PREDICTION OF BRAIN EXTRACELLULAR FLUID CONCENTRATIONS: APPLICATION TO UNDERSTANDING CENTRAL NERVOUS SYSTEM PHARMACOKINETICS AND PHARMACODYNAMICS

John Cory Kalvass

A dissertation submitted to the faculty of the University of North Carolina in partial fulfillment of the requirements for the degree of Doctor of Philosophy in the School of Pharmacy.

Chapel Hill
2006

Approved by:

Advisor: Professor Gary M. Pollack

Reader: Professor Kim L. R. Brouwer

Reader: Professor James E. Hall

Reader: Tristan S. Maurer

Reader: Joseph W. Polli

ABSTRACT

John Cory Kalvass
Prediction of Brain Extracellular Fluid Concentrations: Application to Understanding Central Nervous System Pharmacokinetics and Pharmacodynamics
(Under the direction of Gary M. Pollack, Ph.D.)

This project was pursued to evaluate the applicability of *in vivo* brain extracellular fluid concentrations, obtained via brain-homogenate equilibrium dialysis, to assess extent of CNS penetration and provide estimates of CNS biophase concentrations. Parallel experimentation was conducted to define the impact of blood-brain barrier (BBB) efflux on opioid pharmacokinetics/pharmacodynamics (PK/PD), and to evaluate mathematical approaches for assessing efflux transport kinetics. Steady-state unbound plasma-to-unbound brain concentration ratios and *in vivo* P-gp efflux ratios were determined in mice and used to evaluate extent of CNS distribution for 34 drugs. PK/PD studies were conducted with seven opioids to estimate ED_{50}, serum EC_{50}, and brain EC_{50}; relevant *in vitro* and clinical parameters were used to construct *in vitro*-to-preclinical and preclinical-to-clinical comparisons of opioid potency. PK/PD studies were conducted in P-gp-deficient mice to assess the influence of BBB efflux transport on CNS PK/PD for opioid substrates of P-gp. Comprehensive mathematical modeling was employed to evaluate the influence of efflux, or efflux inhibition, on brain exposure, and to evaluate several potential metrics of efflux. The unbound plasma-to-unbound brain concentration ratio proved to be a valuable parameter for assessing the CNS distribution of drugs (equivalent to or superior to the *in vivo* P-gp efflux ratio). Opioid PK/PD studies indicated that, for centrally-active agents, unbound brain $EC_{50,u}$

was the best descriptor of *in vivo* intrinsic potency, resulting in a *in vitro*-to-*in vivo* correlation of r^2~0.8. P-gp-mediated efflux attenuated central activity of fentanyl, methadone, and loperamide by decreasing brain-to-plasma ratios, but did not influence brain EC_{50}. BBB efflux also decreased fentanyl, methadone, and loperamide brain:plasma equilibration half-life by ~2-fold, consistent with mathematical predictions. Mathematical modeling revealed that 50% inhibition of BBB efflux results in brain exposure increasing ≤2-fold; conventional mathematical treatment of efflux inhibition data overestimates K_m and IC_{50}. New mathematical relationships for expressing efflux activity and calculating K_m and IC_{50} developed in this project overcomes limitations of conventional mathematical treatment. Knowledge of unbound brain concentrations and the influence of BBB efflux transport is important in developing a comprehensive understanding of CNS PK/PD for individual compounds or for members of a compound set.

ACKNOWLEDGEMENTS

To my advisor, Dr. Gary M. Pollack, for his guidance, knowledge, and selfless commitment of time.

To my committee members: Dr. Kim L.R. Brouwer, Dr. James E. Hall, Dr. Tristan S. Maurer, and Joseph W. Polli for their commitment of time and suggestions.

I would also thank Dr. Maciej Zamek-Gliszczynski for his friendship and support, Beverly Mowrey for her friendship and constant support as a study and writing partner as well as a willing proofreader of my work, Rong Zhao for her insightful scientific discussions, Emily Olson for collaboration with the PK/PD mouse studies, and Arlene Bridges for bioanalytical support.

Finally, I would like to this opportunity thank my wife, Leslie Kalvass, for her encouragement, love, and unwavering faith in me. In addition, I would like to thank my friends and family for their encouragement and support.

TABLE OF CONTENTS

LIST OF TABLES……..…..……..…….…....viii

LIST OF FIGURES……...……....x

LIST OF ABBREVIATIONS……...…….……xiii

CHAPTER

1 Challenges Associated with Quantitating, Optimizing, and Predicting Brain Exposure……..……...……1

2 Kinetic Considerations for the Quantitative Assessment of Efflux Activity and Inhibition: Implications for Understanding and Predicting the Effects of Efflux Inhibition……...…….....44

3 Clinical Inhibition of P-glycoprotein at the Blood-Brain Barrier: A Pharmacokinetic and Pharmacodynamic Assessment..…...…..….83

4 Use of Plasma and Brain Unbound Fractions to Assess the Extent of Brain Distribution of Thirty-four Drugs: Comparison of Unbound Concentration Ratios to In Vivo P-glycoprotein Efflux Ratios…….....……..…114

5 Use of Loperamide as a Phenotypic Probe of Mdr1a Status in CF-1 Mice……..141

6 Influence of Blood-Brain Barrier P-glycoprotein on Brain Penetration and Antinociceptive Effects of Model Opioids……..…….....156

7 Pharmacokinetics and Pharmacodynamics of Seven Opioids in P-gp-Competent Mice: Assessment of Unbound Brain EC_{50} and Correlation of In Vitro, Preclinical, and Clinical Data……...…..182

8 Pharmacokinetics and Pharmacodynamics of Alfentanil in P-glycoprotein-Competent- and P-glycoprotein-Deficient Mice: P-glycoprotein Efflux Alters Alfentanil Brain Disposition and Antinociception…….....…….214

9 Perspectives on the Role of Brain Tissue Exposure in the Central Nervous System Pharmacodynamics: Phenomenology, Predictability, and a Roadmap for Drug Discovery……..……238

LIST OF TABLES

Table 1.1 Opioid characteristics……...……42

Table 2.1 Apical, cellular, and basolateral compartments of various model systems……..….74

Table 2.2 Relationships between efflux ratio, permeability-surface area products, and efflux activity…….……75

Table 2.3 Comparison of methods for the calculation of experimental parameters……..……76

Table 2.4 Influence of P-gp-efflux on the brain-to-plasma ratio ($K_{p,brain}$) and brain equilibration rate constant ($K_{brain,eq}$) of P-gp substrates……..…77

Table 3.1 Relationship between P-gp inhibitor perfusate concentration and the degree of P-gp inhibition determined by in situ brain perfusion……..….108

Table 3.2 Preclinical inhibition of P-gp at the BBB…….……109

Table 3.3 In vitro potency and C_{max} of P-gp inhibitors tested clinically……111

Table 3.4 Clinical studies evaluating CNS activity of loperamide and altered P-gp function at the blood brain barrier…….……112

Table 3.5 Effect of P-gp inhibitor on central activity of suspected P-gp substrates…….……..….113

Table 4.1 Conditions used for HPLC-MS/MS analysis for each drug……..….134

Table 4.2 Unbound fractions and $K_{p,brain}$ values for 34 drugs……136

Table 4.3 Classification of drugs based on discrepancies between in vivo P-gp efflux ratio and $[plasma]_{,u}/[brain]_{,u}$ ratio…….……..137

Table 6.1 Parameter estimates from PK-PD modeling…….……173

Table 6.2 Parameter estimates for loperamide in FVB mice……..……...…174

Table 7.1 Parameter estimates from PK-PD modeling……..….203

Table 7.2 Additional parameters used for correlation of i*n vitro*, preclinical, and clinical data…….204

Table 8.1 PK-PD parameters for alfentanil in *mdr1a*(-/-) and *mdr1a*(+/+) mice……231

LIST OF FIGURES

Figure 1.1 Chemical structure of selected *mu* opioid agonists……...……...43

Figure 2.1 Three-compartment model consistent with efflux attenuating the initial rate of flux in the A-to-B direction……...…78

Figure 2.2 Influence of GF-120918 on the brain uptake of quinidine……..……79

Figure 2.3 Theoretical relationship between efflux activity (PS_{efflux}) and permeability-surface area product (PS)……80

Figure 2.4 Theoretical relationship between efflux activity (PS_{efflux}) and asymmetry (ER_{α}), absorptive (ER_B), secretory (ER_A), or intracellular (ER_C) efflux ratio……...……81

Figure 2.5 Correlation between *in situ* and *in vivo* P-gp efflux ratios……..…….82

Figure 4.1 The CNS distributional behavior of each drug based on the plot scheme above……137

Figure 4.2 Comparison of the P-gp efflux ratio and the $[plasma]_{,u}/[brain]_{,u}$ ratio of (A) opioids, (B) triptans, (C) protease inhibitors and (D) antihistamines……139

Figure 4.3 Comparison of the P-gp efflux ratio and the $[plasma]_{,u}/[brain]_{,u}$ ratio of all 34 marketed drugs…….……140

Figure 5.1 Results of the hotplate latency test following a 2-mg/kg s.c. dose of loperamide……..…153

Figure 5.2 Comparison between the hotplate latency results and the loperamide brain-to-serum ratio following a 2-mg/kg s.c. dose of loperamide (4 hr)……154

Figure 5.3 Representative RT-PCR gel indicating the presence of a 1.3 Kb product only in those mice that were phenotyped/ genotyped *mdr1a*(+/+)……..……155

Figure 6.1 Pharmacokinetic-pharmacodynamic model for opioid disposition and antinociception in mice……175

Figure 6.2 Time course of serum (●) and brain (▲) concentrations following s.c. administration of opioids ……..……..176

Figure 6.3 Time course of antinociception following s.c. administration of opioids……..177

Figure 6.4 Relationship between antinociception and opioid serum concentration ……178

Figure 6.5 Relationship between antinociception and opioid brain concentration ……..…179

Figure 6.6 Time course of opioid $K_{p,brain}$ in *mdr1a*(-/-) and *mdr1a*(+/+) mice……..….180

Figure 6.7 Pharmacokinetics/pharmacodynamics of loperamide in FVB mice……..….181

Figure 7.1 Pharmacokinetic-pharmacodynamic model for opioid disposition and antinociception in mice……...……..205

Figure 7.2 Time course of antinociception (◆), serum (●) and brain (▲) concentrations following (A) 0.2-mg/kg s.c. dose of alfentanil; (B) 0.9-mg/kg s.c. dose of fentanyl; (C) 50-mg/kg s.c. dose of loperamide; (D) 25-mg/kg s.c. dose of meperidine;(E) 2-mg/kg s.c. dose of methadone; (F) 3.6-mg/kg s.c. dose of morphine; or (G) 0.001-mg/kg s.c. dose of sufentanil in CF-1 *mdr1a*(+/+) mice……..……206

Figure 7.3 Relationship between plasma concentration and antinociception for *mu* opioid agonists……..207

Figure 7.4 Relationship between brain concentration and antinociception for *mu* opioid agonists……..….208

Figure 7.5 Time course of opioid $K_{p,brain}$ in CF-1 mice……..…..209

Figure 7.6 Correlation analysis for various *in vivo* measures relative to *in vitro* potency……..210

Figure 7.7 Correlation between mouse serum and human plasma EC_{50}s……..…….211

Figure 7.8 Correlation of equipotent clinical dose with *in vitro* K_is, mouse ED_{50}s, and mouse EC_{50}s…….……212

Figure 7.9 The correlation between human plasma-biophase equilibration half-life ($t_{1/2,Ke0}$) and mouse brain equilibration half-life ($t_{1/2eq,brain}$)……213

Figure 8.1 Pharmacokinetic-pharmacodynamic model for alfentanil disposition and antinociception in mice……232

Figure 8.2 Time course of serum (○) and brain (Δ) concentrations following a 0.067- or 0.2-mg/kg s.c. dose of alfentanil in *mdr1a*(-/-) (open symbols) or *mdr1a*(+/+) (solid symbols) mice, respectively……..233

Figure 8.3 Time course of antinociception following a 0.067- or 0.2-mg/kg s.c. dose of alfentanil in *mdr1a*(-/-) (open symbols) or *mdr1a*(+/+) (solid symbols) mice, respectively. Data are presented as mean ± S.E. (n ≥ 3)……..…….234

Figure 8.4 Relationship between antinociception and serum concentration of alfentanil following a 0.067-[*mdr1a*(-/-) ; ○] or 0.2- [*mdr1a*(+/+); ●] mg/kg s.c. dose……..…….235

Figure 8.5 Relationship between antinociception and brain concentration of alfentanil following a 0.2-[*mdr1a*(-/-); ○] or 0.067- [*mdr1a*(+/+); ●] mg/kg s.c. dose……..236

Figure 8.6 Time course of alfentanil Kp_{brain} in mice following a 0.2-[*mdr1a*(-/-); ○] or 0.067- [*mdr1a*(+/+); ●] mg/kg s.c. dose…….237

Figure 9.1 Proposed flow chart for optimal CNS distributional characteristics for drug candidates…….258

LIST OF ABBREVIATIONS

ABCB1	P-glycoprotein
AUC	Area under the curve
AUEC	Area under the effect curve
BBB	Blood-brain barrier
Bcrp	Breast cancer resistance gene
BCSFB	Blood-cerebrospinal fluid barrier
BECF	Brain extracellular fluid
BEI	Brain efflux index
BMECs	Brain microvessel endothelial cells
BUI	Brain uptake index
CNS	Central nervous system
CSF	Cerebrospinal fluid
CYP	Cytochrome P450
DPDPE	[D-Penicillamine^{2,5}]-enkephalin
$E_2$17βG	17beta-estradiol-D-17beta-glucuronide
EEG	Electroencephalogram
HIV	Human immunodeficiency virus
HPLC	High-performance liquid chromatography
LC-MS/MS	Liquid chromatography-tandem mass spectrometry
mdr1	Multi-drug resistant gene

MPR	Maximum possible response
Mrp	Multidrug resistant protein
MS	Mass spectrometry
MW	Molecular weight
Oat	Organic anion transporter
Oatp	Organic anion transporting polypeptide
PAMPA	Parallel artificial membrane permeation assay
PET	Positron emission tomography
P-gp	P-glycoprotein
PK/PD	Pharmacokinetic-pharmacodynamic
QSAR	Quantitative structure-activity relationships
RT-PCR	Reverse transcription polymerase chain reaction
SNP	Single nucleotide polymorphism

CHAPTER 1

CHALLENGES ASSOCIATED WITH QUANTITATING, OPTIMIZING, AND PREDICTING BRAIN EXPOSURE

"Good" brain penetration may be advantageous or detrimental, depending on the site(s) of therapeutic activity and toxicity. Despite recent advances in elucidating the structural and functional aspects of the blood-brain-barrier (BBB), determining the extent of brain penetration of a drug, drug candidate, or new chemical entity remains a formidable challenge. Numerous experimental approaches have been developed to facilitate the prediction and assessment of the central nervous system (CNS) disposition and action of xenobiotics. The factors that govern CNS pharmacokinetics and pharmacodynamics (BBB permeability, active transport, metabolism, CSF bulk flow, and binding to proteins in plasma and brain) have received significant attention in recent years. However, the inter-relationships between these factors, and the ultimate influence of this interplay on brain exposure and consequent biologic response, are poorly understood.

This introductory chapter has been constructed to review the relevant factors that affect brain disposition, as well as the most common experimental approaches used to study or predict the brain disposition of drugs. The shortcomings of currently-used experimental approaches, as well as gaps in the existing knowledge base relative to CNS pharmacokinetics and pharmacodynamics, are discussed. The rationale for development of more sound approaches for predicting and assessing CNS drug penetration, with emphasis on integrating the influence of BBB efflux transport on brain penetration and evaluating target-organ exposure in the context of pharmacologic response, also receives consideration.

The Blood-Brain Interface

The BBB is a physical and biochemical barrier, comprised of a continuous layer of capillary endothelial cells interconnected by tight junctions and supported by parenchymal

(glial) cells, that controls the flux of molecules between blood and brain tissue (Goldstein and Betz, 1986). Although its precise role is unknown, the BBB is generally accepted to be a protective construct that regulates the chemical microenvironment, including both exogenous and endogenous compounds, within the brain. Diffusion of large or hydrophilic molecules across the BBB is restricted because the brain microvasculature lacks fenestrations (openings), and the endothelial cells that line the microvasculature have low basal pinocytotic activity (Goldstein and Betz, 1986). The passive permeability of compounds across the BBB is related to a variety of physiochemical properties (size, charge, polar surface area, and lipophilicity), with small lipophilic molecules (MW<500) having higher passive permeability than large hydrophilic compounds (Habgood et al., 2000). The brain microvascular endothelial cells express various uptake and efflux transporters, as well as metabolic enzymes (Graff and Pollack, 2004). Uptake transporters allow the passage of essential nutrients, such as glucose and amino acids, whereas the efflux transporter proteins and metabolic enzymes serve as biochemical barriers to substrate influx (Graff and Pollack, 2004). Presumably, these active barrier functions play a predominantly protective role, and therefore recognize chemical agents that may pose a threat to brain homeostasis. However, since activation of inhibition of brain target receptors is a fundamental aspect of CNS therapeutics, and such activation or inhibition by necessity changes the "setpoint" biochemical or electrophysiologic condition of the brain, the biologic pressure to exclude CNS-active agents (even therapeutically beneficial ones) from the brain is high. In order to develop effective CNS therapeutic agents, these protective barriers must be understood, circumvented, or otherwise overcome.

Active Transport Across the Blood-Brain Barrier

Active transport at the BBB is recognized as a significant determinant of brain penetration for many drugs. This section briefly highlights some of the relevant transporters thought to be important for CNS drug disposition. Many of the transporters present at the BBB also are expressed at the blood-cerebrospinal fluid barrier (BCSFB). A comprehensive review of relevant BBB and BCSFB transporters was recently published by Graff and Pollack (2004).

P-glycoprotein

To date, P-glycoprotein (P-gp; ABCB1) is recognized as the most important drug efflux transport protein at the BBB. P-gp-mediated efflux has been shown to elicit larger effects on drug distribution into brain (as high as >60-fold attenuation of the brain:blood partition coefficient [$K_{p,brain}$]) (Kalvass et al., 2004), and P-gp has a larger number of relevant drug substrates as compared to any of the other recognized efflux transport systems. P-gp is a 170-kD ATP-dependent transport protein coded by the multi-drug resistance gene (*mdr1*) first identified for its ability to confer multi-drug resistance in tumor cells (Juliano, 1976; Gros et al., 1986) that restricts brain penetration of a variety of xenobiotics. P-gp mediates excretory (e.g., proximal tubular cells of the kidneys; the canalicular membrane of hepatocytes in the liver) and barrier (e.g., the apical membrane of intestinal enterocytes; the luminal membrane of brain capillary endothelial cells) functions in several tissues, (Thiebaut et al., 1987; Cordon-Cardo et al., 1989; Cordon-Cardo et al., 1990). P-gp appears to play a protective role in mammals by attenuating absorption, facilitating excretion, and restricting distribution of many structurally diverse xenobiotics, including calcium channel blockers, HIV protease inhibitors, immunosuppressants, and opioids (Matheny et al., 2001).

P-gp is expressed on the luminal surface of BBB capillary endothelial cells, allowing it to effectively restrict the brain penetration of P-gp substrates. The availability of mice lacking P-gp has been a valuable tool for elucidating the role of P-gp at the BBB (Chen et al., 2003). Studies with P-gp-deficient mice indicate that P-gp-mediated efflux restricts the brain penetration of P-gp substrates by two processes: attenuating brain uptake and enhancing brain efflux (Kusuhara et al., 1997; Dagenais et al., 2001b). While P-gp-mediated efflux has been demonstrated to restrict the brain penetration of a wide variety of drugs, less is known about the pharmacologic significance of other efflux transporters.

Other BBB Efflux Transport Systems

Bcrp. The breast cancer resistance protein (Bcrp) is an apical efflux transporter, expressed on the luminal side of brain microvasculature, that has been shown to reduce the brain penetration of some drugs (Eisenblatter and Galla, 2002; Aronica et al., 2005). Imatinib mesylate (Gleevec), a selective tyrosine kinase inhibitor used to treat some cancers, is a substrate of Bcrp at the BBB. Brain concentrations of imatinib mesylate were 1.7-fold higher in Bcrp-deficient mice compared to wildtype controls (Breedveld et al., 2005), demonstrating the influence of Bcrp on this particular substrate. However, the attenuation of imatinib mesylate uptake across the BBB by Bcrp is modest, at least in comparison to the influence of P-gp on brain uptake of many substrates.

Mrps. Several multidrug resistance-associated proteins (Mrps) also are expressed at the BBB (Nies et al., 2004). Mrp1 has been implicated in the efflux of 17β-estradiol-D-glucuronide ($E_2$17βG), as the brain efflux of $E_2$17βG is lower in Mrp1-defcient mice than wild type controls (Sugiyama et al., 2003). However, a compelling case for pharmacologic

significance of this transporter at the BBB has yet to be made. The role of Mrp2 at the BBB is more controversial. Several studies have indicated that Mrp2-mediated efflux may reduce the brain penetration and effectiveness of some antiepileptic drugs such as phenytoin (Potschka et al., 2003b); other studies have indicated no such role (Potschka et al., 2003a). Mrp2 is not readily detected in rat brain capillaries with commercially available antibodies. However, the protein has been demonstrated in capillary endothelial cells isolated from the brains of epileptic rats (Hoffmann et al., 2006). In some physiologic disease states, the expression of Mrp2 at the BBB may be unregulated (Gerk and Vore, 2002). Other Mrp isoforms, such as Mrp4, Mrp5 and Mrp6, are thought to be present at the BBB, but their functional activity has not been confirmed (Graff and Pollack, 2004).

Organic anion transporting polypeptide (Oatp) and organic anion transporter (Oat) families of transport proteins are expressed in the brain. Specifically, Oatp1, Oatp2, Oatp3, as well as Oat3, have been isolated from brain tissue. There is some evidence that members of the Oatp family may act as both uptake and efflux transporters, depending on the predominant driving force for flux (Graff and Pollack, 2004; Ho and Kim, 2005). Fexofenadine, digoxin, and DPDPE are substrates for Oatps; DPDPE showed saturable brain uptake that was only unmasked in mice lacking P-gp, which serves to efficiently efflux DPDPE from brain (Dagenais et al., 2001a). Although comprehensive mechanistic studies were not performed, competition experiments suggested that DPDPE may be taken up from the systemic circulation into brain by an Oatp. Cimetidine and pravastatin appear to be Oat substrates (Kusuhara et al., 1999; Takeda et al., 2004).

Even though efflux transport proteins other than P-gp may affect CNS drug disposition, no transporter other than P-gp has been shown to have more than a 3-fold effect on $K_{p,brain}$ of

any drug. However, the knowledge base regarding BBB efflux transporters other than P-gp is relatively limited. The P-gp-deficient knockout mouse model has been in use for over 10 years (Schinkel et al., 1996), and is the single experimental model most responsible for the rapid identification of significant substrates for BBB P-gp, as well as for elucidating the pharmacologic impact of P-gp-mediated efflux transport at the blood-brain interface. Murine knockout models for other putative efflux transporters have become available only recently. Thus, it is possible that other transporters will be shown to have significant influence on the brain distribution of some drugs as the database matures. However, compared to other transport proteins P-gp is expressed at high levels in the BBB. It is possible that P-gp is the most significant efflux transporter at the BBB from a pharmacologic standpoint.

Blood-CSF Barrier and CSF Bulk Flow

Even though cerebrospinal fluid (CSF) is in equilibrium with brain extracellular fluid (BECF) and plasma, the blood-CSF interface is not an efficient route for drug delivery to the CNS. The surface area of the blood-CSF barrier (BCSFB; choroid plexus) is ~0.02% that of the BBB (Kusuhara and Sugiyama, 2001). CSF is formed by the choroid plexus, located anatomically in the ventricles of the brain, and maintains a constant bulk flow away from the brain towards the spinal subarachnoid space where it is reabsorbed into plasma. The CSF is turned over every 5-7 hr or about 4 times a day (Shen et al., 2004). CNS bulk flow and constant CSF turnover can be a significant obstacle for movement of molecules from CSF to BECF. Furthermore, CSF bulk flow may act as a significant clearing mechanism for polar hydrophobic molecules with low BBB permeability (Shen et al., 2004).

Many of the active transporters found in the BBB are also expressed in the BCSFB (Graff and Pollack, 2004). One example of a drug that undergoes active transport across the BSCFB is the protease inhibitor ritonavir, which has been shown to undergo active uptake in the guinea pig choroid plexus (Anthonypillai et al., 2004). In some regards, CSF may be considered as an excretory fluid. Thus, transport proteins such as P-gp that are barrier transporters at the blood-brain interface (oriented in the brain-to-blood direction) appear to be excretory transporters at the blood-CSF interface (oriented in the blood-to-CSF direction) (de Lange, 2004). From the standpoint of CNS protection, this directionality may appear counterintuitive at first. However, due to the relative small surface area at the CSF-brain interface, potential toxicants in the CNS afferent circulation may pose a larger threat, via ability to cross the BBB, than compared to toxicants in CSF.

Brain Metabolism

Various metabolic enzymes and cytochrome P450s, such as CYP2D, CYP2E and CYP2B, are expressed in brain tissue (Graff and Pollack, 2004). Many CNS-active agents, such as nicotine and ethanol, are metabolized by these enzymes. As such, brain metabolism may represent a significant barrier and clearing mechanism for centrally-acting agents (Miksys and Tyndale, 2002; Miksys and Tyndale, 2004). The precise influence of these enzymes on CNS pharmacology, and in particular the potential interplay between metabolic enzymes and barrier transport proteins, has yet to be elucidated.

Protein Binding in Plasma and Brain Tissue

Plasma and brain protein binding influence the distribution of drugs between the systemic circulation and brain tissue. *In situ* brain perfusion studies (see below) have demonstrated that extensive plasma protein binding may attenuate the net rate of drug uptake into the brain by reducing the unbound fraction of the drug available for unrestricted diffusion or interaction with uptake transport proteins (Dagenais et al., 2001b; Mandula et al., 2006; Parepally et al., 2006). Extensive brain tissue binding also affects brain distribution by increasing the apparent distributional volume of the brain ($V_{d,brain}$), resulting in a longer brain half-life and slower time to complete equilibration between brain tissue and blood (Liu et al., 2005). Plasma and brain tissue binding also are known to influence steady-state brain-to-plasma partition coefficients ($K_{p,brain}$) of drugs. In the absence of active processes, the steady-state $K_{p,brain}$ of a drug is entirely a function of unbound fractions in plasma and brain (Gillette, 1971; Kurz et al., 1997; Maurer et al., 2004).

METHODS TO ASSESS BBB PERMEABILITY AND ACTIVE TRANSPORT

Measurement of brain uptake clearance

The brain uptake clearance of a compound is an important determinant of its overall brain pharmacokinetics. Several factors govern the magnitude of brain uptake clearance, including BBB permeability, plasma protein binding, blood flow, and active transport. The *in situ* brain perfusion and the brain uptake index (BUI) are two methods developed to estimate the initial rate of brain uptake, best exemplified by the uptake clearance, of compounds in intact animals.

Brain uptake index method. For the BUI method, the compound of interest is administered intravenously to intact animals, and drug concentrations in brain and plasma are determined over a very short time interval at selected time points post-injection (Oldendorf, 1970). It is necessary for the time interval to be sufficiently short to ensure that brain uptake is still under initial linear conditions (i.e., no diffusion from brain back into blood). The brain uptake clearance is then calculated according to equation 1:

$$K_{p,brain}(t) = Cl_{up} \frac{AUC_{0\rightarrow t}}{[plasma](t)} + V_p \quad (1)$$

where $K_{p,brain}(t)$, Cl_{up}, [plasma](t), $AUC_{0\rightarrow t}$, and Vp represent the brain-to-plasma ratio at time t, brain uptake clearance, plasma concentration at time t, plasma $AUC_{0\rightarrow t}$, and the volume of capillary space, respectively. Blood flow and plasma protein binding are known to affect the brain uptake clearance of compounds. The advantage of the BUI method is that the brain uptake clearance is measured under physiologic blood flow and plasma binding conditions. The disadvantage of the BUI method is that multiple time points (≥3), with several animals examined at each time point, are needed to calculate brain uptake clearance for a single compound. Overall, the experiment is relatively animal consumptive (~9 animals per experiment).

In situ brain perfusion model. The *in situ* brain perfusion method is an alternative approach for determining brain uptake clearance in intact animals (Takasato et al., 1984; Smith, 1996). During an *in situ* brain perfusion experiment, the external carotid artery is cannulated, the cardiac ventricles are severed, and one hemisphere of the brain is perfused with perfusate containing test agent and a vascular space marker (i.e., inulin, sucrose, or mannitol). Shortly after starting the perfusion, the experiment is stopped by decapitation. The duration of the perfusion is short (~0.5 - 2 min), because the method assumes initial

linear uptake conditions (i.e., no diffusion from brain back into blood). Brain uptake clearance is calculated from the mass of test agent in the brain hemisphere after subtracting the drug mass from the brain vascular space (X_{brain}), duration of perfusion (t) and perfusate concentration ([perfusate]).

$$Cl_{up} = \frac{X_{brain}/t}{[perfusate]} \quad (2)$$

An advantage of the *in situ* brain perfusion technique is that the perfusate composition (plasma versus buffer, with or without inhibitor) and flow rate can be controlled precisely. This degree of control allows for the effects of blood flow and plasma binding on brain uptake clearance to be studied. The *in situ* brain perfusion method requires relatively fewer animals to determine brain uptake clearance as compared to the BUI method. Potential disadvantages of this approach include the fact that experiments are not conducted under physiologic conditions (e.g., animals are anesthetized; blood flow is under external control). The technique also requires proficiency in animal surgery (carotid artery cannulation) and is relatively labor-intensive (0.5 - 1 hr per perfusion).

Measurement of brain efflux clearance

The brain efflux index (BEI) is a method developed to study the egress of compounds from brain (Kakee et al., 1996). A test-agent and reference compound (impermeable reference marker, such as inulin) are microinjected into the brain, and the rate of substrate disappearance from brain is determined experimentally by measuring the amount of substrate remaining in brain (corrected for the impermeable reference marker) at varying times post-injection. A pseudo-first-order efflux rate constant (K_{el}) is determined from the slope of the log-transformed % dose remaining versus time relationship. This experimental approach has

utility in addressing specific hypotheses regarding brain efflux. For instance, the BEI method has been used to demonstrate that para-aminohippuric acid undergoes saturable efflux, and BBB efflux clearance of this compound exceeds the BBB uptake clearance (Kakee et al., 1997). Also, it is possible to estimate the brain efflux clearance if the apparent volume of distribution of the brain ($V_{d,brain}$) is known (Okura et al., 2003). Similar to the BUI method, the BEI method requires relatively large numbers of animals for the experiment (≥9 animals per experiment).

Cellular monolayer studies.

Various cell-based permeability assays, including Caco-2, MDCK, and brain microvessel endothelial cells (BMECs), are used to estimate BBB permeability and to assess the influence of transport proteins on BBB membrane permeability (Letrent et al., 1999b; Adachi et al., 2001; Mahar Doan et al., 2002; Garberg et al., 2005). These cell-based systems may be more or less useful depending on the tissue of origin (e.g., colon, brain), the source (primary cell versus immortalized cell lines or preclinical versus human), and whether or not the permeability characteristics are reflective of the BBB. A comprehensive comparison of nine different *in vitro* cell models of BBB transport was published recently (Garberg et al., 2005).

In the typical approach, cells are plated on Transwell® inserts and cultured until to confluency. The cell monolayers form polarized apical and basolateral membranes and tight junctions. Apical-to-basolateral (A-to-B) flux studies are then performed to measure apparent permeability (P_{app}) values of test compounds. Cell lines may be transfected with transport protein(s) of interest, and the influence of transporters on permeability may be assessed by measuring the P_{app} in the A-to-B and B-to-A direction with and without specific transporter

inhibitor(s) (Mahar Doan et al., 2002). Asymmetric P_{app} values indicate that a compound of interest is a substrate for active transport. Often, the transporter activity and the asymmetry in permeability are expressed as the ratio of B-to-A to A-to-B P_{app} values or as the ratio of A-to-B with inhibitor to A-to-B without inhibitor P_{app} values.

In vitro cellular monolayer studies provide a high-throughput method for estimating compound permeability and identifying transporter substrates and inhibitors. However, care must be taken when interpreting results from cellular monolayer studies because the expression and functional activity of transport proteins, as well as membrane permeability characteristics of the cellular monolayers, may not be the same as those of the intact BBB (Garberg et al., 2005).

PAMPA

Parallel artificial membrane permeation assay (PAMPA) technology is based on artificial lipid membranes formed on porous support material, and is useful for estimating passive permeability through biologic membranes (Di et al., 2003). PAMPA is a lower-cost, higher-throughput alternative to cell based monolayer permeability assays (Kansy et al., 1998). However, since the influence of uptake and efflux transport proteins is not accounted for by PAMPA, other experimental systems may need to be used in conjunction with this approach.

OTHER METHODS FOR ASSESSING BRAIN DISPOSTION

Use of the brain-to-plasma ratio in assessing CNS disposition

The brain-to-plasma partition coefficient ($K_{p,brain}$) is the most widely used *in vivo* metric for assessing the extent of CNS distribution. A common assumption underlying the use of

this measure of brain distribution is that compounds with large $K_{p,brain}$ values have more extensive CNS distribution than compounds with small $K_{p,brain}$ values. For example, a $K_{p,brain}$ ratio ≥1 often is used as an arbitrary cutoff to classify compounds as having "good" CNS distribution, while a $K_{p,brain}$ <1 is used as an indicator of "poor" CNS distribution. While this type of classification is common, it may be misleading. It is recognized that tissue partition coefficients such as $K_{p,brain}$ are influenced by the relative binding affinity of a substrate for proteins in plasma versus the proteins in the tissue in question (Gillette, 1971; Kurz et al., 1997). For a compound that distributes solely by passive diffusion, the unbound concentration in tissue will equal the unbound concentration in plasma at distribution equilibrium, and the steady-state tissue partition coefficient then is simply a function of the relative plasma and tissue unbound fractions (i.e., $K_{p,tissue} = f_{u,plasma} / f_{u,tissue}$).

When brain and plasma unbound fractions are similar, then a $K_{p,brain}$ value of ~1 would be consistent with unrestricted distribution solely by passive processes. However, the $K_{p,brain}$ value by itself provides little mechanistic information in the absence of estimates of brain and plasma unbound fractions. A $K_{p,brain}$ value <1 could be the result of more extensive binding to plasma proteins than to proteins in brain tissue. Alternatively, a $K_{p,brain}$ value <1 could reflect significant impairment in CNS distribution due to processes such as efflux transport at the BBB.

Imaging techniques

Non-invasive imaging techniques, such as positron emission tomography (PET), have been used more recently to study brain distribution of drugs both in human and preclinical species (Elsinga et al., 2004). The technique requires specialized equipment and facilities to

label compounds and conduct the experiment. Since the isotopes typically used in PET imaging (i.e., [^{11}C] or [^{18}F]) have relatively short half-lives, the experiments must be conducted over short periods of time. PET imaging cannot differentiate between metabolite and parent, and only provides estimates of total drug levels. Nevertheless, recent studies with the P-gp substrate [^{11}C]verapamil have demonstrated that PET has utility for assessing the consequences of P-gp inhibition. Studies in humans, monkeys, and rats showed that the P-gp inhibitor cyclosporin increased the brain concentrations of [^{11}C]verapamil in a concentration-dependent manner (Lee et al., 2005; Sasongko et al., 2005; Hsiao et al., 2006). These results suggest that imaging approaches hold promise for generating brain uptake data in normal human subjects, albeit under very limited conditions. Regardless, imaging may be the most efficient option for generating clinical data for a variety of purposes, such as evaluating the relevance of data acquired from preclinical animal species or *in vitro* experiments.

Gene knockout model

Animals lacking P-gp, Mrp1, Mrp2, Mrp3, Mrp4, or Bcrp have been created (Schinkel et al., 1994; Sugiyama et al., 2003; Assem et al., 2004; Breedveld et al., 2005; Zelcer et al., 2005; Johnson et al., 2006). An animal knockout model is one of the best ways to study the physiologic role of a transporter at the BBB. To examine the influence of a specific transport protein on CNS distribution, $K_{p,brain}$ can be determined in animals deficient for a particular transporter and compared to that of wild-type control animals. One of the most widely used transporter-deficient animal model is the P-gp-deficient mouse model (Chen et al., 2003). It is obvious that the limiting factor for application of this models is that it only has relevance for assessing the impact of a single transport system (in this case, P-gp) on the CNS

disposition of drugs (Schinkel et al., 1994). In addition, it is possible that the activity of other systems (transport proteins, metabolic enzymes, receptors, or post-receptor signaling) changes in response to loss of the target gene. Thus, careful control experiments must be conducted to rule out non-specific changes in substrate pharmacokinetics and pharmacodynamics. The generation of animal knockout models is labor- and resource-intensive.

DETERMINATION OF BRAIN EXTRACELLULAR FLUID CONCENTRATIONS

Total drug concentrations in the systemic circulation or in brain tissue do not provide adequate information concerning the extent of CNS penetration, nor do they allow estimation of BECF concentrations. The ratio between steady-state BECF concentration and unbound drug concentration in the systemic circulation is a logical metric for gauging drug CNS penetration. Several different methods are used to estimate BECF concentration. To date, microdialysis and measurement of substrate concentrations in cerebral spinal fluid (CSF) represent the two methods used most commonly to estimate BECF concentrations. Both methods have documented utility in addressing specific hypotheses. Microdialysis, for example, facilitates continuous sampling of BECF in a discrete brain region (potentially one of pharmacologic relevance) (de Lange et al., 1997); CSF concentrations are thought to be reflective of BECF concentrations for compounds with high passive permeability across the BBB.

While both approaches can provide useful data, each is associated with significant limitations. Microdialysis is a labor- and animal-intensive technique, requires a number of assumptions regarding the efficiency of substrate recovery by the probe, and may disrupt the

regional integrity of the BBB (de Lange et al., 1997; Sun et al., 2001; Hutchinson et al., 2002). While *in vivo* microdialysis is a powerful tool for obtaining the time course of apparent concentrations in BECF, it clearly is not amenable for the efficient characterization of brain penetration. CSF concentrations, in contrast, may be obtained fairly readily from a variety of animal species. However, substrate concentrations in CSF may not reflect BECF concentrations when there is active transport across the BBB or blood-CSF barrier, or when there is incomplete equilibration between blood, brain tissue, and CSF (conditions typically associated with limited BBB permeability, precisely the characteristic that is most important for evaluation of CNS-active agents) (Ooie et al., 1997b; Ooie et al., 1997a; Takasawa et al., 1997; Shen et al., 2004). Consequently, microdialysis lacks general utility, and CSF concentrations often are a poor surrogate for BECF concentration.

Protein binding in brain tissue homogenate

Brain unbound fraction ($f_{u,brain}$) may be estimated from equilibrium dialysis studies performed with brain tissue homogenate (analogous to the use of equilibrium dialysis in determining the unbound fraction of substrates in serum or plasma). The estimate of $f_{u,brain}$, in combination with total brain concentration determined after substrate administration to the intact animal, provides an estimate of the unbound brain tissue (or BECF) concentration. Brain tissue homogenate equilibrium dialysis experiments are conducted by adding drug to brain tissue homogenate (i.e., diluted brain tissue) and dialyzing the homogenate against drug-free buffer. The unbound fraction then is determined from the concentration ratio of buffer and homogenate at equilibrium. The effect on $f_{u,brain}$ of diluting the brain tissue in the

process of obtaining a homogenate can be corrected mathematically to recover an estimate of the unbound fraction in the intact tissue space (Kalvass and Maurer, 2002).

Recently, a validated 96-well equilibrium dialysis apparatus has become commercially available (Banker et al., 2003). The 96-well format has increased throughput compared to more traditional equilibrium dialysis methods. Furthermore, the experimental setup is much faster, and reduced sample volumes can be used. The 96-well format is useful for conducting parallel studies to determine plasma and brain unbound fractions of different compounds, or of the same compound under a variety of conditions.

Although the brain tissue homogenate equilibrium dialysis technique is useful and relatively high-throughput, for some drugs an aberrant $f_{u,brain}$ may be measured if homogenization unmasks binding sites otherwise not accessible to the substrate in the intact organ. In addition, determination of binding in brain tissue homogenate cannot account for active cellular uptake or efflux, or for substrate sequestration due to pH gradients across different cellular organelles. In theory, other more labor-intensive techniques, such as microdialysis or distribution into brain slices *in vitro* (see below), may provide more accurate estimates of $f_{u,brain.}$

In Vitro Substrate Uptake into Brain Slices

Brain slice partitioning studies are useful for determining $f_{u,brain}$ and $V_{d,brain}$. Viable brain slices can be prepared by relatively straightforward and robust experimental methods (Aitken et al., 1995a; Lipton et al., 1995; Kakee et al., 1997; Daniel et al., 2001). Brain slices are incubated in oxygenated artificial BECF containing drug; the steady-state drug concentration ratio between the slice and BECF can be determined readily. The brain unbound fraction

($f_{u,brain}$) is calculated from the [BECF]/[brain] ratio (Becker and Liu, 2006). Brain slices retain tissue structure and cellular activity (metabolism, transport, and sequestration) hence, brain tissue slices offer advantages over the brain tissue homogenate approach (Aitken et al., 1995b). For example, brain tissue slices were useful for studying the lysosomal sequestration and brain partitioning of psychotropic drugs in gray and white brain matter (Daniel, 2003); brain tissue homogenate would have provided an estimate of partitioning due to only the binding processes per se.

Recently, estimates of $f_{u,brain}$ obtained from brain tissue slices have been compared to those determined in brain tissue homogenate equilibrium dialysis. Results suggest both methods are useful and in many cases produce similar values for $f_{u,brain}$ (Becker and Liu, 2006).

Determination of brain apparent volume of distribution from in vitro brain slice data

The apparent volume of distribution of the brain ($V_{d,brain}$) may be measured from *in vitro* brain slice experiments and used to characterize the distribution of drug between BECF and brain tissue (Kakee et al., 1997; Ooie et al., 1997b). The $V_{d,brain}$ is calculated from BECF concentration ([BECF]) and the mass of drug in the brain (X_{brain}) or brain slice according to the following equation:

$$V_{d,brain} = \frac{X_{brain}}{[BECF]} \quad (3)$$

The $V_{d,brain}$ represents the volume of BECF that contains a mass of drug that is equal to the total mass of drug in the brain.

Recognizing that X_{brain} = [brain]× V_{brain} and that $f_{u,brain}$ = [BECF]/[brain], the equation for $V_{d,brain}$ can be rewritten as:

$$V_{d,brain} = \frac{V_{brain}}{f_{u,brain}} \quad (4)$$

where [brain], V_{brain}, and $f_{u,brain}$ represent total brain concentration, actual brain volume, and brain unbound fraction, respectively. From eq. 4, it is obvious that $V_{d,brain}$ is dependent only on $f_{u,brain}$ since V_{brain} is a fixed quantity representing the actual physical volume of brain tissue.

OPIOIDS

Seven *mu* opioid agonists (alfentanil, fentanyl, loperamide, methadone, meperidine, morphine, and sufentanil) were selected as model CNS drugs for this dissertation project because opioids elicit a readily measurable central effect (antinociception) and the clinical pharmacokinetics and pharmacodynamics of these specific compounds are well understood. Furthermore, the opioids selected come from several different structural classes, have a large range of intrinsic potency values, have varying physiochemical properties, and exhibit different brain distributional characteristics including interactions with BBB P-gp (Figure 1.1 and Table 1.1).

Opioids are used clinically as analgesic, anesthetic, and antidiarrheal agents. The analgesic and anesthetic properties of opioids are attributed to interactions with opioid receptors located predominantly within the CNS, whereas antidiarrheal activity is mediated by specific interactions with intestinal opioid receptors. Most opioids have little separation between CNS-mediated effects and antidiarrheal effects. Because of this lack of separation between biologic responses, constipation is a common side effect of opioids. Conversely, most opioids are not useful as antidiarrheal agents because of CNS side effects (Niemegeers et al., 1979). Consequentially, different opioids with distinctive pharmacokinetics and brain

distributional characteristics have been developed for specific uses. Alfentanil and sufentanil are used primarily as anesthetics, whereas fentanyl, meperidine, methadone, and morphine are used primarily as analgesics. Loperamide lacks CNS activity and is used solely as an antidiarrheal agent (Niemegeers et al., 1979). The aforementioned opioids come from four structural classes: diphenylpropylamines (loperamide and methadone), 4-ax-Phenylpiperidines (morphine), 4-eq-phenylpiperidines (meperidine), and 4-anilinopiperidine (alfentanil. fentanyl, and sufentanil) (Figure 1). The following section provides a brief background and rationale for the selection of each of opioid.

Loperamide was developed in the 1970s as an antidiarrheal agent with low incidence of CNS side effects (Niemegeers et al., 1974b; Niemegeers et al., 1974a). Loperamide is a potent *mu* opioid agonist that generally lacks central activity due to poor brain distributional characteristics. The dose required to produce antidiarrheal activity in rats is 88 times lower than the dose that produces CNS effects (Niemegeers et al., 1979). When loperamide was discovered, it was recognized that it had "poor" brain distribution characteristics, although the underlying reason for the "poor" brain distribution was not known. More recent studies have indicated that loperamide is a P-gp substrate, and that P-gp-mediated efflux attenuates loperamide brain uptake and exposure (Schinkel et al., 1996; Dagenais et al., 2004). Mice lacking P-gp exhibit robust CNS effects at low doses of loperamide, whereas P-gp-competent mice do not display these effects. Similarly, the brain tissue concentrations in mice lacking P-gp are about 60-fold higher than in normal mice (Kalvass et al., 2004).

Alfentanil is an anesthetic agent with a rapid onset and offset of action. Studies indicate that the blood-brain equilibration half-life of alfentanil is very rapid (≤ 1 min) (Upton et al.,

1997). Prior to initiating this dissertation project, alfentanil was not believed to be a P-gp substrate (Wandel et al., 2002).

Fentanyl is used primarily as an analgesic. There is some evidence suggesting that fentanyl is a weak P-gp substrate. The *in situ* brain uptake clearance of fentanyl in P-gp-deficient mice was ~20% higher than in P-gp-competent (Dagenais et al., 2004). In addition, fentanyl-associated antinociception (tail flick assay) was ~80% higher in P-gp-deficient mice than in P-gp-competent mice based on comparisons of the area under the effect vs. time curve (AUEC) in each strain of mouse (Thompson et al., 2000).

Methadone is used as an analgesic agent and to treat heroin addiction. The *in situ* brain uptake clearance of methadone is 2.6-fold higher in P-gp-deficient mice than in P-gp-competent mice. Methadone-associated antinociception (tail flick assay) is 3.6-fold higher in P-gp-deficient mice than in P-gp-competent mice based on AUEC comparisons (Thompson et al., 2000). Rats pretreated with the P-gp inhibitor PSC833 exhibited substantially more antinociception (3.1-fold) and a higher $K_{p,brain}$ (6-fold) than control rats (Rodriguez et al., 2004), consistent with a role of P-gp in modulating methadone-associated pharmacologic responses.

Meperidine is an analgesic opioid with an onset of action that is more rapid than for morphine. Meperidine has the lowest intrinsic potency of the seven opioids selected based on *mu* receptor binding affinity. Meperidine also evidences no apparent influence of P-gp on brain uptake.

Morphine is used clinically as an analgesic. It is the most polar and has the lowest *in situ* brain uptake clearance of the seven selected opioids. Morphine is thought to be a weak P-gp substrate. Previous studies demonstrated that morphine produces more antinociception, and

has a larger $K_{p,brain}$, in P-gp-deficient mice as compared to P-gp-competent animals (Thompson et al., 2000; Zong and Pollack, 2000). Rats pretreated with the P-gp inhibitor GF120918 also exhibited more antinociception and larger $K_{p,brain}$ (~3-fold) than control rats (Letrent et al., 1999a), providing further evidence that morphine interacts with P-gp to some extent.

Sufentanil is the most potent of the opioids selected. It is used as an anesthetic agent. Transepithelial monolayer studies conducted with MDR1-transfected LLC-PK1 cells suggest that sufentanil is not a P-gp substrate (Wandel et al., 2002).

Measurement of opioid activity and pharmacokinetic-pharmacodynamic modeling

The central activity of opioids may be measured by several methods, including the hotplate latency test, the tail flick assay, electroencephalogram (EEG), and electrical vocalization in preclinical species (Chen and Pollack, 1998; Cox et al., 1998; Heinzen and Pollack, 2004). Clinically, the cold pressor test, EEG power spectrum analysis, pupilometry, and respiratory depression are used to measure the central action of opioids (Tayrouz et al., 2001; Lotsch, 2005). Because opioids elicit easily measurable responses in humans and animal models, pharmacokinetic-pharmacodynamic modeling has been used to gain a mechanistic understanding of various aspects of opioid pharmacology. For example, Cox et al. (1998) established an *in vitro*-to-*in vivo* potency correlation between *in vitro* receptor affinity and *in vivo* pharmacodynamic parameter estimates obtained from pharmacokinetic-pharmacodynamic modeling of the electroencephalogram effect of three synthetic opioids in rats. A recent review on clinical pharmacokinetic-pharmacodynamic modeling of opioids has

been published (Lotsch, 2005), and provides an excellent summary of the disposition and action of opioids, including the drugs selected for analysis in this project.

Influence of P-gp-mediated efflux on opioid antinociception

Few pharmacokinetic-pharmacodynamic modeling studies have been performed to provide understanding of the precise mechanism(s) by which P-gp-mediated efflux modulates opioid-associated antinociception. One study conducted with morphine in P-gp-competent and P-gp-deficient mice suggest that P-gp-mediated efflux attenuated morphine-associated antinociception solely by decreasing $K_{p,brain.}$ This conclusion was supported by the fact that ED_{50} was higher in P-gp-competent than P-gp-deficient mice, while there was no difference in brain EC_{50} between the P-gp-competent and P-gp-deficient mice (i.e., P-gp simply regulated morphine flux between blood and brain, but had no influence on morphine once it reached the brain tissue compartment (Zong and Pollack, 2000)).

In contrast, a study conducted with the metabolically-stable opioid-peptide DPDPE concluded that P-gp-mediated efflux attenuated DPDPE-associated antinociception in two ways: by reducing the $K_{p,brain,ss}$ of DPDPE, necessitating larger doses and higher systemic concentrations to achieve similar brain concentrations; and by increasing the brain tissue EC_{50}. It was hypothesized that parenchymal expression of P-gp increased the brain EC_{50} of DPDPE by redistributing DPDPE away from the receptor biophase (Chen and Pollack, 1998).

The morphine and DPDPE studies used tail flick and hotplate latency tests, respectively, to measure central opioid response. This difference in experimental approach may account for the apparent differences in the mechanisms by which P-gp modulates opioid

pharmacology. Additional pharmacokinetic-pharmacodynamic studies with other opioids that express a range of interactions with P-gp may provide a better understanding of the mechanism(s) by which P-gp-mediated efflux attenuates the brain penetration and alters the CNS activity of drugs.

***IN VITRO*-TO-*IN VIVO* CORRELATION OF POTENCY**

In drug discovery, *in vitro* assays and preclinical animal studies are widely used to assess compound potency and to identify compound(s) that will have the desired clinical pharmacologic response. There is a range of options for assessing compound potency, including *in vitro* binding or receptor functional assays, and *in vivo* animal studies to determine dose-response or concentration-response relationships. *In vitro* binding and functional assays, by nature, are designed to estimate the intrinsic potency at the receptor of interest.

Ideally, i*n vitro* potency should translate to or predict *in vivo* potency. Very often this is the case, as strong correlations between *in vitro* potency and *in vivo* ED_{50} or EC_{50} have been established for many compounds from diverse therapeutic classes (Leysen et al., 1983; Visser et al., 2003). However, when there is no correlation between *in vitro* and *in vivo* potency measures, the validity of the *in vitro* assay, the animal model, or the target may be questioned. Hence, establishing strong *in vitro*-to-*in vivo* correlations is a necessity for drug development, because it aids in target validation and boosts confidence in the *in vitro* and *in vivo* pharmacology models. Historically, *in vitro*-to-*in vivo* correlations have been established by comparing an *in vitro* measure of potency, such as K_i or EC_{50} from a cell-based functional assay, with ED_{50}. Although the ED_{50} is not necessarily the best measure of intrinsic drug

potency, it has been widely used for two primary reasons: 1) sensitive bioanalytical assays (HPLC or LC-MS/MS) required to determine EC_{50} were not routinely available until more recently (1970s and 1990s, respectively); and 2) dose versus effect studies are relatively straightforward. *In vitro*-to-*in vivo* correlations with ED_{50} are most likely to be successful for compounds that have large differences in intrinsic potency and relatively similar pharmacokinetics.

If compounds possess large differences in pharmacokinetics, improved *in vitro*-to-*in vivo* correlations may be achieved using EC_{50}. Commonly, EC_{50} is estimated from the plasma concentration vs. effect relationship. Pharmacokinetic-pharmacodynamic modeling often is used to obtain estimates of EC_{50} from *in vivo* data, and is a powerful tool for exploring mechanisms of drug disposition and action.

The best *in vitro*-to-*in vivo* potency correlations are achieved when the biophase concentration-effect relationship is known. Total plasma and unbound plasma concentrations are the most widely used surrogates for the biophase concentration. However, these surrogates do not always reflect actual biophase concentrations. The divergence between biophase and systemic concentrations is especially true for compounds that act on targets within the CNS, since the BBB restricts the CNS distribution of many compounds.

Given these considerations, it is important to accurately determine CNS biophase concentrations in order to make better *in vitro* to *in vivo* correlations for centrally active compounds. When compounds have "good" BBB permeability and are not substrates for transporters, *in vitro*-to-*in vivo* correlations can be constructed using unbound plasma or CSF concentrations as a surrogate for CNS biophase concentrations. When unbound plasma or CSF concentrations are not reflective of CNS biophase concentrations, such as when a

compound has "poor" BBB permeability or is subject to active brain uptake or efflux, other methods for estimating CNS biophase concentrations may be needed.

THE EXTENT AND RATE OF CNS DISTRIBUTION

Depending on whether or not CNS activity is desired, the extent and rate of brain penetration of a compound may be important. Predicting or determining the extent and rate of brain penetration remains a challenge, despite the development of methodologies to assess BBB passive permeability, uptake clearance, efflux clearance, and interaction with transporters.

The extent of CNS penetration is dependent on the ratio of unbound uptake and efflux clearances (Liu and Chen, 2005). When distribution between brain and blood occurs solely by passive diffusion, this ratio is unity. If CNS distribution is impaired by active efflux, metabolism, or CSF bulk flow, the ratio will be less than unity, and if CNS distribution is enhanced by active uptake the ratio will be greater than unity.

$$\text{extent} \propto \frac{\text{unbound uptake clearance}}{\text{unbound efflux clearance}} \propto \frac{\text{passive permeability + active uptake}}{\text{passive permeability + active efflux + CSF bulk flow + metabolism}} \quad (5)$$

The rate of equilibration between blood and brain is dependent on the ratio of efflux clearance and brain apparent volume of distribution (Liu and Chen, 2005; Liu et al., 2005). Since the brain apparent volume of distribution is inversely proportional to $f_{u,brain}$ (equation 4), the rate of equilibration is also proportional to the product of efflux clearance and $f_{u,brain}$.

$$\text{rate} \propto \frac{\text{efflux clearance}}{V_{d,brain}} \propto \text{efflux clearance} \times f_{u,brain} \quad (6)$$

or

$$\text{rate} \propto (\text{passive permeability} + \text{active efflux} + \text{CSF bulk flow} + \text{metabolism}) \times f_{u,brain} \quad (7)$$

The previous equations illustrate that the extent and rate of brain penetration are dependent on multiple factors, with no single factor being dominant. Approaches that consider only one factor, such as only passive permeability or affinity for a given efflux transporter, fail to provide sufficient information for proper prediction and evaluation of CNS distributional properties. Low passive permeability or affinity for efflux transport proteins per se does not necessarily indicate that a compound will have a poor extent or rate of CNS distribution. If passive permeability is sufficiently large compared to CSF bulk flow, no other active processes are present (i.e., metabolism and active transport), and if $f_{u,brain}$ is large, then it is possible for a compound with low passive permeability to have unimpaired and rapid CNS distribution. Similarly, a compound that undergoes active efflux may have unimpaired and rapid CNS distribution if active efflux is counterbalanced by active uptake.

ASSESSMENT OF EFFLUX KINETICS

Numerous approaches exist to measure and express efflux kinetics. However, little consensus exists for the quantitation and expression of efflux activity. Efflux activity has been expressed qualitatively as efflux ratios, permeability surface area products, and in terms of flux (Adachi et al., 2001; Gao et al., 2001). Most commonly, parameters associated with efflux kinetics (K_m or IC_{50}) are obtained by fitting a sigmoidal E_{max} model to permeability or flux data. The resulting EC_{50} then is used interchangeably as K_m or IC_{50} depending on the type of study (saturation or inhibition) (Chen et al., 2002; Troutman and Thakker, 2003a). This type of data analysis has been unsatisfactory, for efflux kinetics are poorly understood, and unexplained and complex observations are commonly encountered. For example, recently it has been reported that:

1. The K_m and IC_{50} of a substrate or inhibitor towards an efflux transporter are highly dependent on the cell line or experimental model (Taub et al., 2005).
2. The K_m of a substrate increases as a function of transporter expression (Balakrishnam and Polli, 2005; Balakrishnan et al., 2005).
3. Efflux produces non-symmetric effects on the A-to-B and B-to-A permeabilities (Troutman and Thakker, 2003a; Troutman and Thakker, 2003b).
4. Differential inhibition of efflux in different tissues (P-gp inhibition in blood > testes > BBB) has been reported (Choo et al., 2006).

Various models have been proposed to describe efflux kinetics. However, based on current understanding of these models, the above noted observations could not have been predicted. Different models or approaches are necessary to better predict and understand efflux kinetics.

PROJECT OVERVIEW

The primary purposes of this dissertation project were as follows: 1) to explore kinetic model(s) of efflux to better understand efflux kinetics with emphasis on risk assessment of clinical P-gp inhibition at the BBB, 2) to devise methodology to better assess the extent of CNS distribution of drugs, and 3) to use pharmacokinetic-pharmacodynamic modeling with opioids to assess the influence of P-gp-mediated efflux on opioid brain penetration and antinociception, and to determine the best surrogate of *in vivo* intrinsic potency for CNS active drugs.

Unexpected and complex experimental observations related to efflux transport have been reported in the literature. Current models and understanding of efflux kinetics do not adequately predict or explain these observations. Furthermore, the clinical risk of efflux

inhibition at the BBB is not well-defined. A better understanding of the relationship between efflux inhibition and kinetic parameters is critical for appropriate data interpretation, standardization in calculating and expressing the influence of efflux transport, and predicting the clinical significance of efflux inhibition. The first goal of this dissertation project was to develop an alternative mathematical model for expressing and assessing efflux transport kinetics. The results of this model were applied to recent unexpected and complex experimental observations concerning efflux kinetics (Chapter 2) and towards the assessment of clinical risk of P-gp inhibition at the BBB (Chapter 3).

A second goal of this project was to evaluate the steady-state unbound plasma-to-unbound brain concentration ratio ($[plasma]_{,u}/[brain]_{,u}$) as a method for assessing the extent of CNS distribution of drugs (Chapter 4). The $[plasma]_{,u}/[brain]_{,u}$ ratio is expected to be equal to the *in vivo* P-gp efflux if P-gp-mediated efflux is the only active process affecting brain disposition. Using this principle, studies were conducted to compare the degree of CNS distributional impairment expressed as the $[plasma]_{,u}/[brain]_{,u}$ ratio to the P-gp efflux ratio for 34 marketed drugs. Opioids, triptans, protease inhibitors, and antihistamines (n = 24 total) were included in the study because these classes of agents are known to include P-gp substrates, and the extent to which these compounds distribute into the CNS may have important implications regarding safety and efficacy. In addition, 10 marketed drugs from various drug classes with either poor CNS distribution or BBB efflux also were included as part of the analysis.

The third goal of this project was to define the impact of BBB efflux on opioid pharmacokinetics/pharmacodynamics (Chapter 5, 6, and 8) and to evaluate the applicability of *in vivo* brain extracellular fluid concentrations, obtained via brain-homogenate equilibrium

dialysis to estimate CNS biophase concentrations (Chapter 7). Pharmacokinetic/ pharmacodynamic studies were conducted with seven opioids to estimate ED_{50}, serum EC_{50}, and brain EC_{50}; relevant *in vitro* and clinical parameters were used to construct *in vitro*-to-preclinical and preclinical-to-clinical comparisons of opioid potency (Chapter 7).

In summary, the overall goal of this research project was to evaluate a brain equilibrium dialysis method for predicting *in vivo* brain extracellular fluid concentrations in order to assess CNS penetration, as well as to provide a context for concentration-effect relationships for CNS-active drugs. Furthermore, a considerable portion of this project was devoted to mathematically and experimentally assessing the impact of BBB efflux on CNS pharmacokinetics and pharmacodynamics.

REFERENCES

1. Adachi Y, Suzuki H and Sugiyama Y (2001) Comparative studies on in vitro methods for evaluating in vivo function of MDR1 P-glycoprotein. *Pharm Res* **18:**1660-1668.

2. Aitken PG, Breese GR, Dudek FF, Edwards F, Espanol MT, Larkman PM, Lipton P, Newman GC, Nowak TS, Jr. and Panizzon KL (1995a) Preparative methods for brain slices: a discussion. *J Neurosci Methods* **59:**139-149.

3. Aitken PG, Breese GR, Dudek FF, Edwards F, Espanol MT, Larkman PM, Lipton P, Newman GC, Nowak TS, Jr., Panizzon KL and et al. (1995b) Preparative methods for brain slices: a discussion. *J Neurosci Methods* **59:**139-149.

4. Anthonypillai C, Sanderson RN, Gibbs JE and Thomas SA (2004) The distribution of the HIV protease inhibitor, ritonavir, to the brain, cerebrospinal fluid, and choroid plexuses of the guinea pig. *J Pharmacol Exp Ther* **308:**912-920.

5. Aronica E, Gorter JA, Redeker S, van Vliet EA, Ramkema M, Scheffer GL, Scheper RJ, van der Valk P, Leenstra S, Baayen JC, Spliet WG and Troost D (2005) Localization of breast cancer resistance protein (BCRP) in microvessel endothelium of human control and epileptic brain. *Epilepsia* **46:**849-857.

6. Assem M, Schuetz EG, Leggas M, Sun D, Yasuda K, Reid G, Zelcer N, Adachi M, Strom S, Evans RM, Moore DD, Borst P and Schuetz JD (2004) Interactions between hepatic Mrp4 and Sult2a as revealed by the constitutive androstane receptor and Mrp4 knockout mice. *J Biol Chem* **279:**22250-22257.

7. Balakrishnam A and Polli JE (2005) Bias in estimation of transporter kinetic parameters: Interplay of transporter expression level and substrate affinity. *J Clin Pharmacol* **45:**1087.

8. Balakrishnan A, Sussman DJ and Polli JE (2005) Development of stably transfected monolayer overexpressing the human apical sodium-dependent bile acid transporter (hASBT). *Pharm Res* **22:**1269-1280.

9. Banker MJ, Clark TH and Williams JA (2003) Development and validation of a 96-well equilibrium dialysis apparatus for measuring plasma protein binding. *J Pharm Sci* **92:**967-974.

10. Becker S and Liu X (2006) Evaluation of the utility of brain slice methods to study brain penetration. *Drug Metab Dispos* **34:**855-861.

11. Breedveld P, Pluim D, Cipriani G, Wielinga P, van Tellingen O, Schinkel AH and Schellens JHM (2005) The effect of Bcrp1 (Abcg2) on the in vivo pharmacokinetics and brain penetration of imatinib mesylate (gleevec): Implications for the use of breast cancer resistance protein and P-glycoprotein inhibitors to enable the brain penetration of imatinib in patients. *Cancer Research* **65:**2577-2582.

12. Chen C, Liu X and Smith BJ (2003) Utility of Mdr1-gene deficient mice in assessing the impact of P-glyco-protein on pharmacokinetics and pharmacodynamics in drug discovery and development. *Curr Drug Metab* **4:**272-291.

13. Chen C and Pollack GM (1998) Altered disposition and antinociception of [D-penicillamine(2,5)] enkephalin in mdr1a-gene-deficient mice. *J Pharmacol Exp Ther* **287:**545-552.

14. Chen W, Yang JZ, Andersen R, Nielsen LH and Borchardt RT (2002) Evaluation of the permeation characteristics of a model opioid peptide, H-Tyr-D-Ala-Gly-Phe-D-Leu-OH (DADLE), and its cyclic prodrugs across the blood-brain barrier using an in situ perfused rat brain model. *J Pharmacol Exp Ther* **303:**849-857.

15. Choo EF, Kurnik D, Muszkat M, Ohkubo T, Shay SD, Higginbotham JN, Glaeser H, Kim RB, Wood AJ and Wilkinson GR (2006) Differential in Vivo Sensitivity to Inhibition of P-Glycoprotein Located in Lymphocytes, Testes, and the Blood-Brain Barrier. *J Pharmacol Exp Ther*.

16. Cordon-Cardo C, O'Brien JP, Boccia J, Casals D, Bertino JR and Melamed MR (1990) Expression of the multidrug resistance gene product (P-glycoprotein) in human normal and tumor tissues. *J Histochem Cytochem* **38:**1277-1287.

17. Cordon-Cardo C, O'Brien JP, Casals D, Rittman-Grauer L, Biedler JL, Melamed MR and Bertino JR (1989) Multidrug-resistance gene (P-glycoprotein) is expressed by endothelial cells at blood-brain barrier sites. *Proc Natl Acad Sci U S A* **86:**695-698.

18. Cox EH, Kerbusch T, Van der Graaf PH and Danhof M (1998) Pharmacokinetic-pharmacodynamic modeling of the electroencephalogram effect of synthetic opioids in the rat: correlation with the interaction at the mu-opioid receptor. *J Pharmacol Exp Ther* **284:**1095-1103.

19. Dagenais C, Ducharme J and Pollack GM (2001a) Uptake and efflux of the peptidic delta-opioid receptor agonist. *Neurosci Lett* **301:**155-158.

20. Dagenais C, Graff CL and Pollack GM (2004) Variable modulation of opioid brain uptake by P-glycoprotein in mice. *Biochem Pharmacol* **67:**269-276.

21. Dagenais C, Zong J, Ducharme J and Pollack GM (2001b) Effect of mdr1a P-glycoprotein gene disruption, gender, and substrate concentration on brain uptake of selected compounds. *Pharm Res* **18:**957-963.

22. Daniel WA (2003) Mechanisms of cellular distribution of psychotropic drugs. Significance for drug action and interactions. *Prog Neuropsychopharmacol Biol Psychiatry* **27:**65-73.

23. Daniel WA, Wojcikowski J and Palucha A (2001) Intracellular distribution of psychotropic drugs in the grey and white matter of the brain: the role of lysosomal trapping. *Br J Pharmacol* **134:**807-814.

24. de Lange EC (2004) Potential role of ABC transporters as a detoxification system at the blood-CSF barrier. *Adv Drug Deliv Rev* **56:**1793-1809.

25. de Lange EC, Danhof M, de Boer AG and Breimer DD (1997) Methodological considerations of intracerebral microdialysis in pharmacokinetic studies on drug transport across the blood-brain barrier. *Brain Res Brain Res Rev* **25:**27-49.

26. Di L, Kerns EH, Fan K, McConnell OJ and Carter GT (2003) High throughput artificial membrane permeability assay for blood-brain barrier. *Eur J Med Chem* **38:**223-232.

27. Eisenblatter T and Galla HJ (2002) A new multidrug resistance protein at the blood-brain barrier. *Biochem Biophys Res Commun* **293:**1273-1278.

28. Elsinga PH, Hendrikse NH, Bart J, Vaalburg W and van Waarde A (2004) PET Studies on P-glycoprotein function in the blood-brain barrier: how it affects uptake and binding of drugs within the CNS. *Curr Pharm Des* **10:**1493-1503.

29. Gao J, Murase O, Schowen RL, Aube J and Borchardt RT (2001) A functional assay for quantitation of the apparent affinities of ligands of P-glycoprotein in Caco-2 cells. *Pharm Res* **18:**171-176.

30. Garberg P, Ball M, Borg N, Cecchelli R, Fenart L, Hurst RD, Lindmark T, Mabondzo A, Nilsson JE, Raub TJ, Stanimirovic D, Terasaki T, Oberg JO and Osterberg T (2005) In vitro models for the blood-brain barrier. *Toxicol In Vitro* **19:**299-334.

31. Gerk PM and Vore M (2002) Regulation of expression of the multidrug resistance-associated protein 2 (MRP2) and its role in drug disposition. *J Pharmacol Exp Ther* **302:**407-415.

32. Gillette JR (1971) Factors affecting drug metabolism. *Ann NY Acad Sci* **179**.

33. Goldstein GW and Betz AL (1986) The blood-brain barrier. *Sci Am* **255:**74-83.

34. Graff CL and Pollack GM (2004) Drug transport at the blood-brain barrier and the choroid plexus. *Curr Drug Metab* **5:**95-108.

35. Gros P, Ben Neriah YB, Croop JM and Housman DE (1986) Isolation and expression of a complementary DNA that confers multidrug resistance. *Nature* **323:**728-731.

36. Habgood MD, Begley DJ and Abbott NJ (2000) Determinants of passive drug entry into the central nervous system. *Cell Mol Neurobiol* **20:**231-253.

37. Heinzen EL and Pollack GM (2004) Pharmacodynamics of morphine-induced neuronal nitric oxide production and antinociceptive tolerance development. *Brain Res* **1023:**175-184.

38. Ho RH and Kim RB (2005) Transporters and drug therapy: implications for drug disposition and disease. *Clin Pharmacol Ther* **78:**260-277.

39. Hoffmann K, Gastens AM, Volk HA and Loscher W (2006) Expression of the multidrug transporter MRP2 in the blood-brain barrier after pilocarpine-induced seizures in rats. *Epilepsy Res* **69:**1-14.

40. Hsiao P, Sasongko L, Link JM, Mankoff DA, Muzi M, Collier AC and Unadkat JD (2006) Verapamil P-glycoprotein transport across the rat blood-brain barrier: cyclosporine A concentration-inhibition analysis and comparison with human data. *J Pharmacol Exp Ther*.

41. Hutchinson PJ, O'Connell MT, Kirkpatrick PJ and Pickard JD (2002) How can we measure substrate, metabolite and neurotransmitter concentrations in the human brain? *Physiol Meas* **23:**R75-109.

42. Johnson BM, Zhang P, Schuetz JD and Brouwer KL (2006) Characterization of transport protein expression in multidrug resistance-associated protein (mrp) 2-deficient rats. *Drug Metab Dispos* **34:**556-562.

43. Juliano R (1976) Drug-resistant mutants of Chinese hamster ovary cells possess an altered cell surface carbohydrate component. *J Supramol Struct* **4:**521-526.

44. Kakee A, Terasaki T and Sugiyama Y (1996) Brain efflux index as a novel method of analyzing efflux transport at the blood-brain barrier. *J Pharmacol Exp Ther* **277:**1550-1559.

45. Kakee A, Terasaki T and Sugiyama Y (1997) Selective brain to blood efflux transport of para-aminohippuric acid across the blood-brain barrier: in vivo evidence by use of the brain efflux index method. *J Pharmacol Exp Ther* **283:**1018-1025.

46. Kalvass JC, Graff CL and Pollack GM (2004) Use of loperamide as a phenotypic probe of mdr1a status in CF-1 mice. *Pharm Res* **21:**1867-1870.

47. Kalvass JC and Maurer TS (2002) Influence of nonspecific brain and plasma binding on CNS exposure: implications for rational drug discovery. *Biopharm Drug Dispos* **23:**327-338.

48. Kansy M, Senner F and Gubernator K (1998) Physicochemical high throughput screening: parallel artificial membrane permeation assay in the description of passive absorption processes. *J Med Chem* **41:**1007-1010.

49. Kurz A, Ikeda T, Sessler DI, Larson MD, Bjorksten AR, Dechert M and Christensen R (1997) Meperidine decreases the shivering threshold twice as much as the vasoconstriction threshold. *Anesthesiology* **86:**1046-1054.

50. Kusuhara H, Sekine T, Utsunomiya-Tate N, Tsuda M, Kojima R, Cha SH, Sugiyama Y, Kanai Y and Endou H (1999) Molecular cloning and characterization of a new multispecific organic anion transporter from rat brain. *J Biol Chem* **274:**13675-13680.

51. Kusuhara H and Sugiyama Y (2001) Efflux transport systems for drugs at the blood-brain barrier and blood-cerebrospinal fluid barrier (Part 1). *Drug Discov Today* **6:**150-156.

52. Kusuhara H, Suzuki H, Terasaki T, Kakee A, Lemaire M and Sugiyama Y (1997) P-Glycoprotein mediates the efflux of quinidine across the blood-brain barrier. *J Pharmacol Exp Ther* **283:**574-580.

53. Lee YJ, Maeda J, Kusuhara H, Okauchi T, Inaji M, Nagai Y, Obayashi S, Nakao R, Suzuki K, Sugiyama Y and Suhara T (2005) In vivo evaluation of P-glycoprotein function at the blood-brain barrier in nonhuman primates using [11C]verapamil. *J Pharmacol Exp Ther*.

54. Letrent SP, Pollack GM, Brouwer KR and Brouwer KL (1999a) Effects of a potent and specific P-glycoprotein inhibitor on the blood-brain barrier distribution and antinociceptive effect of morphine in the rat. *Drug Metab Dispos* **27:**827-834.

55. Letrent SP, Polli JW, Humphreys JE, Pollack GM, Brouwer KR and Brouwer KL (1999b) P-glycoprotein-mediated transport of morphine in brain capillary endothelial cells. *Biochem Pharmacol* **58:**951-957.

56. Leysen JE, Gommeren W and Niemegeers CJ (1983) [3H]Sufentanil, a superior ligand for mu-opiate receptors: binding properties and regional distribution in rat brain and spinal cord. *Eur J Pharmacol* **87:**209-225.

57. Lipton P, Aitken PG, Dudek FE, Eskessen K, Espanol MT, Ferchmin PA, Kelly JB, Kreisman NR, Landfield PW and Larkman PM (1995) Making the best of brain slices: comparing preparative methods. *J Neurosci Methods* **59:**151-156.

58. Liu X and Chen C (2005) Strategies to optimize brain penetration in drug discovery. *Curr Opin Drug Discov Devel* **8:**505-512.

59. Liu X, Smith BJ, Chen C, Callegari E, Becker SL, Chen X, Cianfrogna J, Doran AC, Doran SD, Gibbs JP, Hosea N, Liu J, Nelson FR, Szewc MA and Van Deusen J (2005) Use of a physiologically based pharmacokinetic model to study the time to reach brain equilibrium: an experimental analysis of the role of blood-brain barrier permeability, plasma protein binding, and brain tissue binding. *J Pharmacol Exp Ther* **313:**1254-1262.

60. Lotsch J (2005) Pharmacokinetic-pharmacodynamic modeling of opioids. *J Pain Symptom Manage* **29:**S90-103.

61. Mahar Doan KM, Humphreys JE, Webster LO, Wring SA, Shampine LJ, Serabjit-Singh CJ, Adkison KK and Polli JW (2002) Passive permeability and P-glycoprotein-mediated efflux differentiate central nervous system (CNS) and non-CNS marketed drugs. *J Pharmacol Exp Ther* **303:**1029-1037.

62. Mandula H, Parepally JM, Feng R and Smith QR (2006) Role of site-specific binding to plasma albumin in drug availability to brain. *J Pharmacol Exp Ther* **317:**667-675.

63. Matheny CJ, Lamb MW, Brouwer KR and Pollack GM (2001) Pharmacokinetic and pharmacodynamic implications of P-glycoprotein modulation. *Pharmacotherapy* **21:**778-796.

64. Maurer TS, Debartolo DB, Tess DA and Scott DO (2004) Relationship between Exposure and Nonspecific Binding of Thirty-Three Central Nervous System Drugs in Mice. *Drug Metab Dispos*.

65. Miksys S and Tyndale RF (2004) The unique regulation of brain cytochrome P450 2 (CYP2) family enzymes by drugs and genetics. *Drug Metab Rev* **36:**313-333.

66. Miksys SL and Tyndale RF (2002) Drug-metabolizing cytochrome P450s in the brain. *J Psychiatry Neurosci* **27:**406-415.

67. Niemegeers CJ, Lenaerts FM and Janssen PA (1974a) Loperamide (R 18 553), a novel type of antidiarrheal agent. Part 1: in vivo oral pharmacology and acute toxicity. Comparison with morphine, codeine, diphenoxylate and difenoxine. *Arzneimittelforschung* **24:**1633-1636.

68. Niemegeers CJ, Lenaerts FM and Janssen PA (1974b) Loperamide (R 18 553), a novel type of antidiarrheal agent. Part 2: in vivo parenteral pharmacology and acute toxicity in mice. Comparison with morphine, codeine and diphenoxylate. *Arzneimittelforschung* **24:**1636-1641.

69. Niemegeers CJ, McGuire JL, Heykants JJ and Janssen PA (1979) Dissociation between opiate-like and antidiarrheal activities of antidiarrheal drugs. *J Pharmacol Exp Ther* **210:**327-333.

70. Nies AT, Jedlitschky G, Konig J, Herold-Mende C, Steiner HH, Schmitt HP and Keppler D (2004) Expression and immunolocalization of the multidrug resistance proteins, MRP1-MRP6 (ABCC1-ABCC6), in human brain. *Neuroscience* **129:**349-360.

71. Okura T, Saito M, Nakanishi M, Komiyama N, Fujii A, Yamada S and Kimura R (2003) Different distribution of morphine and morphine-6 beta-glucuronide after intracerebroventricular injection in rats. *Br J Pharmacol* **140:**211-217.

72. Oldendorf WH (1970) Measurement of brain uptake of radiolabeled substances using a tritiated water internal standard. *Brain Res* **24:**372-376.

73. Ooie T, Terasaki T, Suzuki H and Sugiyama Y (1997a) Kinetic evidence for active efflux transport across the blood-brain barrier of quinolone antibiotics. *J Pharmacol Exp Ther* **283:**293-304.

74. Ooie T, Terasaki T, Suzuki H and Sugiyama Y (1997b) Quantitative brain microdialysis study on the mechanism of quinolones distribution in the central nervous system. *Drug Metab Dispos* **25:**784-789.

75. Parepally JM, Mandula H and Smith QR (2006) Brain Uptake of Nonsteroidal Anti-Inflammatory Drugs: Ibuprofen, Flurbiprofen, and Indomethacin. *Pharm Res*.

76. Potschka H, Fedrowitz M and Loscher W (2003a) Brain access and anticonvulsant efficacy of carbamazepine, lamotrigine, and felbamate in ABCC2/MRP2-deficient TR- rats. *Epilepsia* **44:**1479-1486.

77. Potschka H, Fedrowitz M and Loscher W (2003b) Multidrug resistance protein MRP2 contributes to blood-brain barrier function and restricts antiepileptic drug activity. *J Pharmacol Exp Ther* **306:**124-131.

78. Rodriguez M, Ortega I, Soengas I, Suarez E, Lukas JC and Calvo R (2004) Effect of P-glycoprotein inhibition on methadone analgesia and brain distribution in the rat. *J Pharm Pharmacol* **56:**367-374.

79. Sasongko L, Link JM, Muzi M, Mankoff DA, Yang X, Collier AC, Shoner SC and Unadkat JD (2005) Imaging P-glycoprotein transport activity at the human blood-brain barrier with positron emission tomography. *Clin Pharmacol Ther* **77:**503-514.

80. Schinkel AH, Smit JJ, van Tellingen O, Beijnen JH, Wagenaar E, van Deemter L, Mol CA, van der Valk MA, Robanus-Maandag EC, te Riele HP and et al. (1994) Disruption of the mouse mdr1a P-glycoprotein gene leads to a deficiency in the blood-brain barrier and to increased sensitivity to drugs. *Cell* **77:**491-502.

81. Schinkel AH, Wagenaar E, Mol CA and van Deemter L (1996) P-glycoprotein in the blood-brain barrier of mice influences the brain penetration and pharmacological activity of many drugs. *J Clin Invest* **97:**2517-2524.

82. Shen DD, Artru AA and Adkison KK (2004) Principles and applicability of CSF sampling for the assessment of CNS drug delivery and pharmacodynamics. *Adv Drug Deliv Rev* **56:**1825-1857.

83. Smith QR (1996) Brain perfusion systems for studies of drug uptake and metabolism in the central nervous system. *Pharm Biotechnol* **8:**285-307.

84. Sugiyama D, Kusuhara H, Lee YJ and Sugiyama Y (2003) Involvement of multidrug resistance associated protein 1 (Mrp1) in the efflux transport of 17beta estradiol-D-17beta-glucuronide (E217betaG) across the blood-brain barrier. *Pharm Res* **20:**1394-1400.

85. Sun H, Bungay PM and Elmquist WF (2001) Effect of capillary efflux transport inhibition on the determination of probe recovery during in vivo microdialysis in the brain. *J Pharmacol Exp Ther* **297:**991-1000.

86. Takasato Y, Rapoport SI and Smith QR (1984) An in situ brain perfusion technique to study cerebrovascular transport in the rat. *Am J Physiol* **247:**H484-493.

87. Takasawa K, Terasaki T, Suzuki H, Ooie T and Sugiyama Y (1997) Distributed model analysis of 3'-azido-3'-deoxythymidine and 2',3'-dideoxyinosine distribution in brain tissue and cerebrospinal fluid. *J Pharmacol Exp Ther* **282:**1509-1517.

88. Takeda M, Noshiro R, Onozato ML, Tojo A, Hasannejad H, Huang XL, Narikawa S and Endou H (2004) Evidence for a role of human organic anion transporters in the muscular side effects of HMG-CoA reductase inhibitors. *Eur J Pharmacol* **483:**133-138.

89. Taub ME, Podila L, Ely D and Almeida I (2005) Functional assessment of multiple P-glycoprotein (P-gp) probe substrates: Influence of cell line and modulator concentration on P-gp activity. *Drug Metab Dispos*.

90. Tayrouz Y, Ganssmann B, Ding R, Klingmann A, Aderjan R, Burhenne J, Haefeli WE and Mikus G (2001) Ritonavir increases loperamide plasma concentrations without evidence for P-glycoprotein involvement. *Clin Pharmacol Ther* **70:**405-414.

91. Terenius L (1975) Comparison between narcotic "receptors" in the guinea-pig ileum and the rat brain. *Acta Pharmacol Toxicol (Copenh)* **37:**211-221.

92. Thiebaut F, Tsuruo T, Hamada H, Gottesman MM, Pastan I and Willingham MC (1987) Cellular localization of the multidrug-resistance gene product P-glycoprotein in normal human tissues. *Proc Natl Acad Sci U S A* **84:**7735-7738.

93. Thompson SJ, Koszdin K and Bernards CM (2000) Opiate-induced analgesia is increased and prolonged in mice lacking P-glycoprotein. *Anesthesiology* **92:**1392-1399.

94. Troutman MD and Thakker DR (2003a) Efflux ratio cannot assess P-glycoprotein-mediated attenuation of absorptive transport: asymmetric effect of P-glycoprotein on absorptive and secretory transport across Caco-2 cell monolayers. *Pharm Res* **20:**1200-1209.

95. Troutman MD and Thakker DR (2003b) Rhodamine 123 requires carrier-mediated influx for its activity as a P-glycoprotein substrate in Caco-2 cells. *Pharm Res* **20:**1192-1199.

96. Upton RN, Ludbrook GL, Gray EC and Grant C (1997) The cerebral pharmacokinetics of meperidine and alfentanil in conscious sheep. *Anesthesiology* **86:**1317-1325.

97. Visser SA, Wolters FL, Gubbens-Stibbe JM, Tukker E, Van Der Graaf PH, Peletier LA and Danhof M (2003) Mechanism-based pharmacokinetic/pharmacodynamic modeling of the electroencephalogram effects of GABAA receptor modulators: in vitro-in vivo correlations. *J Pharmacol Exp Ther* **304:**88-101.

98. Wandel C, Kim R, Wood M and Wood A (2002) Interaction of morphine, fentanyl, sufentanil, alfentanil, and loperamide with the efflux drug transporter P-glycoprotein. *Anesthesiology* **96:**913-920.

99. Zelcer N, van de Wetering K, Hillebrand M, Sarton E, Kuil A, Wielinga PR, Tephly T, Dahan A, Beijnen JH and Borst P (2005) Mice lacking multidrug resistance protein 3 show altered morphine pharmacokinetics and morphine-6-glucuronide antinociception. *Proc Natl Acad Sci U S A* **102:**7274-7279.

100. Zong J and Pollack GM (2000) Morphine antinociception is enhanced in mdr1a gene-deficient mice. *Pharm Res* **17:**749-753.

Table 1.1 Opioid characteristics

	MW	LogD $pH_{7.4}$ Scifinder	BBB permeability [c]	Potency *in vitro* Ki (nM) [a]	P-gp substrate
alfentanil	416.5	1.5	-	7.1	no*
fentanyl	336.5	2.2	high	1.3	weak
loperamide	477.0	4.1	moderate	1.1 [b]	strong
meperidine	247.3	1.6	high	1160	no
methadone	309.6	2.6	moderate	45	moderate
morphine	287.3	0.42	low	54	weak
sufentanil	386.6	2.5	-	0.088	no*

[a] (Leysen et al., 1983)

[b] (Terenius, 1975)

c (Dagenais et al., 2004); Classified based on *mdr1a*(-/-) *in situ* brain uptake clearances (low < 85; moderate 85 to 170; high >170 $ml \bullet min^{-1} \bullet 100g^{-1}$)

* based on available data at the inception of this dissertation project

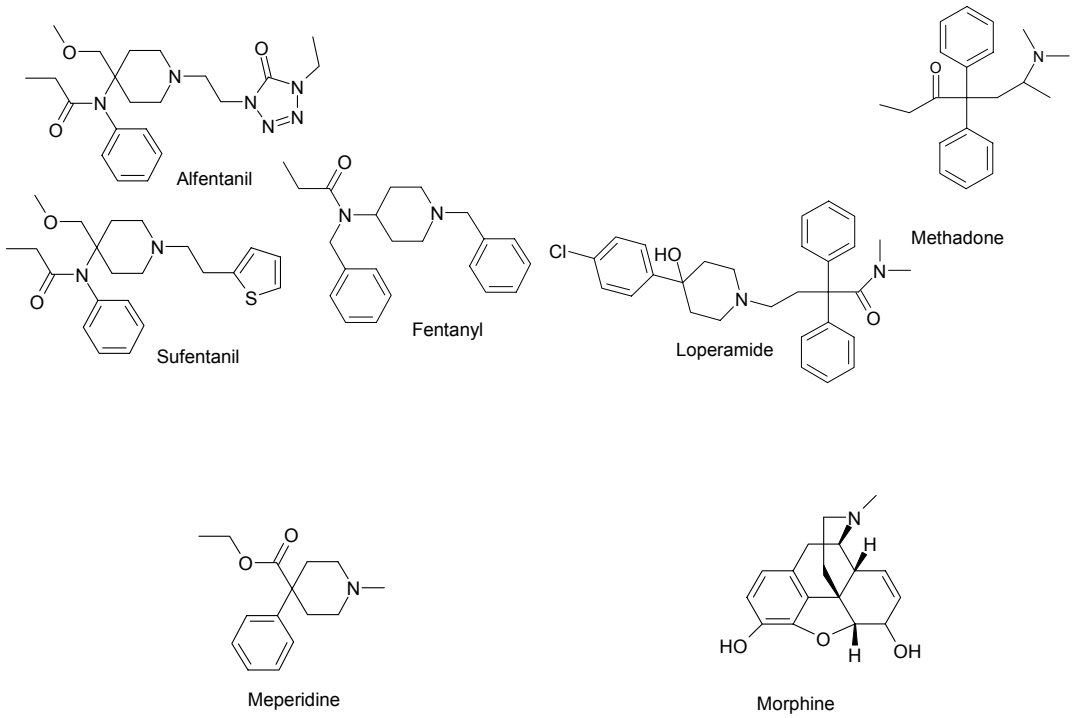

Figure 1.1. Chemical structure of selected *mu* opioid agonists

CHAPTER 2

KINETIC CONSIDERATIONS FOR THE QUANTITATIVE ASSESSMENT OF EFFLUX ACTIVITY AND INHIBITION: IMPLICATIONS FOR UNDERSTANDING AND PREDICTING THE EFFECTS OF EFFLUX INHIBITION

This chapter has been submitted for publication in *Pharmaceutical Research* and is presented in the style of that journal.

Abbreviations:

ϕ_i: degree of efflux inhibition

ER_α: asymmetry efflux ratio ($PS_{B\rightarrow A}/PS_{A\rightarrow B}$) or steady-state ($C_A / C_B$)

ER_A: apical efflux ratio ($PS_{0,B\rightarrow A}/ PS_{B\rightarrow A}$) or steady-state ($C_{A,0} / C_A$)

ER_B: basolateral efflux ratio ($PS_{I,A\rightarrow B} / PS_{A\rightarrow B}$) or steady-state ($C_{B,I} / C_B$)

ER_C: cellular efflux ratio ($PS_{I,A\rightarrow C} / PS_{A\rightarrow C}$) or steady-state ($C_{C,I,} / C_C$)

[I]: inhibitor concentration

IC_{50}: 50% inhibitory concentration

K_i: inhibitor constant

K_m: Michaelis-Menten constant

PS: observed permeability-surface area product

PS_0: permeability-surface area product in the absence of efflux inhibition

PS_I: permeability-surface area product when efflux is completely inhibited or saturated; passive permeability-surface area product

[S]: substrate concentration

Subscripts:

A: apical

B: basolateral

C: cellular

app: apparent

max: maximum

0: absence of efflux inhibition

I: efflux is completely inhibited or saturated

A→B: apical to basolateral; apical compartment dosed

B→A: basolateral to apical; basolateral compartment dosed

A→C: apical to cellular; apical compartment dosed

Abstract

Purpose. Unexpected and complex experimental observations related to efflux transport have been reported in the literature. This work was conducted to develop relationships between efflux activity (PS_{efflux}) as a function of commonly-studied kinetic parameters [permeability-surface area product (PS), efflux ratio (ER), degree of efflux inhibition (ϕ_i), 50% inhibitory concentration (IC_{50}), and Michaelis-Menten constant (K_m)].

Methods. A three-compartment model (apical, cellular, and basolateral) was used to derive flux equations relating the initial rate of flux and steady-state mass transfer in the presence or absence of active efflux. Various definitions of efflux ratio (ER) were examined in terms of permeability-surface area products. The efflux activity (PS_{efflux}) was expressed in terms of ER and PS. The relationships between PS_{efflux} and PS, ER, ϕ_i, IC_{50}, and K_m were solved mathematically. Simulations and examples from the literature were used to illustrate the resulting mathematical relationships.

Results. The relationships derived according to a three-compartment model differed fundamentally from commonly-accepted approaches for determining PS_{efflux}, ϕ_i, IC_{50} and K_m. Based on the model assumptions and mathematical derivations, currently used mathematical relationships erroneously imply that efflux activity is proportional to change in PS (i.e., flux or P_{app}) and thus underestimate PS_{efflux} and ϕ_i, and overestimate IC_{50} and K_m.

Conclusions. An understanding of the relationship between efflux inhibition and kinetic parameters is critical for appropriate data interpretation, standardization in calculating and expressing the influence of efflux transport, and predicting the clinical significance of efflux inhibition.

INTRODUCTION

Xenobiotic efflux transporters such as P-glycoprotein (P-gp) influence drug disposition, efficacy, and safety. Inhibition of efflux transporters may have beneficial (e.g., increased absorption, enhanced presentation to the target site) or adverse (e.g., unexpected or dangerous drug interactions) effects (1). Specific efflux inhibitors are in development to increase oral bioavailability, to target therapeutics to the central nervous system (CNS), and to reverse multidrug resistance (MDR) in cancer (2-4). In addition, drug-drug interactions at the level of efflux transporters have been identified and represent an area of increasing interest (5-7).

Various *in vitro* and *in vivo* models have been developed to identify substrates and inhibitors of efflux transporters and to predict the effects of efflux inhibition on drug disposition and action. These models include cell monolayers (Caco-2 and transfected MDCKII cells), perfused organs (brain, liver, kidney, and intestine), and intact animals (transporter-deficient animals [e.g. mdr1a/b knockout]; co-administration of efflux inhibitors *in vivo*) (8-11). The predictive utility of these models depends on accurate determination of efflux activity (PS_{efflux}), substrate affinity (K_m), inhibitor potency (IC_{50}), and the degree of efflux inhibition (ϕ_i). Unfortunately, the relationships between PS_{efflux} and these other experimental parameters are poorly understood leading to data misinterpretation and inaccurate *in vitro-in vivo* predictions.

Several experimental strategies comprised of different designs and data analysis methods have been used to study apical efflux. Often, observation in one experimental system is used to predict behavior in another system. For example, Caco-2 monolayer flux studies are used to make predictions of intestinal drug absorption in humans. Kinetic, molecular, and

computational models are proposed to provide a better understanding of experimental observations and to make predictions of system behavior. Various types of models with differing degrees of complexity have been proposed for apical efflux (8, 12-14). Even though the models differ in complexity and details, most share some common elements: distinct apical, basolateral, and cellular compartments, with efflux transport located on the apical membrane. A comprehensive understanding of system behavior for the most basic model structure, one that incorporates the fewest assumptions, is an important first step in critically evaluating the kinetic consequences of efflux transport.

In the present work, a simple kinetic model based on the prototypical efflux transporter P-gp was constructed and used to derive the theoretical relationships between PS_{efflux} and experimental parameters (K_m, IC_{50}, and ϕ_i). The resulting mathematical relationships were compared to commonly-accepted approaches for calculating PS_{efflux}, ϕ_i, K_m, and IC_{50}. Kinetic considerations suggest that commonly-used relationships for determining the experimental parameters PS_{efflux}, K_m, and IC_{50} may be confounded by the efflux activity of the model system as well as the choice of substrate.

THEORETICAL

The simplest kinetic model consistent with efflux attenuating initial rate of apical-to-basolateral (A-to-B) flux is a three-compartment system (Figure 2.1) in which PS_A and PS_B represent the passive permeability-surface area product of the apical and basolateral membrane, respectively, and PS_{efflux} represents the permeability-surface area product due to efflux transport. This scheme has been used to represent apical efflux (8, 14) and is capable of representing the *in vitro* and *in vivo* models used to study the impact of efflux transporters (Table 2.1). The kinetic model associated with this scheme can be described by the following set of differential equations:

$$\frac{dX_A}{dt} = C_C(PS_A + PS_{efflux}) - C_A PS_A \quad (1\text{-}1)$$

$$\frac{dX_C}{dt} = C_A PS_A + C_B PS_B - C_C(PS_A + PS_B + PS_{efflux}) \quad (1\text{-}2)$$

$$\frac{dX_B}{dt} = C_C PS_B - C_B PS_B \quad (1\text{-}3)$$

where dX_A/dt, dX_B/dt and dX_C/dt represent the substrate flux into and out of the apical, basolateral, and cellular compartments, respectively; C_A, C_B, and C_C represent substrate concentration in each compartment; PS_A and PS_B represent the passive permeability-surface area product of the apical and basolateral membranes; and PS_{efflux} represents the permeability-surface area product of efflux activity. When substrate concentrations approach or exceed the K_m for the efflux transport protein then:

$$PS_{efflux} = \frac{PS_{efflux,max}}{C_C + K_m} \quad (1\text{-}4)$$

where $PS_{efflux,max}$ equals maximal efflux activity.

Initial Rate of B-to-A Flux in the Presence or Absence of Active Efflux

Assuming initial unidirectional flux into the apical compartment (i.e., X_A=0) and rapid equilibration between the basolateral and cellular compartments ($dX_C/dt = 0$), the flux in the B-to-A direction and the concentration in the cellular compartment (C_C) can be described by equations (2-1) and (2-2), respectively.

$$\frac{dX_A}{dt} = C_C(PS_A + PS_{efflux}) \tag{2-1}$$

$$C_C = \frac{C_B PS_B}{(PS_A + PS_B + PS_{efflux})} \tag{2-2}$$

Substitution of equation (2-2) into equation (2-1) yields the B-to-A flux equation:

$$\frac{dX_{A,B\rightarrow A}}{dt} = \frac{C_B \times PS_B \times (PS_A + PS_{effflux})}{PS_A + PS_B + PS_{efflux}} \tag{2-3}$$

In the absence of efflux ($PS_{efflux} = 0$), the flux in the B-to-A direction is given by:

$$\frac{dX^{w/o\ efflux}_{A,B\rightarrow A}}{dt} = \frac{C_B \times PS_B \times PS_A}{PS_A + PS_B} \tag{2-4}$$

Initial Rate of A-to-B Flux in the Presence or Absence of Active Efflux

Assuming initial unidirectional flux into the basolateral compartment (i.e., X_B=0) and rapid equilibration between the apical and cellular compartments ($dX_C/dt = 0$), the flux in the A-to-B direction and the concentration in the cellular compartment (C_C) can be described by equations (3-1) and (3-2), respectively.

$$\frac{dX_B}{dt} = C_C PS_B \tag{3-1}$$

$$C_C = \frac{C_A PS_A}{(PS_A + PS_B + PS_{efflux})} \tag{3-2}$$

Substitution of equation (3-2) into equation (3-1) yields the A-to-B flux equation:

$$\frac{dX_{B,A\rightarrow B}}{dt} = \frac{C_A \times PS_A \times PS_B}{PS_A + PS_B + PS_{efflux}} \tag{3-3}$$

In the absence of efflux ($PS_{efflux} = 0$), A-to-B flux is given by equation (3-4).

$$\frac{dX^{w/o\ efflux}_{B,A\rightarrow B}}{dt} = \frac{C_A \times PS_A \times PS_B}{PS_A + PS_B} \tag{3-4}$$

Initial Rate of Cellular Influx

Assuming initial unidirectional uptake into the cellular compartment (i.e., $X_C=0$), flux into the cellular compartment (C_C) can be described by equations (4-1) and (4-2) following administration into the apical and basolateral compartments, respectively.

$$\frac{dX_C}{dt} = C_A PS_A \tag{4-1}$$

$$\frac{dX_C}{dt} = C_B PS_B \tag{4-2}$$

Steady-State Concentrations in Compartments A, B, and C

The steady-state substrate concentration in compartments A, B, and C can be determined by solving differential equations (1-1), (1-2), and (1-3) for concentration at infinite time after administration of mass X_0 to the system:

$$C_{A(t=\infty)} = \frac{X_{A(t=\infty)}}{V_A} = \frac{X_0(PS_A + PS_{efflux})}{(PS_{efflux} \times V_A) + PS_A(V_A + V_B + V_C)} \tag{5-1}$$

$$C_{B(t=\infty)} = \frac{X_{B(t=\infty)}}{V_B} = \frac{X_0 \times PS_A}{(PS_{efflux} \times V_A) + PS_A(V_A + V_B + V_C)} \tag{5-2}$$

$$C_{C(t=\infty)} = \frac{X_{C(t=\infty)}}{V_C} = \frac{X_0 \times PS_A}{(PS_{efflux} \times V_A) + PS_A(V_A + V_B + V_C)} \quad (5\text{-}3)$$

In the absence of active efflux, the steady-state concentrations in compartments A, B, and C are equivalent, and may be expressed as:

$$C^{w/o\ efflux}_{(t=\infty)\ (t=\infty)} = \frac{X_0}{(V_A + V_B + V_C)} \quad (5\text{-}4)$$

Definition of Basolateral Efflux Ratio and Efflux Activity

The basolateral efflux ratio (ER_B) can be defined as the ratio of the initial rate of flux in the A-to-B direction when efflux is inhibited completely [eq. (3-4)] divided by the initial rate of flux in the A-to-B direction when efflux is not inhibited [eq. (3-3)]:

$$ER_B = \frac{\frac{dX^{w/o\ efflux}_{B,A\rightarrow B}}{dt}}{\frac{dX_{B,A\rightarrow B}}{dt}} = \frac{PS_A + PS_B + PS_{efflux}}{PS_A + PS_B} \quad (6\text{-}1)$$

Alternatively, ER_B can be defined as the steady-state concentration in the basolateral compartment when efflux is inhibited completely [eq. (5-4)] divided by the steady-state concentration in the basolateral compartment when efflux is not inhibited [eq. (5-2)]:

$$ER_{B(t\rightarrow\infty)} = \frac{C_B^{w/o\ efflux}}{C_B} = 1 + \frac{PS_{efflux} \times V_A}{PS_A(V_A + V_B + V_C)} \quad (6\text{-}2)$$

Efflux activity (PS_{efflux}) can be expressed in terms of ER_B by rearrangement of equations (6-1) and (6-2):

$$PS_{efflux} = (PS_A + PS_B)(ER_B - 1) \quad (6\text{-}3)$$

$$PS_{efflux} = \frac{(V_A + V_B + V_C)}{V_A} PS_A(ER_{B(t\rightarrow\infty)} - 1) \quad (6\text{-}4)$$

Definition of Asymmetry Efflux Ratio and Efflux Activity

Assuming that donor compartment concentrations are identical (C_A=C_B), the asymmetry efflux ratio (ER_α) can be defined as the ratio of the initial rate of flux in the B-to-A direction [eq. (2-3)] divided by the initial rate of flux in the A-to-B direction [eq. (3-3)]:

$$ER_\alpha = \frac{\frac{dX_{A,B\to A}}{dt}}{\frac{dX_{B,A\to B}}{dt}} = \frac{PS_A + PS_{efflux}}{PS_A} \quad (7\text{-}1)$$

Alternatively, ER_α can be defined as the apical steady-state concentration [eq. (5-1)] divided by the steady-state concentration in the basolateral compartment [eq. (5-2)]:

$$ER_{\alpha(t\to\infty)} = \frac{C_A}{C_B} = \frac{PS_A + PS_{efflux}}{PS_A} \quad (7\text{-}2)$$

Efflux activity (PS_{efflux}) then can be solved in terms of ER_α as:

$$PS_{efflux} = PS_A (ER_\alpha - 1) \quad (7\text{-}3)$$

$$PS_{efflux} = PS_A (ER_{\alpha(t\to\infty)} - 1) \quad (7\text{-}4)$$

Definition of Cellular Efflux Ratio and Efflux Activity

The cellular efflux ratio (ER_C) can be defined as the ratio of the initial rate of flux in the A-to-C direction when efflux is inhibited completely [eq. (4-1)] divided by the initial rate of flux in the A-to-C direction when efflux is not inhibited [eq. (4-1)]:

$$ER_C = \frac{\frac{dX^{w/o\ efflux}_{C,A\to C}}{dt}}{\frac{dX_{C,A\to C}}{dt}} = 1 \quad (8\text{-}1)$$

Alternatively, ER_C can be defined as the steady-state concentration in the cellular compartment when efflux is inhibited completely [eq. (5-4)] divided by the steady-state concentration in the cellular compartment when efflux is not inhibited [eq. (5-3)]:

$$ER_{C(t\to\infty)} = \frac{C_C^{\text{w/o efflux}}}{C_C} = 1 + \frac{PS_{efflux} \times V_A}{PS_A(V_A + V_B + V_C)} \tag{8-2}$$

Efflux activity (PS_{efflux}) can be expressed in terms of ER_C as:

$$PS_{efflux} = \frac{(V_A + V_B + V_C)}{V_A} PS_A(ER_{C(t\to\infty)} - 1) \tag{8-3}$$

Definition of Apical Efflux Ratio and Efflux Activity

The apical efflux ratio (ER_A) can be defined as the ratio of the initial rate of flux in the B-to-A direction when efflux is not inhibited [eq. (2-3)] divided by the initial rate of flux in the B-to-A direction when efflux is inhibited completely [eq. (2-4)]:

$$ER_A = \frac{\frac{dX_{A,B\to A}}{dt}}{\frac{dX_{A,B\to A}^{\text{w/o efflux}}}{dt}} = \frac{(PS_A + PS_B)(PS_A + PS_{efflux})}{PS_A(PS_A + PS_B + PS_{efflux})} \le \frac{(PS_A + PS_B)}{PS_A} \tag{9-1}$$

Alternatively, ER_A can be defined as the steady-state concentration in the apical compartment when efflux is not inhibited [eq. (5-1)] divided by the observed steady-state concentration in the apical compartment when efflux is inhibited completely [eq. (5-4)]:

$$ER_{A(t\to\infty)} = \frac{C_A}{C_A^{\text{w/o efflux}}} = \frac{(PS_A + PS_{efflux})(V_A + V_B + V_C)}{(PS_{efflux} \times V_A) + PS_A(V_A + V_B + V_C)} \le \frac{V_A + V_B + V_C}{V_A} \tag{9-2}$$

Efflux activity (PS_{efflux}) then can be expressed in terms of ER_A as:

$$PS_{efflux} = \frac{(PS_A + PS_B)PS_A(ER_A - 1)}{(PS_A + PS_B) - (PS_A \times ER_A)} \tag{9-3}$$

$$PS_{efflux} = \frac{(V_A + V_B + V_C)PS_A(ER_A - 1)}{(V_A + V_B + V_C) - (V_A \times ER_A)} \quad (9\text{-}4)$$

RESULTS AND DISCUSSION

Efflux activity is proportional to the quantity ER-1, not to attenuation or enhancement of flux

The mathematical relationships derived from the three-compartment model in figure 2.1, indicate that efflux attenuates flux in the A-to-B direction and enhances flux in the B-to-A direction. However, neither the attenuation of flux in the A-to-B nor the enhancement of flux in the B-to-A direction is proportional to the efflux activity (PS_{efflux}) [eq. (2-3) and (3-3); illustrated in Figure 2.3]. In contrast, according to the three-compartment model, [Table 2.2; illustrated in Figure 2.4; and eq. (6-3), (6-4), (7-3), (7-4), and (8-3)], PS_{efflux} is proportional to the ER_B-1, ER_α-1, and ER_C-1. The fact that PS_{efflux} is not proportional to flux but is proportional to ER_B-1, ER_α-1, and $ER_{C(t\infty)}$-1 has important implications regarding the calculation of PS_{efflux}, K_m, and IC_{50}.

Numerous approaches with little consensus have been proposed to calculate and express PS_{efflux} (Table 2.3). Often, PS_{efflux} is calculated directly from the magnitude of attenuation or enhancement in flux caused by efflux. Since the magnitude of attenuation and enhancement in flux is not proportional to PS_{efflux}, and therefore should not be used to calculate PS_{efflux} directly, we propose a novel method, consistent with the three-compartment model in figure 2.1, for calculating and expressing PS_{efflux}.

From previous mathematical derivations, PS_{efflux} can be defined in terms of PS_A, PS_B, and efflux ratios (Table 2.2), and is proportional to ER_α-1, ER_B-1, and $ER_{C(t\rightarrow\infty)}$-1 (Table 2.2; illustrated in Figure 2.4). However, in most experimental designs, PS_A and PS_B are not

determined, but the passive permeability-surface area product in the A-to-B direction ($PS_{I,A\rightarrow B}$) is measured. The $PS_{I,A\rightarrow B}$ can be expressed in terms of PS_A and PS_B as follows:

$$PS_{I,A\rightarrow B} = \frac{PS_A \times PS_B}{PS_A + PS_B} \qquad (10\text{-}1)$$

If PS_A and PS_B are assumed to be equal, rearrangement of equation (10-1) indicates that PS_A and PS_B equal $2PS_{I,A\rightarrow B}$. PS_{efflux} can be expressed in terms of $PS_{I,A\rightarrow B}$ and ER by substituting $2PS_{I,A\rightarrow B}$ for PS_A and PS_B into equations (6-3), (7-3), and (8-3), yielding equations (10-2), (10-3), and (10-4) respectively:

$$PS_{efflux} = 4PS_{I,A\rightarrow B}(ER_B - 1) \qquad (10\text{-}2)$$

$$PS_{efflux} = 2PS_{I,A\rightarrow B}(ER_\alpha - 1) \qquad (10\text{-}3)$$

$$PS_{efflux} = 2PS_{I,A\rightarrow B}\frac{(V_A + V_B + V_C)}{V_A}(ER_{C(t\rightarrow\infty)} - 1) \qquad (10\text{-}4)$$

From the preceding equations, the exact value of PS_{efflux} can be calculated from commonly-obtained experimental parameters, namely efflux ratio and passive permeability. In qualitative terms, PS_{efflux} is proportional to the product of (ER-1) and passive permeability. This relationship differs from other commonly-cited approaches for expressing PS_{efflux}; however, it is kinetically sound (based on the inherent assumptions of the model in Figure 2.1), and it is intuitive in that the efflux ratio of a substrate is dependent on both efflux activity and the substrate passive permeability. Expressing PS_{efflux} in terms of $PS_{I,A\rightarrow B}$ and ER also is convenient, and allows for precise quantitation and comparison of PS_{efflux} between different substrates, model systems, and laboratories.

As in the case for PS_{efflux}, flux should not be used to directly calculate K_m or IC_{50}. This is true, because, when determining K_m or IC_{50} it is necessary to relate substrate or inhibitor concentrations to the value PS_{efflux} and because flux is not proportional to PS_{efflux}. Instead of

using flux, K_m and IC_{50} may be calculated directly from the change in ER_α-1, ER_B-1, or $ER_{C(t\rightarrow\infty)}$-1 since ER-1 is proportional to PS_{efflux}. The difference between calculating IC_{50} directly from the change in P_{app} versus ER-1 can be illustrated with a recent example from the literature. Although numerous relevant data sets can be found in the literature, a data set from Chen et. al. (2002) was chosen due to the high quality of the data and the extensive characterization of the Michaelis-Menten profile (Figure 2.2) (15). The conclusions drawn from consideration of this experimental data set are generalizable to other situations. Briefly, the investigators used an *in situ* rat brain perfusion technique to examine the ability of the P-gp inhibitor GF-120918 to inhibit the P-gp-mediated efflux of quinidine. Various concentrations of GF-120918 were examined; as concentrations of GF-120918 were increased, the P_{app} value for quinidine increased to a plateau of ~13-fold. In such experiments, the $IC_{50,app}$ of the inhibitor often is calculated by fitting a modified Michaelis-Menten equation to the P_{app} vs. inhibitor concentration data. In order to illustrate why $IC_{50,app}$ should not be calculated in this manner, we used a modified Michaelis-Menten equation to calculate both the $IC_{50,app}$ (from the P_{app} and GF-120918 concentration data) and the "true" IC_{50} (from ER and GF-120918 data). Even though the same experimental data were used in calculating $IC_{50,app}$ and $IC_{50,}$ the $IC_{50,app}$ (0.56 μM) was 13-fold higher than the IC_{50} (0.042 μM). It is clear that the $IC_{50,app}$ calculated from P_{app} data differs fundamentally from the IC_{50} calculated from ER data. Since changes in P_{app} are not proportional to changes in PS_{efflux}, IC_{50} and K_m should not be calculated by fitting a modified Michaelis-Menten equation to P_{app} data. Mathematical treatment of IC_{50} and K_m will be explored in further detail in a later section; at this point, we simply demonstrate that calculating IC_{50} or K_m from flux or P_{app} values is not equivalent to calculations based on ER values.

B-to-A flux (secretory flux) is minimally sensitive to efflux activity

Apical efflux clearly enhances flux in the B-to-A direction. However, this enhancement is not proportional to either efflux activity (PS_{efflux}) or ER_A-1 [eq. (2-3) and (9-1); (illustrated in Figures 3 and 4)]. The fold increase in the B-to-A flux is given by the ER_A in equation (9-1):

$$ER_A = \frac{\frac{dX_{A,B\rightarrow A}}{dt}}{\frac{dX_{A,B\rightarrow A}}{dt}^{w/o\ efflux}} = \frac{(PS_A + PS_B)(PS_A + PS_{efflux})}{PS_A(PS_A + PS_B + PS_{efflux})} \leq \frac{(PS_A + PS_B)}{PS_A} \qquad (9\text{-}1)$$

Taking into account the model assumptions discussed previously, the maximum value of ER_A is $(PS_A + PS_B) / PS_A$ (i.e., 2, assuming $PS_A = PS_B$). In other words, if passive permeabilities across the apical and basolateral membranes are similar, then the maximum increase in B-to-A flux that efflux can cause is 2-fold. Therefore, measuring the effect of efflux on permeability in the B-to-A direction is uninformative, as flux in the B-to-A direction is not proportional to, and is in fact minimally sensitive to PS_{efflux}.

Experimental evidence is consistent with this predicted behavior. For example, the B-to-A flux of loperamide, amprenavir, and eletriptan in MDR1-transfected MDCK cell monolayers increased only 1.5- to 2.1-fold despite a 10-, 29-, and 45-fold decrease in A-to-B flux, respectively (16). Another experimental observation consistent with a maximum 2-fold increase in B-to-A flux is the influence of P-gp-mediated efflux on the equilibration half-life of the fentanyl, alfentanil, methadone, loperamide across the blood-brain barrier (BBB). These opioids were used as *in vivo* probes in P-gp-competent and P-gp-deficient mice to assess the influence of P-gp-mediated efflux on brain-to-plasma ratio ($K_{p,brain}$) and the pseudo-first-order rate constant governing the time-dependent approach of the brain-to-

plasma ratio to its equilibrium value ($K_{eq,brain}$). Based on the principle that $K_{eq,brain}$ is influenced only by the rate of egress from the brain, $K_{eq,brain}$ should be directly proportional to $PS_{B\rightarrow A}$. Thus, the fold change in $K_{eq,brain}$ can be expressed in terms of ER_A. In contrast, the fold change in brain-to-plasma ratio can be expressed in terms ER_{α}. So by studying the effect of P-gp-mediated efflux on $K_{p,brain}$ and $K_{eq,brain}$, the influence of efflux on the ER_{α} and ER_A can be deduced *in vivo*. P-gp-mediated efflux had a more pronounced effect on the brain-to-plasma ratio (1.9- to 44-fold change) than on the brain equilibration half-life (1.0- to 2.4-fold change). Without examining the experimental observations in terms of ER_A and ER_{α}, the experimental observations in $K_{eq,brain}$ may be difficult to rationalize. However, the results are precisely what would be expected based on the model and associated assumptions (Table 2.4).

Despite these kinetic considerations, for some substrates apical efflux transporters have been reported to increase flux in the B-to-A direction by more than 2-fold. For example, in Caco-2 monolayers the efflux transporter P-gp had a pronounced effect (10-fold) on the B-to-A flux of rhodamine 123, even though P-gp efflux minimally attenuated rhodamine 123 flux in the A-to-B direction (17). In the same Caco-2 studies, rhodamine 123 had low membrane permeability, with A-to-B flux occurring primarily by the paracellular route. However, the B-to-A flux was much higher than the A-to-B flux, and it occurred via the transcellular route, because rhodamine 123 was transported across the basolateral membrane by active uptake. Active uptake of rhodamine 123 across the basolateral membrane violates the assumptions of the basic kinetic model ($PS_{B,inf} \neq PS_{B,eff}$). Therefore, efflux has a more pronounced effect on B-to-A flux than the kinetic scheme would suggest. This phenomenon has been observed for other efflux substrates transported by multiple proteins, such as fexofenadine and digoxin

(18, 19). In cases in which active transport processes are present in addition to efflux, estimates of kinetic efflux parameters (IC_{50}, K_m, or PS_{efflux}) may be confounded by the action of the other transport process(es). Experimental determination of efflux transporter kinetic parameters is difficult when flux is influenced by multiple systems (i.e., active uptake and efflux), because inhibitors often are non-selective and the K_m(s) of additional active process(es) may be less than that of the efflux transporter.

Asymmetry and basolateral efflux ratios are not identical

The basolateral and asymmetry efflux ratios (ER_B and ER_α) are used to characterize the influence of efflux on a given model system and to extrapolate observations from one model system to another (i.e., *in vitro* to *in vivo* predictions). Thus, it is important to understand the relationship between ER_B and ER_α, which may be best understood by examining the relationship between ER_α-1 and ER_B-1 from rearrangement of equations (7-3) and (6-3):

$$ER_\alpha - 1 = \left(\frac{PS_A + PS_{efflux}}{PS_A}\right) - 1 \qquad (11\text{-}1)$$

$$ER_B - 1 = \left(\frac{PS_A + PS_B + PS_{efflux}}{PS_A + PS_B}\right) - 1 \qquad (11\text{-}2)$$

If PS_A=PS_B, then the ratio of ER_α-1 and ER_B-1 equals 2 as shown in equation (11-3).

$$\frac{ER_\alpha - 1}{ER_B - 1} = \frac{\left(\frac{PS_A + PS_{efflux}}{PS_A}\right) - 1}{\left(\frac{PS_A + PS_B + PS_{efflux}}{PS_A + PS_B}\right) - 1} = 2 \qquad (11\text{-}3)$$

Equation (11-3) illustrates that ER_α is larger than ER_B and that when PS_{efflux} is large compared to PS_A, ER_α will equal twice ER_B.

The fact that $ER_\alpha > ER_B$ may explain why the P-gp efflux ratio determined by *in situ* brain perfusion under-predicts the *in vivo* brain-to-plasma efflux ratio. Several studies have examined the influence of P-gp on brain uptake of P-gp substrates, and developed relationships for the difference in brain uptake clearance (Cl_{up}) and brain-to-plasma ratio ($K_{p,brain}$) between P-gp-deficient and P-gp-competent mice. The *in situ* P-gp efflux ratio (9), which is analogous to ER_B and is determined by dividing Cl_{up} in P-gp-deficient mice ($Cl_{up}^{-/-}$) by the brain uptake clearance in P-gp-competent mice ($Cl_{up}^{+/+}$), has been used to predict the *in vivo* P-gp efflux ratio, which is calculated by dividing the $K_{p,brain}$ in P-gp-deficient mice ($K_{p,brain}^{-/-}$) by the $K_{p,brain}$ in P-gp-competent mice ($K_{p,brain}^{+/+}$). In most studies, the *in situ* efflux ratio correlated well with the *in vivo* efflux ratio, although the *in situ* efflux ratio consistently under-predicted the *in vivo* efflux ratio [Figure 2.5; data from references (9, 11, 20, 21) and unpublished observations]. This under-prediction is expected since the *in situ* P-gp efflux ratio is analogous to ER_B and the *in vivo* efflux ratio is analogous to ER_α. Direct predictions can be made by comparing the *in situ* efflux ratio minus one to the *in vivo* efflux ratio minus one. The *in situ* efflux ratio minus one is expected to equal one-half the *in vivo* efflux ratio minus one. When the *in situ* and *in vivo* efflux ratios are compared in this manner, the *in situ* efflux ratio no longer under-predicts the *in vivo* efflux ratio (Figure 2.5).

Apparent IC_{50} and K_m are influenced by efflux activity

The efflux activity (PS_{efflux}) in the presence of efflux inhibition can be expressed as in equation (12-1), where $PS_{efflux,max}$ is the efflux activity in the absence of inhibition, and ϕ_i is the degree of efflux inhibition:

$$PS_{efflux} = PS_{efflux,max} \times (1 - \phi_i) \qquad (12\text{-}1)$$

As derived previously, the efflux activity (PS_{efflux}) is proportional to ER_{α}-1, ER_B-1 and $ER_{C(t\rightarrow\infty)}$-1. When ER-1 and ER_{max}-1 are substituted for PS_{efflux} and $PS_{efflux,max}$ respectively, then equation (12-1) can be rewritten as follows:

$$ER - 1 = (ER_{max} - 1) \times (1 - \phi_i) \tag{12-2}$$

Solving equation (12-2) for ϕ_i yields:

$$\phi_i = \frac{ER_{max} - ER}{ER_{max} - 1} \tag{12-3}$$

From this point forward, the symbol PS will represent any experimental variable that is attenuated by efflux in a manner consistent with the model in Figure 2.1, such as $PS_{A\rightarrow B}$ (i.e., P_{app} or A-to-B flux), cellular partition ratio, or brain-to-plasma ratio. The efflux ratio (ER) can be defined as (PS_I/PS), where PS_I is the value of PS when efflux is inhibited completely and PS is the observed value of PS. When efflux activity is completely inhibited, ER equals unity. In the absence of any efflux inhibition, ER equals $ER_{max,}$ defined as (PS_I/PS_0), where PS_0 is the value of PS in the absence of efflux inhibition. Equation (12-3) can be expressed in terms of PS by substituting (PS_I/PS_0) and (PS_I/PS), for ER_{max} and ER.

$$\phi_i = \frac{PS_I}{PS} \times \frac{(PS - PS_0)}{(PS_I - PS_0)} \tag{12-4}$$

Equation (12-5) represents the standard equation used to calculate ϕ_i in the literature and it differs from equation (12-4) by a factor of PS_I/PS.

$$\phi_{i,app} = \frac{PS - PS_0}{PS_I - PS_0} \tag{12-5}$$

This difference between the kinetically derived equation (12-4) and equation (12-5) has a profound impact on calculating IC_{50}, K_m, and understanding the relationship between PS and ϕ_i (see 2.3). Use of equation (12-5) does not yield true kinetic parameters for the system, but

rather apparent parameters. This can be illustrated by solving equations (12-4) and (12-5) for PS, yielding equations (12-6) and (12-7), respectively:

$$PS = \frac{PS_I \times PS_0}{PS_I + (PS_0 - PS_I) \times \phi_i} \quad (12\text{-}6)$$

$$PS = PS_0 + (PS_I - PS_0) \times \phi_{i,app} \quad (12\text{-}7)$$

Examination of equation (12-7) reveals that the maximum increase in PS due to inhibition is PS_I-PS_0; when $\phi_{i,app}$ equals 50%, the increase in PS equals one-half the maximum possible increase (i.e., the change in PS is directly proportional to $\phi_{i,app}$).

The actual fold change in PS due to efflux inhibition may be expressed in terms of efflux ratios or permeability-surface area products:

$$\text{fold}\,\Delta\,PS = \frac{PS}{PS_0} = \frac{PS_I/PS_0}{PS_I/PS} = \frac{ER_{max}}{ER} \quad (12\text{-}8)$$

Solving equation (12-3) for ER and substituting into equation (12-8) yields:

$$\text{fold}\,\Delta\,PS = \frac{ER_{max}}{ER_{max} - (ER_{max} - 1) \times \phi_i} \quad (12\text{-}9)$$

Assuming $\phi_i = \frac{[I]}{[I] + IC_{50}}$, the maximum fold change in PS at any inhibitor concentration ([I]) is determined by the upper limits of equation (12-9):

$$\frac{[I]}{IC_{50}} + 1 \geq \text{fold}\,\Delta\,PS \leq ER_{max} \quad (12\text{-}10)$$

According to the theoretically-derived equation (12-10), at 50% inhibition ([I] = IC_{50}) the maximum increase in PS is 2-fold. This is contrary to the relationship in equation (12-7). However, it is analogous to the case in which 50% inhibition of a specific clearance pathway (i.e., CYP3A4) will result in at most a 2-fold increase in steady-state concentrations (22).

The difference between the theoretically-derived equation (12-6) and the simple equation (12-7) can be illustrated further by comparing estimates of IC_{50} and K_m obtained from the two equations. The non-linear relationships between PS and IC_{50} derived from the kinetic model in Figure 2.1 can be expressed as in equation (12-11). Similarly, the relationship between PS and K_m can be expressed as in equation (12-12):

$$PS = \frac{PS_I \times PS_0}{PS_I + (PS_0 - PS_I) \times \frac{[I]}{[I] + IC_{50}}} \tag{12-11}$$

$$PS = \frac{PS_I \times PS_0}{PS_I + (PS_0 - PS_I) \times \frac{[S]}{[S] + K_m}} \tag{12-12}$$

Using the relationship in equation (12-7), PS can be expressed in terms of $IC_{50,app}$ or $K_{m,app}$ by substituting $\{[I]/([I]+IC_{50,app})\}$ or $\{[S]/([S]+K_{m,app})\}$ for $\phi_{i,app}$:

$$PS = PS_0 + (PS_I - PS_0) \times \frac{[I]}{[I] + IC_{50,app}} \tag{12-13}$$

$$PS = PS_0 + (PS_I - PS_0) \times \frac{[S]}{[S] + K_{m,app}} \tag{12-14}$$

Differences in $IC_{50,app}$ and $K_{m,app}$ calculated by standard equations in current use vs. those suggested herein can be illustrated by substituting PS from equation (12-11) into equation (12-13) and solving for $IC_{50,app}$ and by substituting PS from equation (12-12) into equation (12-14) and solving for $K_{m,app}$:

$$IC_{50,app} = IC_{50} \times \frac{PS_I}{PS_0} = IC_{50} \times ER_{max} \tag{12-15}$$

$$K_{m,app} = K_m \times \frac{PS_I}{PS_0} = K_m \times ER_{max} \tag{12-16}$$

As can be seen from equations (12-15) and (12-16), current methods used for calculating $K_{m,app}$ or $IC_{50,app}$ will result in over-estimation of these parameters by a factor of ER_{max} (Figure 2.2).

This over-estimation poses a number of potential problems. The ER_{max} for a given model system is dependent on both the efflux activity of the system and the test substrate. When ER_{max} is small, the relative error in $K_{m,app}$ or $IC_{50,app}$ calculated from current methods will be small. However, model systems with high efflux activity and substrates with large ER_{max} are precisely the model systems and substrates that are most sensitive for identifying efflux substrates and inhibitors. The $IC_{50,app}$ of inhibitors should be properly ranked-ordered if testing is conducted with a common probe substrate and in a model system with a consistent efflux activity. However, when inhibitors are tested against dissimilar substrates and in different model systems expressing different efflux activity, then $IC_{50,app}$ and rank ordering of $IC_{50,app}$ may not correspond to the real IC_{50} or even the actual rank order. Lastly, the $IC_{50,app}$ of the same inhibitor will differ between different substrates if the substrates have different ER_{max}. This behavior may confound results or be attributed incorrectly to inhibition at different binding sites on the efflux transporter for different substrates.

The case that $K_{m,app}$ is affected by ER_{max} can be demonstrated by a recently reported study. In the study, which examined the flux of taurocholate through MDCK cell monolayers transfected with apical sodium-dependent bile acid transporter (hASBT), the $K_{m,app}$ of taurocholate increased as a function of hASBT expression. This unexpected and novel observation was attributed to aqueous boundary layer effects (23). Alternatively, since transporter expression and PS_{efflux} are proportional, the observation also is entirely consistent with the expected relationship between $K_{m,app}$ and transporter expression [equation (12-16)].

If the K_m had been calculated in a manner consistent with the kinetic model in figure 2.1 [equation (12-12)], it is likely that that the "true" K_m would have been independent of hASBT expression.

Inhibiting active efflux to reverse MDR or increase drug brain penetration

Arbitrarily, reversal of multidrug resistance (MDR) can be defined as less than a 2-fold difference in intracellular drug concentrations between naïve cells and MDR cells. The change in PS necessary to reverse MDR then can be defined accordingly by:

$$\text{fold}\,\Delta\,\text{PS} \geq \frac{\text{ER}_{\max}}{2} \qquad (13\text{-}1)$$

From equations (13-1) and (12-9), the degree of inhibition required to reverse MDR can be expressed as:

$$\phi_i \geq \frac{\text{ER}_{\max} - 2}{\text{ER}_{\max} - 1} \qquad (13\text{-}2)$$

The degree of efflux inhibition needed to reverse MDR therefore is dependent on ER_{max}. The higher the degree of MDR resistance, the higher the requisite degree of inhibition needed to reverse MDR. The inhibitor concentration necessary to reverse MDR can be determined by solving equation (13-2) for [I], assuming $\phi_i = \frac{[I]}{[I] + K_i}$.

$$[I] \geq (\text{ER}_{\max} - 2)K_i \qquad (13\text{-}3)$$

In equations (13-2) or (13-3), all positive values ϕ_i or [I] indicate the degree of inhibition or the inhibitor concentration necessary to inhibit efflux such that there is less than a two-fold difference in drug resistance between MDR cells and naïve cell lines.

The degree of efflux inhibition necessary to reverse multidrug resistance is not simply a function of inhibitor K_i but is also dependent on ER_{max}. As cells become more resistant due to higher expression of the efflux transporter, the ER_{max} will increase, which will necessitate greater inhibition and consequently higher inhibitor concentrations to reverse MDR. Treatment with an efflux inhibitor will not reverse MDR in all cells equally, and will be less effective in cells possessing the highest degree of MDR. This, in turn, will result in tumors becoming more resistant because the most resistant cells will have a survival advantage. The relationships in equations (13-2) and (13-3) are also applicable to reversing efflux at the blood-brain barrier in order to increase drug delivery of efflux substrates to the brain; substrates with larger values of ER_{max} will require a higher degree of efflux inhibition and higher inhibitor concentrations to overcome efflux.

A relevant case study to illustrate this point comes from a clinical study in which the specific P-gp inhibitor tariquadar was shown to completely inhibit P-gp in T-lymphocytes (using the fluorescent dye $DiOC_2(3)$ as a probe), but was ineffective at inhibiting P-gp at the BBB (using the opioid loperamide as a probe) (24). On first consideration, such observations may seem unexpected, and therefore lead to complex hypotheses to rectify apparently anomalous results. However, these observations are not, in fact, inconsistent. The ER_{max} of DiOC2(3) in T-lymphocytes is ~4, while the ER_{max} of loperamide at the BBB has been estimated in preclinical experiments to be ~65 (25, 26). Based on equations (13-2 and 13-3) and the difference in ER_{max} between DiOC2(3) and loperamide, it is not surprising that complete inhibition of P-gp was observed in T-lymphocytes but not at the BBB.

CONCLUSION

A set of equations, based on a simple three-compartment model, was derived to describe the theoretical relationships between PS_{efflux} and PS, ER, ϕ_i, IC_{50}, and K_m. The resulting relationships show that current mathematical treatment of efflux data is inconsistent with this model. In particular, these relationships mistakenly assume that PS_{efflux} is proportional to the attenuation or enhancement in PS, and that 50% inhibition of efflux activity will result in 50% of the maximum possible change in PS. The theoretical relationships derived herein indicate that such an assumption will lead to an overestimate of ϕ_i, K_m and IC_{50} in proportion to the ER_{max} of the experimental system. These relationships also show that PS_{efflux} is proportional to the passive permeability multiplied by (ER-1), and that 50% inhibition of efflux activity will result in at most a 2-fold increase in PS. In addition, apical efflux has a minimum impact on the B-to-A flux ($\leq$ 2-fold) and consequently B-to-A efflux studies are insensitive approaches for estimating efflux kinetic parameters. Finally, the three-compartment model and kinetic considerations indicate that a larger degree of efflux inhibition is necessary to reverse the effects of efflux when the efflux ratio is large. Viewing efflux activity in terms of efflux ratios rather than change in PS allows for better conceptual understanding and more accurate estimation of kinetic parameters; therefore, it is recommended that efflux ratio be calculated and used when evaluating efflux activity and estimating the degree of efflux inhibition, IC_{50}, or K_m.

REFERENCES

1. C. J. Matheny, M. W. Lamb, K. R. Brouwer, and G. M. Pollack. Pharmacokinetic and pharmacodynamic implications of P-glycoprotein modulation. *Pharmacotherapy* **21**: 778-96 (2001).

2. C. M. Kruijtzer, J. H. Beijnen, H. Rosing, W. W. ten Bokkel Huinink, M. Schot, R. C. Jewell, E. M. Paul, and J. H. Schellens. Increased oral bioavailability of topotecan in combination with the breast cancer resistance protein and P-glycoprotein inhibitor GF120918. *J Clin Oncol* **20**: 2943-50 (2002).

3. H. Thomasand H. M. Coley. Overcoming multidrug resistance in cancer: an update on the clinical strategy of inhibiting p-glycoprotein. *Cancer Control* **10**: 159-65 (2003).

4. E. M. Kemper, C. Cleypool, W. Boogerd, J. H. Beijnen, and O. van Tellingen. The influence of the P-glycoprotein inhibitor zosuquidar trihydrochloride (LY335979) on the brain penetration of paclitaxel in mice. *Cancer Chemother Pharmacol* **53**: 173-8 (2004).

5. R. H. Hoand R. B. Kim. Transporters and drug therapy: implications for drug disposition and disease. *Clin Pharmacol Ther* **78**: 260-77 (2005).

6. J. H. Lin. Drug-drug interaction mediated by inhibition and induction of P-glycoprotein. *Adv Drug Deliv Rev* **55**: 53-81 (2003).

7. A. J. Sadeque, C. Wandel, H. He, S. Shah, and A. J. Wood. Increased drug delivery to the brain by P-glycoprotein inhibition. *Clin Pharmacol Ther* **68**: 231-7 (2000).

8. Y. Adachi, H. Suzuki, and Y. Sugiyama. Comparative studies on in vitro methods for evaluating in vivo function of MDR1 P-glycoprotein. *Pharm Res* **18**: 1660-8 (2001).

9. C. Dagenais, J. Zong, J. Ducharme, and G. M. Pollack. Effect of mdr1a P-glycoprotein gene disruption, gender, and substrate concentration on brain uptake of selected compounds. *Pharm Res* **18**: 957-63 (2001).

10. C. Chen, X. Liu, and B. J. Smith. Utility of Mdr1-gene deficient mice in assessing the impact of P-glyco-protein on pharmacokinetics and pharmacodynamics in drug discovery and development. *Curr Drug Metab* **4**: 272-91 (2003).

11. M. Yamazaki, W. E. Neway, T. Ohe, I. Chen, J. F. Rowe, J. H. Hochman, M. Chiba, and J. H. Lin. In vitro substrate identification studies for p-glycoprotein-mediated transport: species difference and predictability of in vivo results. *J Pharmacol Exp Ther* **296**: 723-35 (2001).

12. T. T. Tran, A. Mittal, T. Aldinger, J. W. Polli, A. Ayrton, H. Ellens, and J. Bentz. The elementary mass action rate constants of P-gp transport for a confluent monolayer of MDCKII-hMDR1 cells. *Biophys J* **88**: 715-38 (2005).

13. J. Bentz, T. T. Tran, J. W. Polli, A. Ayrton, and H. Ellens. The steady-state Michaelis-Menten analysis of P-glycoprotein mediated transport through a confluent cell monolayer cannot predict the correct Michaelis constant Km. *Pharm Res* **22**: 1667-77 (2005).

14. H. Kwon, R. A. Lionberger, and L. X. Yu. Impact of P-glycoprotein-mediated intestinal efflux kinetics on oral bioavailability of P-glycoprotein substrates. *Mol Pharm* **1**: 455-65 (2004).

15. W. Chen, J. Z. Yang, R. Andersen, L. H. Nielsen, and R. T. Borchardt. Evaluation of the permeation characteristics of a model opioid peptide, H-Tyr-D-Ala-Gly-Phe-D-Leu-OH (DADLE), and its cyclic prodrugs across the blood-brain barrier using an in situ perfused rat brain model. *J Pharmacol Exp Ther* **303**: 849-57 (2002).

16. K. M. Mahar Doan, J. E. Humphreys, L. O. Webster, S. A. Wring, L. J. Shampine, C. J. Serabjit-Singh, K. K. Adkison, and J. W. Polli. Passive permeability and P-glycoprotein-mediated efflux differentiate central nervous system (CNS) and non-CNS marketed drugs. *J Pharmacol Exp Ther* **303**: 1029-37 (2002).

17. M. D. Troutmanand D. R. Thakker. Rhodamine 123 requires carrier-mediated influx for its activity as a P-glycoprotein substrate in Caco-2 cells. *Pharm Res* **20**: 1192-9 (2003).

18. N. Petri, C. Tannergren, D. Rungstad, and H. Lennernas. Transport characteristics of fexofenadine in the Caco-2 cell model. *Pharm Res* **21**: 1398-404 (2004).

19. M. E. Taub, L. Podila, D. Ely, and I. Almeida. Functional assessment of multiple P-glycoprotein (P-gp) probe substrates: Influence of cell line and modulator concentration on P-gp activity. *Drug Metab Dispos* (2005).

20. C. Dagenais, C. L. Graff, and G. M. Pollack. Variable modulation of opioid brain uptake by P-glycoprotein in mice. *Biochem Pharmacol* **67**: 269-76 (2004).

21. H. Kusuharaand Y. Sugiyama. Efflux transport systems for drugs at the blood-brain barrier and blood-cerebrospinal fluid barrier (Part 2). *Drug Discov Today* **6**: 206-212 (2001).

22. M. Rowlandand S. B. Matin. Kinetics of drug-drug interactions. *J Pharmacokinet Biopharm* **1**: 553-567 (1973).

23. A. Balakrishnamand J. E. Polli. Bias in estimation of transporter kinetic parameters: Interplay of transporter expression level and substrate affinity. *J Clin Pharmacol* **45**: 1087 (2005).

24. M. Muszkat, D. Kurnik, G. G. Sofowora, J. P. Donahue, G. R. Wilkinson, and A. J. Wood. Tariquidar (TAR, XR-9576) selectively inhibits P-glycoprotein (P-GP) in T-lymphocytes compared to that in the blood-brain barrier (BBB). *Clinical Pharmacology & Therapeutics* **77**: P39-P39 (2005).

25. T. Hulgan, J. P. Donahue, C. Hawkins, D. Unutmaz, R. T. D'Aquila, S. Raffanti, F. Nicotera, P. Rebeiro, H. Erdem, M. Rueff, and D. W. Haas. Implications of T-cell P-glycoprotein activity during HIV-1 infection and its therapy. *J Acquir Immune Defic Syndr* **34**: 119-26 (2003).

26. J. C. Kalvass, C. L. Graff, and G. M. Pollack. Use of loperamide as a phenotypic probe of mdr1a status in CF-1 mice. *Pharm Res* **21**: 1867-70 (2004).

27. K. Yasuda, L. B. Lan, D. Sanglard, K. Furuya, J. D. Schuetz, and E. G. Schuetz. Interaction of cytochrome P450 3A inhibitors with P-glycoprotein. *J Pharmacol Exp Ther* **303**: 323-32 (2002).

28. B. Bauer, D. S. Miller, and G. Fricker. Compound profiling for P-glycoprotein at the blood-brain barrier using a microplate screening system. *Pharm Res* **20**: 1170-6 (2003).

29. M. Barecki-Roach, E. J. Wang, and W. W. Johnson. Many P-glycoprotein substrates do not inhibit the transport process across cell membranes. *Xenobiotica* **33**: 131-40 (2003).

30. J. Zongand G. M. Pollack. Modulation of P-glycoprotein transport activity in the mouse blood-brain barrier by rifampin. *J Pharmacol Exp Ther* **306**: 556-62 (2003).

31. C. Wandel, R. Kim, M. Wood, and A. Wood. Interaction of morphine, fentanyl, sufentanil, alfentanil, and loperamide with the efflux drug transporter P-glycoprotein. *Anesthesiology* **96**: 913-20 (2002).

Table 2.1. Apical, cellular, and basolateral compartments of various model systems

Model system	Apical	Cellular	Basolateral
Cell monolayer	Apical chamber	Cell monolayer	Basolateral chamber
Calcein-AM assay	Extracellular space	Intracellular space	n/a
MDR cell	Extracellular space	Intracellular space	n/a
MDR cell	Extracellular space	Cellular membrane	Intracellular space
Intestine	GI lumen	Epithelial cell	Blood
Kidney	Tubule lumen (urine)	Tubule epithelial cell	Blood
Liver	Canalicular space (bile)	Hepatocyte	Blood
Blood brain barrier	Capillary lumen (blood)	Endothelial cell	Brain

2.2. Relationships between efflux ratio, permeability-surface area products, and efflux activity

Definition of efflux ratio	Assumptions	Efflux activity
$ER_B = \frac{\frac{dX^{w/o\ efflux}_{B,A\to B}}{dt}}{\frac{dX_{B,A\to B}}{dt}} = \frac{PS_A + PS_B + PS_{efflux}}{PS_A + PS_B}$	initial uptake rate (i.e., X_B=0); rapid equilibrium between A and C	$PS_{efflux} = (PS_A + PS_B)(ER_B - 1)$
$ER_{B(t\to\infty)} = \frac{C_B^{w/o\ efflux}}{C_B} = 1 + \frac{PS_{efflux} \times V_A}{PS_A(V_A + V_B + V_C)}$	none	$PS_{efflux} = \frac{(V_A + V_B + V_C)}{V_A} PS_A(ER_B - 1)$
$ER_\alpha = \frac{\frac{dX_{A,B\to A}}{dt}}{\frac{dX_{B,A\to B}}{dt}} = \frac{PS_A + PS_{efflux}}{PS_A}$	initial uptake rate (i.e., X_A=0); rapid equilibrium between B and C initial uptake rate (i.e., X_B=0); rapid equilibrium between A and C	$PS_{efflux} = PS_A(ER_\alpha - 1)$
$ER_{\alpha(t\to\infty)} = \frac{C_A}{C_B} = \frac{PS_A + PS_{efflux}}{PS_A}$	none	$PS_{efflux} = PS_A(ER_\alpha - 1)$
$ER_C = \frac{\frac{dX^{w/o\ efflux}_{C,A\to C}}{dt}}{\frac{dX_{C,A\to C}}{dt}} = 1$	initial uptake rate (i.e., X_C=0)	n/a
$ER_{C(t\to\infty)} = \frac{C_C^{w/o\ efflux}}{C_C} = 1 + \frac{PS_{efflux} \times V_A}{PS_A(V_A + V_B + V_C)}$	none	$PS_{efflux} = \frac{(V_A + V_B + V_C)}{V_A} PS_A(ER_C - 1)$
$ER_A = \frac{\frac{dX_{A,B\to A}}{dt}}{\frac{dX^{w/o\ efflux}_{A,B\to A}}{dt}} = \frac{(PS_A + PS_B)(PS_A + PS_{efflux})}{PS_A(PS_A + PS_B + PS_{efflux})} \le \frac{(PS_A + PS_B)}{PS_A}$	initial uptake rate (i.e., X_A=0); rapid equilibrium between B and C	$PS_{efflux} = \frac{(PS_A + PS_B)PS_A(ER_A - 1)}{(PS_A + PS_B) - (PS_A \times ER_A)}$
$ER_{A(t\to\infty)} = \frac{C_A}{C_A^{w/o\ efflux}} = \frac{(PS_A + PS_{efflux})(V_A + V_B + V_C)}{(PS_{efflux} \times V_A) + PS_A(V_A + V_B + V_C)} \le \frac{V_A + V_B + V_C}{V_A}$	none	$PS_{efflux} = \frac{(V_A + V_B + V_C)PS_A(ER_A - 1)}{(V_A + V_B + V_C) - (V_A \times ER_A)}$

2.3. Comparison of methods for the calculation of experimental parameters

Parameter	Method(s) from literature	Method(s) derived from kinetic theory
IC_{50}	$PS = PS_0 + (PS_I - PS_0) \times \frac{[I]}{[I] + IC_{50,app}}$ (27)	$PS = \frac{PS_I \times PS_0}{PS_I + (PS_0 - PS_I) \times \frac{[I]}{[I] + IC_{50}}}$ $ER - 1 = \left(\frac{PS_I}{PS_0} - 1\right) \frac{IC_{50}}{[I] + IC_{50}}$
K_m	$PS = PS_0 + (PS_I - PS_0) \times \frac{[S]}{[S] + K_{m,app}}$ (28, 29)	$PS = \frac{PS_I \times PS_0}{PS_I + (PS_0 - PS_I) \times \frac{[S]}{[S] + K_m}}$ $ER - 1 = \left(\frac{PS_I}{PS_0} - 1\right) \frac{K_m}{[S] + K_m}$
ϕ_i	$\phi_{i,app} = \frac{PS - PS_0}{PS_I - PS_0}$ (30) $\phi_{i,app} = 1 - \frac{PS_{,B\to A} - PS_{,A\to B}}{PS_{0,B\to A} - PS_{0,A\to B}}$ (31)	$\phi_i = \frac{ER_{max} - ER}{ER_{max} - 1}$ $\phi_i = \frac{PS_I}{PS} \times \frac{(PS - PS_0)}{(PS_I - PS_0)}$ $\phi_i = \frac{PS_{I,A\to B}}{PS_{,A\to B}} \times \left(1 - \frac{PS_{B\to A} - PS_{A\to B}}{PS_{0,B\to A} - PS_{0,A\to B}}\right)$ $\phi_i \geq 1 - \frac{1}{\text{fold}\,\Delta PS}$ [a]
PS_{efflux}	$PS_{efflux,app} = PS_I - PS$ $PS_{efflux,app} \propto PS_I - PS$ $PS_{efflux,app} \propto ER_B$ $PS_{efflux,app} \propto ER_C$ $PS_{efflux,app} \propto ER_\alpha$	$PS_{efflux} = 4PS_{I,A\to B}(ER_B - 1)$ $PS_{efflux} = 2PS_{I,A\to B}(ER_\alpha - 1)$ $PS_{efflux} \propto PS_{I,A\to B}(ER - 1)$
$K_{m,app}$	$K_{m,app} = K_{m,app}$	$K_{m,app} = K_m \times ER_{max}$
$IC_{50,app}$	$IC_{50,app} = IC_{50,app}$	$IC_{50,app} = IC_{50} \times ER_{max}$

Note: Since flux and P_{app} are proportional to PS, flux and P_{app} can be substituted for PS

ER=ER_B,ER_C, or ER_α

[a] rearrangement of equation (12-10)

2.4. Influence of P-gp-efflux on the brain-to-plasma ratio ($K_{p,brain}$) and brain equilibration rate constant ($K_{brain,eq}$) of P-gp substrates

	Fold Change in $K_{p,brain}$ (ER_{α})	Fold change in $K_{brain,eq}$ (ER_A)	Expected change in $K_{brain,eq}$ (ER_A)*
Fentanyl	1.9	1.0	1.3
Alfentanil	2.8	1.4	1.5
Methadone	7.2	2.4	1.8
Loperamide	44	1.9	2

*The expected change in change in $K_{brain,eq}$ was calculated from the fold change in $K_{p,brain}$ and the theoretical relationship between ER_{α} and ER_A.

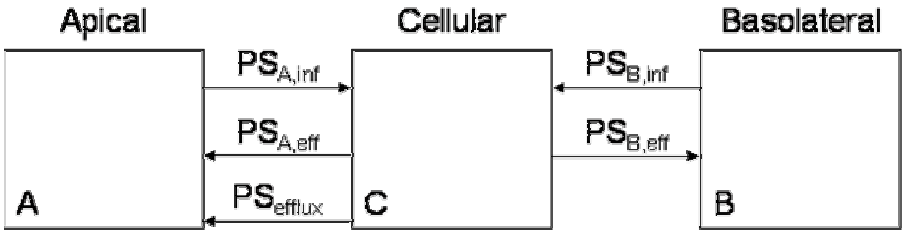

Figure 2.1. **Three-compartment model consistent with efflux attenuating the initial rate of flux in the A-to-B direction.** $PS_{A,inf}$ and $PS_{A,eff}$, represent the passive permeability-surface area product of the apical membrane, whereas, $PS_{B,inf}$ and $PS_{B,eff}$ represent the passive permeability-surface area products of the basolateral membrane. PS_{efflux} represents the permeability-surface area product of efflux activity. It is assumed $PS_{A,inf} = PS_{A,eff} = PS_A$ and $PS_{B,inf} = PS_{B,eff} = PS_B$.

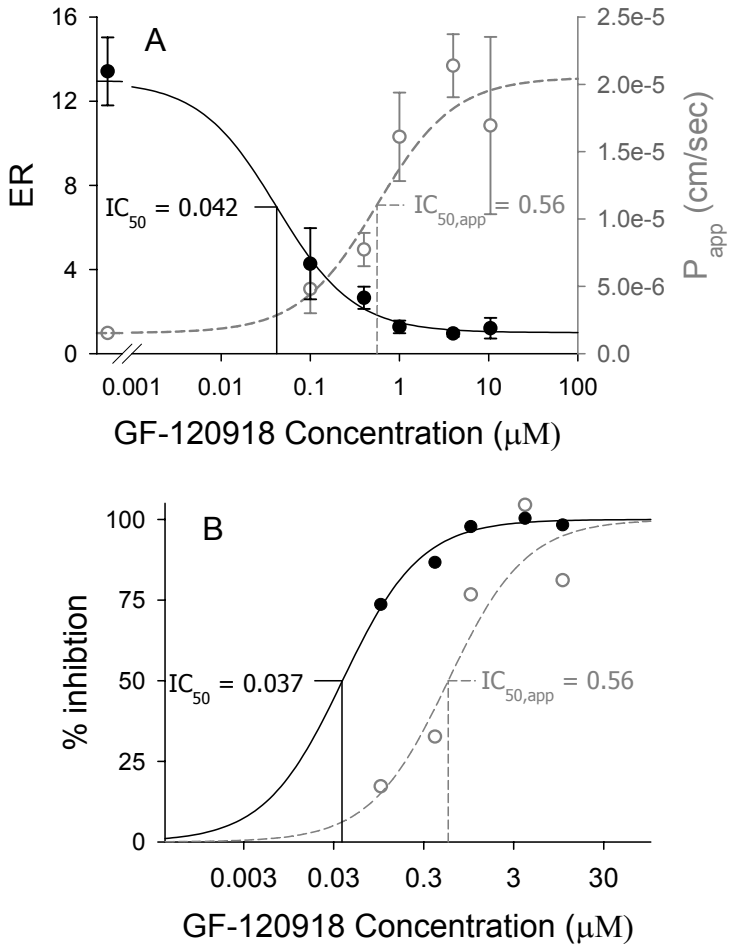

Figure 2.2. **Influence of GF-120918 on the brain uptake of quinidine**. Data from Chen et. al 2002. (A) *In situ* brain perfusion P_{app} and ER values for quinidine were determined in the presence of various concentrations of GF-120918. A modified Michaelis-Menten equation was fitted to either the P_{app} or ER data to obtain estimates of $IC_{50,app}$ and IC_{50} respectively. (B) Inhibition of P-gp mediated efflux was calculated from the P_{app} data using either equation (12-5), a commonly-cited inhibition equation (open symbols), or equation (12-4), a newly derived inhibition equation (solid symbols), and the Michaelis-Menten equation was fitted to the inhibition data to obtain estimates of $IC_{50,app}$ and IC_{50}, respectively. Note that in both panel A and B, $IC_{50,app}$ overestimated $IC_{50,}$ and that $IC_{50,app} = ER_{max} * IC_{50}$.

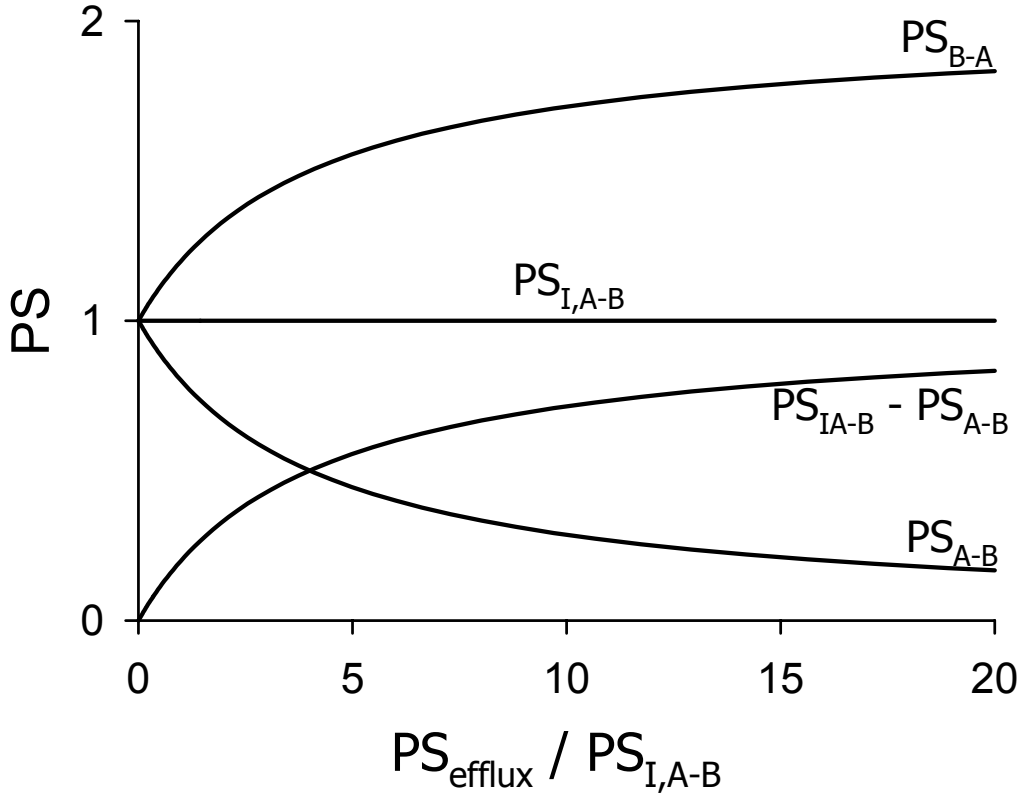

Figure 2.3. **Theoretical relationship between efflux activity (PS_{efflux}) and permeability-surface area product (PS).** Efflux activity was normalized for the A-to-B passive permeability-surface area product ($PS_{I,A-B}$). PS_A and PS_B were assumed to be equal, therefore $PS_{I,A-B} = ½PS_A$. Since P_{app} and flux are proportional to PS, substituting P_{app} or flux for PS will yield the identical relationship.

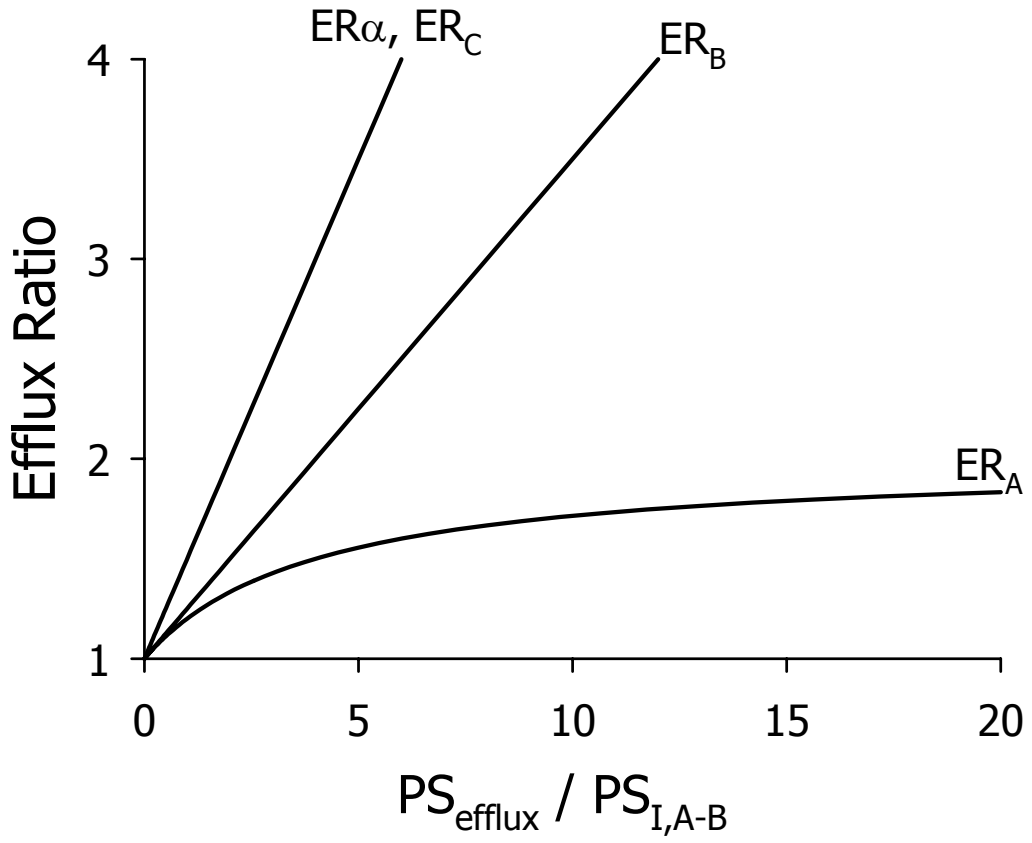

Figure 2.4. **Theoretical relationship between efflux activity (PS_{efflux}) and asymmetry (ER_{α}), absorptive (ER_B), secretory (ER_A), or intracellular (ER_C) efflux ratio.** Efflux activity was normalized for the A-to-B passive permeability-surface area product ($PS_{I,A-B}$). PS_A and PS_B were assumed to be equal, therefore $PS_{I,A-B} = ½PS_A$.

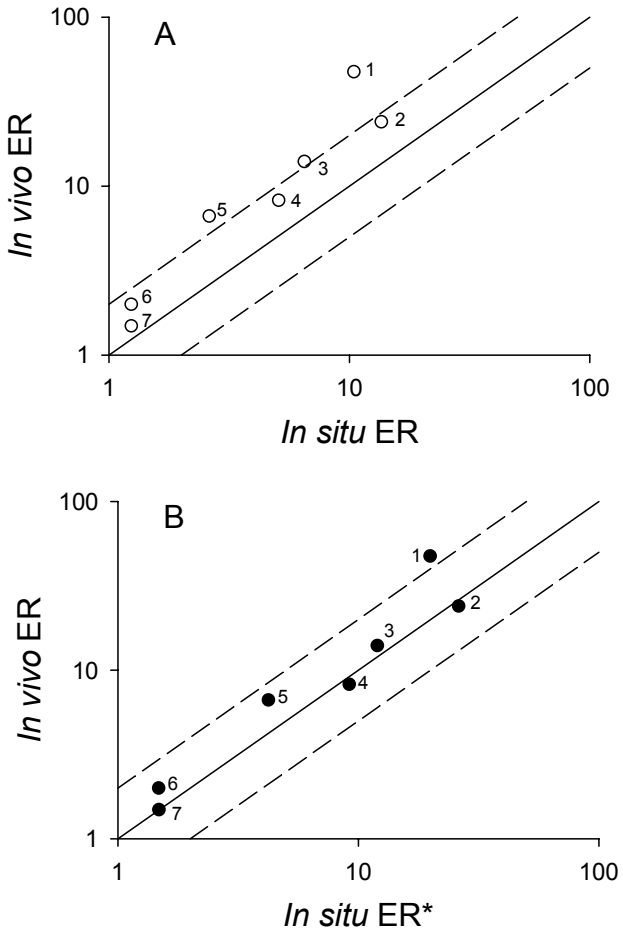

Figure 2.5. **Correlation between *in situ* and *in vivo* P-gp efflux ratios.** (A) *In situ* efflux ratio was by defined as the ratio of brain uptake clearance in P-gp-deficient mice divided by the brain uptake clearance in P-gp-deficient mice. *In vivo* efflux ratio was calculated as the brain-to-plasma ratio of P-gp-deficient mice divided by the brain-to-plasma ratio of P-gp component animals. In panel (B), *in situ* ER* was corrected for differences between ER_A and ER_α (ER* = [(ER-1)x2]+1). Solid line represents line of unity whereas dashed lines represent 2-fold above or below the line of unity. Compound legend is as follows: 1 loperamide, 2 quinidine, 3 ritonavir, 4 verapamil, 5 methadone, 6 fentanyl, 7 morphine.

CHAPTER 3

CLINICAL INHIBITION OF P-GLYCOPROTEIN AT THE BLOOD-BRAIN BARRIER: A PHARMACOKINETIC-PHARMACODYNAMIC ASSESSMENT

This chapter will be submitted for publication in *Clinical Pharmacology and Therapeutics* and is presented in the style of that journal.

Abstract:

Assessment of drug interaction potential is a key aspect of contemporary drug discovery and development. Recent advances in this area have highlighted the importance of genetic polymorphism and chemical inhibition of drug transporters as mechanisms of adverse drug interactions. A principal area of focus has been P-glycoprotein (P-gp) at the blood-brain-barrier (BBB), as this transporter impairs the CNS distribution of many compounds. However, there is little clinical evidence to support the prevalent concern that P-gp substrates or inhibitors are associated with a risk of CNS toxicity secondary to pharmacokinetic-based drug-drug interactions. As a result, there is a fundamental debate as to whether compounds that are P-gp substrates should be selected as candidates for drug development. Clearly, rational decision-making requires a comprehensive understanding of the factors that lead to clinically relevant inhibition of P-gp at the BBB. In this commentary, fundamental pharmacokinetic principles are used to create a framework for the critical evaluation of drug-drug interaction potential for P-gp substrates and inhibitors. In this context, data from *in vitro*, preclinical, and clinical studies are utilized to illustrate key concepts.

P-gp is a member of the ATP-binding cassette family of proteins, which function to excrete a wide variety of potentially toxic molecules from cells. P-gp is localized to the apical plasma membrane domain of cells, where it functions as a key physiologic barrier and clearance mechanism for large molecular weight, lipophilic, uncharged or cationic compounds in the intestine, testes, brain, kidney and liver [1,2] P-gp in intestinal enterocytes transports drugs, as well as certain dietary constituents, back into the gut lumen, thus limiting absorption into mesenteric blood [1-4]. P-gp in capillary endothelial cells of the testes, brain and tumor tissue attenuates the pharmacodynamic effects of its substrates [2], creates an enormous hurdle in chemotherapy [5] , and has been hypothesized to create a sanctuary site for the human immunodeficiency virus [6-8]. Lastly, P-gp in the liver and kidney mediates the biliary and urinary excretion of substrates [1], serving as a determinant of overall systemic exposure.

P-gp inhibition at the BBB

Given its role in limiting oral bioavailability and drug exposure in important target organs, as well as in mediating systemic drug clearance, inhibition of P-gp has garnered considerable attention as a means of enhancing exposure. Although inhibition of P-gp has proven to be successful in improving the oral bioavailability of some substrates [9], attempts at appreciable clinical P-gp inhibition at the BBB have met with limited success [5,10]. To some extent, these failures are surprising. Numerous preclinical studies have demonstrated the importance of P-gp at the BBB [2,11], and large increases in brain penetration of P-gp substrates have been produced by P-gp inhibitors in preclinical models such as *in situ* brain perfusion (Tables 3.1 and 3.2). These results have been used in part to support development of P-gp inhibitors as

adjuncts to therapeutic agents with otherwise impaired access to brain. These observations also have raised concerns about potential unintended drug-drug interactions.

Although several potent P-gp inhibitors have been developed (Table 3.3), appreciable enhancement of CNS drug exposure as a result of P-gp inhibition has not been demonstrated clinically (Table 3.4 and 3.5) due to an inability to achieve unbound systemic concentrations sufficient to elicit appreciable changes in CNS drug disposition. Furthermore, reports of increased CNS exposure due to inhibition of P-gp, inferred from changes in pharmacologic activity, may be secondary to increased systemic drug concentrations due to intestinal P-gp inhibition or to a direct pharmacologic effect of P-gp inhibitors. This commentary explores rational kinetic relationships between the extent of P-gp inhibition and the resultant change in CNS drug exposure. These relationships serve as a framework through which existing data on the consequences of BBB P-gp inhibition may be evaluated.

Theoretical relationship between P-gp inhibition and fold increase in CNS exposure

The fold increase in CNS penetration or exposure (fold Δ CNS) due to P-gp inhibition may be expressed in terms of efflux ratios [eq. (1)], where ER_{max} is the maximum P-gp efflux ratio (i.e., CNS exposure after complete inhibition of P-gp efflux divided by CNS exposure in the absence of P-gp inhibition) and ER_{obs} is the observed P-gp efflux ratio in the presence of a P-gp inhibitor under a specified condition or concentration (i.e., CNS exposure after complete inhibition of P-gp efflux divided by CNS exposure observed under the specified inhibitor condition).

$$\text{fold}\,\Delta\,\text{CNS} = \frac{ER_{max}}{ER_{obs}} \qquad (1)$$

The fractional degree of P-gp inhibition at any inhibitor concentration [I] is given by

$$\left(\phi_i = \frac{[I]}{[I] + K_i} \right) \quad (2)$$

where K_i is the inhibition constant. Now, ER_{obs} can be expressed in terms of ER_{max} and ϕ_I as:

$$ER_{obs} = ER_{max} - (ER_{max} - 1) \times \phi_i \quad (3)$$

By substitution of eq. (3) into eq. (1), the fold Δ CNS can be written as a function P-gp inhibition and ER_{max}

$$\text{fold}\,\Delta\,\text{CNS} = \frac{ER_{max}}{ER_{max} - (ER_{max} - 1) \times \phi_i} \quad (4)$$

Exploring the behavior of eq. (4) at its limits yields the inequality

$$ER_{max} \geq \text{fold}\,\Delta\,\text{CNS} \leq \frac{[I]}{K_i} + 1 \quad (5)$$

The fold increase in exposure due to efflux inhibition is limited by ER_{max} or $([I]/K_i) + 1$, whichever is lower. Thus, when $[I]/K_i=1$ (i.e., 50% inhibition), the maximum increase in CNS exposure is 2-fold irrespective ER_{max}, which influences the fold increase in CNS exposure only when $[I]/K_i$ approaches values in excess of ER_{max}. Eq. (4) and (5) are similar to the equations describing the relationship between fold increase in AUC and the degree of inhibition of a single clearance pathway [12].

The degree of inhibition can be determined from experimental data by rearranging eq. (3) and solving for ϕ_i

$$\phi_i = \frac{ER_{max} - ER_{obs}}{ER_{max} - 1} \quad (6)$$

When ER_{max} is unknown, the minimal extent of P-gp inhibition may be calculated from the fold Δ CNS according to eq. (7).

$$\phi_i \geq 1 - \frac{1}{\text{fold}\,\Delta\,\text{CNS}'} \quad (7)$$

Eq. (6) and (7) represent the theoretical relationship between efflux ratio and the degree of efflux inhibition.

The equations presented herein can be used to predict the magnitude of increase in CNS drug exposure as a result of P-gp inhibition from basic pharmacokinetic parameters prior to conducting complex and costly clinical studies. For example, a recent clinical study evaluated the effect of P-gp inhibition by cyclosporine on CNS exposure to verapamil [13]. Based on the *in vitro* K_i of cyclosporine for inhibition of P-gp (0.2 μM [14]), as well as the unbound fraction of the inhibitor (~0.06 [15,16]), total cyclosporine systemic concentrations in excess of 3.3 μM would be required to produce an appreciable (>2-fold) increase in verapamil CNS exposure. Steady-state cyclosporine concentrations actually attained in the study were 2.8 μM. Eq. (5) would predict an ~84% increase in verapamil CNS exposure at this concentration of cyclosporine. In fact, PET imaging indicated an 88% increase in CNS exposure to ^{11}C-verapamil [13], consistent with theory as outlined in this commentary.

Comprehensive understanding of theory allows application to a variety of experimental issues:

Probe substrate selection

An ideal probe substrate for evaluating the potential influence of a P-gp inhibitor on CNS exposure would have several practical characteristics, including a centrally-mediated pharmacologic response that is easily measured and sensitive to small changes in CNS exposure, be well tolerated, not be a substrate for other transporters, and be available in a formulation for intravenous administration to avoid potential effects of the inhibitor on systemic exposure via modulation of gastrointestinal absorption. The P-gp efflux ratio of an

ideal probe substrate would be ≥3, such that 50% inhibition of P-gp would result in at least a 1.5-fold increase in CNS exposure (eq. 5). Even under such stringent conditions, the pharmacologic measure would require a large dynamic range and sufficient sensitivity to distinguish differences in central effect resulting from a 50% increase in exposure.

One potentially useful substrate for clinical evaluation of BBB P-gp inhibition is the opioid methadone, which is a known P-gp substrate with an efflux ratio in excess of 3 [17,18]. Opioids in general exhibit sensitive and readily-measurable central effects (antinociception, pupil dilation, respiratory depression, and electroencephalogram effects) with clear dose/concentration-effect relationships [19]. Furthermore, methadone is formulated for intravenous administration. One published clinical report was unable to demonstrate appreciable alteration in methadone pharmacodynamics during co-administration with quinidine [20]. However, the dose of quinidine administered would not be expected to produce appreciable enhancement of methadone CNS exposure due to a modest extent of BBB P-gp inhibition (Table 3.3). In addition to methadone, preliminary data from this laboratory indicate that the opioids alfentanil and sufentanil also possess the characteristics of an ideal probe as outlined above.

Several P-gp substrates are known to undergo active uptake across the BBB in addition to P-gp efflux. Surprisingly, in a few studies, administering a P-gp inhibitor actually decreased the CNS exposure of P-gp substrates. Some P-gp inhibitors are not specific and may inhibit other transporters including BBB uptake transporters [21], resulting in a decrease in CNS exposure (e.g., paclitaxel during co-administration with the P-gp inhibitors itraconazol and cyclosporin A; Table 3.2).

Inhibitor selection

A useful model inhibitor, or one proposed to enhance clinical response to a CNS-active agent, must be well-tolerated at concentrations required to modulate BBB P-gp (unbound concentrations at least several fold in excess of the K_i to produce appreciable P-gp inhibition). The inhibitor should be available as an intravenous formulation, such that high oral doses are not required to overcome poor intestinal absorption and first-pass elimination, and to minimize inter-subject variability in systemic inhibitor concentrations. Ideally, the inhibitor should not affect systemic concentrations of probe substrate, so that potential enhancements of CNS exposure may be attributed to inhibition of P-gp at the BBB and not simply to higher systemic probe concentrations; the experimental problems associated with systemic interactions can be overcome by measuring plasma concentrations of the probe substrate. P-gp appears to have multiple binding sites, so for a given inhibitor, the potency and extent of inhibition may vary between P-gp substrates [22]. For example, rifampin can completely abolish P-gp mediated transport of verapamil at the murine BBB. However, at similar concentrations, rifampin is only able to reduce the transport of quinidine by 50% [23]. Therefore, P-gp binding sites should be considered when assessing potential drug interactions. In addition, the inhibitor should be validated in preclinical species at clinically-relevant concentrations prior to clinical use and have no pharmacologic activity of its own.

Few of the currently-available P-gp inhibitors fit the criteria outlined above (Table 3.3), and it is unlikely that inhibition of P-gp at the BBB will exceed ~50%. Of the available inhibitors, cyclosporine A and PSC833 (Valspodar) appear to be the most effective, because the unbound systemic concentrations of these inhibitors can exceed the K_i, albeit at an $[I]/K_i$ ratio that is lower than optimal for extensive BBB P-gp inhibition, they have no central PD

effect, are available as an intravenous formulation, and appear to interact with the various P-gp substrate binding sites (Table 3.3) [13,24]. Quinidine is the third most potent P-gp inhibitor in Table 3.3, however quinidine clinical unbound systemic C_{max} is only 20% greater than its K_i, and it is known to cause respiratory depression, a PD effect that overlaps with opioids [25,26].

Experimental design

A clinical BBB P-gp interaction study employing a pharmacologic measure as a surrogate for CNS drug exposure utilizes a probe substrate and inhibitor with the properties outlined in the preceding sections. Systemic pharmacokinetics of the probe, as well as the pharmacologic effect, should be examined following intravenous administration of the probe substrate alone at a minimum of two different dose levels. The lower dose should elicit a response statistically above placebo, and the higher dose(s) should elicit a response below maximum, but statistically higher than the response produced by the lower dose. These control experiments establish the systemic concentration-effect relationship. Many BBB P-gp interaction studies are confounded by the fact that the inhibitor increases systemic concentrations of the probe substrate (Table 3.4 and 3.5); proper control studies (in the absence of inhibitor) will allow appropriate correction for inhibitor-associated changes in systemic concentrations of the probe. Whenever possible, the study should be conducted under steady-state conditions for the inhibitor. If the steady-state inhibitor concentration approach is not feasible, systemic inhibitor concentrations should be determined throughout the course of the study. Finally, intravenous administration of the inhibitor with probe

placebo should be conducted in order to confirm the absence of inhibitor pharmacologic effects.

Studies using loperamide as a probe substrate

Despite being a potent *mu* opioid agonist, loperamide does not elicit central opioid activity at clinical doses [27] because of limited CNS penetration due to BBB P-gp efflux [28]. Thus, several studies have been performed with loperamide as a probe substrate to study the functional impact of MDR1 genetic polymorphism or chemical inhibition of P-gp at the BBB [29-32].

Clinical and preclinical data suggest that, for most opioids, there is little separation between anti-diarrheal activity and central opioid activity. In studies conducted in rats, loperamide had >70-fold separation between anti-diarrheal activity and CNS effects [33]. Studies in this laboratory have shown that loperamide has an ~60-fold difference in brain penetration and antinociception between P-gp competent and P-gp deficient mice, suggesting P-gp reduces loperamide CNS penetration by 60-70 fold [34]. In P-gp-deficient animals, loperamide is more potent than morphine and methadone at eliciting central opioid effects, indicating that the lack of central opioid effects at clinical doses is likely due to P-gp efflux at the BBB [34-36].

Several reports suggest that the extent of P-gp impairment of CNS exposure is similar between humans and preclinical species [37,38]. Clinical studies and case reports of overdoses demonstrate that loperamide is devoid of measurable CNS effects up to oral doses of 60 mg [27]. At the standard dose of 2 mg, loperamide exhibits no measurable central effects in humans [27]. CNS effects may be observed at doses higher than 60 mg, indicating that there is

at least a 30-fold separation between therapeutic anti-diarrheal effects and central opioid effects. Therefore, for use as a P-gp probe substrate, loperamide must be administered at supra-therapeutic doses (16 to 24 mg) in order to elicit a measurable central pharmacologic effect when P-gp efflux at the BBB is impaired. Using this approach, the impact of inhibition or MDR1 genetic polymorphisms on P-gp function at the BBB has been investigated [29-32]. Two of four studies demonstrated an alteration in the central opioid activity of loperamide, but the results from these studies were not entirely consistent [29,32]. One possible explanation for the inconsistency may be the reliability of central activity of loperamide as a surrogate of P-gp function at the BBB.

Sadeque et al. were the first to demonstrate the potential for clinical drug interactions via P-gp inhibition at the BBB [29]. This study examined the ability of quinidine to increase delivery of loperamide to the brain by inhibiting P-gp. Respiratory response to carbon dioxide rebreathing was used as a marker of central *mu* opioid effects. In a double-blind crossover study, subjects received 600 mg of quinidine or placebo, followed by 16 mg of loperamide one hour later. No respiratory depression was observed for the placebo/loperamide group; however, respiratory depression did occur when loperamide was co-administered with quinidine. Despite a 2.5-fold increase in systemic C_{max} and AUC in the quinidine/loperamide group, the authors ruled out higher systemic concentrations of loperamide as a cause of the CNS effect, because at early time points, respiratory depression was observed only in the quinidine treatment group even though loperamide concentrations were similar to those in the placebo control group.

The functional significance of MDR1 gene mutation in determining the disposition and CNS effects of loperamide also has been investigated [32]. Subjects received placebo or 800

mg of quinidine followed by 24 mg of loperamide one hour later. The central opioid effect of loperamide was monitored by pupilometry. Loperamide pharmacokinetics and central opioid effects were delineated based on MDR1 genotype and whether or not subjects received quinidine. No central opioid effect was observed in either the placebo or quinidine group for subjects homozygous for the MDR1 reference allele. In the other treatment groups (non-homozygous for the MDR1 reference allele), CNS effects were observed only when loperamide was administered with quinidine. When compared to the loperamide C_{max} and AUC of subjects homozygous for the MDR1 reference allele who received placebo, loperamide C_{max} and AUC were 2- to 3.1-fold higher when administered with quinidine. Given that a 24-mg dose of loperamide was administered, a 2- to 3.1-fold increase in C_{max} and AUC would be comparable to the C_{max} and AUC following a 48- to 74-mg dose of loperamide in naive homozygous subjects, assuming linear pharmacokinetics and absorption. In previous dose-escalation studies conducted to assess central opioid activity of loperamide, respiratory depression and pupil diameter were monitored and no central opioid activity was observed in subjects who received loperamide doses up to 60 mg [27]. Since the central opioid activity of loperamide at doses above of 60 mg is unknown, it is possible that the central opioid activity observed in quinidine treated subjects heterozygous for the MDR1 reference allele was predominantly due to increased systemic exposure rather than altered P-gp function at the BBB. However, based on unbound quinidine concentrations and the K_i of the inhibitor (Table 3.3), partial inhibition (~50%) of P-gp at BBB and increased CNS penetration of loperamide (<2-fold) cannot be ruled out. Studies in which equivalent loperamide exposures are achieved need to be conducted in order to determine whether P-gp

inhibition or higher systemic concentrations were responsible for the observed alterations in CNS effects.

Even though higher systemic concentrations in the quinidine-treated group may explain some results with loperamide, discrepancies appear to exist between the two studies. Although larger doses of quinidine and loperamide were used by Skarke et al. [39], no central opioid effects were observed despite higher C_{max} and AUC of loperamide in subjects homozygous for the MDR1 reference allele. One difference between the two studies was the choice of central pharmacodynamic markers: respiratory depression vs. pupil dilatation. Perhaps respiratory depression is a more sensitive marker for central opioid activity. However, this appears not to be the case. In a study evaluating the central pharmacologic effects of morphine, both respiratory depression and pupilometry were equally sensitive at detecting a graded pharmacodynamic response [39]. Another possible explanation is respiratory depression may be caused by quinidine [25,26]. Furthermore, the estimated quinidine C_{max} was within the range associated with development of respiratory depression in susceptible patient populations and preclinical species[40,41]. The effect of 600 mg of quinidine on respiratory depression should be determined in order to rule out the possibility that respiratory depression was caused by quinidine rather than by increased CNS exposure to loperamide to the brain. In one study using 800 mg of quinidine co-administered with morphine, no enhancement in respiratory depression was observed [39], possibly because the respiratory depression caused by morphine masked the effects of quinidine.

The pharmacodynamic changes in the Sadeque et al. study did not correlate with loperamide concentrations [29]. In contrast, in the Skarke et al. study, the time course of miotic effects followed loperamide concentrations. The degree of respiratory depression in the

Sadeque et al. (2000) study peaked prior to maximum loperamide concentrations, then declined as loperamide concentrations continued to increase, which implies the observed respiratory depression may not have been caused by the actions of loperamide. When quinidine is co-administered in studies utilizing respiratory depression as a measure of central opioid activity, secondary measures of CNS activity, such as pupilometry should be used, or a quinidine alone control group should be included to confirm respiratory depression is not caused by the pharmacological actions of quinidine.

One commonality between these studies is that the central opioid effect of loperamide was only observed at doses many multiples (8- to 12-fold) of the standard dose and only after co-administration of a large dose of quinidine. Quinidine more than doubled loperamide systemic exposures compared to placebo control. The magnitude of the pharmacologic effect of loperamide was modest and cannot be attributed entirely to altered function of P-gp at the BBB, because the effect of higher systemic concentrations of loperamide and the effects of quinidine on respiratory depression are not known. In gene-knockout animals lacking P-gp, loperamide is a potent opioid eliciting central effects at low doses [28,34]. The clinical studies to date suggest that chemical inhibition of P-gp at the BBB by quinidine is at best modest, because loperamide elicits only minimal CNS effects at high doses.

Additional studies with loperamide as a probe substrate have been conducted using the human immunodeficiency virus (HIV) protease inhibitor, ritonavir [30]. In a double-blind crossover study, 16 mg of loperamide was co-administered with either placebo or 600 mg ritonavir. Pupilometry, cold pressor test, and transcutaneous P_{CO2} and P_{O2} analysis were performed to assess the central opioid effect produced by loperamide. A modest increase in C_{max} (1.2 fold) was observed in the loperamide/ritonavir group; however, no central opioid

effects were observed in any treatment group. Likewise, other studies produced negative PD results, suggesting that loperamide is a poor probe for P-gp inhibiton at the BBB (Table 3.4).

It may be that loperamide is a poor probe substrate for accessing BBB P-gp function in humans as it cannot be administered at doses that produce some basal level of CNS activity, and it cannot be administered intravenously. Methadone may be an alternate probe choice as it has a moderately high P-gp efflux ratio (5- 25 in preclinical species) [17,18], can be given intravenously, and low doses produce a detectible centrally-mediated PD effect .

MDR1 genetic polymorphisms

No clinical reports of adverse drug interactions due reduction of P-gp function associated with genetic polymorphisms have been forthcoming. Despite identification of numerous human SNPs in the MDR1 gene [42], no null alleles of MDR1 have been isolated. However, a naturally-occurring strain of CF-1 mice, and population of collie dogs, lacking the functional Mdr1 gene product were identified based on neurotoxicity in response to ivermectin, an anti-parasitic P-gp substrate [43,44]. As expected, P-gp protein expression and function in mice heterozygous for the null P-gp allele were half that in animals homozygous for the P-gp reference allele [45]. However, CNS drug penetration to the brain and LD_{50} of avermectin in mice heterozygous of P-gp was similar to mice homozygous for P-gp [45]. If populations of humans homozygous for a null allele of MDR1 were present in significant numbers, many documented examples of adverse reactions to various CNS-active/toxic P-gp substrates (e.g., loperamide, avermectin, ivermectin) would be expected. To date, this has not been demonstrated, suggesting that MDR1 polymorphisms do not confer overt CNS sensitivity to P-gp substrates.

Whether due to chemical inhibition or genetic polymorphism, the maximum possible increase in CNS exposure due to a 50% reduction in P-gp function at the BBB is 2-fold. Within the human population at large, there is normally a large degree of individual variation in systemic pharmacokinetic parameters and consequently in systemic exposure to drugs. Agents that come to market successfully tend to have therapeutic indexes that are sufficiently wide to account for the clinical pharmacokinetic variation. Since systemic exposure to drugs often varies by more than 2-fold, and sometimes by more than an order of magnitude, among individuals in a defined population, a 2-fold increase in CNS penetration due to genetic perturbation or chemical inhibition is unlikely to be the dominant factor in CNS response. Thus, a 50% reduction in BBB P-gp function may be clinically significant only for those agents with extremely narrow therapeutic indices.

Recommendations and concluding remarks

Most clinically-available inhibitors are not sufficiently potent or well-tolerated to achieve unbound systemic concentrations necessary to inhibit P-gp at the BBB, even though they may inhibit P-gp in the gut, and potentially the liver. This situation is due to higher concentrations of inhibitor present in the intestinal tract and portal vein after oral administration as compared to the systemic circulation that delivers substrate to the BBB. At the high systemic concentrations of inhibitor required to modulate BBB P-gp, untoward effects of the inhibitor are more likely to be clinically significant than the magnitude of increase in CNS exposure to a co-administered P-gp substrate.

The anti-diarrheal agent loperamide is an example of how CNS-active P-gp substrates can be developed safely, and experience with this compound suggests that the incidence of

clinically-significant P-gp inhibition at the BBB, as well as genetic polymorphisms affecting P-gp expression or function at the BBB, are exceedingly rare. Loperamide is a very potent opioid agonist; however , due to its large CNS P-gp effect, there is at least a 30-fold safety window between anti-diarrheal and central opioid activity [27]. As detailed above, the large loperamide safety window cannot be easily overcome by clinical inhibition of BBB P-gp activity. Since loperamide has been available over the counter for decades, loperamide CNS effects in the general population would have been documented and linked to P-gp inhibition and/or polymorphisms.

Proper understanding and interpretation of the relationship between the *in vitro* K_i, *in vivo* BBB P-gp inhibition, and the subsequent impact on CNS drug exposure is necessary for the proper design of clinical studies. Using the kinetic concepts presented in this commentary, the extent of enhancement in CNS drug exposure by a P-gp inhibitor can be predicted prior to conducting clinical experimentation. The key principle underlying the analysis of data and the use of mathematical relationships is that unbound systemic inhibitor concentration is the determinant of the extent of P-gp inhibition at the BBB. Although total systemic inhibitor concentrations may exceed the *in vitro* K_i by many fold, if the unbound concentrations are not in adequate excess of the K_i, appreciable BBB P-gp inhibition will not be achieved. Currently-available clinical P-gp inhibitors are not associated with adequate systemic unbound concentrations to cause appreciable increases in CNS exposure to drugs that are P-gp substrates.

References

1. Ho RH and Kim RB (2005) Transporters and drug therapy: implications for drug disposition and disease. *Clin Pharmacol Ther* **78:**260-277.

2. Matheny CJ et al. (2001) Pharmacokinetic and pharmacodynamic implications of P-glycoprotein modulation. *Pharmacotherapy* **21:**778-796.

3. Kim RB et al. (1998) The drug transporter P-glycoprotein limits oral absorption and brain entry of HIV-1 protease inhibitors. *J Clin Invest* **101:**289-294.

4. Tahara H et al. (2005) P-glycoprotein plays a major role in the efflux of fexofenadine in the small intestine and the blood-brain barrier, but only a limited role in its biliary excretion. *Drug Metab Dispos* **33:**963-968.

5. Kemper EM et al. (2004) Modulation of the blood-brain barrier in oncology: therapeutic opportunities for the treatment of brain tumours? *Cancer Treatment Reviews* **30:**415-423.

6. Haas DW et al. (2003) MDR1 gene polymorphisms and phase 1 viral decay during HIV-1 infection: an adult AIDS Clinical Trials Group study. *J Acquir Immune Defic Syndr* **34:**295-298.

7. Pomerantz RJ (2001) Residual HIV-1 RNA in blood plasma of patients taking suppressive highly active antiretroviral therapy. *Biomed Pharmacother* **55:**7-15.

8. Cordon-Cardo C et al. (1990) Expression of the multidrug resistance gene product (P-glycoprotein) in human normal and tumor tissues. *J Histochem Cytochem* **38:**1277-1287.

9. Kruijtzer CM et al. (2002) Increased oral bioavailability of topotecan in combination with the breast cancer resistance protein and P-glycoprotein inhibitor GF120918. *J Clin Oncol* **20:**2943-2950.

10. Kellen JA (2003) The reversal of multidrug resistance: an update. *J Exp Ther Oncol* **3:**5-13.

11. Chen C et al. (2003) Utility of Mdr1-gene deficient mice in assessing the impact of P-glyco-protein on pharmacokinetics and pharmacodynamics in drug discovery and development. *Curr Drug Metab* **4:**272-291.

12. Rowland M and Matin SB (1973) Kinetics of drug-drug interactions. *J Pharmacokinet Biopharm* **1:**553-567.

13. Sasongko L et al. (2005) Imaging P-glycoprotein transport activity at the human blood-brain barrier with positron emission tomography. *Clin Pharmacol Ther* **77:**503-514.

14. Smith AJ et al. (1998) Availability of PSC833, a substrate and inhibitor of P-glycoproteins, in various concentrations of serum. *J Natl Cancer Inst* **90:**1161-1166.

15. Akhlaghi F and Trull AK (2002) Distribution of cyclosporin in organ transplant recipients. *Clin Pharmacokinet* **41:**615-637.

(2000) *Physicians' desk reference PDR*. Medical Economics Co., Oradell, N.J.

17. Wang JS et al. (2004) Brain penetration of methadone (R)- and (S)-enantiomers is greatly increased by P-glycoprotein deficiency in the blood-brain barrier of Abcb1a gene knockout mice. *Psychopharmacology (Berl)* **173:**132-138.

18. Rodriguez M et al. (2004) Effect of P-glycoprotein inhibition on methadone analgesia and brain distribution in the rat. *J Pharm Pharmacol* **56:**367-374.

19. Lotsch J (2005) Pharmacokinetic-pharmacodynamic modeling of opioids. *J Pain Symptom Manage* **29:**S90-103.

20. Kharasch ED et al. (2004) The effect of quinidine, used as a probe for the involvement of P-glycoprotein, on the intestinal absorption and pharmacodynamics of methadone. *Br J Clin Pharmacol* **57:**600-610.

21. Ayrton A and Morgan P (2001) Role of transport proteins in drug absorption, distribution and excretion. *Xenobiotica* **31:**469-497.

22. Pajeva IK and Wiese M (2002) Pharmacophore model of drugs involved in P-glycoprotein multidrug resistance: explanation of structural variety (hypothesis). *J Med Chem* **45:**5671-5686.

23. Zong J and Pollack GM (2003) Modulation of P-glycoprotein transport activity in the mouse blood-brain barrier by rifampin. *J Pharmacol Exp Ther* **306:**556-562.

24. Baekelandt M et al. (2001) Phase I/II trial of the multidrug-resistance modulator valspodar combined with cisplatin and doxorubicin in refractory ovarian cancer. *J Clin Oncol* **19:**2983-2993.

25. Trampuz A et al. (2003) Clinical review: Severe malaria. *Crit Care* **7:**315-323.

26. Jaeger A et al. (1987) Clinical features and management of poisoning due to antimalarial drugs. *Med Toxicol Adverse Drug Exp* **2:**242-273.

27. Jaffe JH et al. (1980) Abuse potential of loperamide. *Clin Pharmacol Ther* **28:**812-819.

28. Schinkel AH et al. (1996) P-glycoprotein in the blood-brain barrier of mice influences the brain penetration and pharmacological activity of many drugs. *J Clin Invest* **97:**2517-2524.

29. Sadeque AJ et al. (2000) Increased drug delivery to the brain by P-glycoprotein inhibition. *Clin Pharmacol Ther* **68:**231-237.

30. Tayrouz Y et al. (2001) Ritonavir increases loperamide plasma concentrations without evidence for P-glycoprotein involvement. *Clin Pharmacol Ther* **70:**405-414.

31. Pauli-Magnus C et al. (2003) No effect of MDR1 C3435T variant on loperamide disposition and central nervous system effects. *Clin Pharmacol Ther* **74:**487-498.

32. Skarke C et al. (2003) Effects of ABCB1 (multidrug resistance transporter) gene mutations on disposition and central nervous effects of loperamide in healthy volunteers. *Pharmacogenetics* **13:**651-660.

33. Niemegeers CJ et al. (1979) Dissociation between opiate-like and antidiarrheal activities of antidiarrheal drugs. *J Pharmacol Exp Ther* **210:**327-333.

34. Kalvass JC et al. (2004) Use of loperamide as a phenotypic probe of mdr1a status in CF-1 mice. *Pharm Res* **21:**1867-1870.

35. Zong J and Pollack GM (2000) Morphine antinociception is enhanced in mdr1a gene-deficient mice. *Pharm Res* **17:**749-753.

36. Thompson SJ et al. (2000) Opiate-induced analgesia is increased and prolonged in mice lacking P-glycoprotein. *Anesthesiology* **92:**1392-1399.

37. Adachi Y et al. (2001) Comparative studies on in vitro methods for evaluating in vivo function of MDR1 P-glycoprotein. *Pharm Res* **18:**1660-1668.

38. Hsiao P et al. (2006) Verapamil P-glycoprotein transport across the rat blood-brain barrier: cyclosporine A concentration-inhibition analysis and comparison with human data. *J Pharmacol Exp Ther*.

39. Skarke C et al. (2003) Respiratory and miotic effects of morphine in healthy volunteers when P-glycoprotein is blocked by quinidine. *Clin Pharmacol Ther* **74:**303-311.

40. Reef VB et al. (1995) Treatment of atrial fibrillation in horses: new perspectives. *J Vet Intern Med* **9:**57-67.

41. Harper CM and Engel AG (1998) Safety and efficacy of quinidine sulfate in slow-channel congenital myasthenic syndrome. *Ann N Y Acad Sci* **841:**203-206.

42. Marzolini C et al. (2004) Polymorphisms in human MDR1 (P-glycoprotein): recent advances and clinical relevance. *Clin Pharmacol Ther* **75:**13-33.

43. Lankas GR et al. (1997) P-glycoprotein deficiency in a subpopulation of CF-1 mice enhances avermectin-induced neurotoxicity. *Toxicol Appl Pharmacol* **143:**357-365.

44. Paul AJ et al. (1987) Clinical observations in collies given ivermectin orally. *Am J Vet Res* **48:**684-685.

45. Umbenhauer DR et al. (1997) Identification of a P-glycoprotein-deficient subpopulation in the CF-1 mouse strain using a restriction fragment length polymorphism. *Toxicol Appl Pharmacol* **146:**88-94.

46. Chen W et al. (2002) Evaluation of the permeation characteristics of a model opioid peptide, H-Tyr-D-Ala-Gly-Phe-D-Leu-OH (DADLE), and its cyclic prodrugs across

the blood-brain barrier using an in situ perfused rat brain model. *J Pharmacol Exp Ther* **303:**849-857.

47. Cisternino S et al. (2003) In vivo saturation of the transport of vinblastine and colchicine by P-glycoprotein at the rat blood-brain barrier. *Pharm Res* **20:**1607-1611.

48. Dagenais C et al. (2004) Variable modulation of opioid brain uptake by P-glycoprotein in mice. *Biochem Pharmacol* **67:**269-276.

49. Arboix M et al. (1997) Multidrug resistance-reversing agents increase vinblastine distribution in normal tissues expressing the P-glycoprotein but do not enhance drug penetration in brain and testis. *J Pharmacol Exp Ther* **281:**1226-1230.

50. Choo EF et al. (2000) Pharmacological inhibition of P-glycoprotein transport enhances the distribution of HIV-1 protease inhibitors into brain and testes. *Drug Metab Dispos* **28:**655-660.

51. Hendrikse NH et al. (1998) Complete in vivo reversal of P-glycoprotein pump function in the blood-brain barrier visualized with positron emission tomography. *Br J Pharmacol* **124:**1413-1418.

52. Bart J et al. (2003) Quantitative assessment of P-glycoprotein function in the rat blood-brain barrier by distribution volume of [11C]verapamil measured with PET. *Neuroimage* **20:**1775-1782.

53. Kemper EM et al. (2003) Increased penetration of paclitaxel into the brain by inhibition of P-Glycoprotein. *Clin Cancer Res* **9:**2849-2855.

54. Chen C and Pollack GM (1999) Enhanced antinociception of the model opioid peptide [D-penicillamine] enkephalin by P-glycoprotein modulation. *Pharm Res* **16:**296-301.

55. Savolainen J et al. (2002) Effects of a P-glycoprotein inhibitor on brain and plasma concentrations of anti-human immunodeficiency virus drugs administered in combination in rats. *Drug Metab Dispos* **30:**479-482.

56. Barraud de Lagerie S et al. (2004) Cerebral uptake of mefloquine enantiomers with and without the P-gp inhibitor elacridar (GF1210918) in mice. *Br J Pharmacol* **141:**1214-1222.

57. Polli JW et al. (1999) Role of P-glycoprotein on the CNS disposition of amprenavir (141W94), an HIV protease inhibitor. *Pharm Res* **16:**1206-1212.

58. Letrent SP et al. (1999) Effects of a potent and specific P-glycoprotein inhibitor on the blood-brain barrier distribution and antinociceptive effect of morphine in the rat. *Drug Metab Dispos* **27:**827-834.

59. Kemper EM et al. (2004) The influence of the P-glycoprotein inhibitor zosuquidar trihydrochloride (LY335979) on the brain penetration of paclitaxel in mice. *Cancer Chemother Pharmacol* **53:**173-178.

60. Desrayaud S et al. (1997) Effect of the P-glycoprotein inhibitor, SDZ PSC 833, on the blood and brain pharmacokinetics of colchicine. *Life Sci* **61:**153-163.

61. Lemaire M et al. (1996) Dose-dependent brain penetration of SDZ PSC 833, a novel multidrug resistance-reversing cyclosporin, in rats. *Cancer Chemother Pharmacol* **38:**481-486.

62. Kusuhara H et al. (1997) P-Glycoprotein mediates the efflux of quinidine across the blood-brain barrier. *J Pharmacol Exp Ther* **283:**574-580.

63. Fromm MF et al. (1999) Inhibition of P-glycoprotein-mediated drug transport: A unifying mechanism to explain the interaction between digoxin and quinidine [seecomments]. *Circulation* **99:**552-557.

64. Malingre MM et al. (2000) Phase I and pharmacokinetic study of oral paclitaxel. *J Clin Oncol* **18:**2468-2475.

65. Weiss J and Haefeli WE (2005) Evaluation of inhibitory potencies for compounds inhibiting P-glycoprotein but without maximum effects: f2-values. *Drug Metab Dispos*.

66. Ward KW and Azzarano LM (2004) Preclinical pharmacokinetic properties of the P-glycoprotein inhibitor GF120918A in the mouse, rat, dog, and monkey. *J Pharmacol Exp Ther*.

67. Malingre MM et al. (2001) Co-administration of GF120918 significantly increases the systemic exposure to oral paclitaxel in cancer patients. *Br J Cancer* **84:**42-47.

68. Heel RC et al. (1982) Ketoconazole: a review of its therapeutic efficacy in superficial and systemic fungal infections. *Drugs* **23:**1-36.

69. Callies S et al. (2004) Population pharmacokinetic model for daunorubicin and daunorubicinol coadministered with zosuquidar.3HCl (LY335979). *Cancer Chemother Pharmacol* **54:**39-48.

70. Newman MJ et al. (2000) Discovery and characterization of OC144-093, a novel inhibitor of P-glycoprotein-mediated multidrug resistance. *Cancer Res* **60:**2964-2972.

71. Chi KN et al. (2005) A phase I pharmacokinetic study of the P-glycoprotein inhibitor, ONT-093, in combination with paclitaxel in patients with advanced cancer. *Invest New Drugs* **23:**311-315.

72. Simon N et al. (1998) Role of lipoproteins in the plasma binding of SDZ PSC 833, a novel multidrug resistance-reversing cyclosporin. *Br J Clin Pharmacol* **45:**173-175.

73. Wigler PW and Patterson FK (1994) Reversal agent inhibition of the multidrug resistance pump in human leukemic lymphoblasts. *Biochim Biophys Acta* **1189:**1-6.

74. Roy L et al. (2002) Quinine pharmacokinetics in chronic haemodialysis patients. *Br J Clin Pharmacol* **54:**604-609.

75. Solary E et al. (2003) Quinine as a multidrug resistance inhibitor: a phase 3 multicentric randomized study in adult de novo acute myelogenous leukemia. *Blood* **102:**1202-1210.

76. Ekins S et al. (2002) Three-dimensional quantitative structure-activity relationships of inhibitors of P-glycoprotein. *Mol Pharmacol* **61:**964-973.

77. van Zuylen L et al. (2000) Role of intestinal P-glycoprotein in the plasma and fecal disposition of docetaxel in humans. *Clin Cancer Res* **6:**2598-2603.

78. van Zuylen L et al. (2002) Disposition of docetaxel in the presence of P-glycoprotein inhibition by intravenous administration of R101933. *Eur J Cancer* **38:**1090-1099.

79. Lee BH et al. (2003) Differential effects of the optical isomers of KR30031 on cardiotoxicity and on multidrug resistance reversal activity. *Anticancer Drugs* **14:**175-181.

80. Eichelbaum M et al. (1984) Pharmacokinetics of (+)-, (-)- and (+/-)-verapamil after intravenous administration. *Br J Clin Pharmacol* **17:**453-458.

81. Tolcher AW et al. (1996) Phase I crossover study of paclitaxel with r-verapamil in patients with metastatic breast cancer. *J Clin Oncol* **14:**1173-1184.

82. Roe M et al. (1999) Reversal of P-glycoprotein mediated multidrug resistance by novel anthranilamide derivatives. *Bioorg Med Chem Lett* **9:**595-600.

83. Stewart A et al. (2000) Phase I trial of XR9576 in healthy volunteers demonstrates modulation of P-glycoprotein in CD56+ lymphocytes after oral and intravenous administration. *Clin Cancer Res* **6:**4186-4191.

84. Kharasch ED et al. (2003) Role of P-glycoprotein in the intestinal absorption and clinical effects of morphine. *Clin Pharmacol Ther* **74:**543-554.

85. Kharasch ED et al. (2004) Quinidine as a probe for the role of p-glycoprotein in the intestinal absorption and clinical effects of fentanyl. *J Clin Pharmacol* **44:**224-233.

86. Drewe J et al. (2000) Effect of P-glycoprotein modulation on the clinical pharmacokinetics and adverse effects of morphine. *Br J Clin Pharmacol* **50:**237-246.

Table 3.1. Relationship between P-gp inhibitor perfusate concentration and the degree of P-gp inhibition determined by *in situ* brain perfusion

Inhibitor EC_{50} (μM)	Inhibitor Concentration (μM)	Probe Substrate	Fold Change in Uptake Clearance	P-gp Inhibition*	Reference
GF120918	0.1	quinidine	3.1	73%	[46]
IC_{50} = 0.030 ± 0.009	0.4	quinidine	5.1	86%	
	1	quinidine	11	97%	
	4	quinidine	14	≥ 99%	
	10.5	quinidine	11	98%	
GF120918	10	AOA-DADLE	61	≥ 99%	[46]
IC_{50} not determined	10	CA-DADLE	190	≥ 99%	
	10	OMCA-DADLE	120	≥ 99%	
PSC833	3	vinblastine	2.0	≥ 50%	[47]
$IC_{50} \leq 3$	3	colchicine	2.5	≥ 60%	
quinidine	4	loperamide	1.5	31%	[48]
IC_{50} = 10 ± 0.4	20	loperamide	2.8	64%	
	100	loperamide	9.6	90%	
quinidine	4	verapamil	1.1	10%	[48]
IC_{50} = 13.5 ± 0.6	20	verapamil	2.2	67%	
	200	verapamil	5.1	≥ 99%	
rifampin	500	quinidine	3.0	76%	[23]
EC_{50} = 170 ± 20	1000	quinidine	3.7	83%	
rifampin	50	verapamil	2.3	69%	[23]
IC_{50} = 21 ± 5	200	verapamil	3.4	86%	
	500	verapamil	4.9	97%	
verapamil	50	quinidine	5.9	95%	[23]
$IC_{50} << 50$	200	quinidine	6.1	95%	
	1000	quinidine	4.3	87%	

*P-gp inhibition was calculated by equation 5.

Table 3.2. Preclinical inhibition of P-gp at the BBB

Inhibitor MED_{50} (mg/kg)	Total Dose (mg/kg)	Probe Substrate	Fold Change in CNS Exposure	P-gp Inhibition*	Reference
amiodarone	25, IP	vinblastine	none	0%	[49]
MED_{50} > 25, IP					
cyclosporin A	1, IV	nelfinavir	none	3.0%	[50]
MED_{50} = 25, IV	4, IV	nelfinavir	1.3	36%	[50]
	12.5, IV	nelfinavir	1.8	30%	[50]
	25, IP	vinblastine	none	0%	[49]
	25, IV	nelfinavir	3.0	69%	[50]
	25, IV	$[C^{11}]$verapamil	3.3	73%	[51]
	50, IV	$[C^{11}]$verapamil	5.3	96%	[51]
	50, IV	$[C^{11}]$verapamil	5.8	≥ 83%	[52]
	50, PO	paclitaxel	1.5 ↓	na	[53]
	50, IV	nelfinavir	2.7	65%	[50]
	175, IP	vinblastine	none	0%	[49]
	200, IP	vinblastine	none	0%	[49]
GF120918	5, IV	DPDPE	1.6	44%	[54]
(Elacridar)	10, IV	nelfinavir	100	≥ 99%	[55]
MED_{50} = 10, IV	10, IP	mefloquine	1.5	≥ 33%	[56]
	50, PO	paclitaxel	3.1	78%	[53]
	100, PO	paclitaxel	4.8	91%	[53]
	100, PO	DPDPE	2.0	71%	[54]
	100, IP	DPDPE	2.7 ↓	na	[54]
	200, PO	paclitaxel	5.2	92%	[53]
	1000, PO	DPDPE	3.0	93%	[54]
	1000, PO	amprenavir	6.7	92%	[57]
	2000, PO	morphine	2.6	≥ 62%	[58]
indinavir	50, IV	nelfinavir	1.3	25%	[50]
MED_{50} > 50, IV					
itraconazol	50, PO	paclitaxel	5.8 ↓	na	[53]
MED_{50} > 50, PO					
ketoconazole	50, IV	nelfinavir	2.0	53%	[50]
MED_{50} = 50, IV					
LY-335979	1, IV	nelfinavir	1.4	38%	[50]
(zosuquidar)	4, IV	nelfinavir	4.1	76%	[50]
MED_{50} = 4, IV	12.5, IV	nelfinavir	11	91%	[50]
	20, IV	paclitaxel	3.2	78%	[59]
	20, IV	paclitaxel	1.3	29%	[59]
	25, PO	paclitaxel	2.2	63%	[59]
	25, IV	nelfinavir	14	92%	[50]
	50, IV	nelfinavir	18	94%	[50]
	80, PO	paclitaxel	3.2	79%	[59]
nelfinavir	50, IV	nelfinavir	none	0%	[50]
MED_{50} > 50, IV					

*P-gp inhibition was calculated by equation 5 or 6.

Table 3.2. continued

Inhibitor MED_{50} (mg/kg)	Total Dose (mg/kg)	Probe Substrate	Fold Change in CNS Exposure	P-gp Inhibition*	Reference
PSC833	1, IV	nelfinavir	1.1 ↓	na	[50]
(valspodar)	4, IV	nelfinavir	3.1	71%	[50]
MED_{50} = 4, IV	9.3, IV	colchicines	> 3.8	≥ 74%	[60]
	10, IV	cyclosporin A	5.0	≥ 80%	[61]
	10, IV	cyclosporin A	5.0	≥ 80%	[61]
	10, IV	vincristine	2.0	≥ 50%	[61]
	10, IV	quinidine	16	97%	[62]
	10, IV	methadone	6.0	≥ 83%	[18]
	10, IV	methadone	4.0	≥ 75%	[18]
	12.5, IV	nelfinavir	12	92%	[50]
	25, PO	paclitaxel	2.2	62%	[53]
	25, IV	nelfinavir	6.9	87%	[50]
	50, IV	nelfinavir	4.8	79%	[50]
	75, PO	paclitaxel	2.4	67%	[53]
quinidine	10, IP	vinblastine	none	0%	[49]
MED_{50} > 100, IP	50, IP	vinblastine	none	0%	[49]
	50, IV	nelfinavir	1.7 ↓	na	[50]
	100, IP	digoxin	none	0%	[63]
rifampin	50, IP	verapamil	1.8	53%	[23]
MED_{50} = 50, IP	50, IP	quinidine	none	na	[23]
	75, IP	verapamil	2.4	72%	[23]
	75, IP	quinidine	none	na	[23]
	100, IP	verapamil	3.0	82%	[23]
	100, IP	quinidine	1.5	40%	[23]
	150, IP	verapamil	3.2	84%	[23]
	150, IP	quinidine	1.8	52%	[23]
ritonavir	25, IV	nelfinavir	1.3	25%	[50]
MED_{50} > 1000, PO	1000, PO	amprenavir	2.4 ↓	na	[57]
saquinavir	50, IV	nelfinavir	none	0%	[50]
MED_{50} > 50, IV					
trifluoperazine	25, IP	vinblastine	none	0%	[49]
MED_{50} > 175, IP	50, IP	vinblastine	none	0%	[49]
	175, IP	vinblastine	none	0%	[49]
verapamil	12.5, IV	nelfinavir	1.1 ↓	na	[50]
MED_{50} = 100, IP	25, IP	vinblastine	none	0%	[49]
	50, IP	vinblastine	none	0%	[49]
	100, IP	DPDPE	4.2	54%	[54]

*P-gp inhibition was calculated by equation 5 or 6.

Table 3.3. In vitro potency and C_{max} of P-gp inhibitors tested clinically

Inhibitor	K_i or IC_{50} (μM)	f_u	C_{max} (μM)	Total C_{max}/K_i	Unbound C_{max}/K_i	References
cyclosporin A	0.2	0.10	3.2	16	1.6	14 16 64
GF120918 (Elacridar)	0.011	< 0.001	0.77	70	< 0.07	65 66 67
ketoconazole	0.15	0.01	6.6	44	0.44	65 68 16
LY335979 (Zosuquidar)	0.001	0.0005*	1.3	130	0.66	65 69
OC144-093 (ONT-093)	0.032	na	8.9	280	na	70 71
PSC833 (Valspodar)	0.02	0.022	6.1	150	3.3	65 72 24
quinidine	2.4	0.16	19	7.7	1.2	65 16 16
quinine	> 2.4	0.063	24	< 11	< 0.69	73 74 75
rifampin	26[†]	0.20	50	1.9	0.38	23 16 16
ritonavir	3.8	0.015	16	4.2	0.063	76 16 16
R101933 (Laniquidar)	~0.085	< 0.02	6.3	~74	< 1.5	77 78
R-verapamil	2.6	0.064	5.1	2.0	0.13	79 80 81
verapamil	0.55	0.11	0.88	1.6	0.18	65 80 16
XR9576 (Tariquidar)	0.016	na	> 0.31	> 19	na	82 83

* Unpublished observation

[†] unbound IC_{50} determined from in vivo mouse studies (mouse plasma fu = 0.12, unpublished observation)

Table 3.4. Clinical studies evaluating CNS activity of loperamide and altered P-gp function at the blood brain barrier

Study design	Fold Δ Systemic Exposure	Altered CNS Activity	Calculated P-gp Inhibition[1]	Theoretical Increase in CNS Penetration[2]	Theoretical CNS Equivalent Dose[3]	Ref
loperamide (2mg), PO Standard dose	none	No	none	none	2	
loperamide (16mg), PO MDR1 gene phenotyping	none	No	none	none	16	[31]
loperamide (16 mg) , PO P-gp inhibition w/ ritonavir (600 mg), PO	1.2	No	12%	1.1	21	[30]
loperamide (16 mg) , PO P-gp inhibition w/ quinidine (600 mg), PO	2.5	Yes	31%	1.4	58	[29]
loperamide (24 mg) , PO MDR1 gene phenotyping P-gp inhibition w/ quinidine (800 mg), PO	2.0 to 3.1	Yes/No	51%	2.0	93 to 150	[32]
loperamide (60 mg) , PO Dose escalation	none	No	none	none	60	[27]

[1] P-gp inhibition calculated from inhibitor fu, observed C_{max}, and K_i according equation 2.
[2] The theoretical increase in CNS penetration was calculated by equation 1.
[3] Calculated by multiplying the (dose of loperamide) x (Δ systemic exposure) x (theoretical increase in CNS penetration)

Table 3.5. Effect of P-gp inhibitor on central activity of suspected P-gp substrates

Probe substrate	Dose	Fold Δ Systemic Exposure	Altered CNS Activity	Ref
morphine (0.15 mg/kg/hr) IV infusion over 1 hr	quinidine 600 mg, PO	not reported	No	[84]
morphine (30 mg/kg), PO	quinidine 600 mg, PO	1.9	minimal; no change in plasma concentration effect relationship	[84]
morphine (0.11 mg/kg/hr) IV infusion over 3 hr	quinidine 800 mg, PO	none	No	[39]
fentanyl (30 µg/kg/hr) IV infusion over 0.083 hr	quinidine 600 mg, PO	not determined	minimal	[85]
fentanyl (2.5 µg/kg), PO	quinidine 600 mg, PO	2.6	yes	[85]
methadone (120 mg/kg/hr) IV infusion over 0.083 hr	quinidine 600 mg, PO	not determined	no	[20]
methadone (10 mg/kg), PO	quinidine 600 mg, PO	increased concentrations during absorptive phase	minimal; no change in plasma concentration effect relationship	[20]
morphine (0.05 mg/kg/hr) IV infusion over 2hr	PSC833 (1 mg/kg/hr) IV infusion over 2hr	none	No	[86]

CHAPTER 4

USE OF PLASMA AND BRAIN UNBOUND FRACTIONS TO ASSESS THE EXTENT OF BRAIN DISTRIBUTION OF THIRTY-FOUR DRUGS: COMPARISON OF UNBOUND CONCENTRATION RATIOS TO *IN VIVO* P-GLYCOPROTEIN EFFLUX RATIOS

This chapter has been submitted for publication in *Drug Metabolism and Disposition* and is presented in the style of that journal.

Abstract

The P-glycoprotein (P-gp)-deficient mouse model is used to assess the influence of P-gp-mediated efflux on the central nervous system (CNS) distribution of drugs. The steady-state unbound plasma-to-unbound brain concentration ratio ($[plasma]_{,u}/[brain]_{,u}$) is an alternative method for assessing CNS distribution of drugs independent of the mechanism(s) involved. The objective of this study was to compare the degree of CNS distributional impairment determined from the *in vivo* P-gp efflux ratio to that determined from the $[plasma]_{,u}/[brain]_{,u}$ ratio. CNS distribution of 34 drugs, including opioids, triptans, protease inhibitors, antihistamines, and other clinically-relevant drugs with either poor CNS distribution or blood-brain barrier (BBB) efflux, was studied. Plasma and brain unbound fractions were determined by equilibrium dialysis. $K_{p,brain}$ and the P-gp efflux ratio were obtained from the literature or determined experimentally. The P-gp efflux ratio and the $[plasma]_{,u}/[brain]_{,u}$ ratio were in concurrence (<3-fold difference) for 21 of the 34 drugs. However, the $[plasma]_{,u}/[brain]_{,u}$ ratio exceeded the P-gp efflux ratio substantially (>4-fold) for 10 of the 34 drugs, suggesting that other, non-P-gp-mediated mechanism(s) may limit the CNS distribution of these drugs. The P-gp efflux ratio exceeded the $[plasma]_{,u}/[brain]_{,u}$ ratio by more than 3-fold for 3 drugs, suggesting the presence of active uptake mechanism(s). These observations indicate that when mechanisms other than P-gp affect CNS distribution (non-P-gp-mediated efflux, poor passive permeability, cerebrospinal fluid (CSF) bulk flow, metabolism, or active uptake), the P-gp efflux ratio may under- or over-estimate CNS distributional impairment. The $[plasma]_{,u}/[brain]_{,u}$ ratio provides a simple mechanism-independent alternative for assessing the CNS distribution of drugs.

Introduction

The efflux transporter P-glycoprotein (P-gp) attenuates the CNS distribution of many drugs, including opioids, triptans, protease inhibitors, and antihistamines. One method used to assess the influence of P-gp on the CNS distribution of compounds is the P-gp-deficient mouse model. The P-gp efflux ratio, calculated from the ratio of brain-to-plasma partition coefficient ($K_{p,brain}$) in P-gp-deficient (*mdr1a*-/-) mice to $K_{p,brain}$ in P-gp-competent (*mdr1a*+/+) mice, reflects the degree to which P-gp-mediated efflux attenuates CNS distribution. However, when other processes influence CNS distribution, the P-gp efflux ratio may be a poor indicator of the degree to which CNS distribution of a compound is impaired.

$K_{p,brain}$ is the most widely used *in vivo* parameter for assessing the extent of CNS distribution. A common assumption is that compounds with large $K_{p,brain}$ values have more extensive CNS distribution than compounds with small $K_{p,brain}$ values. For example, a $K_{p,brain}$ $\geq$1 is often used as an arbitrary cutoff to classify compounds as having "good" CNS distribution, while a $K_{p,brain}$ <<1 is used to classify compounds as having "poor" CNS distribution. While this type of classification is common, it may be misleading. It is recognized that tissue partition coefficients such as $K_{p,brain}$ are influenced by the relative binding affinity of a substrate for proteins in plasma versus the proteins in the tissue in question (Gillette, 1971; Kurz et al., 1997). For a compound that distributes solely by passive diffusion, at distribution equilibrium the unbound concentration in tissue will equal the unbound concentration in plasma, and the steady-state tissue partition coefficient is simply a function of the relative plasma and tissue unbound fractions (i.e., $K_{p,tissue} = f_{u,plasma} / f_{u,tissue}$). When brain and plasma unbound fractions are similar, than a $K_{p,brain}$ ~1 would be

consistent with unrestricted distribution solely by passive processes. However, the $K_{p,brain}$ value by itself provides little information without knowledge of brain and plasma unbound fractions. A $K_{p,brain}$ value <1 could be the result of more extensive binding to plasma proteins than to proteins in brain tissue. Alternatively, a $K_{p,brain}$ value <1 it could reflect significant impairment in CNS distribution due to processes such as efflux transport at the blood-brain barrier (BBB).

Several recent literature reports have utilized the $f_{u,plasma}/f_{u,brain}$ ratio to predict $K_{p,brain}$ and to assess the CNS distribution of compounds. In one published account, the utility of the $f_{u,plasma}/f_{u,brain}$ ratio to predict the $K_{p,brain}$ of CNS discovery compounds was assessed (Kalvass and Maurer, 2002). As expected, the $f_{u,plasma}/f_{u,brain}$ ratio predicted the $K_{p,brain}$ for compounds that did not evidence active efflux at the BBB, and over-predicted $K_{p,brain}$ when active efflux at the BBB limited brain uptake. The degree to which the $f_{u,plasma}/f_{u,brain}$ ratio over-predicted $K_{p,brain}$ was identical to the P-gp efflux ratio for the single member of the compound set for which the P-gp efflux ratio had been determined. Another study used the $f_{u,plasma}/f_{u,brain}$ ratio to predict $K_{p,brain}$ and to assess the CNS distribution of 33 marketed CNS drugs (Maurer et al., 2004). The $f_{u,plasma}/f_{u,brain}$ ratio predicted the $K_{p,brain}$ value for the majority of CNS drugs (25 of 33), indicating that most CNS drugs do not have impaired CNS distribution. In those cases for which the $f_{u,plasma}/f_{u,brain}$ ratio did not predict $K_{p,brain}$, the discrepancy could be explained by active efflux or poor BBB permeability. More recently, for compounds subject to active efflux, the $f_{u,plasma}/f_{u,brain}$ ratio combined with *in vitro* efflux data was shown to provide superior estimates of $K_{p,brain}$ as compared to the $f_{u,plasma}/f_{u,brain}$ ratio alone (Summerfield et al., 2005).

When CNS distribution is impaired, the $f_{u,plasma}/f_{u,brain}$ ratio over-predicts $K_{p,brain}$. The magnitude of the over-prediction is reflective of the degree to which unbound plasma concentrations exceed unbound brain concentrations (eq. 1).

$$\text{Magnitude of over - prediction} = \frac{\left(\frac{f_{u,plasma}}{f_{u,brain}}\right)}{K_{p,brain}} = \frac{\left(\frac{f_{u,plasma}}{f_{u,brain}}\right)}{\frac{[brain]}{[plasma]}} = \frac{[plasma]_u}{[brain]_u} \qquad \text{(eq. 1)}$$

As shown in equation 1, the $f_{u,plasma}/f_{u,brain}$ ratio and $K_{p,brain}$ can be used to calculate the unbound plasma-to-unbound brain concentration ratio $[plasma]_{,u}/[brain]_{,u}$. The $[plasma]_{,u}/[brain]_{,u}$ ratio represents the degree to which unbound plasma concentrations exceed unbound brain concentrations and is meaningful expression of the degree of impairment in CNS distribution. A $[plasma]_{,u}/[brain]_{,u}$ ratio of unity for a given compound, is indicative of unimpaired CNS distribution (i.e., distribution consistent with passive diffusion; $[plasma]_u = [brain]_u$), while a $[plasma]_{,u}/[brain]_{,u}$ ratio greater than unity indicates impairment in CNS distribution (i.e., efflux uptake or poor BBB permeability; $[plasma]_u > [brain]_u$). In contrast, a $[plasma]_{,u}/[brain]_{,u}$ ratio values less than unity is consistent with enhanced CNS distribution (i.e., active uptake; $[plasma]_u < [brain]_u$).

The $[plasma]_{,u}/[brain]_{,u}$ ratio is expected to be equal to the *in vivo* P-gp efflux if P-gp-mediated efflux is the only active process affecting brain disposition. Using this principle, the present study was conducted to compare the degree of CNS distributional impairment expressed as the $[plasma]_{,u}/[brain]_{,u}$ ratio to the P-gp efflux ratio for 34 marketed drugs. Opioids, triptans, protease inhibitors, and antihistamines (n = 24 total) were included in this

analysis because these classes of agents are known to include P-gp substrates, and the extent to which these compounds distribute into the CNS may have important implications regarding safety and efficacy. In addition, 10 marketed drugs from various drug classes with either poor CNS distribution or BBB efflux also were included as part of the analysis.

Material and Methods

Materials. Sufentanil was obtained from Abbott Laboratories (North Chicago, IL). Amprenavir, indinavir, nelfinavir, ritonavir, and saquinavir were obtained through the NIH AIDS Research and Reference Reagent Program, Division of AIDS, NIAID, NIH (Rockville, MD). Olanzapine was obtained from Pfizer Global Material Management (Groton, CT). Eletriptan was extracted from 40-mg tablets obtained from the Roerig Division of Pfizer (New York, NY), and the raw extract was used as a stock solution. Cetirizine, desloratadine, rizatriptan, and zolmitriptan were purchased from Sequoia Research (Oxford, UK). Alfentanil was obtained from Taylor Pharmaceuticals (Decatur, IL). Naratriptan and sumatriptan were purchased from U.S. Pharamcopoeia (Rockville, MD). All other drugs were purchased from Sigma-Aldrich (St. Louis, MO). Solvents and other reagents were obtained from common sources and were of reagent grade or better.

Drug Selection. Twenty-four marketed drugs from four main drug classes (7 opioids, 5 triptans, 5 protease inhibitors, and 7 antihistamines) were chosen for this study because drugs within each class exhibit varying degrees of interaction with BBB P-gp and because the extent of CNS distribution is known to be important to the efficacy and/or toxicity of these drug classes. In addtion, 10 marketed drugs from other drug classes with either poor CNS

distribution or BBB efflux also were chosen to assess the general utility of the approach with as diverse a dataset as possible.

Animals. Male CF-1 *mdr1a*(+/+) and *mdr1a*(-/-) mice (30-40 g; Charles River Laboratories, Inc., Wilmington, MA) were maintained on a 12-h light/dark cycle in a temperature- and humidity-controlled room with access to water and food ad libitum. All procedures involving mice were approved by The Institutional Animal Care and Use Committee of the University of North Carolina and were conducted in accordance with "Principles of Laboratory Animal Care" (NIH Publication No. 85-23, revised in 1985).

Determination of $K_{p,brain}$ from animal studies. $K_{p,brain}$ values in *mdr1a*(-/-) and *mdr1a*(+/+) mice were obtained from the literature or, when published values were not available, were determined experimentally. Separate pharmacokinetic studies were conducted in *mdr1a*(-/-) and *mdr1a*(+/+) mice to determine the $K_{p,brain}$ values for alfentanil, fentanyl, loperamide, and methadone. Briefly, mice received a subcutaneous dose of the opioid, and at designated time points (9 time points, n=4 animals per time point) mice were sacrificed and trunk blood and brain tissue were collected. Plasma was harvested following centrifugation. Brain and plasma samples were stored at -20°C until analysis by HPLC-MS/MS (see below). $K_{p,brain}$ was determined from the ratio of brain to plasma $AUC_{0-\infty}$. $K_{p,brain}$ values for cimetidine, meperidine, ranitidine, and sufentanil were determined under steady-state conditions in *mdr1a*(-/-) and *mdr1a*(+/+) mice. Briefly, osmotic mini pumps (Alzet, Cupertino, CA) were implanted subcutaneously per the manufacture's instructions. Mice were sacrificed and trunk blood and brain tissue collected (n=3) 24 hr later. Plasma was harvested following centrifugation, and brain and plasma samples were stored at -20°C until analysis by HPLC-MS/MS (see below). $K_{p,brain}$ was calculated from the ratio of the 24-

hr brain and plasma concentrations. All other $K_{p,brain}$ values were obtained from the literature.

Equilibrium dialysis experiments. Plasma and brain unbound fractions were determined in a 96-well equilibrium dialysis apparatus (HTDialysis, Gales Ferry, CT) using a previously reported method (Kalvass and Maurer, 2002). Briefly, fresh CF-1 or FVB mouse plasma and brain tissue were obtained the day of the study. Spectra-Por 2 membranes obtained from Spectrum Laboratories Inc. (Rancho Dominguez, CA) were conditioned in HPLC-grade water for 15 min, followed by 30% ethanol for 15 min and 100 mM sodium phosphate buffer (pH 7.4) for 15 min. Brain tissue was diluted 3-fold with 100 mM sodium phosphate buffer (pH 7.4) and homogenized with a sonic probe. The drug of interest was added to plasma and brain homogenate to achieve a final concentration of 3 and 1 μM, respectively; 150-μl aliquots (n=6) were loaded into the 96-well equilibrium dialysis apparatus and dialyzed against and equal volume of 100 mM sodium phosphate (pH 7.4) buffer. The 96-well equilibrium dialysis apparatus was incubated for 4.5 hr in a 155 rpm shaking water bath maintained at 37˚C. Prior experience with the equilibrium dialysis apparatus indicated that equilibrium would be achieved by 4.5 hr (data not shown). After 4.5 hr, 10 μl of matrix sample (plasma or brain homogenate) and 50 μl of buffer sample were removed from the apparatus and added directly to HPLC vials containing 100 μl of methanol containing an appropriate internal standard. A 50-μl aliquot of control buffer was added to the brain homogenate and plasma samples, and either a 10-μl aliquot of control brain homogenate or control plasma was added to the buffer samples to yield identical sample composition between buffer and non-buffer samples. The samples were vortex-mixed, centrifuged, and the supernatant was analyzed by HPLC-MS/MS. Plasma unbound fraction was calculated

from the ratio of concentrations determined from the plasma and buffer samples. Equation 2, a previously described approach to account for the effect of tissue dilution on unbound fraction (Kalvass and Maurer, 2002), was used to calculate the brain unbound fraction:

$$\text{Undiluted } f_u = \frac{1/D}{((1/f_{u,measured}) - 1) + 1/D} \qquad \text{(eq. 2)}$$

where D represents the fold dilution of brain tissue and $f_{u,measured}$ is the ratio of concentrations determined from the buffer and brain homogenate samples

HPLC-MS/MS Analysis of samples. All samples were quantified using either a PE-Sciex API-3000 (Turbo Ionspray source, 500˚C) or an API-4000 (Turbo V Ionspray source, 700˚C, PerkinElmerSciex Instruments, Boston, MA) quadruple mass spectrometer as summarized in Table 4.1. Equilibrium dialysis samples were prepared as described in the equilibrium dialysis section. Plasma and brain samples from animal experiments were prepared as follows. Brain samples were homogenized in water (1:2 v/v) with a sonic probe. An aliquot of homogenate or serum (2 to 25 µl) was transferred to a HPLC vial, and protein was precipitated with 4- to 125-volumes of methanol containing an appropriate internal standard. The sample was vortex-mixed, centrifuged, and the supernatant was analyzed by HPLC-MS/MS. Samples were injected (2-10 µl; CTC Analytics autosampler, Zwingen, Switzerland) onto either a Phenomenex 2.0 × 30 mm, 5 µm Gemini 110A or a Phenomenex 2.0 × 30 mm, 4 µm Synergi Max-RP column (Phenomenex, Torrance, CA) maintained at room temperature. The total run time was 3 min. Analytes were eluted with a linear gradient consisting of ammonium acetate (pH 6.8; 10 mM) ["A"], methanol ["B"] and acetonitrile ["C"] produced by three Shimadzu LC-10ADVP binary pumps. An initial condition (80-95% "A") was ramped to an intermediate condition (5-25% "A") over 2 min, held for 0.5 min at the intermediate condition, and then returned initial conditions in a single step to re-

equilibrate the column (Table 4.1). During the run, the flow rate was increased from 750 to 1500 µl/min over the first 2 min, held at 1500 µl/min for 1 min, and then returned to the initial flow rate of 750 µl/min in a single step. For samples run on the API3000, the flow rate was increased from 500 to750 µl/min over the first 2 min, held at 750 µl/min for 1 min, and then returned to the initial flow rate of 500 µl/min in a single step. The entire column effluent was diverted from the source of the quadrupole mass spectrometer for the first 0.8 min and final 0.5 min of the run. Standards were prepared with either plasma or brain homogenate and were identical in final composition to corresponding samples.

Data analysis. The *in vivo* P-gp efflux ratio for each drug was calculated as the ratio of *mdr1a*(-/-) and *mdr1a*(+/+) $K_{p,brain}$ values. The steady-state $[plasma]_{,u}/[brain]_{,u}$ ratio was calculated for each drug according to equation 3, where $K_{p,brain}$ is the value from P-gp competent mice.

$$\frac{[plasma]_u}{[brain]_u} = \frac{1}{K_{p,brain,}} \times \frac{f_{u,plasma}}{f_{u,brain}} \qquad \text{(eq. 3)}$$

The P-gp efflux ratio and $[plasma]_{,u}/[brain]_{,u}$ ratio were used to assess the distributional behavior of each drug based on the graphical scheme in Figure 4.1. The horizontal and vertical lines represent the point at which the P-gp efflux ratio and the $[plasma]_{,u}/[brain]_{,u}$ ratio equal 3, respectively, as a ≥ 3-fold impairment in CNS distribution was considered meaningful. The figure was divided into four quadrants (I-IV) based on whether the P-gp efflux or $[plasma]_{,u}/[brain]_{,u}$ ratio values were greater than or less than 3. The solid line passing through the origin represents the line of identity ± 3-fold (dashed lines). Drugs were assessed as follows: quadrant I- impaired CNS distribution due to P-gp-mediated efflux; subsections Ia and Ib- impaired CNS distribution due to P-gp with other active process(es) present; quadrant II- impaired CNS distribution due to non-P-gp mechanism; quadrant III- no

impairment in CNS distribution; quadrant IV- P-gp substrate, but CNS distribution is not impaired due to the presence of a compensatory mechanism. The CNS distribution behavior of the protease inhibitors, opioids, antihistamines, and triptans were evaluated separately.

Results

The $K_{p,brain}$, $f_{u,plasma}$, and $f_{u,brain}$ values for all drugs included in this study are reported in Table 4.2. The $K_{p,brain}$ and $f_{u,brain}$ values varied by more than 4 orders of magnitude, whereas the $f_{u,plasma}$ values varied by more than 3 orders of magnitude, among the drugs studied. Vinblastine was unstable in mouse plasma, so the $f_{u,plasma}$ value was reported as equal to or greater than the $f_{u,plasma}$ value determined from the buffer concentrations, assuming complete mass balance.

The P-gp efflux ratio and the $[plasma]_{,u}/[brain]_{,u}$ ratio were compared within each drug class (opioid, antihistamine, triptan, and protease inhibitor; Figure 4.2 A, B, C, and D, respectively). The P-gp efflux ratio and the $[plasma]_{,u}/[brain]_{,u}$ ratio for all 34 drugs examined in this study are compared in Figure 4.3.

The P-gp efflux ratios varied between ~1 and 50 for the examined drugs; 18 of the 34 drugs had a P-gp efflux ratio exceeding 3. The $[plasma]_{,u}/[brain]_{,u}$ ratio varied between ~1 and >1000, with 23 of the 34 drugs having a $[plasma]_{,u}/[brain]_{,u}$ ratio greater than 3. The P-gp efflux ratio and the $[plasma]_{,u}/[brain]_{,u}$ ratio were in concurrence (<3-fold difference) for 21 of the 34 drugs (quadrants I and III). However, the $[plasma]_{,u}/[brain]_{,u}$ ratio exceeded the P-gp efflux ratio substantially (>4-fold) for cetirizine, cimetidine, dexamethasone, digoxin, doxorubicin, fexofenadine, ivermectin, ranitidine, sumatriptan and zolmitriptan (quadrants Ib

and II). The P-gp efflux ratio was more than 3-fold higher than the $[plasma]_{,u}/[brain]_{,u}$ ratio for methadone, ritonavir, and saquinavir (quadrant IV).

Discussion

The P-gp efflux ratio and the $[plasma]_{,u}/[brain]_{,u}$ ratio were in concurrence (<3-fold difference) for 21 of the 34 drugs studied. This concurrence indicates, that for most of the drugs examined, there was little difference between the P-gp efflux ratio and the $[plasma]_{,u}/[brain]_{,u}$ ratio, and that any impairment in CNS disposition would be consistent with P-gp-mediated efflux. The $[plasma]_{,u}/[brain]_{,u}$ ratio exceeded the P-gp efflux ratio substantially (>4-fold) for 10 of the 34 drugs studied (cetirizine, cimetidine, dexamethasone, digoxin, doxorubicin, fexofenadine, ivermectin, ranitidine, sumatriptan, and zolmitriptan), suggesting that other non-P-gp-mediated mechanism(s) may limit the CNS distribution of these drugs. The P-gp efflux ratio exceeded the $[plasma]_{,u}/[brain]_{,u}$ ratio by more than 3-fold for three of the drugs examined (methadone, ritonavir, and saquinavir), suggesting the presence of active uptake mechanism(s). The results for the opioids, triptans, protease inhibitors, and antihistamines are discussed separately in the following paragraphs.

Opioids. Consistent with their clinical use as analgesics, there was minimal impairment in CNS distribution (<3-fold as assessed by both the P-gp efflux ratio and the $[plasma]_{,u}/[brain]_{,u}$ ratio) for, sufentanil, fentanyl, morphine, and meperidine. Alfentanil evidenced modest impairment (~3-fold), consistent with P-gp-mediated efflux. Both methadone and loperamide were significant P-gp substrates (P-gp efflux ratios of 7 and 33, respectively). However, only loperamide had substantial impairment in CNS distribution as assessed by the $[plasma]_{,u}/[brain]_{,u}$ ratio.

The discrepancy between the P-gp efflux ratio and the $[plasma]_{,u}/[brain]_{,u}$ ratio for methadone may indicate the presence of one or more compensatory mechanism(s) (e.g., active uptake) that may have negated the impact of P-gp-mediated efflux. Methadone is a substrate for active uptake in the lung (Chi and Dixit, 1977), so it is plausible methadone also may undergo active uptake across the BBB. The $[plasma]_{,u}/[brain]_{,u}$ ratio predicted that loperamide alone would have substantially reduced central activity, whereas the P-gp efflux ratio predicted that both loperamide and methadone would evidence substantially reduced central activity. Clinically, only loperamide is associated with reduced central activity, so the $[plasma]_{,u}/[brain]_{,u}$ ratio was better able to differentiate between opioids with and without reduced central activity than the P-gp efflux ratio.

Triptans. The $[plasma]_{,u}/[brain]_{,u}$ ratio indicated that all triptans examined have impaired CNS distribution. However, only rizatriptan and eletriptan showed significant impairment due to P-gp (>3-fold). Non-P-gp-mediated mechanism(s) may be responsible for impaired CNS distribution of sumatriptan and zolmitriptan (quadrant II). One non-P-gp-mediated mechanism that may impair the CNS distribution of sumatriptan and zolmitriptan is CSF bulk flow. When passive permeability and brain uptake clearance are very low, CSF bulk flow may represent a significant clearing mechanism from the CNS, ultimately resulting in reduced CNS exposure (Shen et al., 2004). Because sumatriptan and zolmitriptan both have very low passive permeability [less than the paracellular marker mannitol; (Mahar Doan et al., 2002)], it is plausible that CSF bulk flow may limit sumatriptan and zolmitriptan CNS distribution.

If triptans possess a degree of CNS distributional impairment in humans similar to that indicated by the $[plasma]_{,u}/[brain]_{,u}$ ratio, the impaired distribution may have important

implications regarding mechanism of action and CNS side-effect profile of triptans. There is debate as to whether the anti-migraine action of triptans is solely through vascular-mediated events, or whether antinociceptive activity within the brain stem trigeminal nuclei is partially responsible (Dodick and Martin, 2004). In addition, the incidence of CNS side-effects varies between the different triptans. By understanding the inter-relationships between *in vivo* efficacy, incidence of CNS side-effects, and the extent of CNS distribution, the optimal CNS distributional characteristics of triptans may be deduced.

Protease Inhibitors. All of the protease inhibitors examined undergo significant P-gp efflux (P-gp efflux ratio $\geq$ 7, quadrant I and IV). However, the $[plasma]_{,u}/[brain]_{,u}$ ratio indicated that ritonavir and saquinavir, despite being P-gp substrates, do not have impaired CNS distribution (< 3-fold). This observation may be explained if a compensatory mechanism (i.e., active uptake) negates the impact of P-gp-mediated efflux. This explanation is supported by reports demonstrating that both ritonavir and saquinavir are substrates for uptake transporters (Anthonypillai et al., 2004; Su et al., 2004).

Even though it has been thought that ritonavir and saquinavir have poor CNS distribution because of significant P-gp-mediated efflux (in vivo P-gp efflux ratio > 5) and low $K_{p,brain}$ (0.17 and 0.13, respectively), this may not necessarily be the case. The $[plasma]_{,u}/[brain]_{,u}$ ratio indicates that steady-state unbound concentrations in plasma and brain are approximately equal for these agents. Compensatory uptake mechanism(s) may overcome the efflux by P-gp, and the low $K_{p,brain}$ values therefore would simply be a function of more extensive protein binding in plasma than in brain. The binding of ritonavir and saquinavir to plasma proteins is higher than that in the brain. Therefore, based on $f_{u,plasma}$ and $f_{u,brain}$, the $K_{p,brain}$ is expected to be 0.25 and 0.22, respectively, and the $[plasma]_{,u}/[brain]_{,u}$ ratio

indicates the BBB has no net effect on the CNS distribution of ritonavir and saquinavir. These observations suggest that compounds that evidence P-gp-mediated efflux together with low $K_{p,brain}$ ($K_{p,brain} << 1$) may not have impaired CNS distribution if active uptake counters the effects of P-gp efflux and if the low $K_{p,brain}$ can be explained by binding in plasma that exceeds binding in brain. Overall, ritonavir and saquinavir may have better CNS distribution, and thus may be more effective in combating HIV viral infection in the CNS, than previously thought.

Antihistamines. Consistent with their central activity, the sedating antihistamines triprolidine, diphenhydramine, and hydroxyzine had minimal impairment in CNS distribution (quadrant III). The non-sedating histamines desloratadine and cetirizine fell within quadrants I and Ib, respectively, indicating substantial impairment in CNS distribution due to P-gp-mediated efflux. However, the P-gp efflux ratio did not indicate impairment in CNS distribution of the non-sedating antihistamine fexofenadine, whereas the $[plasma]_{,u}/[brain]_{,u}$ ratio suggested significant impairment (quadrant II). Non-P-gp-mediated mechanism(s) may contribute to the impairment in CNS distribution of cetirizine and fexofenadine (quadrants Ib and II). Assuming that loratadine is a pro-drug of desloratadine, only the $[plasma]_{,u}/[brain]_{,u}$ ratio correctly distinguished between the sedating and non-sedating antihistamines.

Other drugs with poor CNS distribution or BBB efflux. Other marketed drugs with poor CNS distribution or BBB efflux were examined along with the opioids, triptans, protease inhibitors, and antihistamines (Figure 4.3). As expected, P-gp substrates such as quinidine, verapamil, and paclitaxel fell within quadrant I (consistent with P-gp being the only efflux mechanism), while efflux substrates for transporters other than P-gp such as ranitidine, digoxin, and doxorubicin fell within quadrants Ib and II (Figure 4.3 and Table 4.3).

Discrepancy between P-gp efflux ratio and the [plasma]$_{,u}$/[brain]$_{,u}$ ratio. The P-gp efflux ratio and the [plasma]$_{,u}$/[brain]$_{,u}$ ratio differed by more than 3-fold for 13 of the 34 drugs examined. In most cases, the difference can be explained by the physiochemical properties, and/or transport characteristics of the individual drugs (Table 4.3). Ten of the 13 drugs for which discrepancy was noted were located in either quadrant Ib or II, indicating more extensive impairment in CNS distribution than predicted by the P-gp efflux ratio. For these 10 drugs, six drugs (digoxin, doxorubicin, ivermectin, cimetidine, dexamethasone, and ranitidine) are known to be substrates for efflux transporters other than P-gp (Table 4.3), two (sumatriptan and zolmitriptan) have very low permeability values (less than mannitol), and two (cetirizine and fexofenadine) have reduced central activity relative to other drugs in the same class. The remaining three of the 13 drugs (methadone, ritonavir, and saquinavir) for which the P-gp efflux ratio and the [plasma]$_{,u}$/[brain]$_{,u}$ ratio differed by more than 3-fold were classified in quadrant IV, indicating less impairment in CNS distribution than indicated by the P-gp efflux ratio. One possible explanation for such drugs is the presence of a compensatory active uptake mechanism. Consistent with this explanation, all three of these drugs are substrates of active uptake (Table 4.3). Although not the intent of this work, additional detailed studies on individual drugs would be useful to confirm whether the discrepancy between the P-gp efflux ratio and the [plasma]$_{,u}$/[brain]$_{,u}$ ratio are real and are not experimental artifacts. For future studies examining the influence of non-P-gp-mediated mechanisms on CNS distribution, the 13 drugs identified as having discrepancies between the P-gp efflux ratio and the [plasma]$_{,u}$/[brain]$_{,u}$ ratio would be logical choices.

Accurate determination of steady-state $K_{p,brain}$ is necessary for accurate determination of the P-gp efflux ratio and the [plasma]$_{,u}$/[brain]$_{,u}$ ratio. In addition, accurate experimental

determination of $f_{u,plasma}$ and $f_{u,brain}$ is required for accurate assessment of the $[plasma]_{,u}/[brain]_{,u}$ ratio. Any error in determining $K_{p,brain}$, $f_{u,plasma}$, or $f_{u,brain}$ may lead to artificial discrepancies between the P-gp efflux ratio and the $[plasma]_{,u}/[brain]_{,u}$ ratio. Any time $K_{p,brain}$ is not accurately determined, the P -gp efflux ratio and the $[plasma]_{,u}/[brain]_{,u}$ ratio may lead to incorrect conclusions regarding the CNS distribution.

In summary the P-gp efflux ratio and $[plasma]_{,u}/[brain]_{,u}$ ratio were similar for most of the drugs examined, indicating P-gp-mediated efflux is the predominate mechanism limiting the CNS distribution of drugs in the selected compound set. The $[plasma]_{,u}/[brain]_{,u}$ ratio differentiated between sedating and non-sedating antihistamines and between opioids with and without reduced central activity, whereas the P-gp efflux ratio did not. Furthermore, when there were differences between the P-gp efflux ratio and the $[plasma]_{,u}/[brain]_{,u}$ ratio, additional supporting evidence was consistent with the $[plasma]_{,u}/[brain]_{,u}$ ratio. When mechanisms other than P-gp affect CNS distribution (non-P-gp-mediated efflux, poor passive permeability, CSF bulk flow, metabolism, or active uptake), the P-gp efflux ratio may under- or over-estimate CNS distributional impairment. The $[plasma]_{,u}/[brain]_{,u}$ ratio provides a simple alternative means for assessing the CNS distribution of drugs independent of the mechanism(s) involved.

References

1. Anthonypillai C, Sanderson RN, Gibbs JE and Thomas SA (2004) The distribution of the HIV protease inhibitor, ritonavir, to the brain, cerebrospinal fluid, and choroid plexuses of the guinea pig. *J Pharmacol Exp Ther* **308:**912-920.

2. Bourdet DL, Pritchard JB and Thakker DR (2005) Differential substrate and inhibitory activities of ranitidine and famotidine toward human organic cation transporter 1 (hOCT1; SLC22A1), hOCT2 (SLC22A2), and hOCT3 (SLC22A3). *J Pharmacol Exp Ther* **315:**1288-1297.

3. Chen C, Hanson E, Watson JW and Lee JS (2003) P-glycoprotein limits the brain penetration of nonsedating but not sedating H1-antagonists. *Drug Metab Dispos* **31:**312-318.

4. Chi CH and Dixit BN (1977) Characterization of (+/-)-methadone uptake by rat lung. *Br J Pharmacol* **59:**539-549.

5. Cvetkovic M, Leake B, Fromm MF, Wilkinson GR and Kim RB (1999) OATP and P-glycoprotein transporters mediate the cellular uptake and excretion of fexofenadine. *Drug Metab Dispos* **27:**866-871.

6. Dodick DW and Martin V (2004) Triptans and CNS side-effects: pharmacokinetic and metabolic mechanisms. *Cephalalgia* **24:**417-424.

7. Evans DC, O'Connor D, Lake BG, Evers R, Allen C and Hargreaves R (2003) Eletriptan metabolism by human hepatic CYP450 enzymes and transport by human P-glycoprotein. *Drug Metab Dispos* **31:**861-869.

8. Gillette JR (1971) Factors affecting drug metabolism. *Ann NY Acad Sci* **179**.

9. Hendrikse NH, Schinkel AH, de Vries EG, Fluks E, Van der Graaf WT, Willemsen AT, Vaalburg W and Franssen EJ (1998) Complete in vivo reversal of P-glycoprotein pump function in the blood-brain barrier visualized with positron emission tomography. *Br J Pharmacol* **124:**1413-1418.

10. Hindmarch I, Shamsi Z and Kimber S (2002) An evaluation of the effects of high-dose fexofenadine on the central nervous system: a double-blind, placebo-controlled study in healthy volunteers. *Clin Exp Allergy* **32:**133-139.

11. Kalvass JC and Maurer TS (2002) Influence of nonspecific brain and plasma binding on CNS exposure: implications for rational drug discovery. *Biopharm Drug Dispos* **23:**327-338.

12. Kemper EM, Cleypool C, Boogerd W, Beijnen JH and van Tellingen O (2004) The influence of the P-glycoprotein inhibitor zosuquidar trihydrochloride (LY335979) on the brain penetration of paclitaxel in mice. *Cancer Chemother Pharmacol* **53:**173-178.

13. Kim RB, Fromm MF, Wandel C, Leake B, Wood AJ, Roden DM and Wilkinson GR (1998) The drug transporter P-glycoprotein limits oral absorption and brain entry of HIV-1 protease inhibitors. *J Clin Invest* **101:**289-294.

14. Kurz A, Ikeda T, Sessler DI, Larson MD, Bjorksten AR, Dechert M and Christensen R (1997) Meperidine decreases the shivering threshold twice as much as the vasoconstriction threshold. *Anesthesiology* **86:**1046-1054.

15. Kusuhara H and Sugiyama Y (2001) Efflux transport systems for drugs at the blood-brain barrier and blood-cerebrospinal fluid barrier (Part 2). *Drug Discov Today* **6:**206-212.

16. Kusuhara H, Suzuki H, Terasaki T, Kakee A, Lemaire M and Sugiyama Y (1997) P-Glycoprotein mediates the efflux of quinidine across the blood-brain barrier. *J Pharmacol Exp Ther* **283:**574-580.

17. Lespine A, Dupuy J, Orlowski S, Nagy T, Glavinas H, Krajcsi P and Alvinerie M (2005) Interaction of ivermectin with multidrug resistance proteins (MRP1, 2 and 3). *Chem Biol Interact*.

18. Mahar Doan KM, Humphreys JE, Webster LO, Wring SA, Shampine LJ, Serabjit-Singh CJ, Adkison KK and Polli JW (2002) Passive permeability and P-glycoprotein-mediated efflux differentiate central nervous system (CNS) and non-CNS marketed drugs. *J Pharmacol Exp Ther* **303:**1029-1037.

19. Maurer TS, Debartolo DB, Tess DA and Scott DO (2004) Relationship between Exposure and Nonspecific Binding of Thirty-Three Central Nervous System Drugs in Mice. *Drug Metab Dispos*.

20. Pariante CM, Makoff A, Lovestone S, Feroli S, Heyden A, Miller AH and Kerwin RW (2001) Antidepressants enhance glucocorticoid receptor function in vitro by modulating the membrane steroid transporters. *Br J Pharmacol* **134:**1335-1343.

21. Polli JW, Jarrett JL, Studenberg SD, Humphreys JE, Dennis SW, Brouwer KR and Woolley JL (1999) Role of P-glycoprotein on the CNS disposition of amprenavir (141W94), an HIV protease inhibitor. *Pharm Res* **16:**1206-1212.

22. Schinkel AH, Mol CA, Wagenaar E, van Deemter L, Smit JJ and Borst P (1995a) Multidrug resistance and the role of P-glycoprotein knockout mice. *Eur J Cancer* **31A:**1295-1298.

23. Schinkel AH, Smit JJ, van Tellingen O, Beijnen JH, Wagenaar E, van Deemter L, Mol CA, van der Valk MA, Robanus-Maandag EC, te Riele HP and et al. (1994) Disruption of the mouse mdr1a P-glycoprotein gene leads to a deficiency in the blood-brain barrier and to increased sensitivity to drugs. *Cell* **77:**491-502.

24. Schinkel AH, Wagenaar E, van Deemter L, Mol CA and Borst P (1995b) Absence of the mdr1a P-Glycoprotein in mice affects tissue distribution and pharmacokinetics of dexamethasone, digoxin, and cyclosporin A. *J Clin Invest* **96:**1698-1705.

25. Shen DD, Artru AA and Adkison KK (2004) Principles and applicability of CSF sampling for the assessment of CNS drug delivery and pharmacodynamics. *Adv Drug Deliv Rev* **56:**1825-1857.

26. Su Y, Zhang X and Sinko PJ (2004) Human organic anion-transporting polypeptide OATP-A (SLC21A3) acts in concert with P-glycoprotein and multidrug resistance protein 2 in the vectorial transport of Saquinavir in Hep G2 cells. *Mol Pharm* **1:**49-56.

27. Summerfield S, Stevens AJ, Cutler L, Del Carmen Osuna M, Hammond B, Tang SP, Hersey A, Spalding DJ and Jeffrey P (2005) Improving the In Vitro Prediction of In Vivo CNS Penetration: Integrating Permeability, Pgp Efflux and Free Fractions in Blood and Brain. *J Pharmacol Exp Ther*.

28. Yamazaki M, Neway WE, Ohe T, Chen I, Rowe JF, Hochman JH, Chiba M and Lin JH (2001) In vitro substrate identification studies for p-glycoprotein-mediated transport: species difference and predictability of in vivo results. *J Pharmacol Exp Ther* **296:**723-735.

Table 4.1. Conditions used for HPLC-MS/MS analysis for each drug. Column consisted of either a Phenomenex 2.0 × 30 mm, 5 µm Gemini 110A (column 1) or a Phenomenex 2.0 × 30 mm, 4 µm Synergi Max-RP column (column 2). Mobile phase A, B, C consisted of ammonium acetate (pH 6.8; 10 mM), methanol and acetonitrile, respectively. HPLC gradients with the initial and intermediate gradient conditions also well as the flow rates listed below were conducted as described in the material and methods section. Drugs listed with a flow rate of 750 to 1500 were run on PE-Sciex API4000. All other drugs were run on PE-Sciex API3000.

Drug	MS Polarity	MRM Transition	Column	Initial Condition	Intermediate Condition	Flow Rate (µl/min)	Internal Standard
Alfentanil	+	417.3 / 268.3	1	95% A : 5% B; 30 sec	10% A : 90%B	750 to 1500	Loperamide
Amprenavir	+	506.4 / 245.4	2	80% A : 20% B	5% A : 95% B	750 to 1500	Ritonavir
Cetirizine	+	389.1 / 201.1	2	95% A : 5% B	5% A : 95% B	750 to 1500	Fexofenadine
Cimetidine	+	253.1 / 159.3	1	95% A : 5% B; 30 sec	10% A : 90%B	750 to 1500	Fexofenadine
Desloratadine	+	311.0 / 259.3	2	95% A : 5% B	5% A : 95% B	750 to 1500	Fexofenadine
Dexamethasone	-	391.2 / 307.3	2	90% A : 5% B : 5% C	5% A : 47.5% B : 47.5% C	500 to 750	Doxorubicin
Digoxin	-	779.5 / 649.5	2	85% A : 15% B	5% A : 95% B	500 to 750	Ivermectin
Diphenhydramine	+	256.1 / 167.3	2	95% A : 5% B	5% A : 95% B	750 to 1500	Fexofenadine
Doxorubicin	-	542.2 / 395.5	2	90% A : 5% B : 5% C	5% A : 47.5% B : 47.5% C	500 to 750	Dexamethasone
Eletriptan	+	383.3 / 84.6	1	95% A : 5% B; 30 sec	10% A : 90%B	750 to 1500	Rizatriptan
Fentanyl	+	337.2 / 188.2	2	80% A : 20% B	5% A : 95% B	750 to 1500	Loperamide
Fexofenadine	+	502.3 / 466.4	2	80% A : 20% B	5% A : 95% B	750 to 1500	Loperamide
Hydroxyzine	+	375.1 / 201.1	2	95% A : 5% B	5% A : 95% B	750 to 1500	Fexofenadine
Indinavir	+	614.5 / 421.5	2	80% A : 20% B	5% A : 95% B	750 to 1500	Ritonavir
Ivermectin	-	873.6 / 229.3	2	85% A : 15% B	5% A : 95% B	500 to 750	Digoxin
Loperamide	+	477.4 / 266.0	2	95% A : 5% B	5% A : 95% B	750 to 1500	Methadone
Loratadine	+	383.0 / 337.1	2	95% A : 5% B	5% A : 95% B	750 to 1500	Fexofenadine
Meperidine	+	248.3 / 220.3	1	95% A : 5% B	5% A : 95% B	750 to 1500	Loperamide
Methadone	+	310.3 / 265.1	2	80% A : 20% B	5% A : 95% B	750 to 1500	loperamide
Morphine	+	286.1 / 201.1	1	95% A : 5% B; 30 sec	20% A : 80% B	750 to 1500	Oxycodone (316.0 / 298.0)
Naratriptan	+	336.1 / 98.4	1	95% A : 5% B; 30 sec	10% A : 90%B	750 to 1500	Zolmitriptan
Nelfinavir	+	568.3 / 330.4	2	80% A : 20% B	5% A : 95% B	750 to 1500	Saquinavir
Paclitaxel	-	852.3 / 525.3	1	95% A : 5% B	5% A : 95% B	750 to 1500	Fexofenadine
Quinidine	+	325.2 / 307.3	2	85% A : 15% B	5% A : 95% B	500 to 750	Olanzapine (325.2 / 307.3)
Ranitidine	+	315.1 / 176.2	1	95% A : 5% B; 30 sec	10% A : 90%B	750 to 1500	Fexofenadine
Ritonavir	+	721.5 / 296.4	2	80% A : 20% B	5% A : 95% B	750 to 1500	Saquinavir
Rizatriptan	+	270.3 / 158.3	1	95% A : 5% B; 30 sec	10% A : 90%B	750 to 1500	Zolmitriptan
Saquinavir	+	671.5 / 570.5	2	80% A : 20% B	5% A : 95% B	750 to 1500	Ritonavir
Sufentanil	+	387.2 / 238.4	1	95% A : 5% B	5% A : 95% B	750 to 1500	Loperamide
Sumatriptan	+	296.1 / 58.5	1	95% A : 5% B; 30 sec	10% A : 90%B	750 to 1500	Zolmitriptan

Table 4.1. continued

Drug	MS Polarity	MRM Transition	Column	Initial Condition	Intermediate Condition	Flow Rate (µl/min)	Internal Standard
Triprolidine	+	279.1 / 208.3	2	95% A : 5% B	5% A : 95% B	750 to 1500	Fexofenadine
Verapamil	+	455.4 / 164.9	2	90% A : 5% B : 5% C	5% A : 47.5% B : 47.5% C	500 to 750	Vinblastine
Vinblastine	+	811.6 / 224.1	2	90% A : 5% B : 5% C	5% A : 47.5% B : 47.5% C	500 to 750	Verapamil
Zolmitriptan	+	288.3 / 58.5	1	95% A : 5% B; 30 sec	10% A : 90%B	750 to 1500	Rizatriptan

Table 4.2. Unbound fractions and $K_{p,brain}$ values for 34 drugs. $K_{p,brain}$ values were determined experimental or obtained from the cited reference. Free fractions are reported as mean ± SD (n=6, unless otherwise indicated by [a] n=4, [b] n=5, [c] n= 16, or [d] n=18).

Drug	$f_{u,plasma}$	$f_{u,brain}$	$f_{u,plasma}/f_{u,brain}$	$K_{p,brain}^{-/-}$	$K_{p,brain}^{+/+}$	P-gp efflux ratio	Reference for $K_{p,brain}$
Alfentanil (Al)	0.26 ± 0.04	0.32 ± 0.11	0.81 ± 0.12	0.53	0.19	2.8	
Amprenavir (A)	0.075 ± 0.008	0.091 ± .005	0.82 ± 0.04	1.0	0.072	14	(Polli et al., 1999)
Cetirizine (C)	0.160 ± 0.009	0.072 ± 0.007	2.20 ± 0.10	0.080	0.020	4	(Chen et al., 2003)
Cimetidine (Ci)	0.81 ± 0.07	0.53 ± 0.10	1.53 ± 0.12	0.031	0.033	0.94	
Desloratadine (Dl)	0.055 ± 0.002	0.0071 ± 0.0008	7.7 ± 0.4	14	<1.0	>14	(Chen et al., 2003)
Dexamethasone (Dex)	0.272 ± 0.014	0.098 ± 0.010[b]	2.77 ± 0.14	0.70	0.30	2.3	(Schinkel et al., 1995b)
Digoxin (Dg)	0.33 ± 0.02	0.0156 ± 0.0011	21.2 ± 0.8	1.5	0.08	19	(Schinkel et al., 1995b)
Diphenhydramine (D)	0.33 ± 0.02	0.058 ± 0.003	5,7 ± 0.2	0.70	9.0	1	(Chen et al., 2003)
Doxorubicin (Dox)	0.22 ± 0.03	0.0014 ± 0.0005	160 ± 20	0.0025	0.00077	3.2	(Kusuhara and Sugiyama, 2001)
Eletriptan (Ele)	0.28 ± 0.03	0.055 ± 0.004	5.1 ± 0.3	14	0.30	47	(Evans et al., 2003)
Fentanyl (F)	0.17 ± 0.04	0.07 ± 0.005	2.4 ± 0.2	4.5	2.4	1.7	
Fexofenadine (Fex)	0.35 ± 0.03	0.077 ± 0.014	4.5 ± 0.4	0.30	0.17	1.8	(Cvetkovic et al., 1999)
Hydroxyzine (H)	0.062 ± 0.008	0.014 ± 0.002	4.4 ± 0.3	4.8	3.8	1.3	(Chen et al., 2003)
Indinavir (I)	0.058 ± 0.007	0.100 ± 0.008	0.58 ± 0.03	0.81	0.084	9.6	(Kim et al., 1998)
Ivermectin (Iv)	0.024 ± 0.008[b]	0.00009 ± 0.00007[a]	270 ± 110	2.5	0.094	27	(Schinkel et al., 1995a)
Loperamide (Lop)	0.023 ± 0.005[d]	0.0046 ± 0.0005[c]	5.0 ± 0.3	5.7	0.096	33	
Loratadine (L)	0.0045 ± 0.00017	0.00178 ± 0.00015	2.5 ± 0.1	3.3	1.6	2.1	(Chen et al., 2003)
Meperidine (Me)	0.38 ± 0.03	0.13 ± 0.019	2.9 ± 0.2	7.0	6.8	1.1	
Methadone (M)	0.147 ± 0.007	0.029 ± 0.002	5.07 ± 0.17	20	4.0	7	
Morphine (Mor)	0.50 ± 0.04	0.41 ± 0.11	1.22 ± 0.14	0.72	0.49	1.5	(Schinkel et al., 1995b)
Naratriptan (N)	0.58 ± 0.03	0.23 ± 0.02	2.52 ± 0.10	1.1	0.42	2.6	(Evans et al., 2003)
Nelfinavir (Nel)	0.0010 ± 0.0004	0.00053 ± 0.00004	1.9 ± 0.3	2.6	0.086	30	(Kim et al., 1998)
Paclitaxel (Pax)	0.021 ± 0.002	0.0028 ± 0.0004	8.0 ± 0.5	4.0	0.50	8	(Kemper et al., 2004)
Quinidine (Q)	0.16 ± 0.03	0.037 ± 0.003	4.3 ± 0.4	4.8	0.20	24	(Kusuhara et al., 1997)
Ranitidine (Ra)	0.96 ± 0.05	0.96 ± 0.13	1.00 ± 0.06	0.039	0.022	1.8	
Ritonavir (Rit)	0.0027 ± 0.0005	0.0106 ± 0.0016	0.25 ± 0.02	2.3	0.17	14	(Yamazaki et al., 2001)
Rizatriptan (Riz)	0.62 ± 0.02	0.348 ± 0.014	1.78 ± 0.04	0.85	0.20	4.3	(Evans et al., 2003)
Saquinavir (Sq)	0.00043 ± 0.00007	0.00190 ± 0.00016	0.226 ± 0.017	0.88	0.13	6.8	(Kim et al., 1998)
Sufentanil (Su)	0.054 ± 0.014	0.034 ± 0.010	1.6 ± 0.3	4.8	1.6	3	
Sumatriptan (Sum)	0.63 ± 0.03	0.36 ± 0.03	1.75 ± 0.07	0.22	0.13	1.7	(Evans et al., 2003)
Triprolidine (T)	0.31 ± 0.02	0.092 ± 0.002	3.37 ± 0.09	3.6	5.9	0.61	(Chen et al., 2003)
Verapamil (V)	0.11 ± 0.03	0.033 ± 0.02	3.3 ± 0.9	3.3	0.43	7.7	(Hendrikse et al., 1998)
Vinblastine (Vi)	≥ 0.09	0.0046 ± 0.0004	≥ 20	19	1.7	11	(Schinkel et al., 1994)
Zolmitriptan (Z)	0.98 ± 0.11[b]	0.54 ± 0.08	1.81 ± 0.14	0.085	0.038	2.2	(Evans et al., 2003)

Table 4.3. Classification of drugs based on discrepancies between in vivo P-gp efflux ratio and $[plasma]_{,u}/[brain]_{,u}$ ratio. The classification for each drug was assigned according to the scheme in figure 4.1. Additional evidence from the literature is provided to support of classification of each drug.

Class Ib P-gp efflux + additional mechanism		Class II Weak or no P-gp efflux + additional impairment		Class IV P-gp efflux – compensatory mechanism(s)	
Drug	Additional Evidence	Drug	Additional Evidence	Drug	Additional Evidence
Cetirizine (C)	very low permeability (Mahar Doan et al., 2002)	Cimetidine (Ci)	Non-Pgp efflux transporter(s) (www.tp-search.jp)	Methadone (M)	active uptake (Chi and Dixit, 1977)
Digoxin (Dg)	additional efflux transporter(s) (www.tp-search.jp)	Dexamethasone (Dex)	steroid transporter (Pariante et al., 2001)	Ritonavir (Rit)	active uptake (Anthonypillai et al., 2004)
Doxorubicin (Dox)	additional efflux transporter(s) (www.tp-search.jp)	Fexofenadine (Fex)	reduced CNS activity (Hindmarch et al., 2002)	Saquinavir (Sq)	active uptake (Su et al., 2004)
Ivermectin (Iv)	additional efflux transporter(s) (Lespine et al., 2005)	Ranitidine (Ra)	Non-Pgp efflux transporter(s) (Bourdet et al., 2005)		
		Sumatriptan (Sum)	very low permeability (Mahar Doan et al., 2002)		
		Zolmitriptan (Z)	very low permeability (Mahar Doan et al., 2002)		

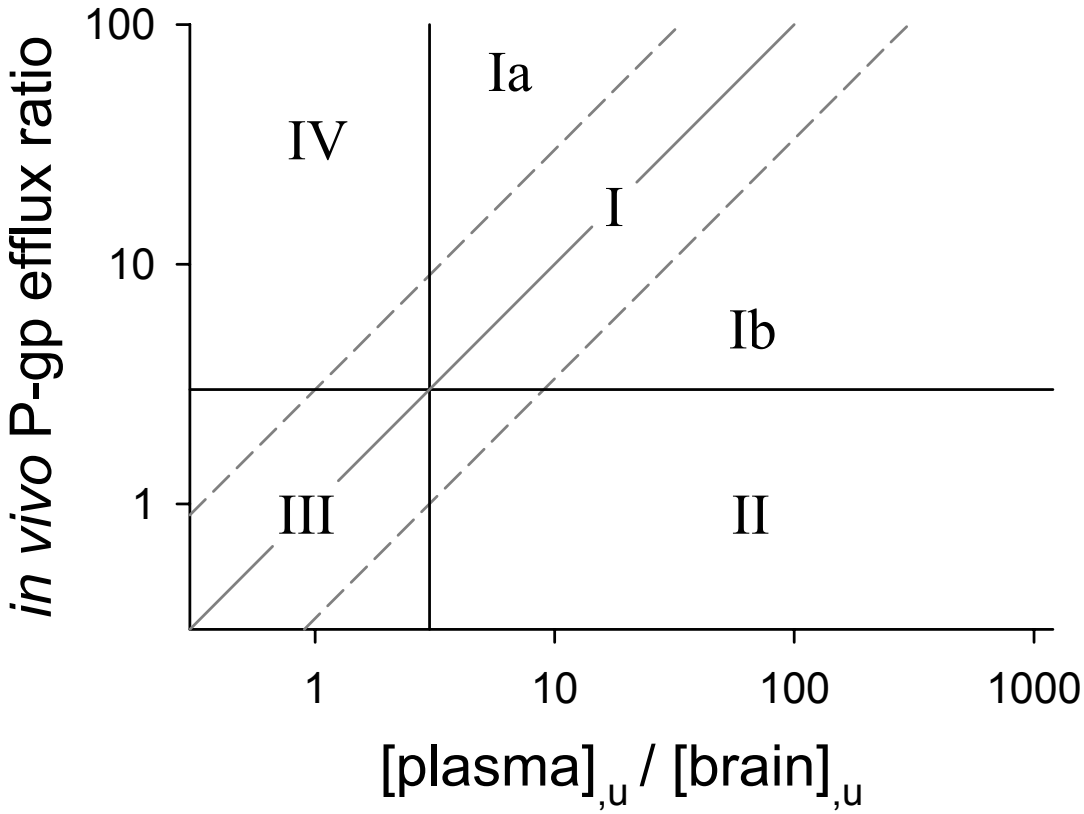

Figure 4.1. The CNS distributional behavior of each drug based on the plot scheme above. The horizontal and vertical lines represent the point at which the P-gp efflux ratio and the $[plasma]_{,u}/[brain]_{,u}$ ratio equal 3, respectively. 3-fold impairment in CNS distribution was considered meaningful. The figure was divided in to four quadrants (I-IV) based on whether the P-gp efflux or ($[plasma]_{,u}/[brain]_{,u}$) ratio values were greater than or less than 3. The solid line passing through the origin represents the line of unity ± 3-fold (dashed lines). Drugs were assessed as follows: (quadrant I) impaired CNS distribution due to P-gp-mediated efflux, (subsections Ia and Ib) impaired CNS distribution due to P-gp with other active process(es) present; (quadrant II) impaired CNS distribution due to non-P-gp mechanism; (quadrant III) no impairment in CNS distribution; (quadrant IV) P-gp substrate, but CNS distribution is not impaired due to compensatory mechanism.

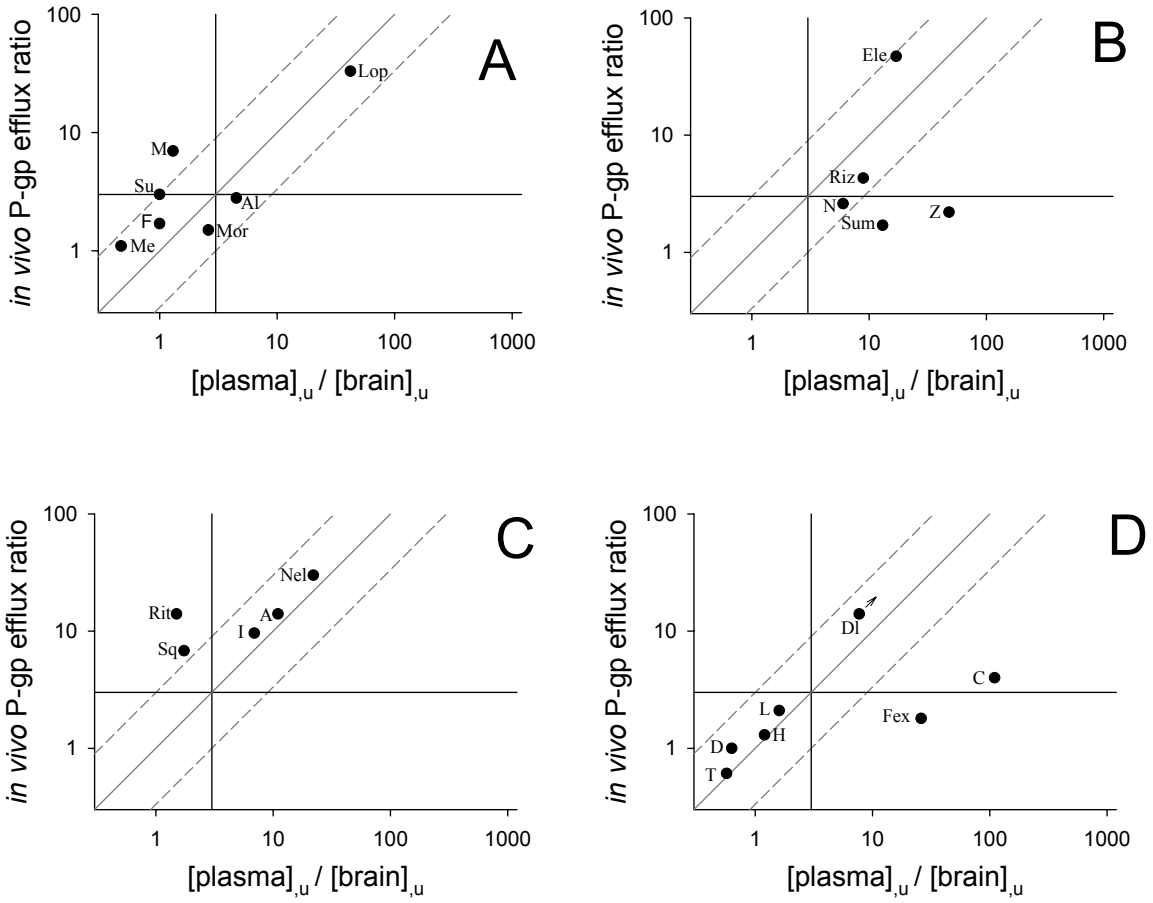

Figure 4.2. Comparison of the P-gp efflux ratio and the $[plasma]_{,u}/[brain]_{,u}$ ratio of (A) opioids, (B) triptans, (C) protease inhibitors and (D) antihistamines. The CNS distributional behavior of each drug was assessed according to the scheme in Figure 4.1. Symbols for drugs are defined in Table 4.2.

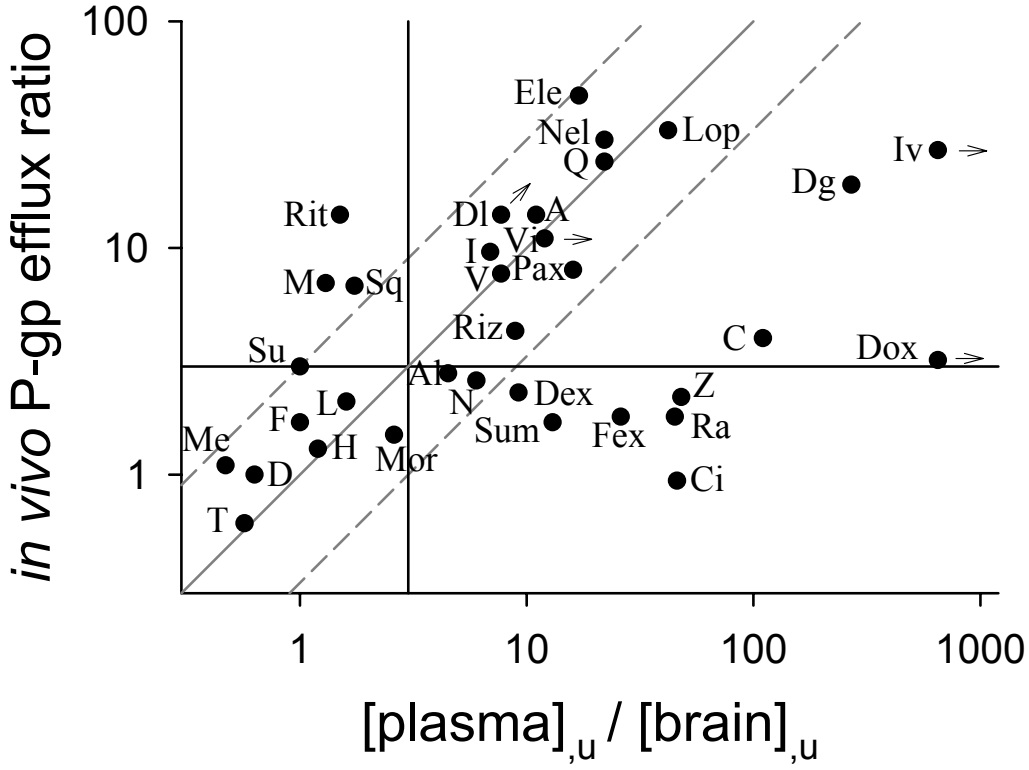

Figure 4.3. Comparison of the P-gp efflux ratio and the $[plasma]_{,u}/[brain]_{,u}$ ratio of all 34 marketed drugs. The CNS distributional behavior of each drug was assessed according to the scheme in Figure 4.1. As expected, P-gp substrates such as quinidine, verapamil, and paclitaxel fell within quadrant I (consistent with P-gp being the only efflux mechanism), while drugs subject to transport by other transporters or with poor BBB permeability, such as ranitidine, digoxin, and doxorubicin fell within quadrants Ib, II, or IV. Symbols for drugs are defined in Table 4.2.

CHAPTER 5

USE OF LOPERAMIDE AS A PHENOTYPIC PROBE OF MDR1A STATUS IN CF-1 MICE

This chapter has been published in *Pharmaceutical Research* and is presented in the style of that journal.

INTRODUCTION

P-glycoprotein (P-gp) is the prototypical multidrug resistance (*MDR*) transport protein. Originally identified based on an ability to impart drug resistance to cancer cells (1), P-gp is by far the most well-characterized of the blood-brain barrier (BBB) efflux transport systems (2). P-gp is a 170-kDa energy-dependent plasma membrane efflux protein and a member of the ABC superfamily of transport systems (3, 4). Experiments performed in mice that lack P-gp expression [e.g., *mdr1a (-/-)* animals] have suggested that the transporter is an important determinant of substrate delivery across the BBB. Although *mdr1a(-/-)* mice do not display a decreased life span and are fertile, they do evidence a marked increase in brain uptake of numerous drugs and other xenobiotics, with a concomitant increase in centrally-mediated pharmacologic response (2), consistent with the absence of P-gp at the blood-brain interface.

A subpopulation of the CF-1 mouse strain (approximately 25%) lacks P-gp expression. Consequently, increased brain penetration of many substrates is observed in these animals. The genetic level of this mutation has been established, and studies have revealed that this inheritance follows a normal Mendelian autosomal pattern (5). In addition, the mutant mice appear to be deficient in P-gp in those tissues that express predominantly the *mdr1a* isoform (i.e., brain and intestine), indicating that this deletion is restricted to the *mdr1a* gene only (6). There are three genes that encode different isoforms of P-gp in mice: *mdr1a* (also known as *mdr*3), *mdr1b* (also known as *mdr*1), and *mdr2* (7). The multidrug resistant phenotype is associated with both mdr1a and mdr1b in mice, while mdr2 is necessary for bile production. Mice lacking the *mdr1a* gene represent a valuable research platform with which to study the potential effects of P-gp on substrate disposition, especially with regards to the CNS. However, while these animals offer the advantage of a lower cost than transgenic (knockout) animals, it is imperative that the investigator know which animals

are phenotypically P-gp-competent or P-gp-deficient. The two sub-strains of mice are virtually identical with regards to gross physiology; spontaneously mutated animals (misidentified as P-gp-competent when they are, in fact, P-gp-deficient) typically are excluded from post-experimental analysis as statistical outliers. Therefore, development of an efficient method to phenotype mice for P-gp function would provide distinct advantages.

In this paper we describe a simple approach for phenotyping mice for BBB P-gp function. This method is benign for P-gp-competent animals, and relatively innocuous even in P-gp-deficient mice.

MATERIALS AND METHODS

Chemicals: Loperamide hydrochloride, (±)-methadone hydrochloride, ribonuclease A (RNase A) and proteinase K were obtained from Sigma-Aldrich (St. Louis, MO). All other chemicals and reagents were the highest grade available from commercial sources.

Animals: Adult CF-1 mice [*mdr1a(+/+)* and *mdr1a(-/-)*, 25-30 g, 6-8 weeks of age] were purchased form Charles River Laboratories (Wilmington, MA) and maintained in a breeding colony in the School of Pharmacy, The University of North Carolina. Male and female mice were housed separately (maximum of 4 per cage) in wire-mesh cages in a temperature- and humidity-controlled room with a 12-hr-dark/12-hr-light cycle, and had unrestricted access to food and water. The experimental protocol was approved by the Institutional Animal Care and Use Committee of the University of North Carolina, and all procedures were conducted according to the "Principles of Laboratory Animal Care" (NIH publication #85-23, revised in 1985).

Behavioral and Dispositional Phenotyping: Mice (n=18; with the experimenter blinded to purported phenotype) received a 2-mg/kg subcutaneous (s.c.) dose of loperamide prepared as a solution in 50% propylene glycol. At 0.25, 2, 4, and 24 hr post-dose, mice were observed for signs of opioid intoxication [i.e., Straub reaction (8)] and loperamide-induced antinociception was determined by the hotplate latency test as previously described (9). Briefly, latency was defined as the time interval between the placement on the hotplate (55ºC; Columbus Instruments, Columbus, OH) and the licking of the hind paws or jumping. To avoid tissue damage, a maximum test latency of 60 sec was used. Baseline latency was determined prior to administration of loperamide.

Following a 2-week wash-out period, mice received a second 2-mg/kg s.c. dose of loperamide, and signs of opioid intoxication and hotplate latencies were determined as after the first dose. The animals were decapitated, and trunk blood and brain tissue were collected following the 4-hr observation. Blood was allowed to clot at room temperature for least 30 min before centrifuging to collect serum. Brain and serum samples were stored at -20ºC until analysis by LC-MS/MS.

Quantitation of Loperamide in Serum and Brain: Brain samples were homogenized in water (1:2 v/v) via sonic probe. A 25-µl aliquot of homogenate or plasma was transferred to an HPLC vial, and protein was precipitated with 250 µl methanol containing internal standard (methadone, 20 ng/ml). The sample was vortex-mixed, centrifuged, and the supernatant was analyzed by LC-MS/MS. Samples were injected (3 µl; Agilent 1100 wellplate autosampler) onto a Phenomenex 2.0 x 30 mm 4 µm Synergi Max-RP column (Phenomenex, Torrance, CA) maintained at room temperature. Analytes were eluted with a linear gradient (750 µl/min) consisting of ammonium acetate (pH 6.8; 10 mM ["A"] and methanol ["B"] produced by an Agilent 1100 series binary pump. An initial concentration of 20% "B" was ramped to a final concentration of 95% over 2 min and held for 1 min. The system was returned to the initial condition in a single step and allowed to equilibrate for 1 min. The entire column effluent was diverted from the Turbo Ionspray of a PE-Sciex API-4000 triple quadrupole mass spectrometer for the first and last min. Loperamide and methadone were measured using multiple reaction monitoring (477.4→266.0 and 310.3→265.1, respectively). Standard curves were prepared in brain homogenate and plasma.

Genotyping of CF-1 Mice: After sacrificing, the distal ~1.5 cm of the tail was removed. Tail tissue was minced and incubated overnight in 250 µl digestion buffer (50 mM Tris, 100 mM NaCl, 10 mM EDTA, 1% SDS, 0.5 mg/ml proteinase K; pH 8; 55ºC). Following digestion, 1.5 µl of RNase (10 mg/ml) was added to each sample, which was incubated at 37°C for 20 min. For DNA extraction, 160 µl of 5 M ammonium acetate was added, samples were mixed by vortex briefly, and centrifuged (16,000 g, 4 min). The supernatant was poured into 600 µl isopropanol (4ºC), gently mixed, and centrifuged (16,000 g, 7 min). The supernatant was discarded and 600 µl ethanol (70%; 4ºC) added. Following centrifugation (16,000 g, 4 min), the supernatant was removed, the pellet was air-dried for ~15 min and suspended in TE buffer (20 µl; 10 mM Tris, 1 mM EDTA, pH 8).

DNA enrichment was conducted with Herculase® Enhanced DNA polymerase kit (Stratagene, La Jolla, CA) and dNTP Mix (Amersham Biosciences, Piscataway, NJ) with the primers 5'CTTTGACTCGGGAGCAGAAG3' (forward) and 5'GAATGAACTGACCTGCCCCA3' (reverse) (UNC Nucleic Acids Core Facility) (10). Following an initial cycle at 94°C for 2 min, PCR was conducted for 35 cycles (94°C for 30 sec, 60°C for 30 sec, 68°C for 10 min). The resulting PCR products were extracted and precipitated as noted above, except that samples were stored at -80ºC for 20 min following isopropanol addition to improve precipitation. The final pellet was dissolved in TE buffer and stored at 4ºC.

A second PCR to isolate the *mdr1a* gene region of interest was conducted using the same conditions as above and the primers 5'CCAGAGCTTGCAGATACCAT3' (forward) and 5'CACGTGTGCTTTCTTCATCG3' (reverse). The resulting products were run on a 1% agarose gel and stained with ethidium bromide. Products were visualized on a VersaDoc

imaging system (Bio-Rad Laboratories, Hercules, CA). Approximate molecular weights for the PCR products were determined using a GeneRuler™ 1kb DNA Ladder (Fermentas Inc., Hanover, MD).

Data Analysis

Where appropriate, a two-tailed Student's *t*-test was used to evaluate the statistical significance of differences between experimental groups. In all cases, $P < 0.05$ was used as the criterion of statistical significance.

RESULTS AND DISCUSSION

Loperamide is an opioid drug used clinically as an anti-diarrheal that normally does not cross the BBB (due to P-gp-mediated efflux) and therefore lacks opiate-like effects in the CNS of animals or man (11). The large P-gp effect (i.e., dependence of the degree of brain uptake on P-gp-mediated efflux) and obvious endpoints for centrally-mediated pharmacologic activity indicated that loperamide may be a useful probe substrate for phenotyping the CF-1 mice (12). In addition, the choice of loperamide as a phenotyping probe substrate offers many advantages over the previously suggested use of the neurotoxin avermectin (5). Loperamide appears to be harmless to the mice, and the opiate-like behavior produced in P-gp-deficient, but not P-gp-competent animals dissipates within 24 hr. Thus, phenotyping with subsequent experimentation can be performed after a minimum washout period. In addition, loperamide is relatively inexpensive and easy to obtain and use.

The present experiments confirmed the *mdr1a* phenotype can be determined with a single 2-mg/kg s.c. dose of loperamide (Figure 5.1). All mice with three consecutive effects of maximum hotplate latency (60 sec; at 0.25, 2 and 4 hr post-dose) showed considerable opioid-like behavior in addition to antinociception, which persisted at least through 4 hr. These behaviors included hunched posture, compulsive circling, decreased coordination, and the classic Straub tail reaction. Opioids contract the sacrococcygeus muscle in mice, which causes a spinal cord reflex resulting in an intense erection of the tail (Straub tail reaction) (8). Although the hot plate assay offers an objective measurement of difference in behavior between P-gp-deficient and P-gp-competent mice following the administration of loperamide, the visual cues indicated by defined behavioral endpoints provided alternative endpoint which was obvious and not dependent upon instrumentation. On the other hand,

mice that did not display 3 consecutive effects of maximum hotplate latency (60 sec) showed no opioid-like behavior, and each of these mice displayed a hotplate latency ≤ 30 sec. No opioid-induced behaviors were noticeable 24 hr post-dose in any of the mice.

In addition to assessing the behavioral effects associated with loperamide administration, loperamide brain-to-serum ratios were determined to confirm that mice identified as P-gp-deficient [presumably *mdr1a*(-/-)] based on pharmacologic activity evidenced increased brain penetration of loperamide (i.e., were phenotypically P-gp-deficient based on transporter function). The loperamide brain-to-serum ratio in mice identified as P-gp-deficient was 10.1 ± 1.0 (mean ± S.E.), while the loperamide brain-to-serum ratio in mice identified as P-gp-competent was 0.155 ± 0.018 (mean ± S.E.), representing a 65-fold higher loperamide brain-to-serum ratio in the absence of P-gp-mediated transport (Figure 5.2). With respect to the identification of P-gp function utilizing a pharmacologic endpoint, no false negatives (Region I in Figure 5.2) or false positives (Region IV I Figure 5.2) were encountered among the 18 animals phenotyped. Thus, the approach appears to provide an accurate identification of P-gp status.

Finally, the mice were genotyped to confirm the presence or absence of the *mdr1a* gene. The subpopulation of CF-1 mice that evidences P-gp deficiency is due to a truncated mRNA with a deleted exon 23 (10). All animals that were identified as phenotypically P-gp-competent based on the hotplate assay evidenced the *mdr1a(+/+)* genotype (Figure 5.3).

While increased substrate uptake into brain has been shown in the presence of chemical inhibitors of P-gp-mediated transport, pharmacokinetic experiments in transport-deficient mice form the foundation of the current understanding of attenuated BBB translocation by P-gp. Use of these animals is imperative to furthering the development of

CNS agents, and an efficient means of phenotyping the mice should prove useful for studying the role of P-gp in drug disposition. The *mdr1a*(-/-) mice displayed clear signs of opioid intoxication (e.g., circling, erect tail, lack of balance) within 15 min of the dose. Therefore, this assay offers a rapid and unambiguous measure via a relatively non-invasive, simple technique.

REFERENCES

1. R. L. Juliano and V. Ling. A surface glycoprotein modulating drug permeability in Chinese hamster ovary cell mutants. *Biochim Biophys Acta* **455**: 152-162 (1976).

2. P. L. Golden and G. M. Pollack. Blood-brain barrier efflux transport. *Journal of Pharm Sci* **92**: 1739-1753 (2003).

3. V. Ling. Multidrug resistance: molecular mechanisms and clinical relevance. *Cancer Chemother Pharmacol* **40 Suppl**: S3-S8 (1997).

4. P. F. Juranka, R. L. Zastawny, and V. Ling. P-glycoprotein: multidrug-resistance and a superfamily of membrane-associated transport proteins. *Faseb J* **3**: 2583-2592 (1989).

5. D. R. Umbenhauer, G. R. Lankas, T. R. Pippert, L. D. Wise, M. E. Cartwright, S. J. Hall, and C. M. Beare. Identification of a P-glycoprotein-deficient subpopulation in the CF-1 mouse strain using a restriction fragment length polymorphism. *Toxicol Appl Pharmacol* **146**: 88-94. (1997).

6. A. H. Schinkel, J. J. M. Smit, O. van Tellingen, J. H. Beijnen, E. Wagenaar, L. van Deemter, C. A. Mol, M. A. van der Valk, E. C. Robanus-Maandag, H. P. te Riele, A. J. Berns, and P. Borst. Disruption of the mouse *mdr1a* p-glycoprotein gene leads to a deficiency in the blood-brain barrier and to increased senstivity to drugs. *Cell* **77**: 491-502 (1994).

7. P. Borst, A. H. Schinkel, J. J. M. Smit, E. Wagenaar, L. van Deemter, A. J. Smith, E. W. H. M. Eijdems, F. Baas, and G. J. R. Zaman. Classical and novel forms of multidrug resistance and the physiological functions of p-glycoproteins in mammals. *Phamac Ther* **60**: 289-299 (1993).

8. M. Narita, T. Suzuki, M. Misawa, and H. Nagase. Antagonism of the morphine-induced Straub tail reaction by k-opioid receptor activation in mice. *Psychopharmacology* **110**: 254-256 (1993).

9. C. Chen and G. M. Pollack. Blood-brain disposition and antinociceptive effects of -D-penicillamine2,5-enkephalin in the mouse. *J Pharmacol Exper Ther* **283**: 1151-1159 (1997).

10. T. R. Pippertand D. R. Umbenhauer. The subpopulation of CF-1 mice deficient in P-glycoprotein contains a murine retroviral insertion in the mdr1a gene. *J Biochem Mol Toxicol* **15**: 83-89 (2001).

11. A. H. Schinkel, E. Wagenaar, C. A. Mol, and L. van Deemter. P-glycoprotein in the blood-brain barrier of mice influences the brain penetration and pharmacological activity of many drugs. *J Clin Invest* **97**: 2517-2524. (1996).

12. A. J. Sadeque, C. Wandel, H. He, S. Shah, and A. J. Wood. Increased drug delivery to the brain by P-glycoprotein inhibition. *Clin Pharmacol Ther* **68**: 231-237 (2000).

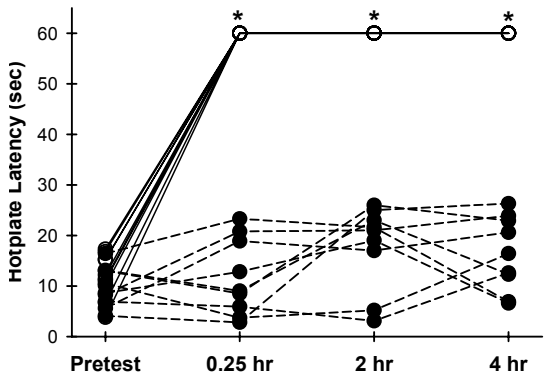

Figure 5.1: Results of the hotplate latency test following a 2-mg/kg s.c. dose of loperamide. ● indicate mice that were phenotypically *mdr1a*(+/+) and o indicate mice that were phenotypically *mdr1a*(-/-). *p< 0.01 vs. pretest

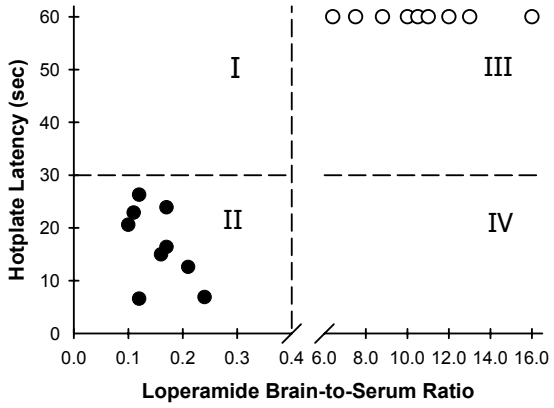

Figure 5.2: Comparison between the hotplate latency results and the loperamide brain-to-serum ratio following a 2-mg/kg s.c. dose of loperamide (4 hr). • indicate mice that were phenotypically *mdr1a*(+/+) and o indicate mice that were phenotypically *mdr1a*(-/-).

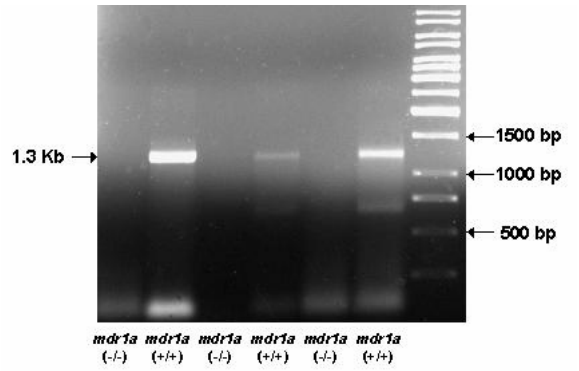

Figure 5.3: Representative RT-PCR gel indicating the presence of a 1.3 Kb product only in those mice that were phenotyped/genotyped *mdr1a*(+/+).

CHAPTER 6

INFLUENCE OF BLOOD-BRAIN BARRIER P-GLYCOPROTEIN ON BRAIN PENETRATION AND ANTINOCICEPTIVE EFFECTS OF MODEL OPIOIDS

This chapter has been submitted for publication in *Journal of Pharmacology and Experimental Therapeutics* and is presented in the style of that journal.

Abstract

This study assessed the pharmacokinetic-pharmacodynamic (PK-PD) implications of variable substrate interactions with blood-brain barrier (BBB) P-glycoprotein (P-gp). Opioids were selected as model compounds because they elicit a readily-measured central effect (antinociception) and evidence a range of interactions with P-gp (loperamide: high; methadone: intermediate; fentanyl: low). P-gp-competent [*mdr1a*(+/+)] and P-gp-deficient [*mdr1a*(-/-)] CF-1 mice received equipotent subcutaneous doses of loperamide, methadone, or fentanyl. FVB [*mdr1a/b*(+/+)] and [*mdr1a/b*(-/-)] mice also received equipotent subcutaneous doses of loperamide in order to assess the potential influence of *mdr1b* on opioid brain penetration and antinociception. The time courses of antinociception and brain/serum concentrations were determined. Brain-to-plasma concentration ratios ($K_{p,brain}$), brain equilibration half-life ($t_{1/2eq,brain}$), and pharmacokinetic/pharmacodynamic parameters were estimated by fitting appropriate kinetic or kinetic/dynamic models to the data. *Mdr1a*(+/+) mice required 50- and 5-fold higher doses of loperamide and methadone, respectively, to produce antinociceptive activity similar to *mdr1a*(-/-) mice. P-gp efflux reduced the $K_{p,brain}$ of loperamide, methadone, and fentanyl by ~40-, ~7-, and ~2-fold, respectively. However, P-gp efflux had no effect on brain EC_{50}, indicating that the only influence of P-gp on loperamide-, methadone-, and fentanyl-associated antinociception was through limiting CNS exposure across the BBB. P-gp efflux decreased brain uptake clearance, $K_{p,brain}$, and $t_{1/2eq,brain}$. The ~2-fold decrease in the time to brain/plasma equilibration for loperamide and methadone is consistent with theoretical considerations for BBB efflux transport, assuming that the egress rate from brain determines brain/plasma equilibration half-life.

Introduction

Several opioids, including fentanyl, methadone, and loperamide, are substrates for the efflux transporter P-glycoprotein (P-gp) (Dagenais et al., 2004). P-gp was first identified in tumor cells for its ability to confer multi-drug resistance against chemotherapy agents (Juliano, 1976; Gros et al., 1986). P-gp is also expressed in several normal organs and tissues, such as the intestine, liver, kidneys, testes, and brain. P-gp expression at these sites appears to serve a protective role by limiting absorption, facilitating excretion, and reducing tissue distribution of potentially harmful xenobiotics, including calcium channel blockers, HIV protease inhibitors, immunosuppressants, and opioids to sensitive tissues, including the brain (Matheny et al., 2001).

While human P-gp is encoded by the MDR1 gene, rodents encode the transporter through two distinct genes, *mdr1a* and *mdr1b*. Two strains of P-gp-deficient mice have been used in a variety of experimental protocols to study the influence of P-gp on the pharmacokinetic and pharmacodynamics of drugs: the CF-1 mouse strain, which naturally lacks the *mdr1a* gene product, and *mdr1a/b* double knockouts, which were developed in the FVB murine line (Schinkel et al., 1994; Chen et al., 2003). The *mdr1a* isoform is expressed on the apical membrane of capillary endothelial cells comprising the BBB, and is thought to be the prominent isoform restricting the entry of P-gp substrates into the brain (Schinkel et al., 1994). In contrast, the *mdr1b* isoform has been reported to be expressed in brain parenchyma (Golden and Pardridge, 2000); the role of *mdr1b* P-gp in attenuating opioid-associated antinociception is unknown. Studies with P-gp-competent and P-gp-deficient mice of both strains have shown that P-gp is responsible for attenuating brain uptake, decreasing brain

tissue concentrations, and reducing the antinociceptive action of some opioids (Schinkel et al., 1996; Chen and Pollack, 1998; Thompson et al., 2000; Dagenais et al., 2004).

It has been proposed that P-gp expression within brain parenchyma may serve as a tertiary barrier to substrate approach to pharmacologic targets such as opioid receptors (Golden and Pollack, 2003). Some experimental evidence supports this hypothesis. For example, the brain tissue EC_{50} of the metabolically stable cyclic opioid peptide [D-penicillamine^{2,5}]-enkephalin (DPDPE) was 10-fold lower in P-gp-deficient as compared to P-gp-competent mice (Chen and Pollack, 1998). It was proposed that the difference in brain tissue EC_{50} was due to P-gp within the brain parenchyma effluxing drug away from the receptor site. However, this explanation remains speculative.

The anti-diarrheal agent loperamide is devoid of central activity at therapeutic doses, despite being a potent *mu* opioid agonist, due to substantial P-gp-mediated efflux (Schinkel et al., 1996). Efflux by BBB P-gp decreases the loperamide brain-to-plasma ratio ($K_{p,brain}$) by ~60-fold (Kalvass et al., 2004). P-gp-mediated efflux also has been reported to decrease the $K_{p,brain}$ for methadone and to attenuate fentanyl-associated antinociception in mice (Thompson et al., 2000; Wang et al., 2004). The effect of P-gp on opioid flux is in the order loperamide > methadone > fentanyl, making this a useful compound set for comprehensive evaluation of the role of P-gp in modulating central opioid response. A side-by-side comparison of the pharmacokinetics and pharmacodynamics of these compounds will allow a better understanding of the effect of P-gp-mediated efflux on brain penetration and antinociception of opioids. The specific goal of the present study was to use a PK-PD modeling approach to assess the influence of P-gp-mediated BBB efflux on the

pharmacokinetics, brain disposition, and antinociception of fentanyl, methadone, and loperamide.

Material and Methods

Materials. Fentanyl, methadone, and loperamide were purchased from Sigma-Aldrich (St. Louis, MO). All other reagents were obtained from common sources and were of reagent grade or better.

Animals. Male CF-1 [*mdr1a*(+/+) and *mdr1a*(-/-)] and FVB [*mdr1a/b(*+/+) and *mdr1a/b(*-/-)] mice (30-40 g; Charles River Laboratories, Inc. Wilmington, MA; and Taconic, Germantown, NY, respectively) were maintained on a 12-h light/dark cycle in a temperature- and humidity-controlled room with access to water and food ad libitum. All procedures involving mice were approved by The Institutional Animal Care and Use Committee of the University of North Carolina and were conducted in accordance with "Principles of Laboratory Animal Care" (NIH Publication No. 85-23, revised in 1985).

Opioid Pharmacokinetics and Pharmacodynamics. Based on the results of pilot studies, 36 *mdr1a*(-/-) and 36 *mdr1a*(+/+) CF-1 mice received equipotent subcutaneous doses of loperamide (1 or 50 mg/kg, respectively), methadone (0.2 or 0.6 mg/kg, respectively), or fentanyl (0.09 mg/kg, respectively). The loperamide and fentanyl doses were prepared in 50/50 propylene glycol/water, whereas the methadone dose was prepared in 0.9% saline. In a separate experiment designed to assess the significance of *mdr1b* on opioid brain penetration and antinociception, 36 *mdr1a/b*(-/-) and 36 *mdr1a/b*(+/+) FVB mice received equipotent subcutaneous doses of loperamide (1 or 25 mg/kg, respectively). For both sets of

experiments, antinociception was assessed; 4 *mdr1a*(-/-) and 4 *mdr1a*(+/+) mice were sacrificed by decapitation for collection of brain tissue and trunk blood at selected time points. Trunk blood was collected in 1.5-ml microcentrifuge tubes and was allowed to clot for ≥ 30 min at room temperature. Serum was harvested following centrifugation. Brain and serum samples were stored at -20°C until analysis by HPLC-MS/MS.

Assessment of Antinociception. Antinociception was assessed with the hot plate latency test as described elsewhere (Chen and Pollack, 1997). Prior to administration of opioids, baseline hotplate latency was determined for each animal in triplicate. Hotplate latency was defined as the time interval between placement on the hot plate (55°C; Columbus Instruments, Columbus, OH) and first observation of a jump or lick of the hind limb(s). Animals with an average baseline latency <25 sec were used in the study. A cut-off latency of 60 sec was used to avoid tissue damage. The degree of antinociception was calculated as:

$$\%\text{MPR} = \frac{\text{test latency - control latency}}{60 - \text{control latency}} \times 100\% \qquad (1)$$

Quantitation of Opioids in Serum and Brain Tissue Samples. Brain samples were homogenized in water (1:2 v/v) via sonic probe. A 25-µl aliquot of homogenate or serum was transferred to a HPLC vial, and protein was precipitated with 100 µl methanol containing internal standard (5 ng/ml loperamide for fentanyl and methadone; 20 ng/ml methadone for loperamide). The sample was vortex-mixed, centrifuged, and the supernatant was analyzed by HPLC-MS/MS. Samples were injected (3 µl; CTC Analytics autosampler, Zwingen, Switzerland) onto a Phenomenex 2.0 x 30 mm, 5 µm Gemini 110A column (Phenomenex, Torrance, CA) maintained at room temperature. The total run time was 3 min.

Analytes were eluted with a linear gradient consisting of ammonium acetate (pH 6.8; 10 mM) ["A"] and methanol ["B"] produced by two Shimadzu LC-10ADVP binary pumps. An initial condition of 5% "B" was ramped to 95% "B" over 2 min, held for 0.5 min, and then returned initial condition of 5% "B" in a single step to re-equilibrate the column. During the run, the flow rate was increased from 750 to 1500 µl/min over the first 2 min, held at 1500 µl/min for 1 min, and then returned the initial flow rate of 750 µl/min in a single step. The entire column effluent was diverted from the source of the PE-Sciex API-4000 quadrupole mass spectrometer (Turbo V Ionspray source, 700˚C, PerkinElmerSciex Instruments, Boston, MA) for the first 1 min and last 0.5 min of the run. Fentanyl, loperamide, and methadone were measured in positive ionization mode using multiple reaction monitoring (337.1→188.3, 477.4→266.0 and 310.3→265.1, respectively). Standard curves were prepared in brain homogenate or serum and were identical in composition to corresponding samples.

Pharmacokinetic-Pharmacodynamic Analysis. A compartmental modeling approach with distribution between serum and brain tissue was used to describe fentanyl, loperamide, and methadone pharmacokinetics. The pharmacokinetic model in Figure 6.1 was fit simultaneously to the serum and brain tissue concentration-time data using nonlinear least-squares regression analysis (WinNonlin 4.1; Pharsight Corporation, Mountain View, CA). The brain volume (V_b) was determined experimentally (13.4 ml/kg) assuming a specific gravity of 1.0 g/ml. All other pharmacokinetic parameters were obtained from fitting the kinetic model to the data. The pharmacodynamic parameters, EC_{50} and γ, were determined

from fitting a sigmoidal E_{max} model to the antinociception versus brain concentration (C) data.

$$\%MPR = \frac{E_{max} \cdot C^{\gamma}}{EC_{50}{}^{\gamma} + C^{\gamma}} \quad (2)$$

E_{max} was defined as 100%, and γ was constrained to the same value for P-gp-competent and P-gp-deficient mice. The time course of brain-to-serum ratio ($K_{p,brain}$) was used to estimate the brain equilibration rate constant (k_{eq}) and steady-state brain-to-serum ratio ($K_{p,brain,ss}$) according to:

$$K_{p,brain} = K_{p,brain,ss}\left(1 - e^{-k_{eq} \cdot t}\right) \quad (3)$$

The brain equilibration half-life ($t_{1/2eq,brain}$) was obtained from k_{eq}:

$$t_{1/2eq,brain} = \frac{\ln(2)}{K_{eq}} \quad (4)$$

Results

In order to achieve similar antinociception between *mdr1a*(+/+) and *mdr1a*(-/-) mice, *mdr1a*(+/+) animals received 5- and 50-fold larger doses of methadone and loperamide, respectively. Consistent with receiving a larger dose, the serum concentrations of methadone and loperamide in *mdr1a*(+/+) mice exceeded those in *mdr1a*(-/-) mice. However, brain tissue concentrations were similar between the two strains of mice. The time course of serum and brain tissue concentrations in the *mdr1a*(-/-) and *mdr1a*(+/+) mice following subcutaneous dose of loperamide, methadone, and fentanyl are reported in Figure 6.2. In general, the brain concentrations for each opioid were similar between the two mouse strains, consistent with the fact that equipotent doses were administered. However, because larger doses were administered to P-gp-competent mice, opioid concentrations in the systemic

circulation were higher in these animals as compared to their P-gp-deficient counterparts, and were approximately dose-proportional. Again consistent with the administration of equipotent doses in the two mouse strains, the magnitude and duration of fentanyl-, methadone-, and loperamide-associated antinociception were similar between *mdr1a*(-/-) and *mdr1a*(+/+) mice (Figure 6.3). The fit of the PK/PD model to the concentration vs. time and antinociception vs. time data is shown in Figures 2 and 3, respectively. Corresponding estimates of pharmacokinetic and pharmacodynamic parameters obtained from the model are reported in Table 6.1.

The systemic pharmacokinetics of fentanyl and methadone did not differ substantially between *mdr1a*(-/-) and *mdr1a*(+/+) mice, so in the implementation of modeling estimates of systemic pharmacokinetic parameters were constrained to the same values for both *mdr1a*(-/-) and *mdr1a*(+/+) mice. However, differences in loperamide systemic pharmacokinetics between P-gp-deficient [*mdr1a*(-/-) and *mdr1a/b*(-/-)] and P-gp-competent [*mdr1a*(+/+) and *mdr1a/b*(+/+)] mice were apparent. Hence, independent estimates of pharmacokinetic parameters were obtained for P-gp-deficient and P-gp-competent mice for this agent. The systemic pharmacokinetics of fentanyl were most consistent with a two-compartment model, whereas a one-compartment model best described the systemic pharmacokinetics of methadone and loperamide (Table 6.1 and 6.2).

The antinociception versus opioid serum and brain concentration relationships are shown in Figures 4 and 5, respectively. For each of the opioids, the antinociception versus serum concentration relationship evidenced a counterclockwise hysteresis, consistent with delayed distribution between serum and the biophase. Compared to *mdr1a*(-/-) mice, the antinociception versus serum concentration relationship in *mdr1a*(+/+) mice was shifted

rightward 1.9-, 7-, and 44-fold for fentanyl, methadone, and loperamide, respectively. In contrast, no hysteresis or rightward shift was observed in the antinociception versus brain concentration relationships. A sigmoidal E_{max} model was capable of adequately describing the relationship between antinociception and brain concentrations. There was no difference in brain EC_{50} between *mdr1a*(-/-) and *mdr1a*(+/+) mice for any of the opioids examined. The brain EC_{50} estimates for loperamide in *mdr1a/b*(-/-) and *mdr1a/b*(+/+) mice were consistent with the brain EC_{50} from *mdr1a*(-/-) and *mdr1a*(+/+) mice (Table 6.1 and 6.2). The time course of $K_{p,brain}$, as well as the antinociception versus serum and brain tissue concentration relationships (Figure 6.7, panels C, D, and E, respectively), were similar between the P-gp-competent CF-1 *mdr1a*(+/+) and FVB *mdr1a/b*(+/+) mice, and between the P-gp-deficient CF-1 *mdr1a*(-/-) and FVB *mdr1a/b*(-/-) mice.

P-gp-mediated efflux reduced the $K_{p,brain}$ of fentanyl, methadone, and loperamide by 1.9-, 7.2-, and 44-fold, respectively (Figure 6.6 and Table 6.1). P-gp efflux did not prolong the brain equilibrium half-life. To the contrary, P-gp efflux decreased the time to brain/plasma equilibration of loperamide and methadone by ~2-fold.

Discussion

Previous studies have indicated that P-gp-mediated efflux attenuates the brain uptake and antinociception of fentanyl, methadone, and loperamide. In this study, a PK/PD modeling approach was used to more fully elucidate the mechanism(s) by which P-gp attenuates brain penetration and antinociception. Multiple mechanisms may be involved, including alteration in systemic pharmacokinetics (e.g., decreased bioavailability or increased clearance),

reduction in brain penetration (e.g., decreased brain uptake and/or increased brain efflux), and alteration of drug distribution within the brain (e.g., increased brain EC_{50}).

Estimates of systemic pharmacokinetic parameters for fentanyl and methadone were similar between *mdr1a*(-/-) and *mdr1a*(+/+) mice, indicating no change in systemic pharmacokinetics due to P-gp-mediated efflux. However, different pharmacokinetic parameters were necessary to fit the model to the loperamide serum concentration vs. time data from the *mdr1a*(-/-), *mdr1a*(+/+), *mdr1a/b*(-/-), and *mdr1a/b*(+/+) mice. This difference in loperamide pharmacokinetics between the different groups of mice may not be due to P-gp-mediated efflux, but rather to non-linear pharmacokinetics.

The loperamide serum concentrations in *mdr1a*(-/-) mice were poorly described by the pharmacokinetic model in 6.1, regardless of whether the one- or two-compartment system was used. The estimate for K_a from the model consistently converged to the maximum value allowed, and had a large associated variance. Since the K_a was large and could not be estimated with reasonable accuracy, the data set was treated as an i.v. bolus and K_a was removed as a fitted parameter. A two-compartment model with bolus input, consistent with this approximation, yielded parameter estimates with the lowest variance, and was best able to fit the serum concentration-time data in *mdr1a*(-/-) mice.

In order to avoid acute toxicity in the P-gp-competent FVB mice, it was necessary to reduce the dose of loperamide by half compared to the P-gp-competent CF-1 mice (25 vs. 50 mg/kg). The increased sensitivity towards loperamide toxicity in the FVB P-gp-competent mice is attributed to lower systemic clearance (28 vs 58 $ml \cdot min^{-1} \cdot kg^{-1}$), not to any innate difference in pharmacology or P-gp activity. Serum and brain tissue concentrations, as well

as antinociception, were similar between the FVB *mdr1a/b*(+/+) and CF-1 *mdr1a*(+/+) mice at one-half the dose.

A counterclockwise hysteresis in the antinociceptive effect versus serum concentration relationship was observed for both *mdr1a*(+/+) and *mdr1a*(-/-) mouse strains, consistent with delayed distribution between the serum and the biophase. The antinociception versus serum concentration relationship shifted rightward in P-gp-competent animals, in proportion to the fold change in $K_{p,brain}$. Similarly, the ED_{50} of loperamide and methadone in P-gp-competent mice shifted rightward ~30-fold and ~5-fold compared to P-gp-deficient mice (data not shown). No hysteresis was observed in the antinociceptive effect versus brain concentration relationship. The brain EC_{50} was identical between P-gp-deficient and P-gp-competent mice. These results are consistent with the brain being the site of opioid action. The loperamide brain EC_{50} estimates for the *mdr1a*(+/+), *mdr1a*(-/-), *mdr1a/b*(+/+), and *mdr1a/b*(-/-) mice were similar suggesting that P-gp (neither the *mdr1a* nor the *mdr1b* gene product) had no effect on brain EC_{50} and that brain EC_{50}s were similar between CF-1 and FVB mouse strains.

Previously, this laboratory demonstrated a 10-fold difference in brain tissue EC_{50} between *mdr1a/b*(-/-) and *mdr1a/b*(+/+) mice for the cyclic opioid peptide DPDPE (Chen and Pollack, 1998). This observation has been used to support the hypothesis that P-gp efflux not only limits access to the brain via the BBB, but parenchymal expression of P-gp may also limit access of P-gp substrates to biophase once the P-gp substrates have crossed the BBB. Another study conducted with morphine indicated that P-gp-mediated efflux had no effect in brain tissue EC_{50} between *mdr1a*(-/-) and *mdr1a*(+/+), even though P-gp efflux increased the ED_{50} by reducing the $K_{p,brain,ss}$ (Zong and Pollack, 2000). Results from this study are consistent with the previous observations for morphine, as there was no difference in brain

EC_{50} of fentanyl, methadone, and loperamide between *mdr1a*(-/-) and *mdr1a*(+/+) mice. However, it should be noted that DPDPE is specific agonist for the delta opioid receptor, whereas fentanyl, methadone, and loperamide are *mu* opioid agonists. Whether this difference has any bearing on P-gp related difference in brain EC_{50} requires further investigation.

P-gp-mediated efflux reduced the $K_{p,brain}$ of fentanyl, methadone, and loperamide by 1.9-, 7.2-, and 44-fold, respectively. These results are consistent with previously reported values for methadone and loperamide (16- and 65-fold, respectively) (Kalvass et al., 2004; Wang et al., 2004). The $K_{p,brain}$ was reduced through the attenuation of brain uptake and the enhancement of brain efflux. This is evident by the fact that the Cl_{up} was smaller, and the Cl_{efflux} was larger, in the P-gp-competent mice compared to P-gp-deficient mice. The effect of P-gp-mediated efflux on brain uptake was generally more significant than on brain efflux. The location of P-gp on the apical membrane of capillary endothelial cells allows it to more effectively attenuate brain uptake than enhance brain efflux (Thiebaut et al., 1989). This is consistent with the present observation that P-gp-mediated efflux attenuated the brain uptake clearance of loperamide by ~20-fold (0.8 vs 0.04 $ml \cdot min^{-1} \cdot kg^{-1}$) and enhanced brain efflux of loperamide only by ~1.5-fold (0.2 vs 0.3 $ml \cdot min^{-1} \cdot kg^{-1}$). Furthermore, the brain equilibration rate constant was about 2-fold higher, and the brain equilibrium half-life was shorter, in P-gp-competent as compared to P-gp-deficient animals. Consistent with P-gp attenuating brain uptake and enhancing brain efflux, P-gp-mediated efflux reduced the extent ($K_{p,brain}$) but not the rate ($K_{eq,brain}$) of brain distribution.

An explanation for why P-gp efflux affects uptake to a larger extent than efflux can be achieved by considering the orientation of P-gp in the BBB, and by taking into account the

diffusional barriers a molecule must transverse to cross the BBB. In order for a molecule to transverse the BBB, it must cross both the apical and basolateral membranes of the endothelial cell. P-gp is present on the apical membrane and pumps in the direction of the capillary lumen (Tsuji et al., 1992). During brain uptake, a drug first encounters the apical membrane followed by the basolateral membrane. The presence of P-gp on the apical membrane allows it to severely limit brain uptake. However, during egress from the brain the drug first encounters the basolateral membrane followed by the apical membrane. In the complete absence of P-gp, the basolateral and apical membranes equally dictate the rate of drug egress from the brain. When P-gp-mediated efflux is present and is sufficiently large, P-gp efflux reduces the resistance of the apical membrane to the point that it is no longer a diffusional barrier, and only the basolateral membrane is a barrier to movement out of the brain. In the absence of efflux, two barriers restrict drug egress from the brain. However, with efflux these two barriers can be effectively reduced to one barrier, resulting in an increase in drug efflux. If the membrane permeability is similar between the apical and basolateral membranes, then P-gp would be expected to increase efflux from the brain by no more than 2-fold. Further evidence supporting this hypothesis is that the brain equilibration half-life, which is inversely proportional to the rate of efflux from the brain, was about 2-fold shorter in the P-gp-competent animals. Other studies indicate a similar effect of BBB efflux on brain equilibration half-life (Letrent et al., 1999; Sugiyama et al., 2003).

In summary this study demonstrated that P-gp-mediated efflux reduced antinociception of fentanyl, methadone, and loperamide by attenuating $K_{p,brain}$. This was evident by rightward-shifts in the antinociception versus serum concentration relationship, identical brain tissue EC_{50} between P-gp-competent and P-gp-deficient mice, and that brain Cl_{up} was increased

while brain Cl_{efflux} was decreased in P-gp-competent mice. Although the extent of brain penetration ($K_{p,brain}$) was reduced by P-gp efflux, the rate of equilibration ($K_{eq,brain}$) of drug between serum and brain was increased by P-gp efflux. The effects of P-gp-mediated efflux on opioid brain penetration and antinociception appear to be due to the *mdr1a* isoform of P-gp.

References

1. Dagenais C, Graff CL and Pollack GM (2004) Variable modulation of opioid brain uptake by P-glycoprotein in mice. *Biochem Pharmacol* **67:**269-276.

2. Juliano R (1976) Drug-resistant mutants of Chinese hamster ovary cells possess an altered cell surface carbohydrate component. *J Supramol Struct* **4:**521-526.

3. Gros P, Ben Neriah YB, Croop JM and Housman DE (1986) Isolation and expression of a complementary DNA that confers multidrug resistance. *Nature* **323:**728-731.

4. Matheny CJ, Lamb MW, Brouwer KR and Pollack GM (2001) Pharmacokinetic and pharmacodynamic implications of P-glycoprotein modulation. *Pharmacotherapy* **21:**778-796.

5. Schinkel AH, Smit JJ, van Tellingen O, Beijnen JH, Wagenaar E, van Deemter L, Mol CA, van der Valk MA, Robanus-Maandag EC, te Riele HP and et al. (1994) Disruption of the mouse mdr1a P-glycoprotein gene leads to a deficiency in the blood-brain barrier and to increased sensitivity to drugs. *Cell* **77:**491-502.

6. Chen C, Liu X and Smith BJ (2003) Utility of Mdr1-gene deficient mice in assessing the impact of P-glyco-protein on pharmacokinetics and pharmacodynamics in drug discovery and development. *Curr Drug Metab* **4:**272-291.

7. Golden PL and Pardridge WM (2000) Brain microvascular P-glycoprotein and a revised model of multidrug resistance in brain. *Cell Mol Neurobiol* **20:**165-181.

8. Schinkel AH, Wagenaar E, Mol CA and van Deemter L (1996) P-glycoprotein in the blood-brain barrier of mice influences the brain penetration and pharmacological activity of many drugs. *J Clin Invest* **97:**2517-2524.

9. Chen C and Pollack GM (1998) Altered disposition and antinociception of [D-penicillamine(2,5)] enkephalin in mdr1a-gene-deficient mice. *J Pharmacol Exp Ther* **287:**545-552.

10. Thompson SJ, Koszdin K and Bernards CM (2000) Opiate-induced analgesia is increased and prolonged in mice lacking P-glycoprotein. *Anesthesiology* **92:**1392-1399.

11. Golden PL and Pollack GM (2003) Blood-brain barrier efflux transport. *J Pharm Sci* **92:**1739-1753.

12. Kalvass JC, Graff CL and Pollack GM (2004) Use of loperamide as a phenotypic probe of mdr1a status in CF-1 mice. *Pharm Res* **21:**1867-1870.

13. Wang JS, Ruan Y, Taylor RM, Donovan JL, Markowitz JS and DeVane CL (2004) Brain penetration of methadone (R)- and (S)-enantiomers is greatly increased by P-glycoprotein deficiency in the blood-brain barrier of Abcb1a gene knockout mice. *Psychopharmacology (Berl)* **173:**132-138.

14. Chen C and Pollack GM (1997) Blood-brain disposition and antinociceptive effects of -D-penicillamine2,5-enkephalin in the mouse. *J Pharmacol Exp Ther* **283:**1151-1159.

15. Zong J and Pollack GM (2000) Morphine antinociception is enhanced in mdr1a gene-deficient mice. *Pharm Res* **17:**749-753.

16. Thiebaut F, Tsuruo T, Hamada H, Gottesman MM, Pastan I and Willingham MC (1989) Immunohistochemical localization in normal tissues of different epitopes in the multidrug transport protein P170: evidence for localization in brain capillaries and crossreactivity of one antibody with a muscle protein. *J Histochem Cytochem* **37:**159-164.

17. Tsuji A, Terasaki T, Takabatake Y, Tenda Y, Tamai I, Yamashima T, Moritani S, Tsuruo T and Yamashita J (1992) P-glycoprotein as the drug efflux pump in primary cultured bovine brain capillary endothelial cells. *Life Sci* **51:**1427-1437.

18. Letrent SP, Pollack GM, Brouwer KR and Brouwer KL (1999) Effects of a potent and specific P-glycoprotein inhibitor on the blood-brain barrier distribution and antinociceptive effect of morphine in the rat. *Drug Metab Dispos* **27:**827-834.

19. Sugiyama D, Kusuhara H, Lee YJ and Sugiyama Y (2003) Involvement of multidrug resistance associated protein 1 (Mrp1) in the efflux transport of 17beta estradiol-D-17beta-glucuronide (E217betaG) across the blood-brain barrier. *Pharm Res* **20:**1394-1400.

Table 6.1. Parameter estimates from PK-PD modeling.

Parameter	fentanyl		methadone		loperamide	
	mdr1a(+/+)	*mdr1a*(-/-)	*mdr1a*(+/+)	*mdr1a*(-/-)	*mdr1a*(+/+)	*mdr1a*(-/-)
K_a (min^{-1})	0.07 ± 0.07		0.55 ± 0.13		0.063 ± 0.015	-
Cl ($ml \cdot min^{-1} \cdot kg^{-1}$)	90 ± 40		127 ± 12		58 ± 7	34 ± 8
V_c ($ml \cdot kg^{-1}$)	2900 ± 2800		8800 ± 600		32000 ± 3000	3000 ± 2000
Cl_d ($ml \cdot min^{-1} \cdot kg^{-1}$)	40 ± 30		-		-	130 ± 140
V_p ($ml \cdot kg^{-1}$)	5000 ± 13000		-		-	4300 ± 1600
Cl_{up} ($ml \cdot min^{-1} \cdot kg^{-1}$)	8 ± 3	10 ± 2	27 ± 4	43 ± 5	0.04 ± 0.06	0.8 ± 0.5
Cl_{efflux} ($ml \cdot min^{-1} \cdot kg^{-1}$)	3.4 ± 1.4	2.2 ± 0.7	5.1 ± 0.9	1.8 ± 0.2	0.3 ± 0.5	0.20 ± 0.11
EC_{50} (ng/g)	6.4 ± 1.1	8.7 ± 1.8	510 ± 60	480 ± 30	104 ± 6	73 ± 12
γ	1.4 ± 0.3		3.7 ± 1.1		2.7 ± 0.5	1.2 ± 0.2
$K_{p,brain}$	2.3 ± 0.2	4.5 ± 0.2	3.3 ± 0.2	24 ± 3	0.115 ± 0.014	5.1 ± 0.9
K_{eq} (min^{-1})	0.14 ± 0.04	0.13 ± 0.02	0.073 ± 0.014	0.029 ± 0.008	0.025 ± 0.010	0.015 ± 0.008
$t_{1/2eq,brain}$ (min)	4.9 ± 1.3	5.2 ± 0.0	9.6 ± 1.8	26 ± 6	27 ± 11	50 ± 20

Parameter estimate ± S.E. from non-linear regression analysis of pooled mouse data.
$t_{1/2eq,brain}$ were calculated from $0.693/K_{eq,brain}$.

Table 6.2. Parameter estimates for loperamide in FVB mice

Parameter	loperamide (FVB mice)	
	mdr1a/b(+/+)	*mdr1a/b*(-/-)
K_a (min^{-1})	0.12±0.04	0.24±0.11
Cl ($ml \cdot min^{-1} \cdot kg^{-1}$)	28±4	100±20
V_c ($ml \cdot kg^{-1}$)	13000±1000	15000±3000
Cl_d ($ml \cdot min^{-1} \cdot kg^{-1}$)	-	-
V_p ($ml \cdot kg^{-1}$)	-	-
Cl_{up} ($ml \cdot min^{-1} \cdot kg^{-1}$)	0.02±0.05	0.88±0.19
Cl_{efflux} ($ml \cdot min^{-1} \cdot kg^{-1}$)	0.2±0.7	0.27±0.06
EC_{50} (ng/g)	82±6	61±5
γ	2.9±0.6	
$K_{p,brain}$	0.13±0.02	18±3
K_{eq} (min^{-1})	0.009±0.003	0.0028±0.0008
$t_{1/2eq,brain}$ (min)	77±20	250±70

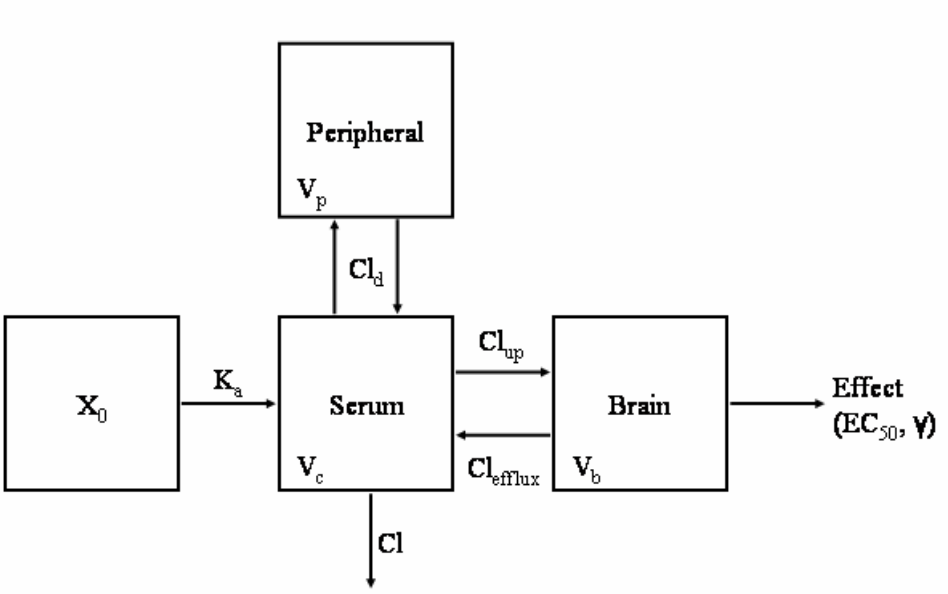

Figure 6.1. Pharmacokinetic-pharmacodynamic model for opioid disposition and antinociception in mice. Pharmacokinetic parameters were obtained by fitting the above model to the time course of serum and brain concentrations of *mdr1*a(-/-) and *mdr1a*(+/+) mice following subcutaneous administration of opioid. Except for loperamide, the absorption rate constant (K_a), central volume (V_c), and systemic clearance (Cl), peripheral volume (V_p), and distributional clearance (Cl_d) were held constant between *mdr1*a(-/-) and *mdr1a*(+/+) mice; whereas, the brain uptake (Cl_{up}) and brain efflux clearances (Cl_{efflux}) were allowed to vary between *mdr1*a(-/-) and *mdr1a*(+/+) mice**.** The brain volume (V_b) was fixed. The effect parameters, EC_{50} and γ, were obtained by fitting a sigmoidal E_{max} model to the brain concentration versus antinociception data. E_{max} was defined as 100%.

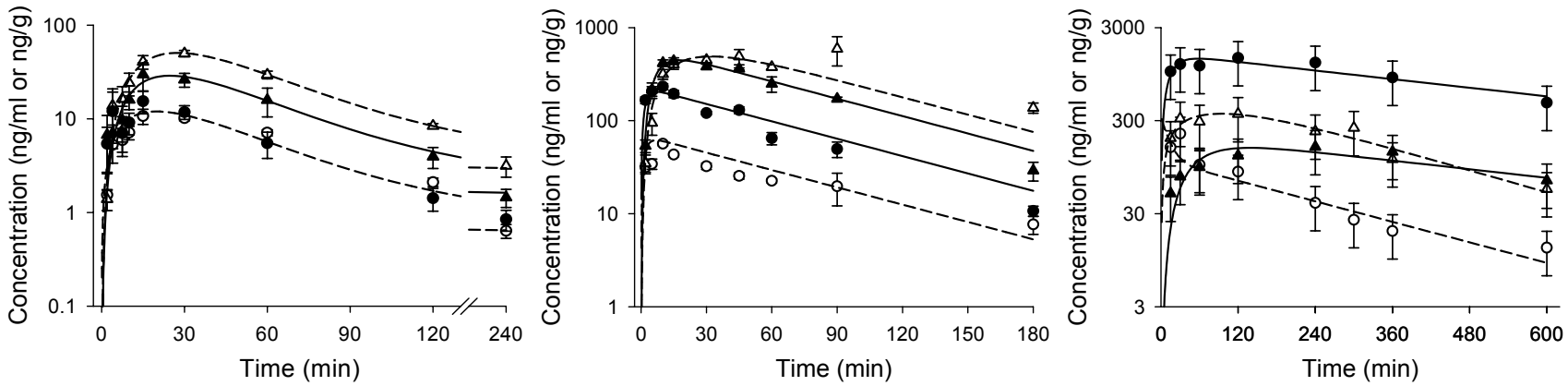

Figure 6.2. Time course of serum (●) and brain (▲) concentrations following s.c. administration of opioids (from left to right: fentanyl [0.09-mg/kg], methadone [0.2- and 0.6-mg/kg], and [1- and 50-mg/kg]) in *mdr1a*(-/-) and *mdr1a*(+/+) mice (open and solid symbols, respectively). Data are presented as mean ± S.E. ($n \geq 3$). Note: At the given doses, nearly equivalent brain concentrations where achieved in *mdr1a*(-/-) and *mdr1a*(+/+) mice, however methadone and loperamide serum concentrations in the *mdr1a*(+/+) mice were much higher than in *mdr1a*(-/-) mice.

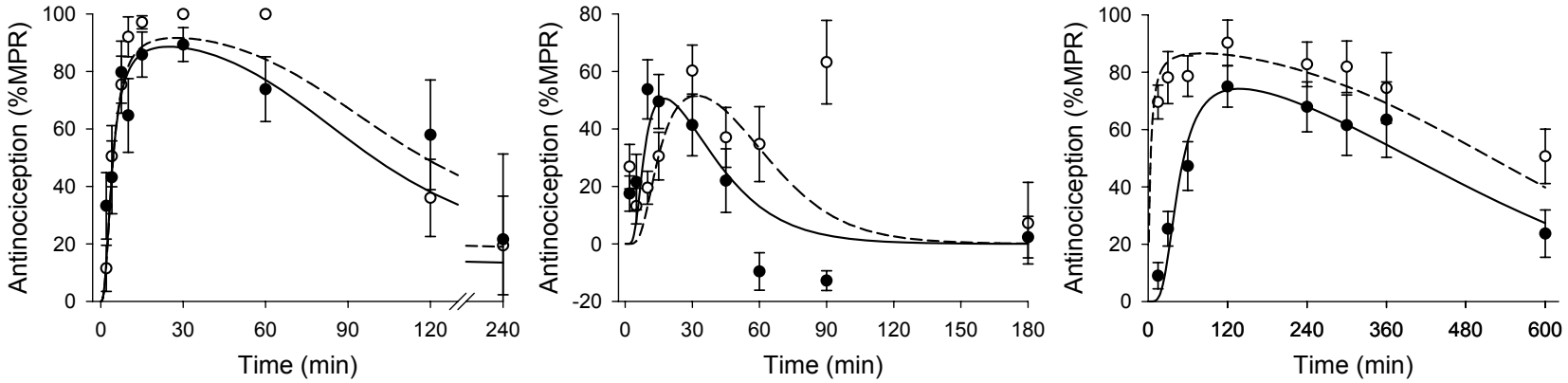

Figure 6.3. Time course of antinociception following s.c. administration of opioids (from left to right: fentanyl, methadone, and loperamide) in *mdr1a*(-/-) and *mdr1a*(+/+) mice (open and solid symbols, respectively). Data are presented as mean ± S.E. (n = 4 to 36).

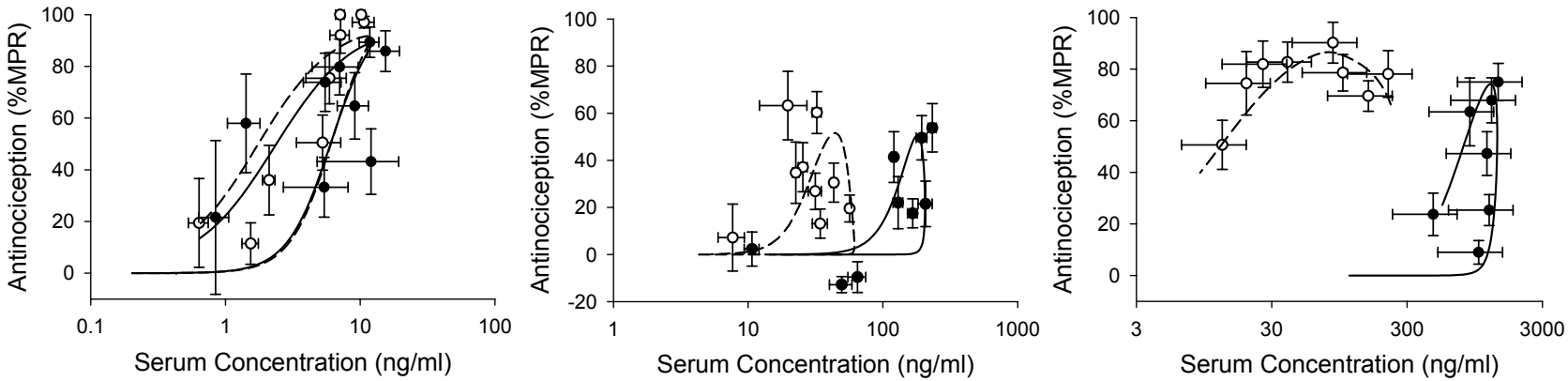

Figure 6.4. Relationship between antinociception and opioid serum concentration (from left to right: fentanyl, methadone, and loperamide) in *mdr1a*(-/-) and *mdr1a*(+/+) mice (open and solid symbols, respectively). Data are presented as mean ± S.E. (n = 4 to 36).

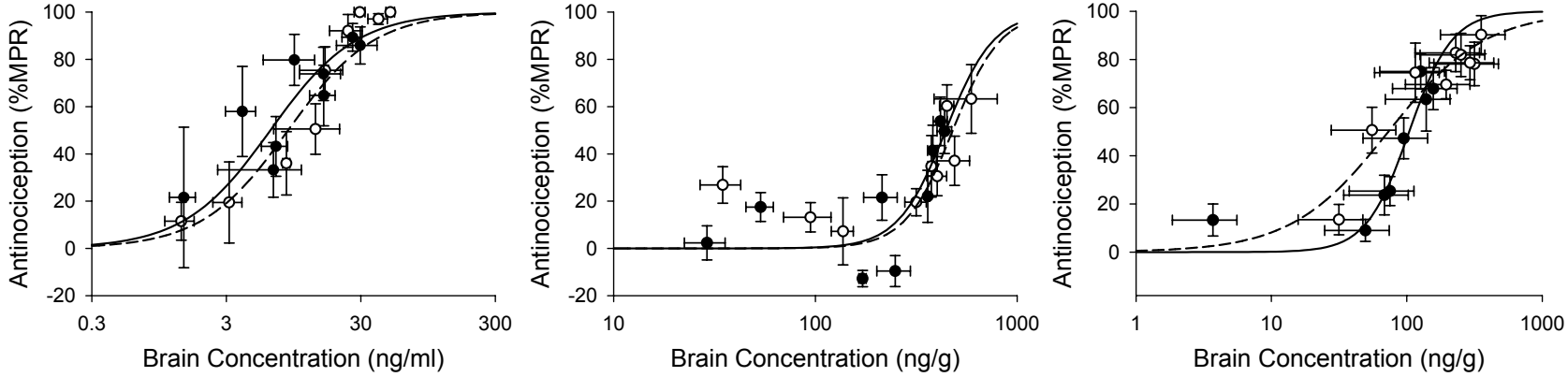

Figure 6.5. Relationship between antinociception and opioid brain concentration (from left to right: fentanyl, methadone, and loperamide) in *mdr1a*(-/-) and *mdr1a*(+/+) mice (open and solid symbols, respectively). Dashed and solid lines represent the fit of a kinetic model to the *mdr1a*(+/+) and *mdr1a*(-/-) data, respectively Data are presented as mean ± S.E. (n = 4 to 36).

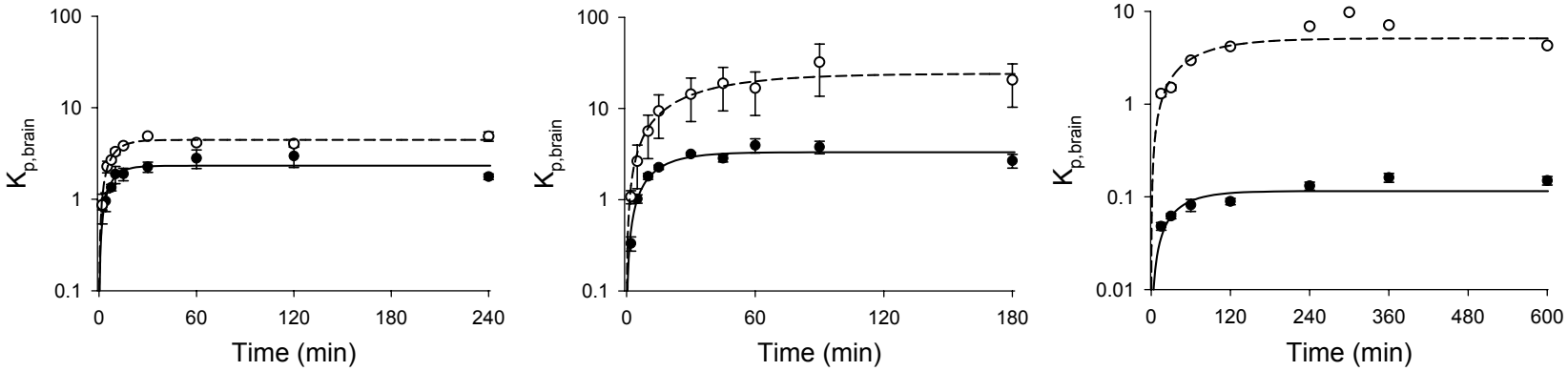

Figure 6.6. Time course of opioid (from left to right: fentanyl, methadone, and loperamide) $K_{p,brain}$ in *mdr1a*(-/-) and *mdr1a*(+/+) mice (open and solid symbols, respectively). Dashed and solid lines represent the fit of a kinetic model to the *mdr1a*(+/+) and *mdr1a*(-/-) data, respectively.

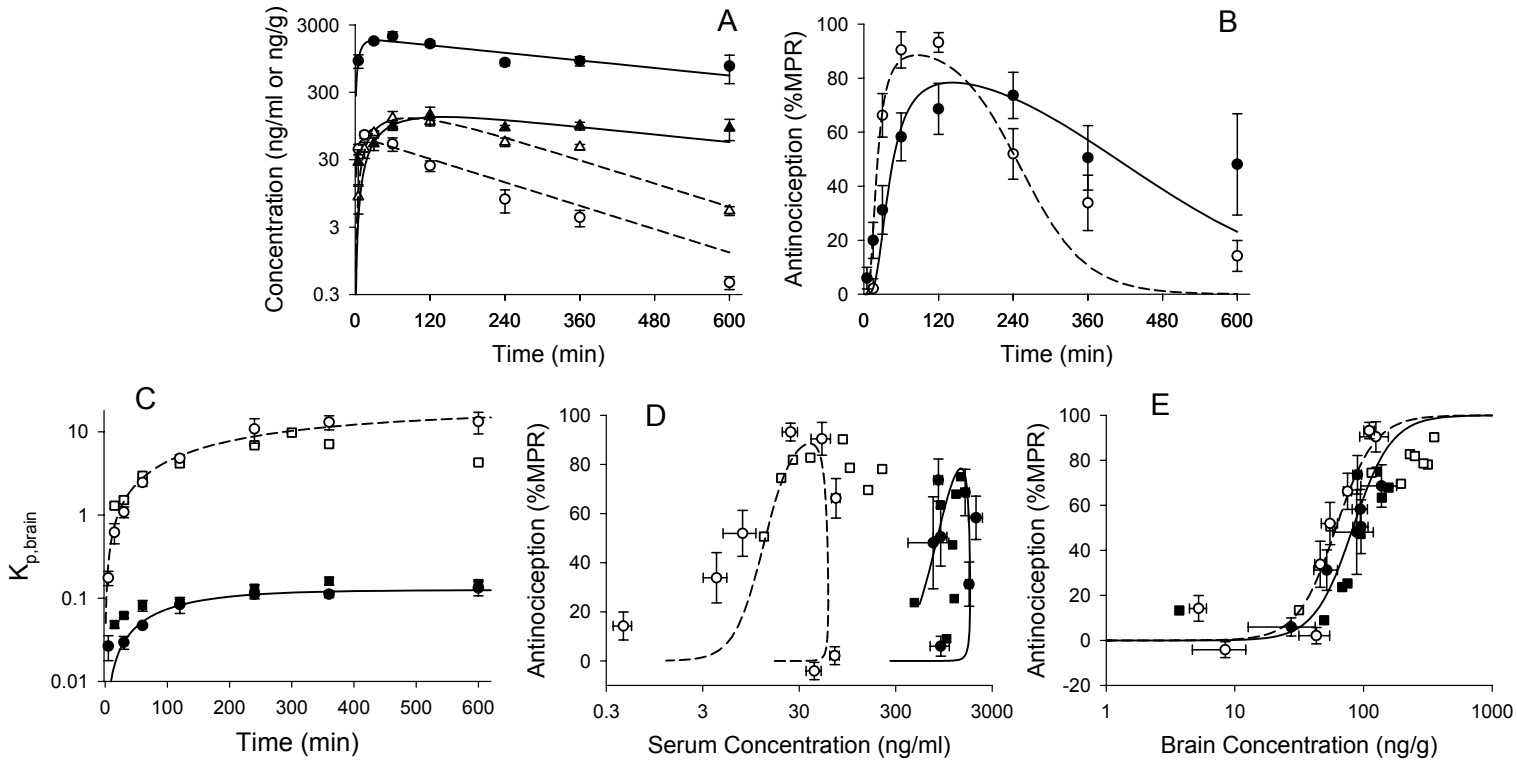

Figure 6.7. Pharmacokinetics/pharmacodynamics of loperamide in FVB mice. Time course of (A) serum (circle) and brain (triangle) concentrations, (B) antinociception, and (C) $K_{p,brain}$ following s.c. administration of 1- and 25-mg/kg dose of loperamide in FVB *mdr1a/b*(-/-) and *mdr1a/b*(+/+) mice, respectively. Antinociception versus serum and brain concentrations are depicted in panels D and E, respectively. Solid and open symbols represent mean data ± S.E. (n = 4 to 36) from P-gp-competent and P-gp-deficient mice, respectively. Solid and dashed lines represent the fit of a PK/PD model to the FVB *mdr1a/b*(+/+) and *mdr1a/b*(-/-) mouse data, respectively. For comparison, squares symbols in panel C, D, and E represent the mean loperamide data obtained from CF-1 mice.

CHAPTER 7

PHARMACOKINETICS AND PHARMACODYNAMICS OF SEVEN OPIOIDS IN P-GP-COMPETENT MICE: ASSESSMENT OF UNBOUND BRAIN EC_{50} AND CORRELATION OF *IN VITRO*, PRECLINICAL, AND CLINICAL DATA

This chapter will be submitted for publication in *Journal of Pharmacology and Experimental Therapeutics* and is presented in the style of that journal.

Abstract

This study was conducted to assess the utility of unbound brain EC_{50} ($EC_{50,u}$) as a measure of *in vivo* potency for centrally-active drugs. Seven *mu* opioid agonists (alfentanil, fentanyl, loperamide, methadone, meperidine, morphine, and sufentanil) were selected as model CNS drugs because they elicit a readily measurable central effect (antinociception) and their clinical pharmacokinetics/pharmacodynamics are well understood. Mice received an equipotent subcutaneous dose of one of the model opioids. The time course of antinociception, serum and brain concentrations was determined. A pharmacokinetic-pharmacodynamic model was used to estimate relevant parameters. *In vitro* potency (K_i) and relevant clinical parameters were obtained from the literature for *in vitro*-to-preclinical and preclinical-to-clinical comparisons. The strongest i*n vitro*-to-*in-vivo* correlation was observed between K_i and brain $EC_{50,u}$ (r^2~0.8). A strong correlation between mouse serum and human plasma EC_{50} was observed (r^2=0.949); the correlation was improved when corrected for protein binding (r^2=0.995). Clinical equipotent i.v. dose was only moderately related to K_i. However, estimates of ED_{50} and EC_{50} (total serum, unbound serum, total brain, and unbound brain) were significant predictors of clinical equipotent i.v. dose; the best correlation was observed for brain $EC_{50,u}$ (r^2=0.982). For each opioid, brain equilibration half-life in mice was almost identical to the plasma effect-site equilibration half-life measured clinically. These results indicate that the mouse is a good model for opioid human brain disposition and clinical pharmacology, and that superior *in vitro*-to-preclinical and preclinical-to-clinical correlations can be achieved with relevant unbound concentrations.

Introduction

In drug discovery, *in vitro* assays and preclinical animal studies are widely used to assess compound potency and to identify compound(s) that may have a desirable clinical response. Several options for assessing compound potency are available, including *in vitro* (receptor binding or functional assays) and *in vivo* (animal studies to determine dose-response or concentration-response relationships) protocols. *In vitro* binding and functional assays, by nature, are designed to estimate the intrinsic potency at the receptor of interest, while *in vivo* experiments take into account the full spectrum of pharmacokinetic and pharmacodynamic processes that ultimately determine biologic response.

Ideally, i*n vitro* potency would translate to or predict *in vivo* potency. Often this is the case, and significant correlations between *in vivo* ED_{50} or EC_{50} and *in vitro* potency have been established for a variety of therapeutic targets (Leysen et al., 1983; Visser et al., 2003). However, when there is no correlation between *in vivo* and *in vitro* potency measures, the validity of the *in vitro* assay, the animal model, and the target may be questioned. Therefore, establishing strong *in vitro*-to-*in vivo* relationships is a necessity for drug development, because it aids in target validation and boosts confidence in the *in vitro* and *in vivo* pharmacology models. Historically, *in vitro*-to-*in vivo* correlations have been established by comparing an *in vitro* measure of potency, such as K_i or EC_{50} from a receptor binding or a cell-based functional assay, with ED_{50}. Although the ED_{50} is not necessarily the best measure of intrinsic drug potency, it has been widely used because it is a straightforward, robust, and readily attainable metric. *In vitro*-to-*in vivo* correlations with ED_{50} are most likely to be successful for a compound set, within a discrete pharmacologic class, that consists of members with large differences in intrinsic potency and relatively similar pharmacokinetics.

For compounds that evidence large differences in pharmacokinetics, improved *vitro*-to-*in vivo* correlations may be obtained by using EC_{50} as opposed to ED_{50}. Commonly, EC_{50} is estimated from the effect vs. plasma concentration relationship. Pharmacokinetic-pharmacodynamic (PK-PD) modeling often is used to obtain estimates of EC_{50} from *in vivo* data, and is a powerful tool for enhancing mechanistic understanding of drug disposition and action.

I*n vitro*-to-*in vivo* potency relationships have maximum predictability when the relationship between biologic response and biophase concentration is known. Total plasma and unbound plasma concentrations are most widely used surrogates for biophase concentrations. However, systemic concentrations do not always reflect biophase concentrations, regardless of whether or not protein binding is taken into account. This is especially for true for compounds that act on targets within the central nervous system (CNS). The blood-brain barrier (BBB) restricts the CNS distribution of many compounds, and in many cases results in temporal dissociation between biophase and systemic concentrations. Therefore, it is important to accurately determine CNS biophase concentrations, or a closely-related surrogate, in order to make better *in vitro*-to-*in vivo* correlations for centrally-active compounds. When compounds have "good" BBB permeability and are not substrates for transporters, *in vitro*-to-*in vivo* correlations can be constructed using unbound plasma or CSF concentrations as a surrogate for CNS biophase concentrations. When unbound plasma or CSF concentrations are not reflective of CNS biophase concentrations, such as when a compound has "poor" BBB permeability or is subject to active brain uptake or efflux, other means for estimating CNS biophase concentrations may be needed. One method for estimating CNS biophase concentrations is simply to multiply total brain concentrations by brain unbound fraction ($f_{u,brain}$).

The present study was conducted to test the hypothesis that the brain $EC_{50,u}$ is the best *in vivo* measure of CNS intrinsic potency. Seven *mu* opioid agonists (alfentanil, fentanyl, loperamide, methadone, meperidine, morphine, and sufentanil) were selected as probe CNS drugs. These agents were selected on the bases of having pronounced differences in potency towards the *mu* opioid receptor (Terenius, 1975; Leysen et al., 1983), differing physiochemical properties (i.e. lipophilicity, unbound fractions, and permeability), and differing extent of CNS distribution (i.e. P-gp or non-P-gp substrate) (Dagenais et al., 2004). PK/PD studies were conducted in mice to determine five measures of *in vivo* potency (ED_{50}; total and unbound EC_{50} for both serum and brain) for each opioid. Estimates of *in vitro* potency (K_i) and relevant clinical parameters were obtained from the literature and used to construct *in vitro*-to-preclinical and preclinical-to-clinical comparisons. The most useful measure of *in vivo* of potency was determined by correlation analysis with the *in vitro* and clinical potency data.

Material and Methods

Materials. Alfentanil was purchased from Taylor Pharmaceuticals (Decatur, IL). Fentanyl, loperamide, methadone, morphine, and oxycodone were purchased from Sigma-Aldrich (St. Louis, MO). Meperidine was obtained from Spectrum Chemicals and Laboratory Products (Gardena, CA). Sufentanil was purchased from Abbott Laboratories (North Chicago, IL). All other reagents were obtained from common sources and were of reagent grade or better.

Animals. Male CF-1 *mdr1a*(+/+) mice (30-40 g; Charles River Laboratories, Inc. Wilmington, MA) were maintained on a 12-h light/dark cycle in a temperature- and humidity-controlled room with access to water and food ad libitum. All procedures involving mice were

approved by The Institutional Animal Care and Use Committee of the University of North Carolina and were conducted in accordance with "Principles of Laboratory Animal Care" (NIH Publication No. 85-23, revised in 1985).

Pharmacokinetic-Pharmacodynamic Study. Based on the results of pilot experiments, a total of 36 *mdr1a*(+/+) CF-1 mice received a single equipotent subcutaneous dose of alfentanil (0.2 mg/kg), fentanyl (0.09 mg/kg), loperamide (50 mg/kg), methadone (0.6 mg/kg), meperidine (25 mg/kg), morphine (3.6 mg/kg), or sufentanil (0.001 mg/kg). Fentanyl and loperamide were prepared in 50/50 propylene glycol/water, whereas the remaining opioids were prepared in 0.9% saline. Antinociception was assessed at selected time points, and 4 mice per opioid were sacrificed by decapitation for collection of brain tissue and blood samples. Trunk blood was collected in 1.5-ml microcentrifuge tubes and was allowed to clot for ≥ 30 min at room temperature. Serum was harvested following centrifugation. Brain and serum samples were stored at -20°C until analysis by HPLC-MS/MS.

Assessment of Antinociception. Antinociception was assessed with the hot plate latency test as described elsewhere (Chen and Pollack, 1997). Prior to opioid administration, baseline hotplate latency was determined for each animal in triplicate. Hotplate latency was defined as the time interval between placement on the hot plate (55°C; Columbus Instruments, Columbus, OH) and the first observation of a jump or lick of a hind limb. Only animals with an average baseline latency < 25 sec were used in this study. A cut-off latency of 60 sec was established to avoid tissue damage. The degree of antinociception was calculated as:

$$\%\text{MPR} = \frac{\text{test latency - control latency}}{60 - \text{control latency}} \times 100\% \qquad \text{(eq. 1)}$$

Evaluation of Protein Binding. Plasma and brain unbound fractions were determined in a 96-well equilibrium dialysis apparatus (HTDialysis, Gales Ferry, CT) using a previously reported method (Kalvass and Maurer, 2002). Briefly, fresh mouse plasma and brain tissue were obtained the day of the study. Spectra-Por 2 membranes obtained from Spectrum Laboratories Inc. (Rancho Dominguez, CA) were conditioned in HPLC water for 15 min, followed by 30% ethanol for 15 min and 100 mM sodium phosphate pH 7.4 buffer for 15 min. Brain tissue was diluted with 3-fold with 100 mM sodium phosphate (pH 7.4) buffer and homogenized with a sonic probe. The drug of interest was added to samples of plasma and brain tissue homogenate (3 and 1 μM, respectively), and 150-μl aliquots (n=6) were loaded into the 96-well equilibrium dialysis apparatus and dialyzed against an equal volume of 100 mM sodium phosphate (pH 7.4) buffer for 4.5 hr in a 155 rpm shaking water bath maintained at 37˚C. Prior experience with the equilibrium dialysis apparatus indicated that equilibrium would be achieved by the end of the specified incubation period (data not shown). Following incubation, 10 μl of matrix (plasma or brain homogenate) and 50 μl of buffer were removed from the apparatus and added directly to HPLC vials containing 100 μl of an appropriate internal standard in methanol. A 50-μl aliquot of control buffer was added to the brain homogenate and plasma samples, and 10 μl aliquot of either control brain homogenate or control plasma was added to the buffer samples, to yield identical matrix composition for all samples prior to analysis. The samples were vortex-mixed, centrifuged, and the supernatant was analyzed by the HPLC-MS/MS as described below. Plasma unbound fraction was calculated from the ratio of concentrations determined in buffer vs. plasma

samples. Equation 2, which accounts for the effect of tissue dilution on unbound fraction (Kalvass and Maurer, 2002), was used to calculate the brain unbound fraction:

$$\text{Undiluted } f_u = \frac{1/D}{((1/f_{u,measured}) - 1) + 1/D} \qquad \text{(eq. 2)}$$

D represents the fold dilution of brain tissue, and $f_{u,measured}$ is the ratio of concentrations determined in buffer vs. brain homogenate samples.

Quantitation of Serum and Brain Concentrations. Brain samples were homogenized in water (1:2 v/v) via sonic probe. An aliquot (2 to 25 µl) of homogenate or serum was transferred to a HPLC vial, and protein was precipitated with 4- to 125-volumes of methanol containing internal standard (5 ng/ml loperamide for alfentanil, fentanyl, meperidine, methadone, and sufentanil; 20 ng/ml methadone for loperamide; and 100 ng/ml oxycodone for morphine). The sample was vortex-mixed, centrifuged, and the supernatant was analyzed by HPLC-MS/MS. Samples were injected (2-10 µl; CTC Analytics autosampler, Zwingen, Switzerland) onto a Phenomenex 2.0 × 30 mm, 5 µm Gemini 110A column (Phenomenex, Torrance, CA) maintained at room temperature. The total run time was 3 min. Analytes were eluted with a linear gradient consisting of ammonium acetate (pH 6.8; 10 mM) ["A"] and methanol ["B"] produced by two Shimadzu LC-10ADVP binary pumps. An initial condition of 5% "B" was ramped to 95% "B" over 2 min, held for 0.5 min, and then returned initial condition of 5% "B" in a single step to re-equilibrate the column. During the run, the flow rate was increased from 750 to 1500 µl/min over the first 2 min, held at 1500 µl/min for 1 min, and then returned the initial flow rate of 750 µl/min in a single step. For the morphine samples, the initial conditions were held for 0.5 minutes before ramping the gradient and flow rate. The entire column effluent was diverted

from the source of the PE-Sciex API-4000 quadrupole mass spectrometer (Turbo V Ionspray source, 700˚C, PerkinElmerSciex Instruments, Boston, MA) for the first 0.8 min and last 0.5 min of the run. Alfentanil, fentanyl, loperamide, methadone, meperidine, morphine, oxycodone, and sufentanil were measured in positive ionization mode using multiple reaction monitoring (417.3→268.3, 337.1→188.3, 477.4→266.0, 248.3→220.3, 310.3→265.2, 286.1→201.1, 316.0→298.0 and 387.2→238.4, respectively). Standard curves were prepared in brain homogenate, serum, plasma, or buffer and were identical in composition to corresponding samples.

Pharmacokinetic-Pharmacodynamic Analysis. A compartmental modeling approach with distribution between serum and brain tissue was used to describe opioid pharmacokinetics. The pharmacokinetic model in Figure 7.1 was fit simultaneously to the serum and brain concentration-time data using nonlinear least-squares regression (WinNonlin 4.1; Pharsight Corporation, Mountain View, CA). The brain volume (V_b) was determined experimentally as 13.4 ml/kg, assuming a specific gravity of 1.0 g/ml. All other pharmacokinetic parameters were obtained from fitting the kinetic model to the data. The pharmacodynamic parameters, EC_{50} and γ, were determined from fitting a sigmoidal E_{max} model to the antinociception versus brain concentration (C) data.

$$\%\mathrm{MPR} = \frac{E_{max} \cdot C^{\gamma}}{EC_{50}{}^{\gamma} + C^{\gamma}} \qquad \text{(eq. 3)}$$

E_{max} was defined as 100%. Serum EC_{50} was calculated from the following equation:

$$\text{serum } EC_{50} = \frac{\text{brain } EC_{50}}{K_{p,brain,ss}} \qquad \text{(eq. 4)}$$

The ED_{50} was calculated, assuming linear pharmacokinetics, from the maximum brain concentration predicted by the PK model (brain C_{max}), the opioid dose (X_0), and the brain EC_{50}.

$$ED_{50} = \frac{\text{brain } EC_{50}}{\text{brain } C_{max}} \times X_0 \qquad \text{(eq. 5)}$$

The time course of the brain-to-serum ratio ($K_{p,brain}$) for each opioid was used to estimate the brain equilibration rate constant (k_{eq}) and steady-state brain-to-serum ratio ($K_{p,brain,ss}$) for that compound according to:

$$K_{p,brain} = K_{p,brain,ss}\left(1 - e^{-k_{eq} \cdot t}\right) \qquad \text{(eq. 6)}$$

The brain equilibration half-life ($t_{1/2eq,brain}$) was obtained from k_{eq}:

$$t_{1/2eq,brain} = \frac{\ln(2)}{K_{eq}} \qquad \text{(eq. 7)}$$

Results

The dose administered to produce equivalent antinociception in mice varied by more than four orders of magnitude between the most and least potent opioid (0.001 vs. 50 mg/kg for sufentanil and loperamide, respectively). Similarly, the calculated mouse ED_{50} varied by nearly five orders of magnitude (Table 7.2). The large range of effective doses was advantageous for subsequent construction of relationships between various *in vitro* and *in vivo* metrics of response.

The pharmacokinetic-pharmacodynamic model adequately described the time course of antinociception, as well as the brain tissue concentration vs. time and serum concentration vs. time relationships, for each of the opioids studied (Figure 7.2). With the exception of fentanyl, the systemic pharmacokinetics of all of the opioids were most effectively modeled with a single compartment system and first-order absorption from the site of administration (Table 7.1 and

Figure 7.2). The disposition of fentanyl required addition of a peripheral distributional compartment with associated parameters (apparent peripheral distributional space [V_p]; distributional clearance [Cl_d]). Estimates of relevant pharmacokinetic parameters for each of the opioids are reported in Table 7.1.

Pharmacokinetic/pharmacodynamic modeling revealed counter-clockwise hysteresis in the antinociception versus serum concentration relationship for each opioid (Figure 7.3). In contrast, all of the opioids exhibited a sigmoidal relationship between antinociception and brain tissue concentration, with no evidence of significant hysteresis behavior associated with temporal dissociation between CNS pharmacokinetics and pharmacodynamics (Figure 7.4). Brain EC_{50} and γ are reported in Table 7.2. Brain EC_{50} estimates differed by more than 3000-fold between the most (sufentanil) and the least (meperidine) potent opioid. Similarly the serum, unbound serum, and unbound brain EC_{50} estimates evidenced a wide range among the seven opioids. Depending on the particular EC_{50} value used as a metric (total brain, unbound brain, total serum, or unbound serum), the rank order of opioid potency differed considerably as a consequence of large differences in $f_{u,plasma}$ and $f_{u,brain}$ among the opioids.

$K_{p,brain,ss}$ values differed by more than 50-fold among the opioids (Table 7.1 and Figure 7.5). The lowest $K_{p,brain,ss}$ was observed for alfentanil (0.19), and the highest for meperidine (6.8). The $t_{1/2eq,brain}$ ranged from 1 to 74 min, with alfentanil and morphine having the shortest and longest $t_{1/2eq,brain}$, respectively (Table 7.1).

In vitro-to-*in vivo* relationships (Figure 7.6) revealed that mouse serum EC_{50} and brain EC_{50} correlated poorly with *in vitro* K_i ($r^2<0.5$). A modest improvement was observed for the correlation between unbound serum $EC_{50,u}$ and K_i ($r^2=0.583$). The strongest relationship was observed between unbound brain $EC_{50,u}$ and K_i ($r^2 < 0.799$).

Preclinical-to-clinical relationships indicated that mouse serum and human plasma EC_{50} estimates were well-correlated (r^2=0.949). Despite the strength of this relationship, the correlation was improved when the EC_{50} values were corrected for binding to plasma proteins (r^2=0.995) (Figure 7.7). Correlations also were explored between human equipotent clinical i.v. dose of the opioids and various estimates of *in vitro* and *in vivo* potency (Figure 7.8). The relationship between equipotent clinical dose and K_i was relatively poor (r^2=0.677). Equipotent clinical i.v. dose correlated more strongly with mouse ED_{50} (r^2=0.932). Equipotent clinical i.v. dose also correlated equally well with total and unbound mouse serum EC_{50} (r^2=0.922 and r^2=0.937, respectively). Somewhat surprisingly, equipotent clinical i.v. dose did not correlate as well with total brain EC_{50} (r^2=0.878) compared to the relationships with metrics obtained from plasma. However, the equipotent clinical i.v. dose correlated most strongly with unbound brain $EC_{50,u}$ values in the mouse (r^2=0.982).

The brain equilibration half-life in mouse determined in the present study ($t_{1/2eq,brain}$) was compared to the apparent plasma-biophase equilibration half-life in humans ($t_{1/2,Ke0}$), obtained from the literature, among the opioids examined in this study. The correlation between clinical $t_{1/2,Ke0}$ and mouse $t_{1/2eq,brain}$ was excellent (r^2=0.988). With the exception of morphine, all of the opioids fell within a factor of 1.4-fold relative to the line of identity (Figure 7.9).

Discussion

An integrated pharmacokinetic/pharmacodynamic modeling strategy yielded an adequate description of the time course of antinociception, serum concentrations, and brain tissue concentrations, for each of the opioids examined in this study. Systemic clearance of these

opioids differed by ~10-fold within the compound set. In contrast, the *in vivo* potency measurements differed up to 30,000-fold. The differences in the range of behavior within the compound set between systemic pharmacokinetics (exemplified by clearance) and pharmacodynamics (as indicated by potency metrics) indicated that factors other than systemic disposition are the primary determinants of the magnitude and time course of antinociceptive response. Among these non-systemic factors, are distribution into the CNS (as indicated by the equilibration half-life), distribution within the CNS (reflected by the brain tissue unbound concentration), and intrinsic potency of the opioid.

Pharmacokinetic/pharmacodynamic modeling revealed counter-clockwise hysteresis in the antinociception versus serum concentration relationship for each opioid (Figure 7.3). The hysteresis behavior was consistent with delayed distribution between the serum and the biophase. In contrast, all of the opioids exhibited a sigmoidal relationship between antinociception and brain tissue concentration, with no evidence of significant hysteresis behavior associated with temporal dissociation between CNS pharmacokinetics and pharmacodynamics (Figure 7.4). Brain EC_{50} and γ are reported in Table 7.2. Brain EC_{50} estimates differed by more than 3000-fold between the most (sufentanil) and the least (meperidine) potent opioid. Similarly the serum, unbound serum, and unbound brain EC_{50} estimates evidenced a wide range among the seven opioids. Depending on the particular EC_{50} value used as a metric (total brain, unbound brain, total serum, or unbound serum), the rank order of opioid potency differed considerably as a consequence of large differences in $f_{u,plasma}$ and $f_{u,brain}$ among the opioids. For instance, loperamide was the least potent of the seven opioid based on total serum EC_{50} values; however, it was the 5^{th}, 4^{th}, and 2^{nd} most potent opioid based on the total brain EC_{50}, unbound serum $EC_{50,u}$, and unbound brain EC_{50u}, values respectively.

In vitro-to-preclinical correlations. Previous studies have established *in vitro*-to-preclinical correlations for opioid potency. Leysen *et al.* (1983) reported a correlation (r^2= 0.81) between *in vitro* K_i (displacement of sufentanil in rat forebrain membranes) and ED_{50} (rat tail withdrawal reflex) for 35 opioids from 5 structural classes, with more >100,000-fold difference in receptor affinity. However, no correlation existed between K_i and ED_{50} if only alfentanil, fentanyl, loperamide, methadone, meperidine, morphine, and sufentanil were included in the analysis ($r^2 < 0.15$) (Niemegeers et al., 1979; Leysen et al., 1983). In the present study, there was a similarly poor correlation ($r^2 = 0.167$) between *in vitro* K_i and mouse ED_{50} for alfentanil, fentanyl, loperamide, methadone, meperidine, morphine, and sufentanil. This lack of correlation can be attributed to differences in pharmacokinetics and biophase distribution characteristics for the seven opioids. The opioids selected for this study came from four different structural classes: diphenyproplamines (loperamide and methadone), 4-ax-phenylpiperidines (morphine), 4-eq-phenylpiperidines (meperidine), and 4-anilinopiperidines (alfentanil, fentanyl, and sufentanil). At least three (fentanyl, methadone, and methadone) are P-gp substrates (Dagenais et al., 2004). Consequently, the opioids examined have different physiochemical properties and CNS (biophase) distribution characteristics. One would anticipate that K_i would be a better predictor of biophase EC_{50} because the confounding influences of pharmacokinetics and biophase distribution are removed.

Total plasma, unbound plasma, and cerebrospinal fluid (CSF) concentrations been used to estimate CNS biophase concentration for *in vitro*-to-*in vivo* correlations. Visser et al. (2003) demonstrated that, for nine $GABA_A$ modulators, *in vitro*-to-*in vivo* correlations could be made between K_i and either total or unbound plasma EC_{50}; however, the unbound plasma EC_{50}

correlated better with K_i than total plasma EC_{50}. Another study demonstrated the *in vitro* K_i of alfentanil, fentanyl, and sufentanil correlated well with the *in vivo* EC_{50} determined from CSF concentrations (Cox et al., 1998).

In this study, total plasma, total brain, unbound plasma, and unbound brain EC_{50} estimates were used to express opioid potency and were evaluated as potential surrogates for biophase EC_{50}. The total serum and total brain EC_{50} were weakly related to *in vitro* K_i ($r^2<0.5$). A modest improvement was observed with unbound serum $EC_{50,u}$ ($r^2=0.583$). However, the strongest relationship was observed between unbound brain $EC_{50,u}$ and K_i ($r^2=0.799$). These results are consistent with unbound brain concentrations serving as the best surrogate for CNS biophase.

Preclinical-to-clinical correlations. Predicting human efficacious plasma concentrations is an important part of drug discovery, since this information is needed for dose selection and assessing relative safety margin. For example, it may be desirable to have more than a 10-fold safety window between projected efficacious and toxic concentrations (e.g., QT prolongation). Often, human efficacious plasma concentrations are predicted from total plasma concentrations in preclinical efficacy models (Danhof et al., 1993; Ito et al., 1993). Assuming the drug has similar pharmacology and plasma protein binding in humans and preclinical models, this prediction should be valid. In the present study, mouse total serum EC_{50} correlated well with human total plasma EC_{50} ($r^2=0.949$), consistent with similarities between mouse and human opioid pharmacology and plasma protein binding. However, the correlation improved when the EC_{50} values were corrected for protein binding ($r^2=0.995$). On average, mouse unbound serum $EC_{50,u}$ over-predicted human unbound human plasma $EC_{50,u}$ by 2.8-fold (data not shown), although the correlation per se was very strong. Thus, it may not be possible to use mouse serum

$EC_{50,u}$ as a predictor of human efficacious serum concentrations for a single opioid in isolation. However, the murine model appears to be a remarkably effective predictor of relative human efficacious serum concentrations among a set of *mu* opioids, even when those compounds are derived from different chemical classes.

The ability to predict human dose from *in vitro* and preclinical data also is important. Clinical dose often correlates with ED_{50} obtained from animal models. For example, Niemegeers et al. (1979) demonstrated that rat ED_{50} determined for antidiarrheal and analgesic activity strongly correlated with clinical dose for 12 opioids. In the present study, the equipotent clinical i.v. dose and mouse ED_{50} correlated well for the 7 opioids examined (r^2=0.932). Although efficacious dose is dependent on many factors, including systemic disposition, target-site pharmacokinetics, and intrinsic potency, the observed differences in efficacious dose appear to be dominated by intrinsic potency. Therefore, any reliable measure of opioid *in vivo* intrinsic potency should correlate well with the clinical equipotent i.v. dose for these opioids.

Various *in vitro* and *in vivo* measures of opioid potency were correlated with clinical equipotent i.v. dose to evaluate predictive potential. The *in vitro* K_i was a weak predictor of equipotent clinical i.v. dose (r^2=0.677). Equipotent clinical dose correlated better with *in vivo* measures, including mouse ED_{50} (r^2=0.932) and total or unbound mouse serum EC_{50} (r^2=0.922 and r^2=0.937, respectively). It was surprising that equipotent clinical dose did not correlate as well with total brain EC_{50}s (r^2=0.879) as with either serum concentration measure or murine effective dose, suggesting that non-specific opioid binding in brain is substantial. As expected, the equipotent clinical dose correlated best with unbound brain $EC_{50,u}$ (r^2=0.982), consistent unbound brain $EC_{50,u}$ being the best measure of *in vivo* intrinsic opioid potency.

It is interesting to note that the $t_{1/2eq,brain}$ determined in mice, derived from the kinetics of drug equilibration between brain tissue and serum, was almost identical to the clinical $t_{1/2,Ke0}$, an inferred value from the kinetics of pharmacologic response in the context of kinetics of systemic disposition (Figure 7.9). Morphine evidenced the largest discrepancy between these metrics, with $t_{1/2,Ke0}$ being 2.4-fold larger than mouse $t_{1/2eq,brain}$. Morphine-6-gluronide, an active metabolite of morphine in humans have (Glare and Walsh, 1991) that is not formed extensively in rodents, possesses a long $t_{1/2,Ke0}$ (> 3600 min (Lotsch, 2005)). Because morphine and its active metabolite exist in combination after morphine administration in humans, the $t_{1/2,Ke0}$ estimate obtained will reflect the contribution of both parent drug and metabolite. The remarkable relationship between $t_{1/2,Ke0}$ and $t_{1/2eq,brain}$, together with the strong interspecies correlation between unbound serum/plasma EC_{50}, suggests that the brain distribution characteristics are similar between humans and mice.

Relative potency and $K_{p,brain}$. Even though all seven opioids examined are *mu* agonists, they do not have the same primary indication. The primary indication of a given opioid appears not to be related to intrinsic opioid potency, but rather to differences in brain distribution characteristics and systemic pharmacokinetics. For example, the two anesthetic opioids, alfentanil and sufentanil, have the shortest mouse systemic half-life (8 and 14 min, respectively) and $t_{1/2eq,brain}$ (1 and 4 min, respectively) of the opioids examined. The short systemic half-life, combined with the short $t_{1/2eq,brain}$, results in a rapid onset and offset of action, allowing for rapid adjustment of response during i.v. infusion. Fentanyl, methadone, meperidine, and morphine, on the other hand, have longer half-lives and $t_{1/2eq,brain}$, rendering them more suitable as analgesics. The brain distribution of loperamide is limited due to P-gp-mediated efflux (Schinkel et al., 1996) allowing

it to act selectively on *mu* opioid receptors in the intestinal tract versus the CNS and conferring ideal antidiarrheal properties. These relationships indicate that systemic pharmacokinetics and biophase distribution characteristics are more important than intrinsic potency for optimizing an opioid action towards a given indication (anesthetic, analgesic, or antidiarrheal). Undoubtedly, potency and biophase distribution characteristics must to be balanced with other properties and considerations (i.e., solubility, permeability, bioavailability, systemic clearance and half-life) to achieve compounds that will be useful clinical agents. However, the current data clearly indicate the importance of target-site pharmacokinetics and activity in determining qualitative, as well as quantitative, clinical response.

$K_{p,brain}$ often is used as a measure of CNS exposure, under the assumption that larger values of $K_{p,brain}$ equate with higher CNS exposure. CNS drug discovery programs have devoted much effort and resources to predicting and maximizing the $K_{p,brain}$ of drug candidates. Although not the main intent of this work, the results presented herein can be used to illustrate the fallacy of pursing this strategy. As previously demonstrated, K_i, ED_{50}, EC_{50}, and equipotent i.v. clinical doses are appropriate parameters for constructing *in vitro*-to-*in vivo* and preclinical-to-clinical correlations. The same cannot be said for $K_{p,brain}$. Even though $K_{p,brain}$ values differed by more than 50-fold among the opioids examined, there was no correlation between $K_{p,brain}$ and any relevant pharmacodynamic parameter ($r^2<0.2$) for K_i, EC_{50}, $EC_{50,u}$, ED_{50}, equipotent i.v. clinical dose, $f_{u,plasma}$, $f_{u,brain}$, $t_{1/2eq,brain}$ and $t_{1/2,Ke0}$). With the exception of loperamide, all of the opioids examined are marketed CNS-active drugs exhibiting $K_{p,brain}$ values ranging between 0.19 and 6.8. This large range of $K_{p,brain}$ values, which was not meaningfully correlated with any relevant measure of opioid action, indicates that $K_{p,brain}$ is not a useful parameter. In contrast to $K_{p,brain}$, the unbound brain and unbound plasma concentrations were useful for *in vitro*-to-*in vivo* and

preclinical-to-clinical predictions, and the ratio of unbound brain to unbound plasma concentrations better reflects pharmacologically relevant brain exposure.

In summary, these results suggest that the mouse is a good model for opioid brain disposition and pharmacology, and that superior *in vitro*-to-preclinical and preclinical-to-clinical correlations can be established when making comparisons between relevant unbound concentrations.

References

1. Chen C and Pollack GM (1997) Blood-brain disposition and antinociceptive effects of -D-penicillamine2,5-enkephalin in the mouse. *J Pharmacol Exp Ther* **283:**1151-1159.

2. Cox EH, Kerbusch T, Van der Graaf PH and Danhof M (1998) Pharmacokinetic-pharmacodynamic modeling of the electroencephalogram effect of synthetic opioids in the rat: correlation with the interaction at the mu-opioid receptor. *J Pharmacol Exp Ther* **284:**1095-1103.

3. Dagenais C, Graff CL and Pollack GM (2004) Variable modulation of opioid brain uptake by P-glycoprotein in mice. *Biochem Pharmacol* **67:**269-276.

4. Danhof M, Mandema JW, Hoogerkamp A and Mathot RA (1993) Pharmacokinetic-pharmacodynamic modelling in pre-clinical investigations: principles and perspectives. *Eur J Drug Metab Pharmacokinet* **18:**41-47.

5. Glare PA and Walsh TD (1991) Clinical pharmacokinetics of morphine. *Ther Drug Monit* **13:**1-23.

6. Inturrisi CE, Colburn WA, Kaiko RF, Houde RW and Foley KM (1987) Pharmacokinetics and pharmacodynamics of methadone in patients with chronic pain. *Clin Pharmacol Ther* **41:**392-401.

7. Ito K, Yajima N, Ohtani H, Yamada Y, Nakamura K, Sawada Y and Iga T (1993) Prediction of the therapeutic dose for beta-stimulants based on preclinical data: application of oral dosage forms and aerosols to asthmatic patients. *J Pharmacokinet Biopharm* **21:**133-144.

8. Kalvass JC and Maurer TS (2002) Influence of nonspecific brain and plasma binding on CNS exposure: implications for rational drug discovery. *Biopharm Drug Dispos* **23:**327-338.

9. Kurz A, Ikeda T, Sessler DI, Larson MD, Bjorksten AR, Dechert M and Christensen R (1997) Meperidine decreases the shivering threshold twice as much as the vasoconstriction threshold. *Anesthesiology* **86:**1046-1054.

10. Leysen JE, Gommeren W and Niemegeers CJ (1983) [3H]Sufentanil, a superior ligand for mu-opiate receptors: binding properties and regional distribution in rat brain and spinal cord. *Eur J Pharmacol* **87:**209-225.

11. Lotsch J (2005) Pharmacokinetic-pharmacodynamic modeling of opioids. *J Pain Symptom Manage* **29:**S90-103.

12. Meuldermans WE, Hurkmans RM and Heykants JJ (1982) Plasma protein binding and distribution of fentanyl, sufentanil, alfentanil and lofentanil in blood. *Arch Int Pharmacodyn Ther* **257:**4-19.

13. Niemegeers CJ, McGuire JL, Heykants JJ and Janssen PA (1979) Dissociation between opiate-like and antidiarrheal activities of antidiarrheal drugs. *J Pharmacol Exp Ther* **210:**327-333.

14. Schinkel AH, Wagenaar E, Mol CA and van Deemter L (1996) P-glycoprotein in the blood-brain barrier of mice influences the brain penetration and pharmacological activity of many drugs. *J Clin Invest* **97:**2517-2524.

15. Terenius L (1975) Comparison between narcotic "receptors" in the guinea-pig ileum and the rat brain. *Acta Pharmacol Toxicol (Copenh)* **37:**211-221.

16. Visser SA, Wolters FL, Gubbens-Stibbe JM, Tukker E, Van Der Graaf PH, Peletier LA and Danhof M (2003) Mechanism-based pharmacokinetic/pharmacodynamic modeling of the electroencephalogram effects of GABAA receptor modulators: in vitro-in vivo correlations. *J Pharmacol Exp Ther* **304:**88-101.

17. Wood M and Alastair JJ (1990) *Drugs and anesthesia: pharmacology for anesthesiologist*. Williams & Wilkins, Baltimore.

Table 7.1. Parameter estimates from PK-PD modeling.

Parameter	alfentanil	fentanyl	loperamide	meperidine	methadone	morphine	sufentanil
K_a (min^{-1})	0.35 ± 0.03	0.07 ± 0.07	0.063 ± 0.015	0.39 ± 0.18	0.55 ± 0.13	0.27 ± 0.04	0.32 ± 0.12
Cl ($ml \cdot min^{-1} \cdot kg^{-1}$)	82 ± 3	90 ± 40	58 ± 7	190 ± 40	127 ± 12	95 ± 5	19 ± 3
V_c ($ml \cdot kg^{-1}$)	1000 ± 60	3000 ± 3000	32000 ± 3000	6100 ± 1200	8800 ± 600	2900 ± 180	400 ± 80
Cl_d ($ml \cdot min^{-1} \cdot kg^{-1}$)	-	40 ± 30	-	-	-	-	-
V_p ($ml \cdot kg^{-1}$)	-	5000 ± 13000	-	-	-	-	-
Cl_{up} ($ml \cdot min^{-1} \cdot kg^{-1}$)	4 ± 3	8 ± 3	0.04 ± 0.06	100 ± 40	27 ± 4	9.5 ±0.5	37 ± 14
Cl_{efflux} ($ml \cdot min^{-1} \cdot kg^{-1}$)	22 ± 17	3.4 ± 1.4	0.3 ± 0.5	8 ± 4	5.1 ± 0.9	1.9 ± 1.4	12 ± 5
EC_{50} (ng/g)	9.2 ± 1.7	6.4 ± 1.1	100 ± 6	2200 ± 110	510 ± 60	38 ± 4	1.0 ± 0.2
γ	1.8 ± 0.4	1.4 ± 0.3	2.7 ± 0.5	7.8 ± 4.2	3.7 ± 1.1	2.3 ± 0.5	2.5 ± 1.3
$K_{p,brain}$	0.195 ± 0.0087	2.3 ± 0.2	0.115 ± 0.014	6.8 ± 0.5	3.3 ± 0.2	1.1 ± 0.6	2.1 ± 0.3
K_{eq} (min^{-1})	0.64 ± 0.09	0.14 ± 0.04	0.025 ± 0.010	0.13 ± 0.03	0.073 ± 0.014	0.009 ± 0.006	0.16 ± 0.06
$t_{1/2eq,brain}$ (min)	1.08 ± 0.16	4.9 ± 1.3	27 ± 11	5.4 ± 1.1	9.6 ± 1.8	74 ± 45	4.3 ± 1.6

Parameter estimate ± S.E. from non-linear regression analysis of pooled *mdr1a*(+/+) mouse data.

$t_{1/2eq,brain}$ were calculated from $0.693/K_{eq,brain}$.

Table 7.2. Additional parameters used for correlation of *in vitro*, preclinical, and clinical data.

Parameter	alfentanil	fentanyl	loperamide	meperidine	methadone	morphine	sufentanil
In Vitro Ki (nM) [a]	19	1.6	0.50 [b]	193	2.2	5.7	0.10
Mouse ED_{50} (mg/kg)	0.079	0.020	36	3.2	2.2	0.94	0.00041
Mouse $f_{u,plasma}$ [c]	0.26	0.17	0.029	0.36	0.15	0.50	0.054
Mouse $f_{u,brain}$ [c]	0.33	0.070	0.0047	0.13	0.029	0.41	0.034
Human Plasma EC_{50} (nM) [d]	1337	24	n.a.	6034 [e]	1151	195	1.8
Human Equipotent IV dose (mg) [f]	0.75	0.10	n.a.	90	8.75	10	0.015
Human $t_{1/2,Ke0}$ (min) [d]	1.0	5.8	n.a.	-	12	178	6.2
Human $f_{u,plasma}$	0.079 [g]	0.156 [g]	-	0.35 [e]	0.125 [h]	0.75 [i]	0.75 [g]

[a] (Leysen et al., 1983)
[b] (Terenius, 1975)
[c] (Kalvass and Pollack, 2006)
[d] Average from EEG power spectrum analysis, analgesia (cancer pain), pain tolerance, and/or post operative analgesia; (Lotsch, 2005)
[e] Unbound potency of meperidine is 20 time less than alfentanil; (Kurz et al., 1997)
[f] (Wood and Alastair, 1990)
[g], [h], and [i] (Meuldermans et al., 1982), (Inturrisi et al., 1987), and (Glare and Walsh, 1991), respectively

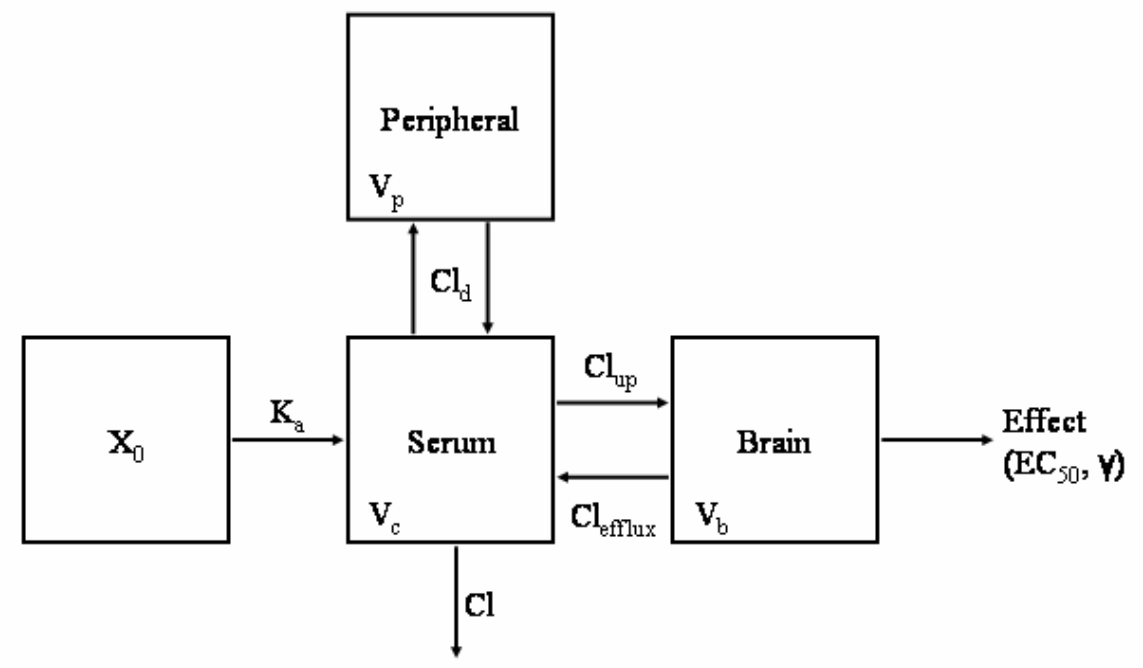

Figure 7.1. Pharmacokinetic-pharmacodynamic model for opioid disposition and antinociception in mice. Pharmacokinetic parameters were obtained by fitting the model to the time course of serum and brain concentrations in *mdr1a*(+/+) mice following subcutaneous administration. The absorption rate constant (K_a), central volume (V_c), systemic clearance (Cl), peripheral volume (V_p), distributional clearance (Cl_d), brain uptake clearance (Cl_{up}), and brain efflux clearance (Cl_{efflux}) were estimated for each opioid**.** The brain volume (V_b) was fixed. The effect parameters, EC_{50} and γ, were obtained by fitting a sigmoidal E_{max} model to the brain concentration versus antinociception data. E_{max} was defined as 100%.

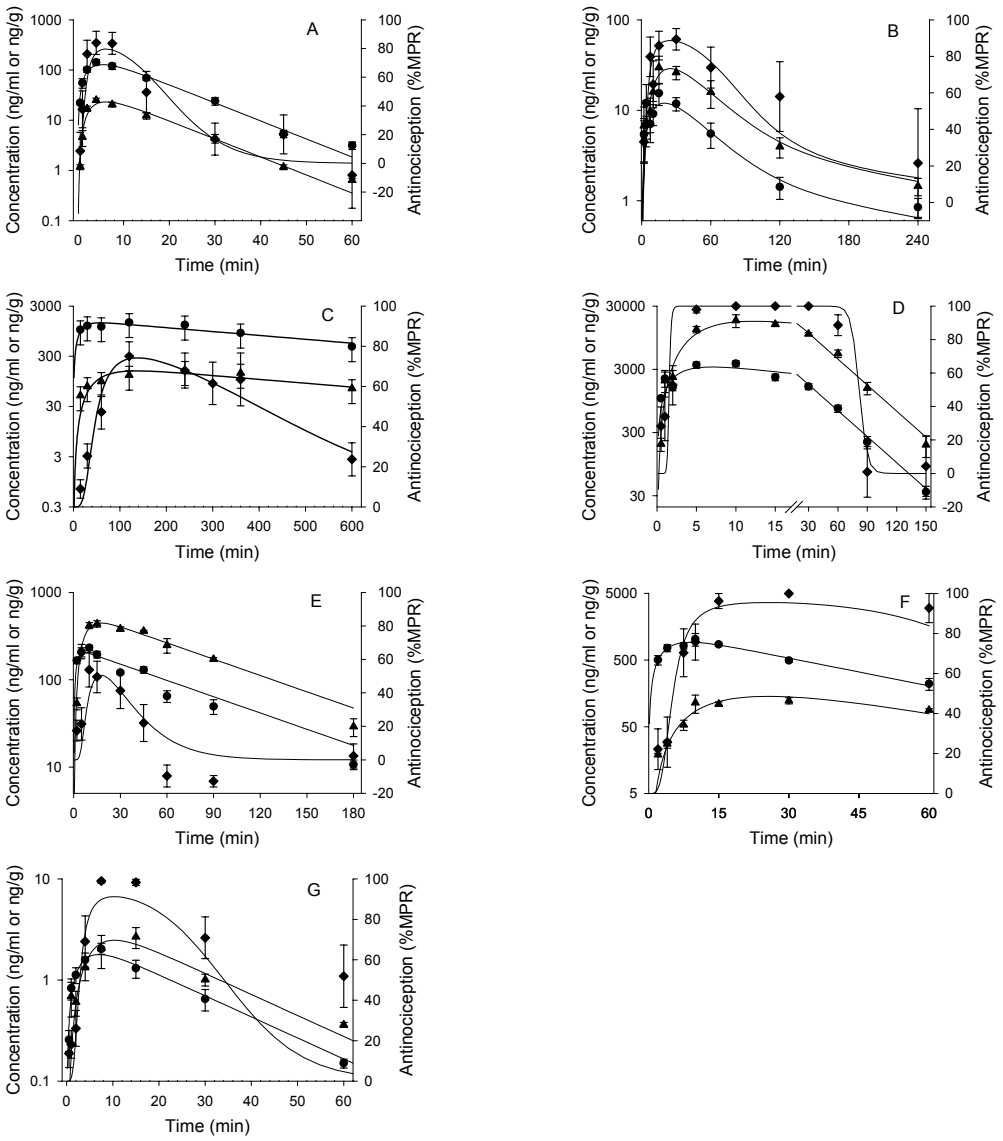

Figure 7.2. Time course of antinociception (◆), serum (●) and brain (▲) concentrations following (A) 0.2-mg/kg s.c. dose of alfentanil; (B) 0.9-mg/kg s.c. dose of fentanyl; (C) 50-mg/kg s.c. dose of loperamide; (D) 25-mg/kg s.c. dose of meperidine; (E) 2-mg/kg s.c. dose of methadone; (F) 3.6-mg/kg s.c. dose of morphine; or (G) 0.001-mg/kg s.c. dose of sufentanil in CF-1 *mdr1a*(+/+) mice. Data are presented as mean ± S.E. [concentration data ($n \geq 3$); antinociception (n = 4 to 36)]. Lines represent the fit of the PK-PD model to the antinociception and concentration data.

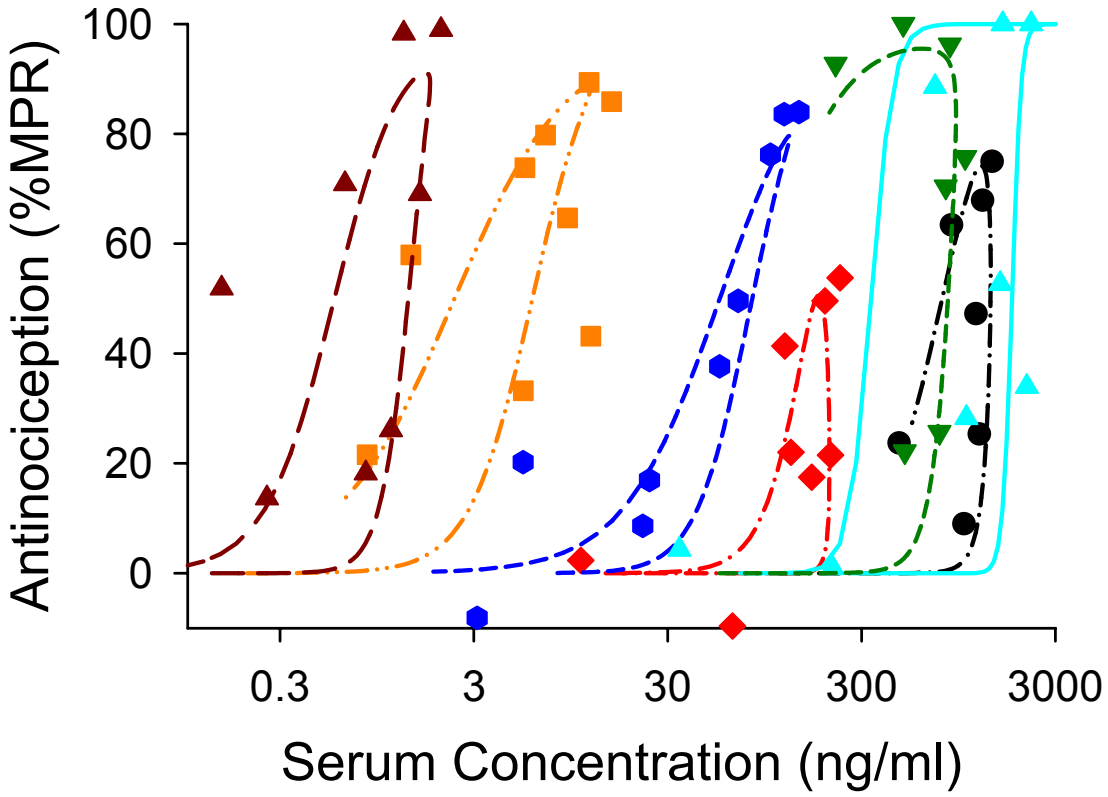

Figure 7.3. Relationship between plasma concentration and antinociception for *mu* opioid agonists. Symbols represent data from *mdr1a*(+/+) mice. Lines represent the fit of the PK/PD model to the antinociception-serum concentration data. Symbols are as follows: ▲ sufentanil, ■ fentanyl, ⬢ alfentanil, ◆ methadone, ▲ meperidine, ▼morphine, and ● loperamide. All opioids exhibited a counter-clockwise hysteresis in the antinociception versus serum concentration relationship. Data are presented as means [serum concentration (n = 2 to 4); antinociception (n = 4 to 36)].

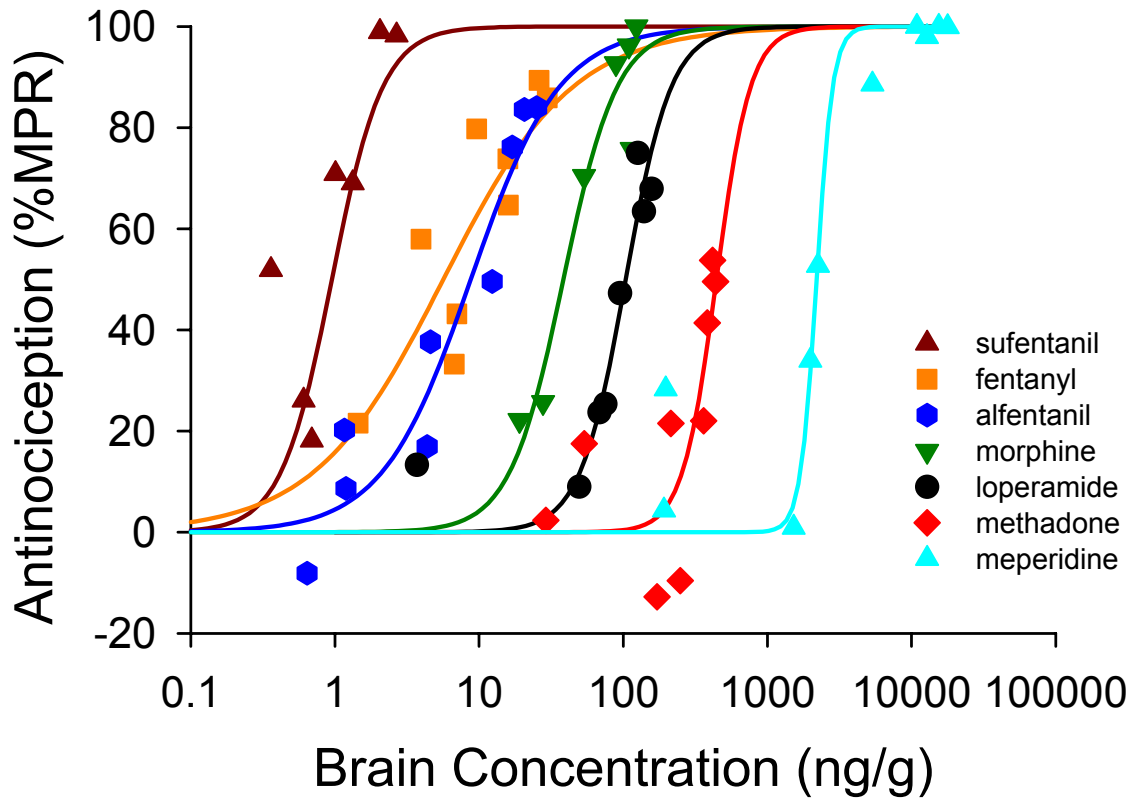

Figure 7.4. Relationship between brain concentration and antinociception for *mu* opioid agonists. Symbols represent data from *mdr1a*(+/+) mice. Lines represent the fit of a sigmoidal E_{max} model to the antinociception-brain concentration data. Data are presented as means [brain concentration (n = 2 to 4); antinociception (n = 4 to 36)].

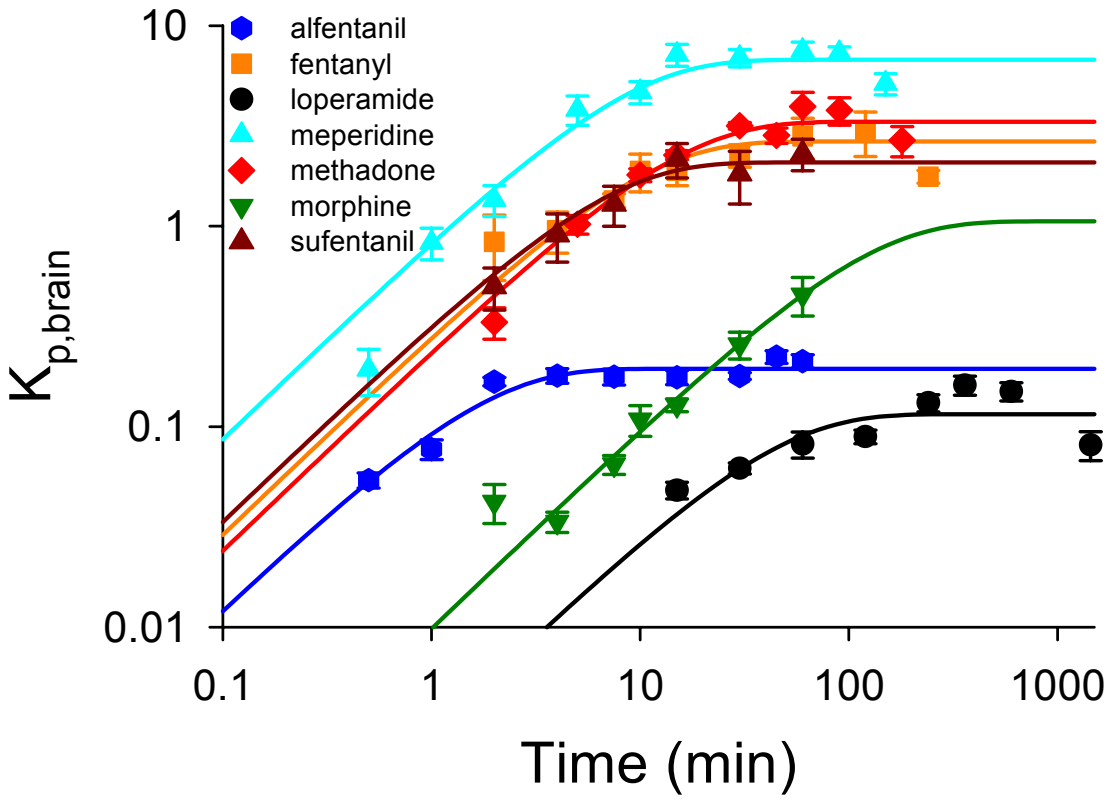

Figure 7.5. Time course of opioid $K_{p,brain}$ in CF-1 mice. Solid lines represent the fit of a kinetic model to the data. Data are presented as mean ± S.E. ($n \geq 3$).

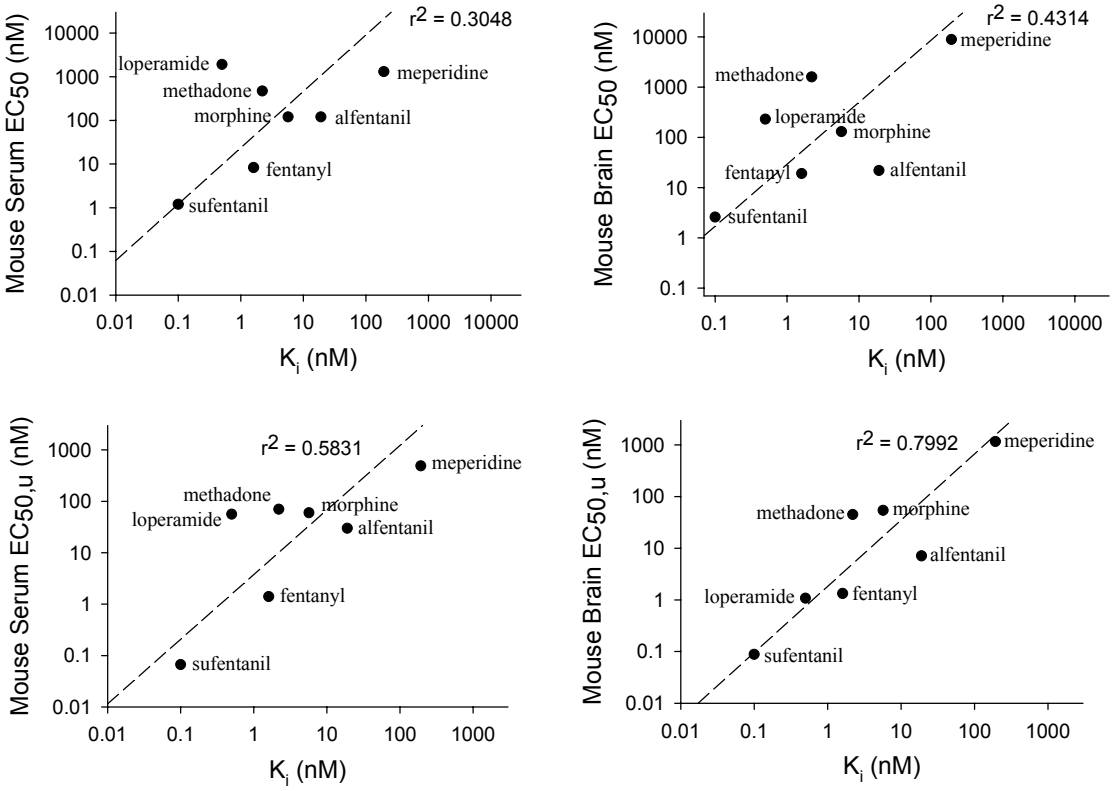

Figure 7.6. Correlation analysis for various *in vivo* measures relative to *in vitro* potency. The dashed line represents the line from log-log orthogonal regression analysis.

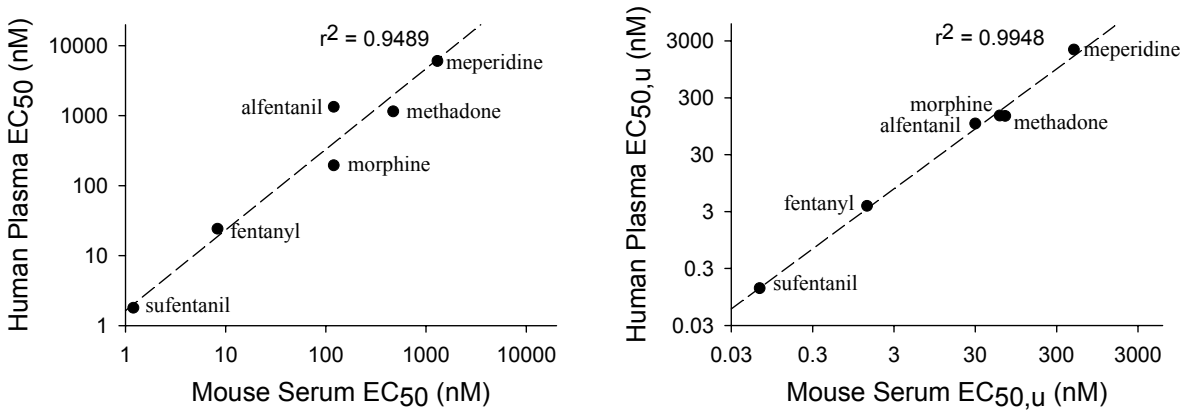

Figure 7.7. Correlation between mouse serum and human plasma EC_{50}s**.** The dashed line represents the line from log-log orthogonal regression analysis.

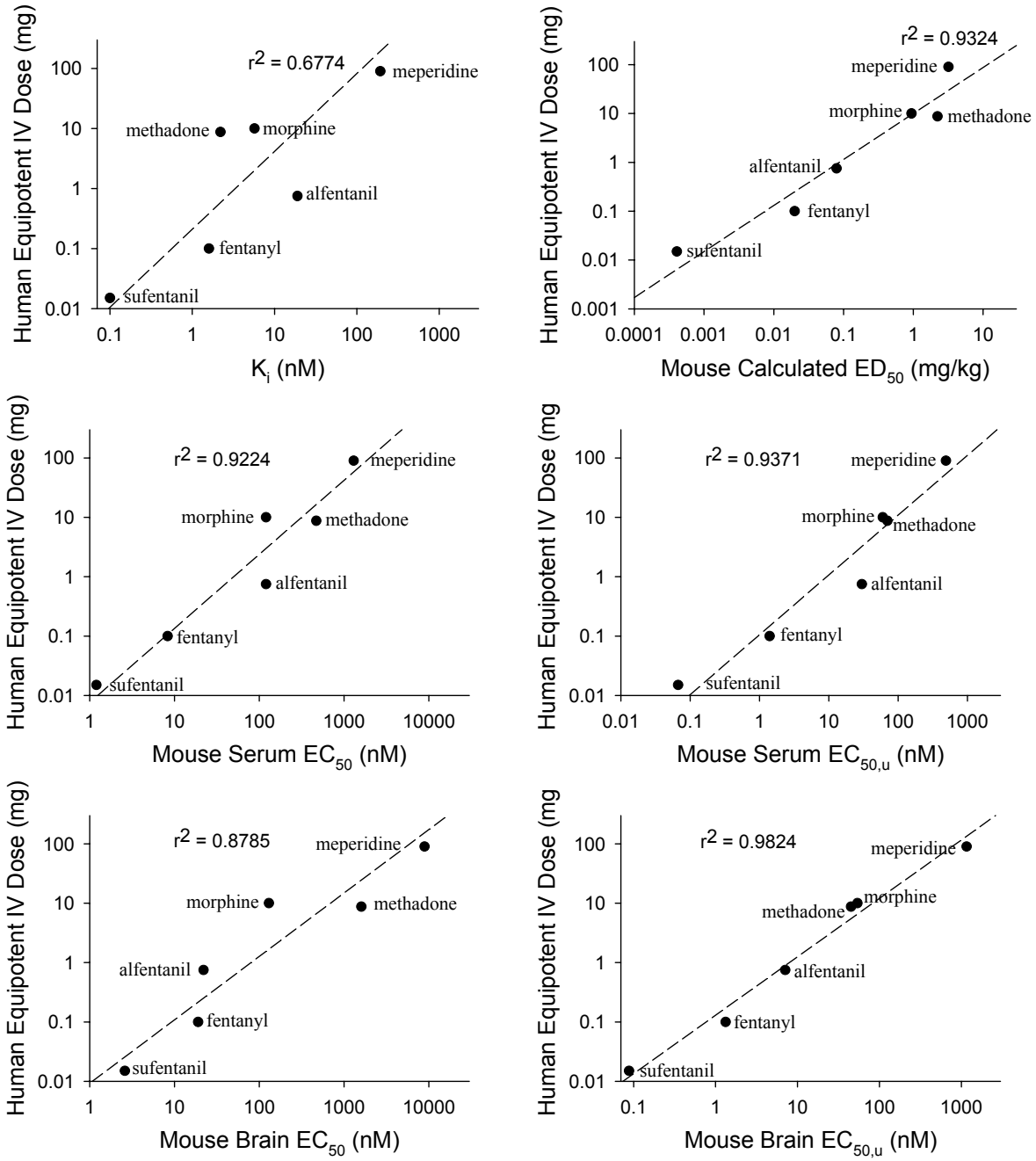

Figure 7.8. Correlation of equipotent clinical dose with *in vitro* K_is, mouse ED_{50}s, and mouse EC_{50}s. The dashed line represents the line from log-log orthogonal regression analysis.

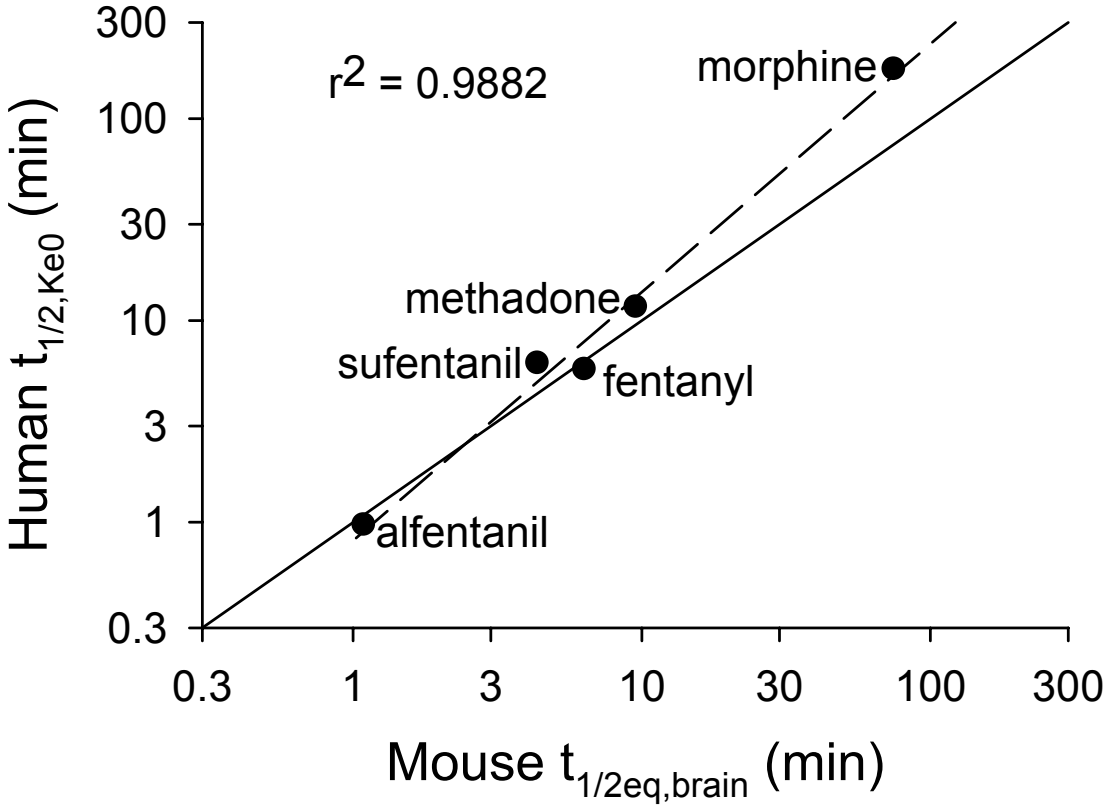

Figure 7.9. The correlation between human plasma-biophase equilibration half-life ($t_{1/2,Ke0}$) and mouse brain equilibration half-life ($t_{1/2eq,brain}$). The solid line represents the line of unity; the dashed line represents the line from log-log orthogonal regression analysis. With the exception of morphine, all of the opioids fell within 1.4-fold of the line of unity.

CHAPTER 8

PHARMACOKINETICS AND PHARMACODYNAMICS OF ALFENTANIL IN P-GLYCOPROTEIN-COMPETENT AND P-GLYCOPROTEIN-DEFICIENT MICE: P-GLYCOPROTEIN EFFLUX ALTERS ALFENTANIL BRAIN DISPOSITION AND ANTINOCICEPTION

This chapter has been submitted for publication in *Drug Metabolism and Disposition* and is presented in the style of that journal.

Abstract

Previous studies have indicated that P-glycoprotein (P-gp) attenuates the CNS penetration and central activity of some opioids. The impact of P-gp-mediated efflux on the disposition and efficacy of the synthetic opioid alfentanil currently is unknown. In this study, P-gp-competent [*mdr1a*(+/+)] and P-gp-deficient [*mdr1a*(-/-)] mice were used to investigate the impact of P-gp-mediated efflux on the systemic pharmacokinetics, brain disposition, and central activity of alfentanil. Equipotent doses of alfentanil were administered to *mdr1a*(+/+) and *mdr1a*(-/-) mice (0.2 and 0.067 mg/kg, respectively), and the time course of brain and serum concentrations, as well as antinociception, were determined. A pharmacokinetic-pharmacodynamic (PK-PD) model was fit to the data and used to assess the impact of P-gp on parameters associated with alfentanil disposition and action. The *mdr1a*(+/+) mice were less sensitive to alfentanil than *mdr1a*(-/-) mice, requiring a 3-fold higher dose to produce similar antinociception. PK-PD modeling revealed no differences in alfentanil systemic pharmacokinetics between P-gp expressers and nonexpressers. However, the steady-state brain-to-serum concentration ratio ($K_{p,brain,ss}$) was ~3-fold lower in *mdr1a*(+/+) mice compared to *mdr1a*(-/-) mice (0.19±0.01 versus 0.54±0.04, respectively). Consistent with the ~3-fold lower $K_{p,brain,ss}$, the antinociception versus serum concentration relationship in *mdr1a*(+/+) mice was shifted ~3-fold rightward compared to *mdr1a*(-/-) mice. However, there was no difference in the antinociception versus brain concentration relationship, or in the brain tissue EC_{50} (11±1.8 versus 9.2±1.7 ng/g), between *mdr1a*(+/+) and *mdr1a*(-/-) mice. These results indicate that alfentanil is an *in vivo* P-gp substrate, and are consistent with the hypothesis that P-gp-mediated efflux attenuates antinociception by reducing alfentanil $K_{p,brain,ss}$.

Introduction

P-glycoprotein (P-gp) is the 170-kD protein product of the multi-drug resistance gene (*mdr1*) first identified for its ability to confer multi-drug resistance in tumor cells (Juliano, 1976; Gros et al., 1986). P-gp mediates excretory and barrier functions in several tissue (e.g., proximal tubular cells of the kidneys, the canalicular membrane of hepatocytes in the liver, the apical membrane of intestinal enterocytes, and the luminal membrane of brain capillary endothelial cells) (Thiebaut et al., 1987; Cordon-Cardo et al., 1989; Cordon-Cardo et al., 1990). P-gp appears to play a protective role in intact mammals by attenuating absorption, facilitating excretion, and restricting distribution to several tissue sites, including the central nervous system (CNS), of many structurally diverse xenobiotics, including calcium channel blockers, HIV protease inhibitors, immunosuppressants, and opioids (Matheny et al., 2001).

Concomitant administration of P-gp inhibitors with P-gp substrates may lead to clinically significant drug interactions (Ho and Kim, 2005). For example, although the anti-diarrheal agent loperamide is a potent opioid agonist, it is not centrally active due, in part, to P-gp-mediated efflux at the blood-brain barrier (BBB) (Schinkel et al., 1996). However, when loperamide and the P-gp inhibitor quinidine were co-administered to subjects, respiratory depression was observed, which was attributed to an increase in loperamide brain concentration caused by P-gp inhibition (Sadeque et al., 2000). While the precise mechanism of this interaction has not been verified, the potential for enhanced central effects of P-gp substrates due to P-gp inhibition is nonetheless clear.

Studies have demonstrated that P-gp attenuates the brain distribution and central activity of several opioids. For example, (Thompson et al., 2000) showed that fentanyl, morphine, and methadone resulted in increased and prolonged antinociception in *mdr1a*(-/-) mice

compared to *mdr1a*(+/+) mice. Similarly, the cyclic peptide opioid DPDPE produced increased antinociception in *mdr1a*(-/-) mice as opposed to their P-gp-expressing counterparts (Chen and Pollack, 1998). The P-gp inhibitor GF120918 was able to restore DPDPE-mediated antinociception in *mdr1a*(+/+) mice to levels observed in the *mdr1a*(-/-) mice (Chen and Pollack, 1999). The P-gp inhibitor verapamil also was capable of increasing morphine brain concentrations and morphine-associated antinociception in *mdr1a*(+/+) mice (Zong and Pollack, 2000).

Alfentanil is a synthetic opioid used for the induction of surgical anaesthesia and the management of post-surgical pain. The alfentanil dose needs to be individualized based on numerous factors, including pathological condition, use of other medicines, and the type and duration of the surgical procedure (Scholz et al., 1996). Because alfentanil is a CYP3A4 substrate, CYP3A4 activity is another important determinant of the required alfentanil dose (Kharasch and Thummel, 1993). Many compounds are substrates of both CYP3A4 and P-gp. If alfentanil is a P-gp substrate, P-gp may be a determinant of the required alfentanil dose, a possible a source of inter-patient variability, and a potential locus of drug-drug interactions.

The impact of P-gp-mediated efflux on the pharmacokinetics and central pharmacodynamics of the alfentanil is unknown. Initial pilot experiments in this laboratory indicated P-gp-mediated efflux reduces alfentanil-associated antinociception. To investigate these observations further, and to evaluate whether P-gp efflux activity may contribute to inter-patient variability in alfentanil response or serve as a locus of drug-drug interactions, the present study was undertaken to determine the impact of P-gp-mediated efflux on the systemic pharmacokinetics, brain disposition, and central activity of alfentanil. A PK-PD

modeling approach was employed to assess the mechanism(s) by which P-gp-mediated efflux influences alfentanil-associated antinociception.

Material and Methods

Materials. Alfentanil was obtained from Taylor Pharmaceuticals (Decatur, IL) and loperamide was purchased from Sigma-Aldrich (St. Louis, MO). All other reagents were obtained from common sources and were of reagent grade or better.

Animals. Male CF-1 *mdr1a*(+/+) and *mdr1a*(-/-) mice (30-40 g; Charles River Laboratories, Inc. Wilmington, MA) were maintained on a 12-h light/dark cycle in a temperature- and humidity-controlled room with access to water and food ad libitum. All procedures involving mice were approved by The Institutional Animal Care and Use Committee of the University of North Carolina and were conducted in accordance with "Principles of Laboratory Animal Care" (NIH Publication No. 85-23, revised in 1985).

PK/PD Study. Based on the results of pilot studies, 36 *mdr1a*(-/-) and 36 *mdr1a*(+/+) mice received equipotent subcutaneous doses of alfentanil in physiological saline (0.067 and 0.2 mg/kg, respectively). At 0.5, 1, 2, 4, 8, 15, 30, 45 and 60 min post-administration, antinociception was assessed, and 4 *mdr1a*(-/-) and 4 *mdr1a*(+/+) mice were sacrificed by decapitation for collection of brain tissue and trunk blood. Trunk blood was collected in 1.5-ml microcentrifuge tubes and was allowed to clot for ≥ 30 min at room temperature. Serum was harvested following centrifugation. Brain and serum samples were stored at -20°C until analysis by HPLC-MS/MS.

Assessment of Antinociception. Antinociception was assessed with the hot plate latency test as described elsewhere (Chen and Pollack, 1997). Prior to administration of alfentanil, baseline hotplate latency was determined for each animal in triplicate. Hotplate latency was defined as the time interval between placement on the hot plate (55°C; Columbus Instruments, Columbus, OH) and first observation of a jump or lick of the hind limb(s).

Animals with an average baseline latency < 25 sec were used in the study. A cut-off latency of 60 sec was used to avoid tissue damage. The degree of antinociception was calculated as:

$$\%\text{MPR} = \frac{\text{test latency - control latency}}{\text{60 - control latency}} \times 100\% \quad (1)$$

Quantitation of Alfentanil in Serum and Brain. Brain samples were homogenized in water (1:2 v/v) with a sonic probe. A 25-µl aliquot of homogenate or serum was transferred to a HPLC vial, and protein was precipitated with 100 µl methanol containing internal standard (loperamide, 5 ng/ml). The sample was vortex-mixed, centrifuged, and the supernatant was analyzed by HPLC-MS/MS. Samples were injected (3 µl; CTC Analytics autosampler, Zwingen, Switzerland) onto a Phenomenex 2.0 × 30 mm, 5 µm Gemini 110A column (Phenomenex, Torrance, CA) maintained at room temperature. The total run time was 3 min. Analytes were eluted with a linear gradient consisting of ammonium acetate (pH 6.8; 10 mM) ["A"] and methanol ["B"] produced by two Shimadzu LC-10ADVP binary pumps. An initial condition of 5% "B" was ramped to 95% "B" over 2 min, held for 0.5 min, and then returned initial condition of 5% "B" in a single step to re-equilibrate the column. During the run, the flow rate was increased from 750 to 1500 µl/min over the first 2 min, held at 1500 µl/min for 1 min, and then returned the initial flow rate of 750 µl/min in a single step. The entire column effluent was diverted from the source of the PE-Sciex API-4000 "quadrupole mass spectrometer (Turbo V Ionspray source, 700˚C, PerkinElmerSciex Instruments, Boston, MA) for the first 1 min and last 0.5 min of the run. Alfentanil and loperamide were measured in positive ionization mode using multiple reaction monitoring (417.3→268.3 and 477.4→266.0, respectively). Standards were prepared in brain homogenate and serum and fitted with a quadratic equation with 1/y weighting (0.1-500 ng/ml). Accuracy of standards was within ± 15%.

Pharmacokinetic-Pharmacodynamic Analysis. A compartmental modeling approach with distribution between serum and brain tissue was used to describe alfentanil pharmacokinetics. The pharmacokinetic model shown schematically in Figure 8.1 was fit simultaneously to the serum and brain concentration data from both *mdr1a*(-/-) and *mdr1a*(+/+) mice using nonlinear least-squares regression (WinNonlin 4.1; Pharsight Corporation, Mountain View, CA). The absorption rate constant (k_a), central volume (V_c), and systemic clearance (Cl) did not differ between *mdr1a*(-/-) and *mdr1a* +/+ mice, and therefore were assumed to be identical when fitting the model to the data from both mouse strains simultaneously; the brain uptake (Cl_{up}) and brain efflux (Cl_{efflux}) clearances were allowed to vary between *mdr1a*(-/-) and *mdr1a*(+/+) mice**.** The brain volume (V_b) was determined experimentally as 13.4 $ml \cdot kg^{-1}$, assuming a specific gravity of 1.0 g/ml. The pharmacodynamic parameters, EC_{50} and γ, were determined directly from fitting a sigmoidal E_{max} model to the antinociception versus brain concentration (C) data:

$$\%MPR = \frac{E_{max} \cdot C^{\gamma}}{EC_{50}{}^{\gamma} + C^{\gamma}} \qquad (2)$$

E_{max} was defined as 100%, and γ was constrained to the same value for *mdr1a*(-/-) and *mdr1a*(+/+) mice. The time course of the brain-to-serum concentration ratio ($K_{p,brain}$) was used to estimate the brain equilibration rate constant (k_{eq}) and steady-state brain-to-serum ratio ($K_{p,brain,ss}$) according to:

$$K_{p,brain} = K_{p,brain,ss}\left(1 - e^{-k_{eq} \cdot t}\right) \qquad (3)$$

The brain equilibration half-life ($t_{1/2eq,brain}$) was obtained from k_{eq}:

$$t_{1/2eq,brain} = \frac{\ln(2)}{K_{eq}} \qquad (4)$$

Results

Alfentanil Pharmacokinetics. Alfentanil was absorbed rapidly following subcutaneous administration, with peak serum and brain concentrations achieved in less than 10 minutes (Figure 8.2). Alfentanil clearance was high (~equivalent to hepatic blood flow), assuming complete absorption from the subcutaneous site, and half-life was short ($t_{1/2}$ < 15 min). Alfentanil serum concentrations were 3-fold lower in the *mdr1a*(-/-) mice, consistent with those animals receiving a 3-fold lower dose than their transporter-competent counterparts. However, the time course of brain concentrations in the *mdr1a*(-/-) and *mdr1a*(+/+) mice were nearly superimposable (Figure 8.2). Both the systemic and brain tissue pharmacokinetics were capable of being described by the pharmacokinetic model (Figure 8.2 and Table 8.1). Pharmacokinetic-parameter estimates obtained from the pharmacokinetic model are reported in Table 8.1.

Alfentanil Pharmacodynamics. Pilot experiments indicated that, at equivalent doses, antinociceptive activity was lower in *mdr1a*(+/+) mice than in *mdr1a*(-/-) mice (data not shown). However, at a 3-fold higher dose (0.20 mg/kg vs 0.067 mg/kg), the magnitude and duration of antinociception in *mdr1a*(+/+) were identical to those in *mdr1a*(-/-) mice (Figure 8.3). In both *mdr1a*(+/+) and *mdr1a*(-/-) mice, alfentanil had a rapid onset of antinociception, a peak effect of ~85% MPR, and a rapid offset of action with nociceptive response returning to baseline within 60 min of administration. Consistent with a lower alfentanil potency in *mdr1a*(+/+) mice (due to P-gp-mediated efflux from the brain) , there was a 3-fold rightward shift in the serum concentration-effect relationship in transporter-competent versus transporter-deficient mice (Figure 8.4). There was no difference in the brain concentration effect relationship, nor brain EC_{50}s, between the *mdr1a*(+/+) and

mdr1a(-/-) mice (Figure 8.5; Table 8.1). The PK-PD model adequately described the time course of antinociception, the serum concentration-effect relationships, and the brain concentration-effect relationships in both mouse strains (Figures 3, 4, and 5, respectively). The PK-PD model indicated the presence of a slight counterclockwise hysteresis in the antinociceptive effect versus serum concentration relationship (Figure 8.4). However, there was no hysteresis in the antinociceptive effect versus brain concentration relationship (Figure 8.5). Pharmacodynamic parameter estimates obtained from the PK-PD model are reported in Table 8.1.

Alfentanil Brain Disposition. Equilibration of alfentanil between brain and serum occurred rapidly, with state-steady $K_{p,brain}$ reached within approximately 4 min. The time course of alfentanil $K_{p,brain}$ is shown in Figure 8.6. The $K_{p,brain,ss}$ was less than unity for both *mdr1a*(+/+) and *mdr1a*(-/-) mice, and the $K_{p,brain,ss}$ in *mdr1a*(-/-) mice was 3-fold higher than in *mdr1a*(+/+) mice (Table 8.1; Figure 8.6). Estimates of Cl_{up} and Cl_{efflux} differed between *mdr1a*(+/+) and *mdr1a*(-/-) mice, with Cl_{up} increased (1.6-fold) and Cl_{efflux} decreased (1.6-fold) in *mdr1a*(-/-) mice. The $t_{1/2eq,brain}$ was short ($\leq$ 1.5 min) in both *mdr1a*(+/+) and *mdr1a*(-/-) mice. However, $t_{1/2eq,brain}$ was ~1.5-fold longer in *mdr1a*(-/-) mice (Table 8.1). Consistent with implicit assumptions of the PK model, the ratios of Cl_{up}/Cl_{efflux} (0.18 and 0.47 in *mdr1a*(+/+) and *mdr1a*(-/-) mice, respectively) were comparable to the respective $K_{p,brain,ss}$ values (Table 8.1).

Discussion

The ATP-dependent efflux transporter P-gp is the protein product of the *mdr1* gene, and is expressed in variety of tissues including the luminal membrane of the BBB (Cordon-Cardo et al., 1989; Cordon-Cardo et al., 1990). Several studies have indicated that some opioids have reduced brain penetration and attenuated central activity due to P-gp-mediated efflux (Chen and Pollack, 1998; Thompson et al., 2000; Zong and Pollack, 2000; Dagenais et al., 2004). The influence of P-gp on the pharmacokinetics and central pharmacodynamics of the synthetic opioid alfentanil had not been explored previously. Pilot experiments in this laboratory indicated that alfentanil produced less antinociception in *mdr1a*(+/+) mice than in *mdr1a*(-/-) mice, consistent with P-gp-mediated efflux at the BBB. In this study, the time course of antinociception, as well as serum and brain concentrations of alfentanil, were evaluated in *mdr1a*(+/+) and *mdr1a*(-/-) mice in order to investigate the impact of P-gp-mediated efflux on the systemic pharmacokinetics, brain disposition, and central activity of alfentanil.

In order to achieve a similar degree of antinociception in both *mdr1a*(+/+) and *mdr1a*(-/-) mice, the dose administered to *mdr1a*(+/+) mice was three-fold higher than that in transporter-deficient animals. Even though the doses were different, pharmacokinetic modeling indicated no difference in systemic pharmacokinetics between *mdr1a*(+/+) and *mdr1a*(-/-) mice (Table 8.1). This result was not unexpected since P-gp often has minimal impact on systemic pharmacokinetics following subcutaneous or intravenous administration.

In contrast to the serum pharmacokinetics, P-gp had a pronounced effect on alfentanil brain pharmacokinetics. The $K_{p,brain,ss}$ of *mdr1a*(+/+) mice was ~3-fold lower compared to *mdr1a*(-/-) mice (0.19 vs. 0.54). The decrease in $K_{p,brain,ss}$ was accompanied by a ~1.6-fold

decrease in Cl_{up} and ~1.6-fold increase in Cl_{efflux}. These observations are consistent with the hypothesis that P-gp decreases $K_{p,brain,ss}$ by both attenuating brain uptake and enhancing brain efflux. Similar observations have been reported for other P-gp substrates (Kusuhara et al., 1997). The brain and serum concentrations of alfentanil equilibrated rapidly, with a $t_{1/2,eq,,brain} \leq 1.5$ min. This value is similar to previously reported estimates from humans (Lotsch, 2005). Unexpectedly, the $t_{1/2,eq,,brain}$ was shorter in the *mdr1a*(+/+) mice (Table 8.1). This observation may be explained by the fact that $t_{1/2,eq,,brain}$ is inversely proportional to Cl_{efflux}, and that P-gp increased Cl_{efflux} (~1.6-fold) thereby causing a proportional decrease in the $t_{1/2,eq,,brain}$ in *mdr1a*(+/+) mice (~1.4-fold). Interestingly, this result implies that P-gp-mediated efflux may reduce equilibration time between brain and systemic concentrations. Previously, the short $t_{1/2,eq,,brain}$ of alfentanil had been attributed in part to a small $K_{p,brain,ss}$ (Upton et al., 1997). In this study, the $K_{p,brain,ss}$ of alfentanil was less than unity for both *mdr1a*(+/+) and *mdr1a*(-/-) mice, indicating two important points: first, that a small $K_{p,brain,ss}$ may indeed facilitate rapid equilibrium between systemic and brain concentration, and second, that a $K_{p,brain,ss}$ greater than unity may not be needed, or even desirable, for CNS drug with rapid onset and offset of action.

PK-PD modeling indicated a ~3-fold rightward shift in the antinociception versus serum concentration relationship for *mdr1a*(+/+) mice compared to *mdr1a*(-/-) mice. PK-PD modeling also revealed a slight counterclockwise hysteresis in the antinociception versus serum concentration relationship for both *mdr1a*(+/+) and *mdr1a*(-/-) mice. However, there was no hysteresis in the antinociception versus brain concentration relationship, and the brain tissue EC_{50}s between *mdr1a*(+/+) and *mdr1a*(-/-) mice were not different. These observations are consistent with brain concentrations driving antinociception, and provide

compelling evidence that P-gp efflux attenuates alfentanil antinociception by reducing $K_{p,brain,ss}$.

This study is the first to show that alfentanil is a P-gp substrate. In contrast, an earlier study that examined the transcellular flux of alfentanil across L-MDR1 (expressing P-gp) and LLC-PK1 cell monolayers concluded alfentanil was not a P-gp substrate and had low affinity towards P-gp (IC_{50} > 50 μM) (Wandel et al., 2002). There are at least three possible explanations for the difference in results between these two studies. First, there might be species differences in the P-gp-mediated transport of alfentanil. This study evaluated the *in vivo* effects of murine P-gp (*mdr1a*), whereas the previous work studied the human form of P-gp (*MDR1*) *in vitro*. However, species differences in P-gp are unlikely, since human and murine P-gp share 80% sequence homology, and they are known to have similar substrate specificity (Chen et al., 2003). Secondly, basal activity of endogenous efflux transporter(s) in the LLC-PK1 and L-MDR1 cell lines may have masked P-gp-mediated transport of alfentanil, for flux was higher in the basolateral-to-apical direction in both the P-gp-expressing L-MDR1 and control LLC-PK1 cell monolayers. Thirdly, *in vitro* systems often are less sensitive than intact animal models for identifying weak P-gp substrates.

Alfentanil is a CYP3A4 substrate in humans, and has been used as a noninvasive clinical probe to evaluate CYP3A4 activity (Kharasch et al., 2005). The degree of miosis produced by alfentanil has been shown to correlate well with alfentanil plasma concentrations, and as such alfentanil-pupilometry studies have been used to evaluate CYP3A4 activity and to conduct drug-drug interaction studies. An assumption of such studies is that any increase or decrease in alfentanil-induced miosis is due primarily to changes in CYP3A4 activity (inhibition or induction). The present results showing that alfentanil is P-gp substrate

indicate that alfentanil-pupilometry studies may have the potential to detect alterations in P-gp activity. Previous pupilometry studies conducted with the P-gp substrates morphine, fentanyl, methadone, and loperamide have shown that inhibition of P-gp at the BBB by the P-gp inhibitor quinidine is modest (Kharasch et al., 2003; Skarke et al., 2003; Kharasch et al., 2004a; Kharasch et al., 2004b). Since quinidine is one of the most potent compounds capable of inhibiting P-gp that is in clinical use, the likelihood of significant inhibition of P-gp at the BBB appears remote. However, future drug-drug interaction studies conducted with alfentanil should be assessed carefully to ensure that any observed drug-drug interaction is not caused by P-gp inhibition.

In summary, the present study indicated that alfentanil is a P-gp substrate, and that P-gp-mediated efflux attenuates alfentanil antinociception by reducing $K_{p,brain,ss}$. These observations may have important implications regarding inter-individual differences in alfentanil pharmacodynamics and for the risk of drug-drug interactions. Additional studies may be warranted to assess the clinical relevance of P-gp efflux as a determinant of alfentanil pharmacotherapy.

References

1. Chen C, Liu X and Smith BJ (2003) Utility of Mdr1-gene deficient mice in assessing the impact of P-glyco-protein on pharmacokinetics and pharmacodynamics in drug discovery and development. *Curr Drug Metab* **4:**272-291.

2. Chen C and Pollack GM (1997) Blood-brain disposition and antinociceptive effects of -D-penicillamine2,5-enkephalin in the mouse. *J Pharmacol Exp Ther* **283:**1151-1159.

3. Chen C and Pollack GM (1998) Altered disposition and antinociception of [D-penicillamine(2,5)] enkephalin in mdr1a-gene-deficient mice. *J Pharmacol Exp Ther* **287:**545-552.

4. Chen C and Pollack GM (1999) Enhanced antinociception of the model opioid peptide [D-penicillamine] enkephalin by P-glycoprotein modulation. *Pharm Res* **16:**296-301.

5. Cordon-Cardo C, O'Brien JP, Boccia J, Casals D, Bertino JR and Melamed MR (1990) Expression of the multidrug resistance gene product (P-glycoprotein) in human normal and tumor tissues. *J Histochem Cytochem* **38:**1277-1287.

6. Cordon-Cardo C, O'Brien JP, Casals D, Rittman-Grauer L, Biedler JL, Melamed MR and Bertino JR (1989) Multidrug-resistance gene (P-glycoprotein) is expressed by endothelial cells at blood-brain barrier sites. *Proc Natl Acad Sci U S A* **86:**695-698.

7. Dagenais C, Graff CL and Pollack GM (2004) Variable modulation of opioid brain uptake by P-glycoprotein in mice. *Biochem Pharmacol* **67:**269-276.

8. Gros P, Ben Neriah YB, Croop JM and Housman DE (1986) Isolation and expression of a complementary DNA that confers multidrug resistance. *Nature* **323:**728-731.

9. Ho RH and Kim RB (2005) Transporters and drug therapy: implications for drug disposition and disease. *Clin Pharmacol Ther* **78:**260-277.

10. Juliano R (1976) Drug-resistant mutants of Chinese hamster ovary cells possess an altered cell surface carbohydrate component. *J Supramol Struct* **4:**521-526.

11. Kharasch ED, Hoffer C, Altuntas TG and Whittington D (2004a) Quinidine as a probe for the role of p-glycoprotein in the intestinal absorption and clinical effects of fentanyl. *J Clin Pharmacol* **44:**224-233.

12. Kharasch ED, Hoffer C and Whittington D (2004b) The effect of quinidine, used as a probe for the involvement of P-glycoprotein, on the intestinal absorption and pharmacodynamics of methadone. *Br J Clin Pharmacol* **57:**600-610.

13. Kharasch ED, Hoffer C, Whittington D and Sheffels P (2003) Role of P-glycoprotein in the intestinal absorption and clinical effects of morphine. *Clin Pharmacol Ther* **74:**543-554.

14. Kharasch ED and Thummel KE (1993) Human alfentanil metabolism by cytochrome P450 3A3/4. An explanation for the interindividual variability in alfentanil clearance? *Anesth Analg* **76:**1033-1039.

15. Kharasch ED, Walker A, Hoffer C and Sheffels P (2005) Sensitivity of intravenous and oral alfentanil and pupillary miosis as minimally invasive and noninvasive probes for hepatic and first-pass CYP3A activity. *J Clin Pharmacol* **45:**1187-1197.

16. Kusuhara H, Suzuki H, Terasaki T, Kakee A, Lemaire M and Sugiyama Y (1997) P-Glycoprotein mediates the efflux of quinidine across the blood-brain barrier. *J Pharmacol Exp Ther* **283:**574-580.

17. Lotsch J (2005) Pharmacokinetic-pharmacodynamic modeling of opioids. *J Pain Symptom Manage* **29:**S90-103.

18. Matheny CJ, Lamb MW, Brouwer KR and Pollack GM (2001) Pharmacokinetic and pharmacodynamic implications of P-glycoprotein modulation. *Pharmacotherapy* **21:**778-796.

19. Sadeque AJ, Wandel C, He H, Shah S and Wood AJ (2000) Increased drug delivery to the brain by P-glycoprotein inhibition. *Clin Pharmacol Ther* **68:**231-237.

20. Schinkel AH, Wagenaar E, Mol CA and van Deemter L (1996) P-glycoprotein in the blood-brain barrier of mice influences the brain penetration and pharmacological activity of many drugs. *J Clin Invest* **97:**2517-2524.

21. Scholz J, Steinfath M and Schulz M (1996) Clinical pharmacokinetics of alfentanil, fentanyl and sufentanil. An update. *Clin Pharmacokinet* **31:**275-292.

22. Skarke C, Jarrar M, Schmidt H, Kauert G, Langer M, Geisslinger G and Lotsch J (2003) Effects of ABCB1 (multidrug resistance transporter) gene mutations on disposition and central nervous effects of loperamide in healthy volunteers. *Pharmacogenetics* **13:**651-660.

23. Thiebaut F, Tsuruo T, Hamada H, Gottesman MM, Pastan I and Willingham MC (1987) Cellular localization of the multidrug-resistance gene product P-glycoprotein in normal human tissues. *Proc Natl Acad Sci U S A* **84:**7735-7738.

24. Thompson SJ, Koszdin K and Bernards CM (2000) Opiate-induced analgesia is increased and prolonged in mice lacking P-glycoprotein. *Anesthesiology* **92:**1392-1399.

25. Upton RN, Ludbrook GL, Gray EC and Grant C (1997) The cerebral pharmacokinetics of meperidine and alfentanil in conscious sheep. *Anesthesiology* **86:**1317-1325.

26. Wandel C, Kim R, Wood M and Wood A (2002) Interaction of morphine, fentanyl, sufentanil, alfentanil, and loperamide with the efflux drug transporter P-glycoprotein. *Anesthesiology* **96:**913-920.

27. Zong J and Pollack GM (2000) Morphine antinociception is enhanced in mdr1a gene-deficient mice. *Pharm Res* **17:**749-753.

Table 8.1. PK-PD parameters for alfentanil in *mdr1a*(-/-) and *mdr1a*(+/+) mice

Parameter	weighting	*mdr1a*(-/-)	*mdr1a*(+/+)
K_a (min^{-1})		0.35 ± 0.03	
Cl ($ml \cdot min^{-1} \cdot kg^{-1}$)	1/y	82 ± 3	
V_c ($ml \cdot kg^{-1}$)	1/y	1000 ± 60	
$t_{1/2}$ (min)	-	12 ± 0.6 [a]	
Cl_{up} ($ml \cdot min^{-1} \cdot kg^{-1}$)	1/y	7 ± 5	4 ± 3
Cl_{efflux} ($ml \cdot min^{-1} \cdot kg^{-1}$)	1/y	13 ± 12	22 ± 17
V_b ($ml \cdot kg^{-1}$)	-	13.4 (fixed)	
EC_{50} (ng/g)	uniformed	9.2 ± 1.7	11 ± 1.8
γ	uniformed	1.8 ± 0.4	
$K_{p,brain}$	1/y	0.54 ± 0.04	0.195 ± 0.008
K_{eq} (min^{-1})	1/y	0.46 ± 0.10	0.64 ± 0.09
$t_{1/2eq,brain}$ (min)	-	1.5 ± 0.3	1.08 ± 0.16

Parameter estimate ± S.E. from nonlinear least-squares regression analysis of pooled *mdr1a*(-/-) or *mdr1a*(+/+) mouse data.

Ka, Cl, Vc, Vb, and γ were constrained to the same value for *mdr1a*(-/-) or *mdr1a*(+/+) mice.

$t_{1/2}$ and $t_{1/2eq,brain}$ were calculated from $0.693/(V_c/Cl)$ and $0.693/K_{eq,brain}$, respectively.

[a] Propagation of error was used to calculated SE.

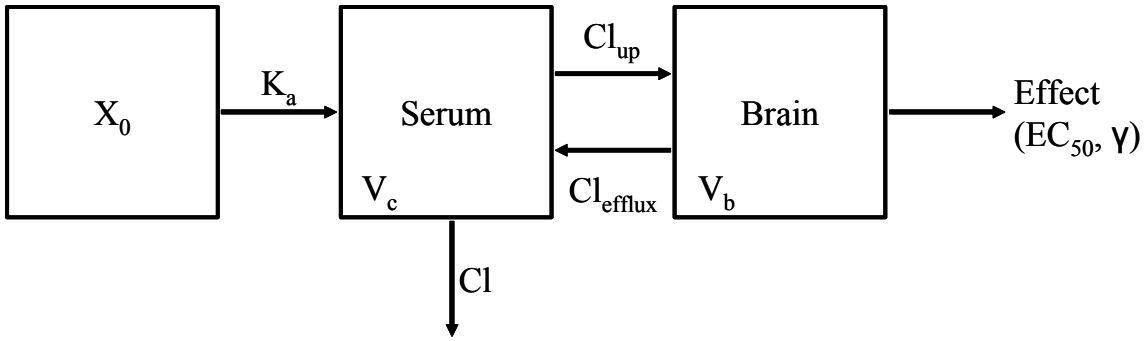

Figure 8.1. Pharmacokinetic-pharmacodynamic model for alfentanil disposition and antinociception in mice. Pharmacokinetic parameter were obtained by fitting the above model to the time course of serum and brain concentrations of *mdr1a*(-/-) and *mdr1a*(+/+) mice following subcutaneous administration of alfentanil. The absorption rate constant (K_a), central volume (V_c), and systemic clearance (Cl) were held constant between *mdr1a*(-/-) and *mdr1a*(+/+) mice; whereas, the brain uptake (Cl_{up}) and brain efflux clearances (Cl_{efflux}) were allowed to vary between *mdr1a*(-/-) and *mdr1a*(+/+) mice**.** The brain volume (V_b) was fixed. The effect parameters, EC_{50} and γ, were obtained by fitting a sigmoidal E_{max} model to the brain concentration versus antinociception data. E_{max} was defined as 100%, and γ was constrained to the same value for *mdr1a*(-/-) and *mdr1a*(+/+) mice.

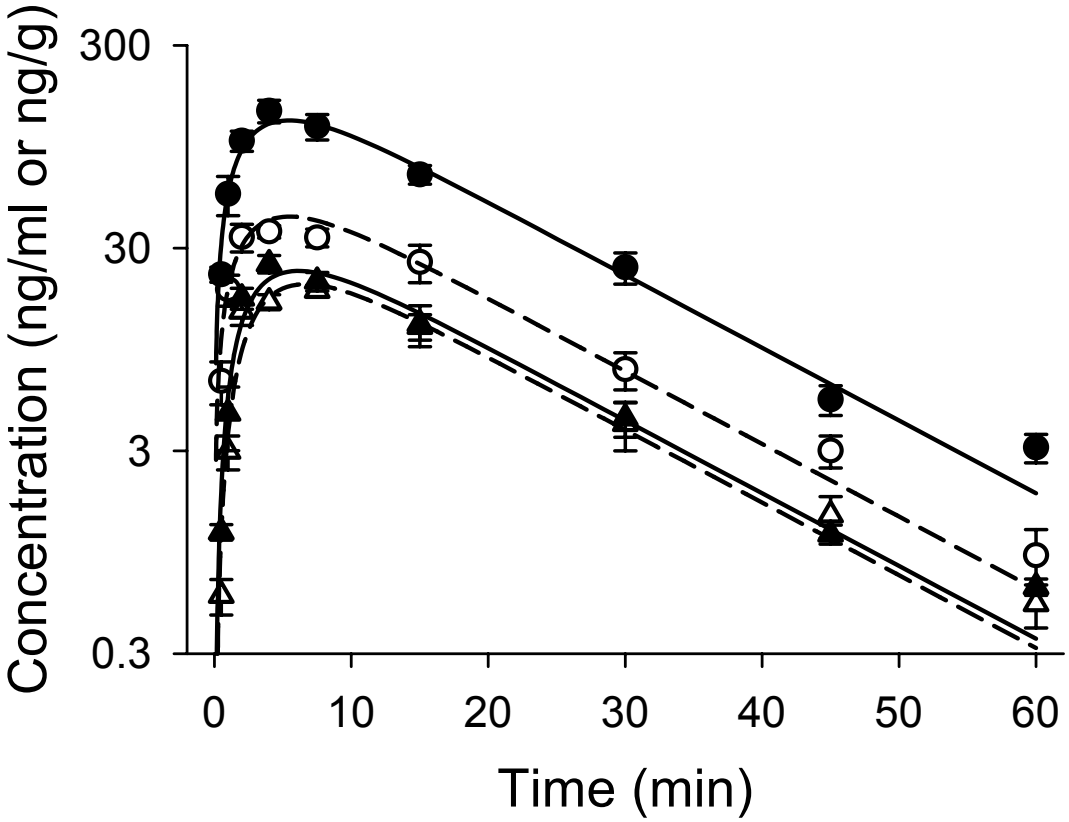

Figure 8.2. Time course of serum (●) and brain (▲) concentrations following a 0.067- or 0.2-mg/kg s.c. dose of alfentanil in *mdr1a*(-/-) (open symbols) or *mdr1a*(+/+) (solid symbols) mice, respectively. Data are presented as mean ± S.E. ($n \geq 3$). Dashed and solid lines represent the fit of the PK model to the concentration data for *mdr1a*(-/-) and *mdr1a*(+/+) mice, respectively.

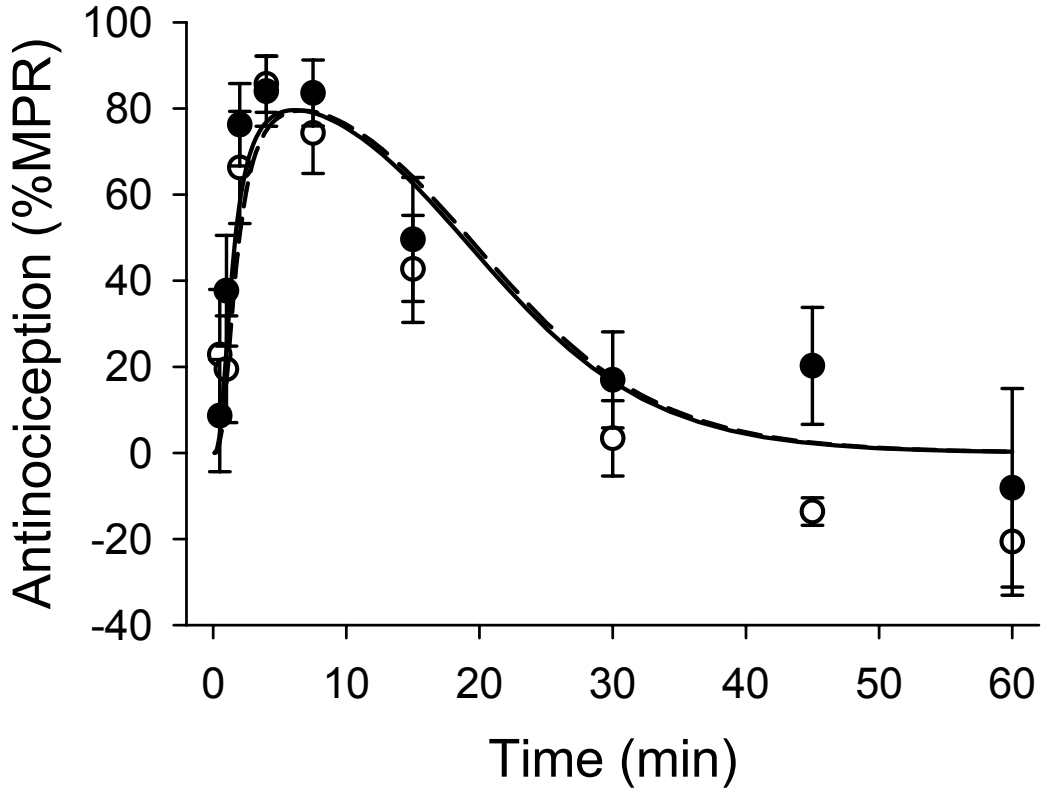

Figure 8.3. Time course of antinociception following a 0.067- or 0.2-mg/kg s.c. dose of alfentanil in *mdr1a*(-/-) (open symbols) or *mdr1a*(+/+) (solid symbols) mice, respectively. Data are presented as mean ± S.E. ($n \geq 3$). Dashed and solid lines represent the fit of the PK-PD model to the antinociception data for *mdr1a*(-/-) and *mdr1a*(+/+) mice, respectively.

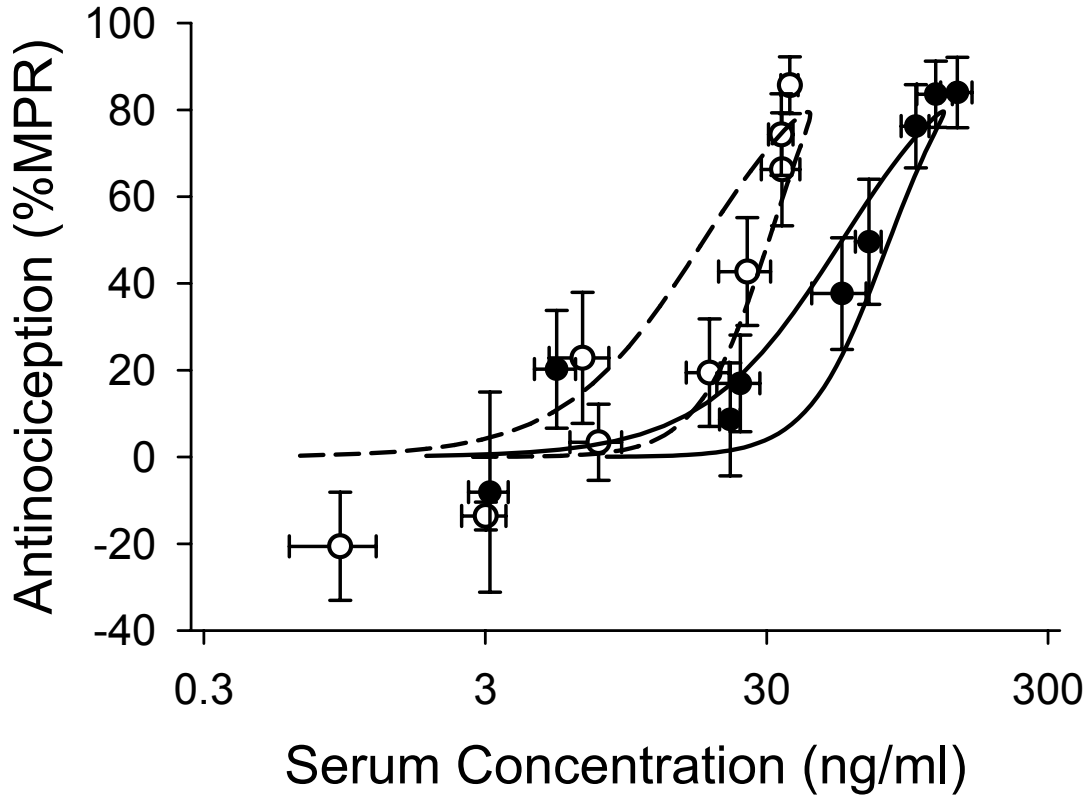

Figure 8.4. Relationship between antinociception and serum concentration of alfentanil following a 0.067- [*mdr1a*(-/-); ○] or 0.2- [*mdr1a*(+/+); ●] mg/kg s.c. dose**.** Data are presented as mean ± S.E. [concentration data (n ≥ 3); antinociception (n = 4 to 33)]. Dashed and solid lines represent the fit of the PK-PD model to the antinociception and serum concentration data for *mdr1a*(-/-) and *mdr1a*(+/+) mice, respectively. A slight counterclockwise hysteresis is present for both *mdr1a*(-/-) and *mdr1a*(+/+) mouse strains.

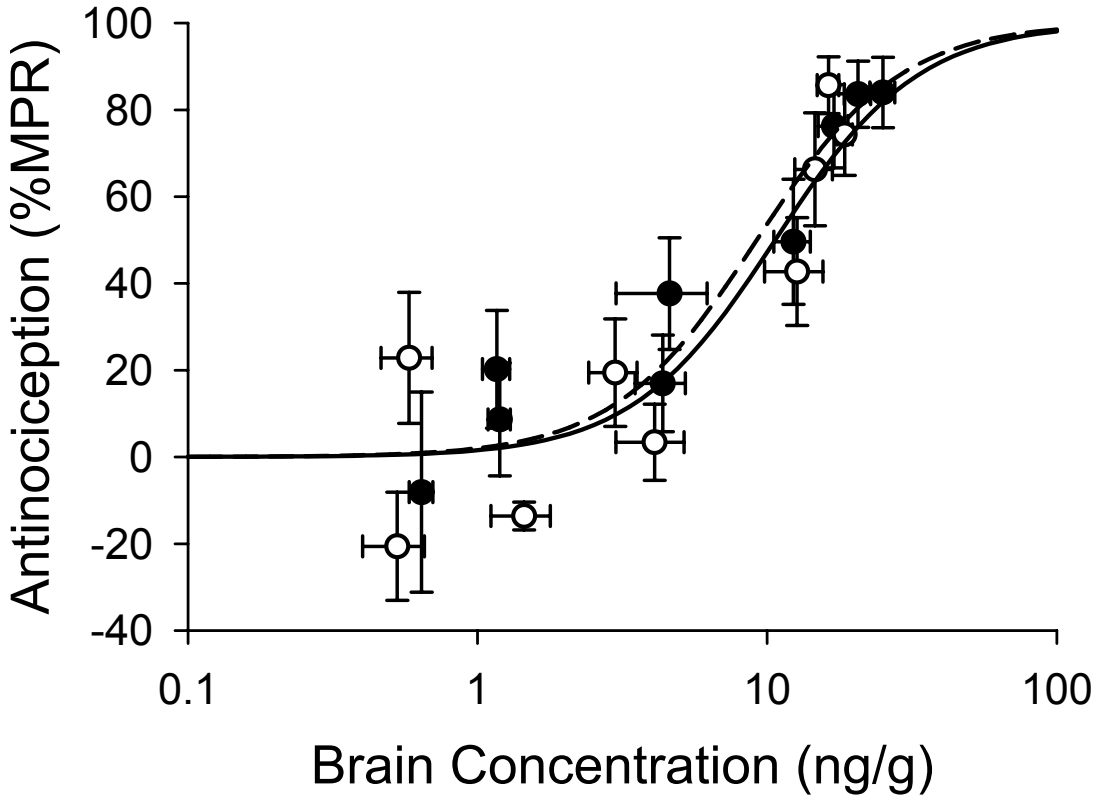

Figure 8.5. Relationship between antinociception and brain concentration of alfentanil following a 0.067- [*mdr1a*(-/-); ○] or 0.2- [*mdr1a*(+/+); ●] mg/kg s.c. dose**.** Data are presented as mean ± S.E. [concentration data (n ≥ 3); antinociception (n = 4 to 33)]. Dashed and solid lines represent the fit of a sigmoidal E_{max} model to the effect data obtained from *mdr1a*(-/-) and *mdr1a*(+/+) mice, respectively. Gamma was constrained to the same value for both mouse strains.

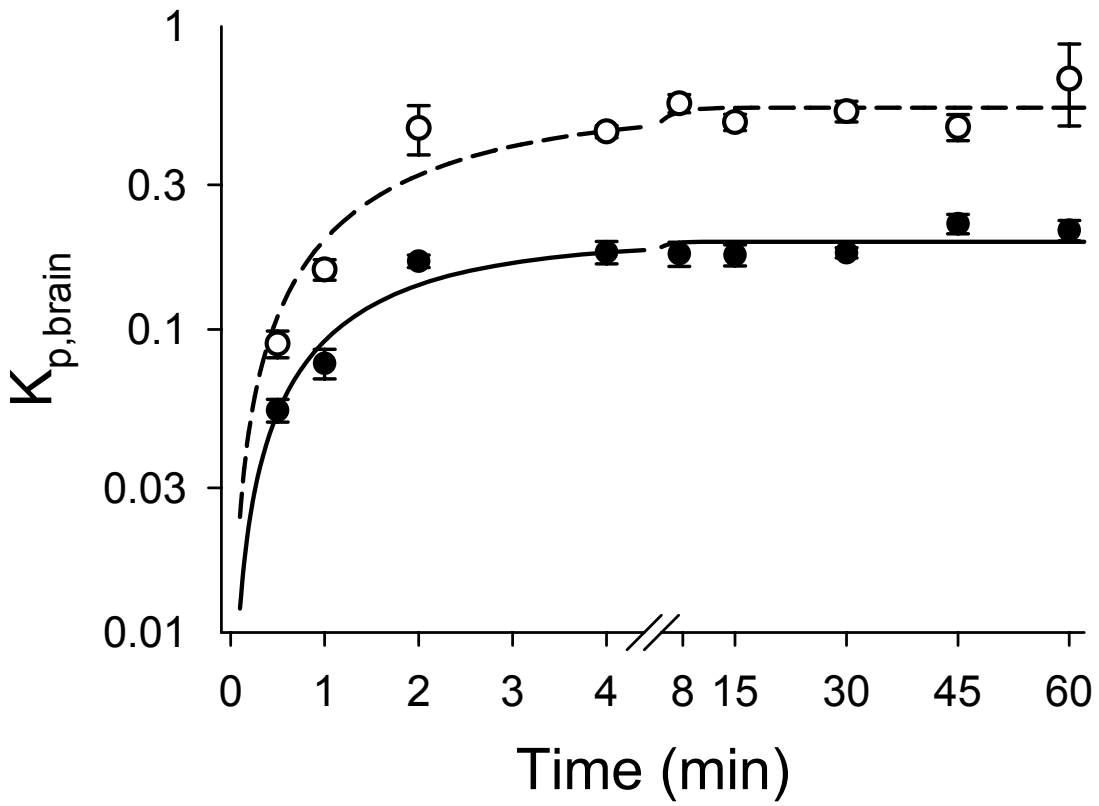

Figure 8.6. Time course of alfentanil $K_{p,brain}$ in mice following a 0.067- [*mdr1a*(-/-); ○] or 0.2- [*mdr1a*(+/+); ●] mg/kg s.c. dose. Data are presented as mean ± S.E. (n ≥ 3). Dashed and solid lines represent the fit of a kinetic model to the *mdr1a*(-/-) and *mdr1a*(+/+) data, respectively.

CHAPTER 9

PERSPECTIVES ON THE ROLE OF BRAIN TISSUE EXPOSURE IN CENTRAL NERVOUS SYSTEM PHARMACODYNAMICS: PHENOMENOLOGY, PREDICTABILITY, AND A ROADMAP FOR DRUG DISCOVERY

The exposure of brain tissue to a pharmacologic agent, together with the intrinsic ability of that agent to elicit a biologic effect mediated by a central nervous system (CNS) target, are the primary determinates of *in vivo* CNS activity for the agent. Depending on the particular disease state, target, mechanism of action, and overt effect, CNS activity may be beneficial or detrimental; in many cases, a single agent will have the capacity to produce both therapeutic and toxic effects in the CNS, mediated by either the same or different target receptors. Evaluating intrinsic activity is a straightforward process in contemporary drug discovery, and typically relies on the ability of a compound to interact (activate or inhibit) with a single target receptor (typically a protein). However, CNS exposure is more complex, as it is influenced by numerous physicochemical, biochemical, and physiologic factors. These factors typically include blood-brain barrier (BBB) passive permeability, active transport in the uptake and/or efflux directions, biotransformation in CNS tissues, cerebrospinal fluid (CSF) bulk flow, and binding to proteins in blood and brain tissue.

Although this dissertation project was multifaceted, the central theme was ***exposure of brain tissue to pharmacologic agents*** that mediate therapeutic and/or toxic effects via CNS targets. Specifically, it was recognized that two particular categories of pharmacokinetic phenomena, protein binding and membrane transport, are often important determinants of net brain uptake and, ultimately, *in vivo* exposure. A comprehensive understanding of the factors that determine brain exposure, and in particular translating that understanding into methods for predicting exposure, must include these important processes. In addition to considering the mechanistic determinants of brain exposure, it also is important to develop an appropriate mathematical framework for the quantitative expression of the influence of individual processes on exposure. Consequently, significant effort was invested in exploring metrics of

efflux transport, an important barrier function that limits brain exposure for many compounds, and in considering relatively straightforward experimental approaches that might indicate the predominant mechanisms of limited brain exposure for an individual compound such that further experimentation may proceed in a directed manner. The intent of this chapter is to draw together the various elements of this dissertation, to place those elements in the context of contemporary literature, and to extend those elements to suggest potential directions for future investigation.

Apical efflux kinetics and clinical risk associated with efflux inhibition at the BBB

Apical efflux transporters at the BBB attenuate brain exposure for many compounds. Although efflux transport is a well-documented phenomenon that occurs in a variety of tissues, and can be viewed as either limiting substrate distribution into a protected space or facilitating removal from an excretory organ, the kinetics of efflux transport often are misunderstood. For example, unexpected, apparently contradictory, and seemingly complex experimental observations related to efflux transport have been reported in the literature (see Chapters 1 and 2). Commonly used experimental models, together with the mathematical framework for expressing efflux transport in a quantitative manner, often do not satisfactorily explain these observations or predict *in vivo* behavior. Consequently, new mathematical relationships for efflux transport were derived, and their utility is explored in Chapter 2. These relationships were based on a simple kinetic scheme, and provided a mathematical scaffolding to improved understanding, prediction, and communication of the effects of efflux transport on brain tissue exposure to substrates. Importantly, the mathematical

relationships that were derived in this effort showed that several apparently unexpected experimental observations were entirely predictable based on standard kinetic theory.

It must be noted that the mathematical relationships derived as a significant component of this dissertation project differ fundamentally from many commonly used relationships. Current approaches for the treatment of efflux transport data mistakenly assume that the K_m and the IC_{50} for a particular efflux transport protein are identical to the EC_{50} of a substrate or inhibitor for that transporter. Conventional treatment of efflux transport data also over-estimates K_m and IC_{50}, improperly expresses efflux activity, and imply that 50% inhibition of efflux transport activity will result in 50% of the maximum effect on substrate flux. The newly derived relationships express K_m, IC_{50}, and efflux transport activity in a manner consistent with a standard and parsimonious kinetic model, and predict a maximum 2-fold change in substrate flux (or ultimately brain tissue exposure) when efflux transport is inhibited 50%. The discrepancy between the currently accepted relationships and the newly derived mathematical approaches has important implications for appropriate selection of substrates and inhibitors, experimental design, data interpretation, standardizing expression of efflux transport activity, and predicting the clinical significance of efflux transport inhibition (Chapters 2 and 3).

Since inhibition of efflux transport at the BBB could potentially increase brain tissue exposure to a pharmacologic agent, thereby modulating biologic activity, the clinical risk of P-gp inhibition at the BBB was assessed in context of the newly-derived mathematical relationships (Chapter 3). Based on these relationships, the fold increase in brain tissue exposure will be less than or equal to the quantity $1 + ([I]_u / K_i)$, where K_i and $[I]_u$ represent the inhibitory constant and unbound inhibitor concentration, respectively. Analysis of

currently available P-gp inhibitors indicated that despite the potential for drug-drug interactions (DDI) at the locus of BBB P-gp-mediated transport, current inhibitors do not achieve sufficiently high unbound concentrations in the systemic circulation to appreciably increase brain exposure of substrate molecules (Table 3.3). Only one out of the fourteen inhibitors examined was capable of achieving clinical unbound concentrations more than 2-fold above the respective K_i (Valspodar, $[I]_u/Ki=3.3$). However, since Valspodar is not an FDA approved agent, one must conclude that the risk of clinically significant P-gp inhibition at the BBB mediated by currently-approved drugs is small. This conclusion is substantiated further by the fact that loperamide, an opioid P-gp substrate with a higher intrinsic potency than morphine (based on intrinsic *mu* receptor affinity) that is excluded from the brain due to P-gp-mediated efflux at the BBB (Schinkel et al., 1996), has no appreciable CNS activity even when co-administered with potent P-gp inhibitors (Sadeque et al., 2000; Tayrouz et al., 2001; Skarke et al., 2003). Thus, it appears unlikely that drug-drug interactions will result in untoward effects in the CNS unless such interactions also change the circulating concentrations of the substrate (due to inhibition of clearance, for example) or the therapeutic window is extremely narrow.

When BBB efflux transport is inhibited significantly, it is logical to speculate that the expected change in BBB uptake clearance, efflux clearance, and brain exposure of a substrate for that efflux transporter can be predicted. Indeed, for a given substrate the efflux ratio, unbound inhibitor concentration, and K_i can be used, in the context of the mathematical relationships derived in Chapter 2, to predict the outcome of a transport-mediated drug-drug interaction on brain exposure. However, it must be pointed out that to date no comprehensive preclinical pharmacokinetic-pharmacodynamic studies have been conducted to determine

whether the concentration-effect relationships for efflux inhibitors behaves in a manner consistent with the relationships proposed in Chapter 2. This limitation could be overcome by selecting P-gp inhibitors and substrates from different structural classes, with experimental determination of dose-effect, concentration-effect, and time-effect relationships for each combination of substrate and inhibitor. If the *in vitro* K_i is determined accurately and the time course of brain and plasma concentrations for both substrate and inhibitor are measured, the resulting data would be amendable to comprehensive pharmacokinetic-pharmacodynamic analysis. Pharmacokinetic-pharmacodynamic modeling could be used to test specific hypotheses, such as the hypothesis that unbound plasma inhibitor concentration serves as the driving force for BBB P-gp inhibition, and that P-gp inhibition at the BBB occurs in a manner consistent with mathematical relationships derived in Chapter 2. In addition, i*n vitro*-to-*in vivo* potency correlations for various inhibitors could be constructed. Such correlations would allow a better mechanistic understanding of BBB efflux transport inhibition and therefore provide better predictions and risk assessment for clinical efflux inhibition at the BBB.

Since brain tissue exposure is influenced by BBB efflux transport, it would be advantageous to identify efflux transport substrates and inhibitors quickly and efficiently. One method for identifying substrates and inhibitors is through the establishment of quantitative structure-activity relationships (QSAR) and *in silico* models (Wang et al., 2003; Wang et al., 2005; Srinivas et al., 2006). QSAR models have the potential to reduce the costs and time needed to identify substrates and inhibitors of interest (Ekins et al., 2000). One limitation of QSAR and *in silico* models is that the models are only as good as the data set used to generate them. Current QSAR models for identifying P-gp substrates and inhibitors

have been created with data sets consisting primarily of kinetic parameters (K_m, IC_{50}, or V_{max}) that were calculated using conventional mathematical approaches (Ekins et al., 2002). Since conventional mathematical treatment of efflux data may overestimate the values of these kinetic parameters, it is reasonable to speculate that the QSAR relationships may be biased based on these results. Appropriate kinetic analysis of transport data may result in more reliable QSAR relationships.

P-gp is the predominant efflux transporter that attenuates the brain exposure of drugs. The role of other mechanisms and transporters that affect brain exposure to various drugs is not well documented (Graff and Pollack, 2004). To assess the role of P-gp- and non-P-gp-mediated mechanisms on brain exposure, the $[plasma]_u/[brain]_u$ ratio and the *in vivo* P-gp efflux ratio were evaluated for a total of 34 drugs. Using these simple metrics, a classification system for evaluating brain exposure was developed. This classification system was capable of assessing whether a compound was excluded from the brain entirely by P-gp, partially by P-gp, or only by non-P-gp-mediated mechanisms. In addition, the classification system was able to identify compounds with active brain uptake. Of the 34 drugs examined, 21 were classified as having P-gp-mediated efflux as the sole mechanism limiting brain exposure. Three drugs (methadone, ritonavir, and saquinavir) had $[plasma]_u/[brain]_u$ and *in vivo* P-gp efflux ratios consistent with active uptake. Ten drugs (digoxin, doxorubicin, ivermectin, cimetidine, dexamethasone, ranitidine sumatriptan, zolmitriptan, cetirizine, and fexofenadine) were classified as having non-P-gp-mediated mechanism(s) that limited brain exposure. The compounds identified as having either active uptake or non-P-gp-mediated mechanisms limiting brain exposure would make an ideal compound set for additional study,

because the potential influence of active uptake and non-P-gp-mediated efflux on brain exposure could be further elucidated.

Total brain exposure is dependent on plasma and brain tissue protein binding, as plasma and brain unbound fraction influences the brain-to-plasma partition coefficient ($K_{p,brain}$). This concept has been demonstrated in several key reports (Kalvass and Maurer, 2002; Maurer et al., 2004; Summerfield et al., 2005). Over the last several years, the $f_{u,brain}$ and $f_{u,plasma}$ values obtained from equilibrium dialysis experiments have been determined and reported in the literature for over 100 drugs and discovery compounds (Kalvass and Maurer, 2002; Maurer et al., 2004; Summerfield et al., 2005; Becker and Liu, 2006). The $f_{u,brain}$ and $f_{u,plasma}$ values for 34 additional compounds were added as a result of this dissertation project. With the available $f_{u,brain}$ and $f_{u,plasma}$ data, it may be possible to a create an *in silico* model to predict $f_{u,brain}$ and $f_{u,plasma}$ for diverse compounds. *In silico* estimates of $f_{u,brain}$ and $f_{u,plasma}$ may reduce the need to determine protein binding experimentally, and may provide a useful context for predicting and assessing *in vivo* $K_{p,brain}$.

At the inception of this dissertation project, many opioids, including DPDPE, fentanyl, morphine, loperamide and methadone, were known to be P-gp substrates to some (varying) extent (Schinkel et al., 1996; Chen and Pollack, 1998; Dagenais et al., 2004). At the time, alfentanil and sufentanil were not believed to be P-gp substrates (Wandel et al., 2002). Studies conducted as part of this dissertation project identify alfentanil and sufentanil as P-gp substrates (Chapters 4 and 8). Both alfentanil and sufentanil had a higher $K_{p,brain}$ (~3-fold), and alfentanil had an increased antinociceptive response, in P-gp-deficient mice as compared to P-gp-competent animals. The clinical significance of the observation that these compounds

are P-gp substrates is not known. However, based on the relatively small P-gp effect (~3-fold) and for the reasons outlined in Chapter 3, the clinical significance is likely to be small.

Previous pharmacokinetic-pharmacodynamic studies indicated that P-gp-mediated efflux attenuates antinociception and brain penetration of some opioids. However, the precise mechanism(s) by which P-gp attenuates antinociception and brain penetration are not clear (Chen and Pollack, 1998; Thompson et al., 2000; Zong and Pollack, 2000). One pharmacokinetic-pharmacodynamic study conducted with morphine in P-gp-competent and P-gp-deficient mice showed that P-gp-mediated efflux reduced morphine-associated antinociception solely by lowering $K_{p,brain}$ (Zong and Pollack, 2000). Another study (Chen and Pollack, 1998) conducted with the metabolically-stable opioid-peptide DPDPE in P-gp-competent and P-gp-deficient mice showed P-gp-mediated efflux reduced DPDPE-associated antinociception by two apparent mechanisms: by decreasing $K_{p,brain}$ (i.e., by impeding net brain uptake) and by increasing the brain tissue EC_{50}. (i.e., by impeding the approach of DPDPE to the pharmacologic receptor). One question raised by the discrepancy between the morphine and DPDPE studies is whether P-gp-mediated efflux attenuates the antinociception of other opioids in a manner more consistent with that of morphine or that of DPDPE.

This important question was answered through comprehensive pharmacokinetic-pharmacodynamic studies conducted with four opioids (alfentanil, fentanyl, loperamide, and methadone) in P-gp-competent and P-gp-deficient mice [CF-1 *mdr1a*(+/+) and *mdr1a*(-/-)] (Chapter 6). One additional study with loperamide was conducted in FVB *mdr1a/b*(+/+) and *mdr1a/b*(-/-) mice to evaluate the possible influence of *mdr1b* on opioid disposition and response. Alfentanil, fentanyl, loperamide, and methadone were selected as model opioid P-

gp substrates because they exhibit a range of interaction with P-gp (Dagenais et al., 2004). Pharmacokinetic-pharmacodynamic modeling revealed identical brain tissue EC_{50} values in P-gp-competent and P-gp-deficient mice for each of the opioids, and that P-gp-mediated efflux attenuated opioid-associated antinociception only by decreasing $K_{p,brain}$. *Mdr1b* had no noticeable effect on loperamide brain penetration or antinociception. The lower $K_{p,brain}$ values observed in P-gp-competent mice were accompanied by a decrease in brain uptake clearance and an increase in brain efflux clearance, consistent with the known influence of BBB P-gp on substrate flux between brain tissue and the systemic circulation. The enhancement in brain efflux (~2-fold or less) was less than the decrease in brain uptake (up to 20-fold for loperamide). Consistent with the ~2-fold increase in efflux clearance, brain equilibration half-life was ~2-fold shorter in P-gp-competent mice. The relative changes in uptake and efflux clearances were entirely consistent with predictions based on the theoretical considerations for BBB efflux presented in Chapter 2.

***In vitro* prediction of brain equilibration half-life**

The rate and extent of brain equilibration are important aspects of CNS pharmacokinetics. The rate of CNS distribution can be characterized by the brain equilibration half-life ($t_{1/2brain,eq}$). The parameter $t_{1/2brain,eq}$ influences the onset and offset of CNS activity. In some cases, such as for a rapidly-acting anesthetic agent, a short $t_{1/2brain,eq}$ is desired; in other cases, a long $t_{1/2brain,eq}$ may be preferable.

The ability to predict $t_{1/2brain,eq}$ from *in vitro* data would aid in the selection drug candidates with desirable CNS pharmacokinetics. The $t_{1/2brain,eq}$ is dependent on $f_{u,brain}$ and unbound brain efflux clearance (Liu et al., 2005; Syvanen et al., 2006). In the absence of active processes

(metabolism or active transport), unbound efflux clearance is dependent solely on the passive permeability of a given compound through the BBB. Even in the presence of active apical efflux, unbound efflux clearance still is predominately dependent on BBB passive permeability, because, as outlined in Chapter 2, brain efflux clearance is minimally affected by apical active efflux (≤2-fold increase efflux clearance). Because efflux clearance is predominately dependent on BBB passive permeability, the *in vivo* $t_{1/2brain,eq}$ should be amenable to estimation from $f_{u,brain}$ and *in vitro* estimates of BBB passive permeability.

In the present project, high-quality *in vivo* measures of $t_{1/2brain,eq}$ were obtained for seven opioids. The $t_{1/2brain,eq}$ differed by more than 70-fold among these opioids. Although it was clearly beyond the scope of this project, this data set would be ideal for testing the predictive value of various BBB passive permeability assays (*in vitro* cell monolayers, PAMPA, *in situ* brain uptake clearance) in combination with $f_{u,brain}$ to estimate *in vivo* $t_{1/2brain,eq}$. Correlations between observed and predicted $t_{1/2brain,eq}$ could be constructed to determine the best surrogate for brain efflux clearance or BBB passive permeability.

In vitro-to-preclinical and preclinical-to-clinical correlations

Understanding relevant brain exposure is a requisite step in understanding the CNS pharmacokinetics and pharmacodynamics for any compound for which equilibration between brain tissue and the systemic circulation is not rapid. Whereas total brain tissue concentrations and $K_{p,brain}$ are relatively easy to determine in a discovery setting, unbound brain concentrations are more informative. This dissertation project was conducted in part to assess the utility of unbound brain $EC_{50,u}$ as a measure of *in vivo* potency for centrally acting drugs. Seven *mu* opioid receptor agonists (alfentanil, fentanyl, loperamide, methadone,

meperidine, morphine, and sufentanil) were selected as model CNS drugs. In separate groups, mice received a single equipotent subcutaneous dose of one opioid. The time course of antinociception, as well as serum and brain concentrations, were determined, and a pharmacokinetic-pharmacodynamic model was fit to the concentration and effect data to estimate relevant parameters associated with opioid disposition and action. Estimates of *in vitro* potency (K_i) and relevant clinical parameters were obtained from the literature and used to construct *in vitro*-to-preclinical and preclinical-to-clinical relationships. The strongest i*n vitro*-to-*in-vivo* correlation was observed between K_i and unbound brain $EC_{50,u}$ (r^2=0.799). A strong correlation between mouse serum and human plasma EC_{50} estimates was observed (r^2=0.949). However, the correlation was improved when the data were corrected for plasma protein binding (r^2=0.995). K_i correlated only moderately with clinical equipotent i.v. dose among these opioids (r^2=0.677). However, estimates of ED_{50} and various EC_{50} metrics (total serum, unbound serum, total brain, and unbound brain) correlated strongly with clinical equipotent i.v. dose, with the strongest correlation observed for unbound brain $EC_{50,u}$. These results indicate that superior *in vitro*-to-preclinical and preclinical-to-clinical correlations can be achieved when comparisons are based on relevant unbound concentrations.

Does CSF sampling, microdialysis, brain slice partitioning, or equilibrium dialysis provide the "best" estimate of unbound brain concentration?

Determination of the brain extracellular fluid concentrations (BECF) of compounds of interest has utility in assessing the extent of CNS penetration and estimating CNS biophase concentrations. This dissertation project relied on a brain homogenate equilibrium dialysis method to measure brain unbound fraction ($f_{u,brain}$) of various drugs. The $f_{u,brain}$ of each

compound was then multiplied by the corresponding total brain concentrations to estimate unbound brain (or BEFC) concentrations. The unbound concentrations proved useful in assessing the extent of CNS penetration and estimating CNS biophase concentrations of the compounds examined (Chapters 4 and 7).

Other methods obviously have been used to estimate brain unbound concentrations, such as measurement of CSF concentration, use of microdialysis for direct assessment of unbound concentration, or examination of substrate partitioning in brain slices (Hutchinson et al., 2002; Shen et al., 2004; Becker and Liu, 2006). Even though brain homogenate equilibrium dialysis studies are relatively high-throughput, easy to perform, and provide reasonable estimates of brain unbound concentration, it is unknown whether brain homogenate equilibrium dialysis studies provide the most optimal and accurate estimate of brain unbound concentrations. A side-by-side comparison of each of the four methods would allow for determination of the "best" method for estimating brain unbound concentrations. While such a comparison was envisioned at the beginning of this dissertation project, it was de-prioritized as the utility of other aspects of the project became increasingly clear.

In determining the "best" method, considerations for the relative accuracy, as well as the assay throughput, is necessary. It is possible that one method may be the most accurate in all circumstances, but also may be the most labor- and resource-intensive. If very little difference in estimated brain unbound concentrations exists among the different methods, then the least labor- and animal-intensive (and highest throughput) method would have a clear advantage.

Use of other drug classes to correlate unbound brain concentration with CNS effects

Opioids were used as model CNS drugs to evaluate the utility of unbound brain concentrations for assessing the extent of CNS distribution and estimating CNS biophase concentrations. The approach used for opioids in this body of work could easily be extended to other relevant drug classes, such as antihistamines. Antihistamines generally are used for the treatment or prevention of symptoms related to allergic reactions. However, some first-generation antihistamines have sedation as a major CNS side effect, and even have been used as sleep aids (Welch et al., 2002). Second- and third-generation antihistamines have low BBB permeability and/or undergo active efflux, thus avoiding the CNS side effects associated with earlier antihistamines (Chen et al., 2003; Uhr et al., 2003). Because antihistamines have diverse brain distributional characteristics and varying propensity to cause CNS effects, examination of the CNS pharmacokinetics/pharmacodynamics (preclinical and clinical), as well as the relationship between *in vitro* and *in vivo* potency, would contribute to the understanding of central action of drugs, and ultimately allow for better *in vitro*-to-*in vivo* predictions.

Optimal CNS distributional characteristics

The optimal CNS distributional characteristics of a drug are dependent on whether CNS activity is desired or not, and whether a drug has intrinsic CNS or systemic activity. If CNS activity is not desired and a compound has no intrinsic CNS activity, then the CNS distributional characteristics of a compound are irrelevant. In contrast, if a compound possess both systemic and CNS activity, such as some opioids and antihistamines, then the CNS distributional characteristics should be optimized, if possible, for the intended indication (CNS or systemic). Figure 9.1 illustrates a proposed flow chart for optimization of CNS

distributional characteristics of drug candidates that incorporates many of the issues examined in this dissertation project.

If the intended indication for a drug is a systemic target, brain exposure should be minimized; however, if the intended indication is a CNS target, brain exposure (relative to systemic exposure) should be maximized, with brain concentrations then regulated by the kinetics of drug administration. The $[plasma]_u/[brain]_u$ ratio is one approach for assessing relative brain exposure irrespective of the specific mechanisms that determine flux between the systemic circulation and brain, as well as within the various compartments of the CNS (BBB passive permeability, active transport, metabolism, and CSF bulk flow). CNS-active compounds generally possess low values of $[plasma]_u/[brain]_u$ [i.e.,1 to 3; (Maurer et al., 2004)] whereas non-CNS active compounds generally are characterized by high values of $[plasma]_u/[brain]_u$ (i.e., >3; Chapter 4). Another important determinant of CNS activity for a given compound is the brain equilibration half-life. This parameter is of particular importance when considered relative to the frequency of drug administration. If a compound is administered acutely, a long brain equilibration half-life will result in a slower onset of CNS action and attenuated CNS activity. A short brain equilibration half-life will result in more rapid onset action and, possibly, a more robust pharmacologic effect, as a larger fraction of the administered dose will accumulate in brain prior to removal from the systemic circulation. If a drug is administered chronically, brain equilibration half-life is not as important, because steady-state brain concentrations eventually will be achieved regardless of the brain equilibration half-life.

Both the extent and rate of brain exposure are dependent on multiple factors, with no single process being dominant. Approaches that consider only one factor, such as passive

permeability or affinity for a given efflux transport protein, fail to provide sufficient information for proper prediction and evaluation of CNS distributional properties. Low passive permeability, or high intrinsic efflux clearance mediated by a transport protein such as P-glycoprotein, is not necessarily an indicator that a given compound will have either a low extent or a slow rate of CNS distribution. If passive permeability is sufficiently large compared to CSF bulk flow, no other active processes are present (i.e., metabolism and active transport), and $f_{u,brain}$ is large, then it is possible for a compound with low passive permeability to have unimpaired and rapid CNS distribution. Similarly, a compound that undergoes active efflux may have unimpaired and rapid CNS distribution if the efflux mechanism is counterbalanced by an active uptake process.

Conclusions

This dissertation project demonstrated the utility of unbound brain concentrations, estimated with equilibrium dialysis, in assessing the extent of CNS penetration. In addition, unbound brain concentrations appeared to represent an optimal surrogate measure for biophase concentrations, at least in the context of opioid pharmacokinetics-pharmacodynamics across a relatively wide range of *mu* opioid agonists. Comprehensive pharmacokinetic-pharmacodynamic experiments and associated mathematical modeling demonstrated the influence of BBB efflux on opioid disposition and action in the CNS. The results of this project provide important new information for improved understanding of CNS pharmacokinetic-pharmacodynamic relationships; for correlating *in vitro*, preclinical, and clinical data; and for exploring the impact of efflux transport on drug disposition and action. Finally, novel approaches to expressing transport kinetics, and the impact of transport

inhibition on target-site exposure, provide a means for obtaining more physiologically- and pharmacologically-relevant estimates of important kinetic parameters.

REFERENCES

1. Becker S and Liu X (2006) Evaluation of the utility of brain slice methods to study brain penetration. *Drug Metab Dispos* **34:**855-861.

2. Chen C, Hanson E, Watson JW and Lee JS (2003) P-glycoprotein limits the brain penetration of nonsedating but not sedating H1-antagonists. *Drug Metab Dispos* **31:**312-318.

3. Chen C and Pollack GM (1998) Altered disposition and antinociception of [D-penicillamine(2,5)] enkephalin in mdr1a-gene-deficient mice. *J Pharmacol Exp Ther* **287:**545-552.

4. Dagenais C, Graff CL and Pollack GM (2004) Variable modulation of opioid brain uptake by P-glycoprotein in mice. *Biochem Pharmacol* **67:**269-276.

5. Ekins S, Kim RB, Leake BF, Dantzig AH, Schuetz EG, Lan LB, Yasuda K, Shepard RL, Winter MA, Schuetz JD, Wikel JH and Wrighton SA (2002) Application of three-dimensional quantitative structure-activity relationships of P-glycoprotein inhibitors and substrates. *Mol Pharmacol* **61:**974-981.

6. Ekins S, Waller CL, Swaan PW, Cruciani G, Wrighton SA and Wikel JH (2000) Progress in predicting human ADME parameters in silico. *J Pharmacol Toxicol Methods* **44:**251-272.

7. Graff CL and Pollack GM (2004) Drug transport at the blood-brain barrier and the choroid plexus. *Curr Drug Metab* **5:**95-108.

8. Hutchinson PJ, O'Connell MT, Kirkpatrick PJ and Pickard JD (2002) How can we measure substrate, metabolite and neurotransmitter concentrations in the human brain? *Physiol Meas* **23:**R75-109.

9. Kalvass JC and Maurer TS (2002) Influence of nonspecific brain and plasma binding on CNS exposure: implications for rational drug discovery. *Biopharm Drug Dispos* **23:**327-338.

10. Liu X, Smith BJ, Chen C, Callegari E, Becker SL, Chen X, Cianfrogna J, Doran AC, Doran SD, Gibbs JP, Hosea N, Liu J, Nelson FR, Szewc MA and Van Deusen J (2005) Use of a physiologically based pharmacokinetic model to study the time to

reach brain equilibrium: an experimental analysis of the role of blood-brain barrier permeability, plasma protein binding, and brain tissue binding. *J Pharmacol Exp Ther* **313:**1254-1262.

11. Maurer TS, Debartolo DB, Tess DA and Scott DO (2004) Relationship between Exposure and Nonspecific Binding of Thirty-Three Central Nervous System Drugs in Mice. *Drug Metab Dispos*.

12. Sadeque AJ, Wandel C, He H, Shah S and Wood AJ (2000) Increased drug delivery to the brain by P-glycoprotein inhibition. *Clin Pharmacol Ther* **68:**231-237.

13. Schinkel AH, Wagenaar E, Mol CA and van Deemter L (1996) P-glycoprotein in the blood-brain barrier of mice influences the brain penetration and pharmacological activity of many drugs. *J Clin Invest* **97:**2517-2524.

14. Shen DD, Artru AA and Adkison KK (2004) Principles and applicability of CSF sampling for the assessment of CNS drug delivery and pharmacodynamics. *Adv Drug Deliv Rev* **56:**1825-1857.

15. Skarke C, Jarrar M, Schmidt H, Kauert G, Langer M, Geisslinger G and Lotsch J (2003) Effects of ABCB1 (multidrug resistance transporter) gene mutations on disposition and central nervous effects of loperamide in healthy volunteers. *Pharmacogenetics* **13:**651-660.

16. Srinivas E, Murthy JN, Rao AR and Sastry GN (2006) Recent advances in molecular modeling and medicinal chemistry aspects of phospho-glycoprotein. *Curr Drug Metab* **7:**205-217.

17. Summerfield S, Stevens AJ, Cutler L, Del Carmen Osuna M, Hammond B, Tang SP, Hersey A, Spalding DJ and Jeffrey P (2005) Improving the In Vitro Prediction of In Vivo CNS Penetration: Integrating Permeability, Pgp Efflux and Free Fractions in Blood and Brain. *J Pharmacol Exp Ther*.

18. Syvanen S, Xie R, Sahin S and Hammarlund-Udenaes M (2006) Pharmacokinetic consequences of active drug efflux at the blood-brain barrier. *Pharm Res* **23:**705-717.

19. Tayrouz Y, Ganssmann B, Ding R, Klingmann A, Aderjan R, Burhenne J, Haefeli WE and Mikus G (2001) Ritonavir increases loperamide plasma concentrations without evidence for P-glycoprotein involvement. *Clin Pharmacol Ther* **70:**405-414.

20. Thompson SJ, Koszdin K and Bernards CM (2000) Opiate-induced analgesia is increased and prolonged in mice lacking P-glycoprotein. *Anesthesiology* **92:**1392-1399.

21. Uhr M, Grauer MT and Holsboer F (2003) Differential enhancement of antidepressant penetration into the brain in mice with abcb1ab (mdr1ab) P-glycoprotein gene disruption. *Biol Psychiatry* **54:**840-846.

22. Wandel C, Kim R, Wood M and Wood A (2002) Interaction of morphine, fentanyl, sufentanil, alfentanil, and loperamide with the efflux drug transporter P-glycoprotein. *Anesthesiology* **96:**913-920.

23. Wang RB, Kuo CL, Lien LL and Lien EJ (2003) Structure-activity relationship: analyses of p-glycoprotein substrates and inhibitors. *J Clin Pharm Ther* **28:**203-228.

24. Wang YH, Li Y, Yang SL and Yang L (2005) Classification of substrates and inhibitors of P-glycoprotein using unsupervised machine learning approach. *J Chem Inf Model* **45:**750-757.

25. Welch MJ, Meltzer EO and Simons FE (2002) H1-antihistamines and the central nervous system. *Clin Allergy Immunol* **17:**337-388.

26. Zong J and Pollack GM (2000) Morphine antinociception is enhanced in mdr1a gene-deficient mice. *Pharm Res* **17:**749-753.

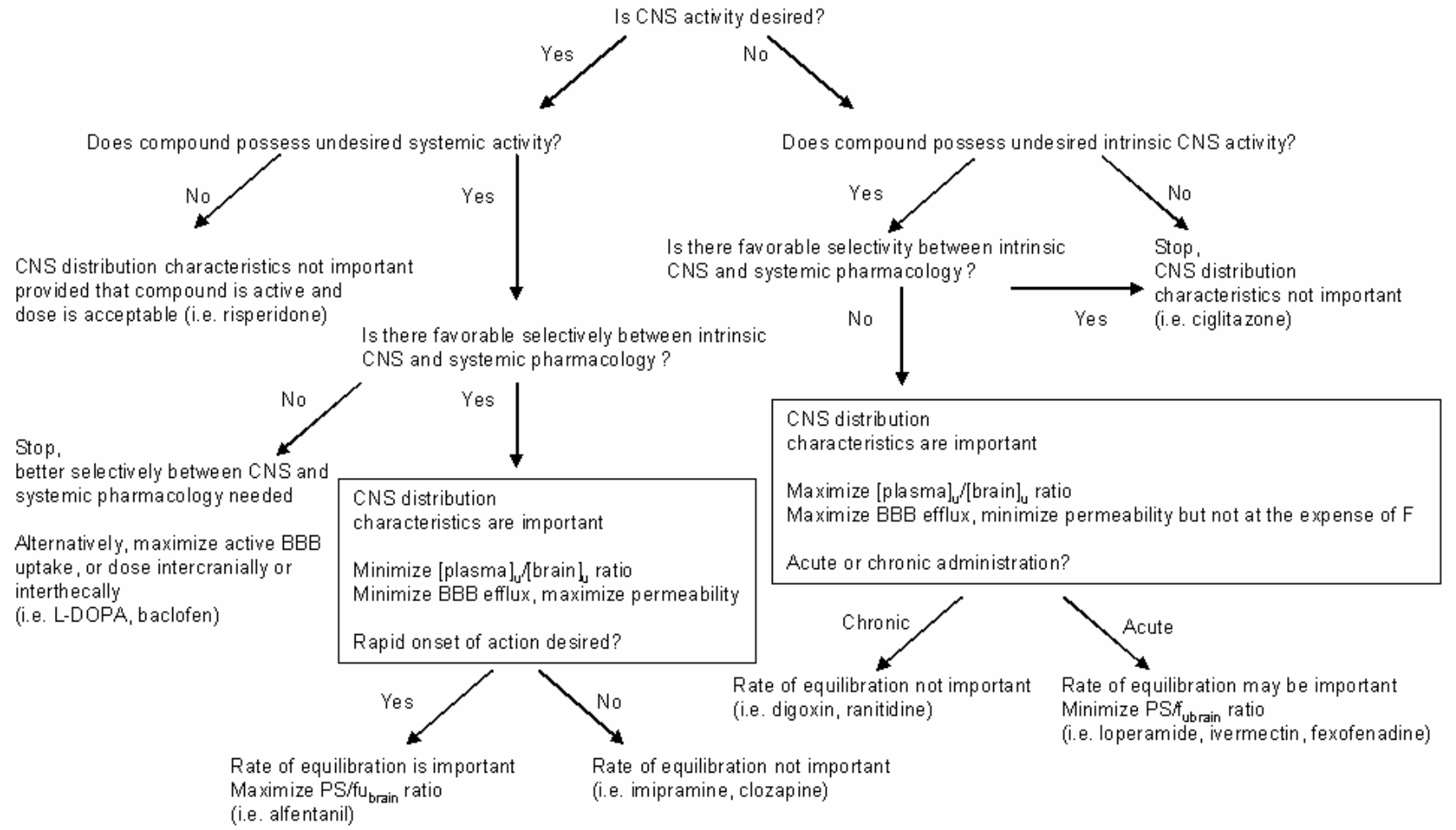

Figure 9.1. Proposed flow chart for optimal CNS distributional characteristics for drug candidates. PS, F, $f_{u,brain}$, $[plasma]_u$, and $[brain]_u$ represent passive permeability surface area product, bioavailability, unbound brain fraction, and plasma and brain unbound fractions, respectively.